

**CENTER FOR THE STUDY OF METALS IN THE
ENVIRONMENT
Final Report**

Submitted to:
U.S. Environmental Protection Agency
1200 Pennsylvania N.W.
Washington, DC 20460

Project Officer: Iris Goodman

Submitted by:
University of Delaware

In Cooperation with:
**Colorado School of Mines
Manhattan College
University of Missouri – Rolla
University of Wyoming**

Period of Performance: April 2, 2002 – May 31, 2006

Table of Contents

CENTER FOR THE STUDY OF METALS IN THE ENVIRONMENT	1
Unit World Model for Metals in Aquatic Environments	1
Introduction.....	1
Approach.....	2
Effects Concentration and Bioavailability	2
Unit World Model Design and Testing.....	3
Project Summaries	3
Ranville, J. and Ross, P. Colorado School of Mines “Ecotoxicology of Mining-Related Metal Oxides in a High Gradient Mountain Stream”	4
Allen, H. E. University of Delaware “Modeling Cu and Zn Desorption Kinetics from Soil Particles”	5
Di Toro, D. M. University of Delaware and Carbonaro R. Manhattan College “Quantitative Structure Activity Relationships for Toxicity and Fate Parameters of Metal and Metal Compounds”	5
Di Toro, D. M. University of Delaware and Farley, K. Manhattan College “Developing a Unit World Model for Metals in Aquatic Environments”	6
Sondhi, A., Imhoff, P., Allen, H. E., and Dentel, S. K. University of Delaware “Evaluation of Automobile Sources for Metals in Urban Areas”	6
Sparks, D. and Peltier, E. University of Delaware and van der Lelie, D. Brookhaven National Laboratory “The Impact of Surface Precipitation on Sequestration and Bioavailability of Metals in Soils”	7
Wronkiewicz, D. J., Adams, C. D. and Mendoza, C. University of Missouri-Rolla “Transport Processes of Mining Related Metals in the Black River of Missouri’s New Lead Belt”	7
Meyer, J. S. University of Wyoming “A Test of the Biotic Ligand Model: Fish Exposed to Time-varying Concentrations of Copper and Zinc”	8
References.....	8
APPENDIX I	11
Research Project Reports	11
Ecotoxicology of Mining-Related Metal Oxides in a High Gradient Mountain Stream	12
Introduction.....	13
Background.....	13
Clear Creek Watershed	14
Methods	16
Water and Sediment Sampling.....	16
Chemical Analysis	16
Sorption Experiments.....	17
Surface Complexation Modeling	17
Results and Discussion	19
Component 1: Evaluation of methods for the determination of metal distribution between dissolved and particulate phases.....	19

Component 2: Temporal variations in the geochemistry of Clear Creek	20
Component 3: Spatial Trends in Stream Geochemistry.....	25
Component 4: Laboratory sorption experiments using field-derived materials	28
Component 5: Sequential extraction Analysis of Field-derived materials from Clear Creek	30
Overall Summary	31
Literature Cited.....	34
 Modeling Cu and Zn Desorption Kinetics from Soil Particles	 35
Introduction.....	36
Materials and Methods.....	38
Model Description	40
Results.....	43
Kinetics of Cu and Zn desorption from soils	43
Kinetics of Zn sorption on and desorption from soils.....	47
Kinetics of Cu sorption on and desorption from soils	51
Conclusion	53
Literature Cited	54
 Quantitative Structure Activity Relationships for Toxicity and Fate Parameters of Metals and Metal Compounds	 57
Introduction.....	58
Approach.....	59
Lactic Acid LFER for WHAM V	59
Irving-Rossotti Slopes.....	61
Irving-Rossotti LFERs for WHAM V	62
Estimating Metal-Ligand Binding	63
Analysis Methods	66
Thermodynamic Constant Selection Criteria and Ionic Strength Corrections.....	66
Regression Analysis.....	66
Results and Discussions.....	66
Martell-Hancock LFERs.....	66
Irving-Rossotti Slopes for Negatively-Charged Oxygen Donor Atoms.....	70
First Row Transition Metals	72
Alkaline Earth Metals	73
Lanthanides and Actinides.....	73
Other Metal Ions	74
Relationship of Proton and Metal Ligand Complexes.....	74
Relationship Between the Irving-Rossotti Slope and C_A^{aq}	75
Applications for Irving-Rossotti Slopes	76
Conclusions.....	77
Literature Cited.....	77
 Developing a Unit World Model for Metals in Aquatic Environments.....	 79

Introduction.....	80
Approach.....	80
Review of Current Models for Metal Speciation and Organic Carbon Cycling.....	81
Windermere Humic Aqueous Model (WHAM, Model V) (Tipping, 1994).....	82
SEM-AVS (Di Toro et al. 1990; Di Toro et al. 1992).....	82
Biotic Ligand Model (BLM) (Di Toro et al. 2001).....	82
Preliminary Modeling Studies.....	83
Perch Lake, Canada.....	84
Lake Baldegg, Switzerland.....	86
WHAM V Calculations for K_D	87
Development of UWM: Tier 1 Model for Metals in Lakes.....	90
Tier 1 Model Applications.....	91
Model Results.....	92
Unit World Model for Streams and Rivers.....	94
Probabilistic Dilution Modeling.....	94
Metal Partitioning Analysis.....	95
WHAM6 Results.....	96
Sorption to Algae.....	96
Delaware Bay Chemical Speciation.....	99
Literature Cited.....	99
Evaluation of Automobile sources for Metals in Urban Areas.....	103
Introduction.....	104
Material and Methods.....	105
Break Pad Wear Debris.....	105
Leaching Solution and Chemical Reagents.....	106
Analytical Equipment.....	106
Experimental Design.....	106
Representative elementary mass.....	106
Total metal content.....	106
Dissolution/leaching of copper.....	107
Particle distribution.....	107
Specific surface areas.....	107
Results.....	108
Total Metal Content and Important Elements in Brake Wear Debris.....	108
Surface Area of Natural and Artificial Brake Wear Debris.....	109
Distribution of Copper in Artificial and Natural Wear Debris.....	109
Density Measurement.....	110
Dissolution/Leaching of Metals and Elements at pH 4.3.....	111
Dissolution/Leaching of Metals and Elements at pH 6.1.....	113
Comparison of Dissolution at pH 4.3 and 6.1.....	114
Estimating Copper Emissions from Natural Wear Debris with Artificial Wear Debris.....	114
Particle Size Distribution of Artificial, Natural and LACT Brake Wear Debris.....	115

Prediction and confirmation of bimetallic oxides	117
Discussion	119
Literature Cited	121
The Impact of Surface Precipitation on Sequestrian and Bioavailability of Metals in Soils.....	123
Objectives and Background Information	124
Approach.....	126
Precipitate Formation in Ni Amended Laboratory Soils	126
Metal Speciation	127
Metal Desorption/Dissolution Studies	127
Thermodynamic Analysis	128
Nickel Bioavailability	128
Modeling Ni Sorption and Deorption Kinetics	128
Results.....	130
Thermodynamic Stability of Ni LDH Precipitate Phases	130
Precipitate Formation on Laboratory Contaminated Soils.....	131
Short term kinetics of Ni precipitate formation	133
Ni desorption from aged soils	134
Metal bioavailability	134
Modeling Ni Sorption and Desorption Kinetics	135
Summary and Conclusions	138
Acknowledgements.....	139
Literature Cited	139
Transport Processes of Mining Related Metals in the Black River of Missouri's New Lead Belt.....	142
Introduction.....	143
Objectives	143
Background.....	143
Regional Geology and Geography.....	143
Experimental Procedures	145
Site Selection, Sampling Dates and Locations	145
Sampling and analytical procedures	147
Analytical Precision and Accuracy.....	148
Results and Discussion	149
Regional Ssediments – Background Metal Concentrations.....	149
West Fork Sediments – Mineralogy	149
West Fork Sediments – Chenistry	150
West Fork Water Column - Chemistry	153
West Fork Batch Metal Adsorption Test	155
Clearwater Lake Sediment Core Studies	157
Sequentially Extracted Metals	159
Hydrologic Characterization of the West Fork of the Black River	159
Big River and Associated Tributary Sediments – Chemistry	159

Big River and Associated Tributary Sediments – Mineralogy	160
Big River Tailings Pile Water - Chemistry	163
Big River Water - Chemistry	163
Dissolution Processes Occurring in Tailings Piles	164
Metal Concentration Changes with Transport Distance	165
Particulate Control on Contaminant Metal Transport.....	167
Particulate Organics	167
Clays	169
Mn and Fe oxyhydroxide	169
Sulfides	173
Flood Effects on Contaminant Metal Transport	173
Conclusions.....	175
Literature Cited.....	176
A Test of the Biotic Ligand Model: Fish Exposed to Time-varying Concentrations of Copper and Zinc.....	177
Introduction.....	178
Methods	179
Toxicity Tests	179
Physical and Chemical Analyses	180
Models	180
Biotic ligand model.....	180
One-Compartment Uptake-Depuration Models.....	181
Statistical Analyses	183
Results and Discussion	184
Fitting the OCUD Model to the Continuous-Exposure LC50 Data.....	184
Fitting the OCUD Model to the Continuous-Exposure LA50 Data	186
Observed versus Predicted Pulse-Exposure LA50	191
Framework for Using the Linked BLM-OCUD Model for Predicting Acute Toxicity of Copper.....	193
Conclusions.....	194
Acknowledgements.....	195
Literature Cited.....	195
APPENDIX II.....	197
Publications.....	197
Ecotoxicology of Mining-Related Metal Oxides in a High Gradient Mountain Stream	198
Presentations:	199
Poster	199
Peer-Reviewed Papers	200
Published Abstracts.....	201
Modeling Cu and Zn Desorption Kinetics from Soil Particles.....	202
Papers	203

Manuscripts in Preparation	203
Presentations	203
Quantitative Structure Activity Relationships for Toxicity and Fate Parameters of Metals and Metal Compounds	204
Presentations	205
Books	205
Papers	205
Developing a Unit World Model for Metals in Aquatic Environments.....	206
Presentations	207
Papers	208
Evaluation of Automobile sources for Metals in Urban Areas.....	209
Papers (to be submitted)	210
The Impact of Surface Precipitation on Sequestrian and Bioavailability of Metals in Soils.....	211
Presentations	212
Published Article.....	213
Transport Processes of Mining Related Metals in the Black River of Missouri's New Lead Belt.....	214
A Test of the Biotic Ligand Model: Fish Exposed to Time-varying Concentrations of Copper and Zinc.....	217
Journal articles containing acknowledgement of funding from CSME that either were published or have been accepted for publication in scientific journals:	218
Books published:.....	218
Book chapters published:.....	218
Manuscripts containing acknowledgement of funding from CSME that are in review for publication in scientific journals:	219
Manuscripts containing acknowledgement of funding from CSME that are in preparation for submission to scientific journals:.....	219
Presentations at scientific meetings:	219
APPENDIX III.....	222
Students Supported	222

CENTER FOR THE STUDY OF METALS IN THE ENVIRONMENT

Final Report

April 2, 2002 – May 31, 2006

The Center for the Study of Metals in the Environment is a multi-institutional consortium of scientists and engineers working to further the understanding of processes affecting the fate and effects of metals in aquatic and terrestrial ecosystems. Significant gaps in the ability to predict the fate and effects of metals in both aquatic and terrestrial systems continue to hamper appropriate risk assessments and cost-effective risk management. In these situations, decisions include many assumptions and the application of safety factors. The focus of the Center is to develop appropriate information so that regulatory decisions will be based on sound scientific principles. Much of the existing methodology for hazard identification and for risk assessment is based on experience with persistent organic pollutants such as DDT and PCBs. The large differences in environmental behavior and potential for toxicity between organic compounds and metals are not incorporated into these methods. Assessment methodology is currently focused on the extent to which chemicals exhibit PBT (persistent, bioaccumulative, and toxic) characteristics. All three characteristics are important aspects of the assessment of risk, but their applicability to metals and the evaluation of metals data for these criteria differ from organic compounds.

As a replacement for the current methods for evaluating the effect of metals in the environment, the Center is developing a model for the behavior of metal compounds that can be used as a tool in the hazard assessment of metals and metal compounds. This model will include the physical and chemical mechanisms that control the fate and resulting bioavailability of metals discharged to natural waters. In particular the transformations that affect metal fate and toxicity will be included. It is anticipated that it would be similar to the Unit World models, for example EUSES that are used for evaluating PBT organic chemicals. Metal behavior in watersheds, streams, lakes and reservoirs will be considered. The focus of the research efforts is to provide the information necessary to formulate and parameterize the model.

Unit World Model for Metals in Aquatic Environments

Introduction

There is a clear need for methods that can be used for evaluating the environmental hazard associated with the release of metals and metal compounds to the environment (Adams et al., 2000). The purpose of the Unit World Model (UWM) is to provide such a framework. The idea for a UWM comes from the fugacity and regional models developed for organic chemicals (Mackay 1979, 1991, Mackay et al. 1992). Models of this sort have previously been applied in various forms to pesticides (USEPA, 1986a) and industrial organic chemicals (European Commission, 1996). The UWM for metals is structured such that it can be used to estimate both

the exposure and effects of metal and metal compounds. It incorporates the necessary metal specific processes that differentiate the behavior of metals from organic chemicals.

Approach

The Unit World Model is designed to represent the major processes that determine the fate and transport of metals in the aquatic environment. In the water column these processes include solubilization for particulate metal compounds, speciation among inorganic and organic dissolved ligands, and partitioning to suspended particles. The WHAM series of aqueous speciation models (Tipping, 1994) have been extensively calibrated and are well suited for incorporation in the UWM. A metal particle sorption model (SCAMP) has also recently become available (Lofts and Tipping 1998). Although not as well calibrated, it provides a useful starting point.

The sorption of metals to water column particulate matter leads to the transfer of the metal to the bottom sediments. Hence, sediments are the ultimate repositories of metals in aquatic settings. A number of sediment models have been developed that successfully predict levels of sulfide (AVS–Acid Volatile Sulfide) and partitioned metal (SEM) in sediments and resulting fluxes of dissolved metal from the sediments to the overlying water column (Di Toro et al., 1996; Carbonaro, 1999; Di Toro et al., 2001). Therefore the frameworks exist for at least most of the processes, in various stages of development, for the water column and sediment compartments.

Effects Concentration and Bioavailability

In addition to the exposure concentrations in the water column and sediment, it is necessary to predict the effects to be expected. The traditional method is to use an effects concentration for the water column and the sediment. For the water column the EPA Water Quality Criteria (Stephan et al., 1985, USEPA 1986b, 1996) or the PNEC (Predicted No Effect Concentration) derived following the EU Technical Guidelines (EU, 1996) are possibilities. However, these criteria make only limited bioavailability corrections (for water hardness only). This is a much more critical issue for metals than for organic chemicals. To remedy this situation, the Biotic Ligand Model (BLM) has recently been developed (USEPA, 1999, 2000; Di Toro, et al., 2001; Paquin et al., 2002). It incorporates the WHAM speciation model and in addition models the competitive metal binding at the toxic site of action (the Biotic Ligand). BLMs are currently available for copper and silver (Di Toro, et al., 2001; Santore et al., 2001), zinc (Santore et al., 2002) and are under development for cadmium, nickel and lead.

The situation in the sediment is similar. There are guideline values that do not take bioavailability into account—the sediment PNEC—or which are empirical and therefore are not predictive of individual metal toxicity (e.g. Long and Morgan, 1991; Field et al., 2002).

For metals, EPA has developed sediment quality guidelines that are causally related to metal effects and do take bioavailability into account. They are based on the relative magnitudes of acid volatile sulfide AVS and simultaneously extractable metal SEM, and organic carbon (Di Toro et al., 1990, 1992; Ankley et al., 1993, 1996; USEPA, 2000).

Unit World Model Design and Testing

The design of the UWM is based on the processes required for calculating both the exposure concentration and the variables required for making the bioavailability corrections for the effects concentration. Since the model is expected to be used for site-specific evaluations as well as in regulatory settings, it needs to be predictive to the extent possible. This forces a more complex model structure than would be necessary for a strictly evaluative model with fixed physical, chemical and biological variables. The UWM is being built using a water column/sediment eutrophication model as a basis (Di Toro, 2001). Modern eutrophication models compute most of the required auxiliary variables required for metal modeling—carbon and sulfur cycles—and water column/sediment models for manganese and iron are also available, which are required for metal partitioning.

The steps in producing the model are to synthesize the available components into a unified modeling framework, and then to test the model with laboratory and field data for a variety of metals. The testing will begin with experiments in which a suite of metals were added to freshwater (Diamond et al., 1990) and marine (Santschi et al., 1987) mesocosms, and a long term dosing experiments to a Canadian lake (Hesslein, 1980). There is one data set (O'Connor 1988) that can be used for calibrating the model to freshwater streams. However, it is somewhat limited and it was not collected using modern clean techniques. It is anticipated that most of the data for streams will need to be generated.

Project Summaries

The Center's Science Advisory Committee (SAC) met in May 2003 to review proposals for research. Nine projects, each of which had been proposed for a 3-year period, were approved. During the course of the projects some personnel changes took place. The principal change resulted from Dr. Dominic Di Toro leaving Manhattan College and moving to the University of Delaware. The two projects that he directed began at Manhattan College, but were moved to the University of Delaware. These projects are

Investigator	Institution	Project Title
Ranville, J./ Ross, P.	Colorado School of Mines	Ecotoxicology of Mining-Related Metal Oxides in a High Gradient Mountain Stream
Allen, H. E.	University of Delaware	Modeling Cu and Zn Desorption Kinetics from Soil Particles
+Church, T.	University of Delaware	Metal Speciation in Watersheds
Di Toro, D. M./ Farley, K.	University of Delaware Manhattan College	Developing a Unit World Model for Metals in Aquatic Environments
Imhoff, P./ Allen, H. E./ Dentel, S. K.	University of Delaware	Evaluation of Automobile Sources for Metals in Urban Areas
Sparks, D.	University of Delaware	The Impact of Surface Precipitation on Sequestration and Bioavailability of Metals in Soils

*Capitani, J.F./ Di Toro, D. M.	Manhattan College University of Delaware	Quantitative Structure Activity Relationships for Toxicity and Fate Parameters of Metal and Metal Compounds
~Wronkiewicz, D. Adams, C. D.	University of Missouri-Rolla	Transport Processes of Mining Related Metals in the Black River of Missouri's New Lead Belt
Meyer, J. S.	University of Wyoming	A Test of the Biotic Ligand Model: Fish Exposed to Time-varying Concentrations of Copper and Zinc

+ coPI added – Luther, III G.W.
* Replaced as coPI at Manhattan College by Carbonaro, R. Di Toro, D.M. present PI – no change in scope of work
~coPI added – Mendoza, C.

Reports of the results of activities for each of these projects are contained in Appendix I. Publications are listed in Appendix II and Students Supported are listed in Appendix III. A brief summary of each project is presented here.

Ranville, J. and Ross, P. Colorado School of Mines “Ecotoxicology of Mining-Related Metal Oxides in a High Gradient Mountain Stream”

This project supported Unit World Model (UWM) development for metal transport in streams, by providing field data sets for calibration. Much of the previous data has been collected for lentic systems and data on high-gradient systems is lacking. Clear Creek (CC) and North Fork Clear Creek (NFCC), a major tributary to CC, located west of Denver CO, were the focus of investigation. The streams receive high loads of Fe, Mn, Cu, and Zn from abandoned mines. The dominance of hydrous ferric oxide (HFO) and hydrous manganese oxide (HMO) in the sediments also allowed the testing of existing surface complexation models (SCM) for predicting the distribution of metals between sediment and dissolved phases, a key component of the UWM. There were five components of the work, the results of which were as follows. First, direct analysis (acid-digestions of sediments retained on filters) is statistically the same as the difference method (unfiltered metal concentration minus filtered metal concentration) for determining suspended sediment-associated metals. Second, seasonal changes in stream discharge results in significant changes in water chemistry and the suspended sediment concentration and composition, over both time and space. Observed particulate Cu and Zn compared favorably to SCM predictions if both HFO and HMO phases were considered and dissolved organic carbon (DOC) was included as a competing ligand present in the aqueous phase. Third, similar measurements and SCM predictions were made at a larger number of sites along NFCC. Downstream variations in the distribution of Cu and Zn between the dissolved and suspended sediment phases were reasonably well predicted, however Zn spatial data was not as well represented as was the Zn seasonal data. Fourth, the SCM was applied to pH-variable adsorption experiments performed in the laboratory using field collected HFO and HMO. In general the comparison between the SMC predictions and the measurements was better for Cu than for Zn. Finally, sequential extractions were performed on suspended sediments. The results further suggest that Cu and Zn are mostly associated with oxide phases such as HFO and HMO and to a lesser extent organic phases. Results suggest that current SCMs can be used in the UWM to provide accurate predictions of metal sorption to sediments in which HFO and HMO are present.

Allen, H. E. University of Delaware “Modeling Cu and Zn Desorption Kinetics from Soil Particles”

In this project, the effect of solution chemistry and soil composition on trace metal sorption and desorption kinetics was investigated. Based on the experimental results, predictive kinetics models were formulated and successfully used to describe the kinetics of trace metals sorption and desorption on a variety of soils. A number of soil samples were selected to test the effect of soil composition. The solution pH has significant effect on the Cu and Zn sorption and desorption kinetics. DOM greatly enhanced Cu release but had little effect on Zn. Among all soil components, soil organic matter is the dominant phase controlling Cu and Zn sorption and desorption kinetics. The kinetics models were formulated and successfully used to describe the Cu and Zn sorption and desorption kinetics. For Zn, a two-site kinetics model was necessary. The soil organic carbon (SOC) is the major model parameter accounting for the effect of soil properties on Zn sorption and desorption kinetics. The organic carbon normalized sorption rate coefficients can be applied to different soils based on their SOC concentrations. One set of rate coefficients can be applied to different influent Zn concentrations. The sorption rate coefficients were dependent on solution pH which was accounted for by Zn and proton competition. Cu showed different kinetics behavior and a one-site kinetics model was sufficient. DOM effect can be accounted for by DOM complexation of copper ions. Although the kinetics model assuming the linear binding, the nonlinearity of Cu binding to soils was also considered by incorporating the equilibrium models into the kinetics model, such as Windermere Humic Aqueous Model (WHAM) VI. The equilibrium model was used to predict the partition coefficient at every Cu loading. The WHAM VI based kinetics model successfully described Cu sorption and desorption kinetics for a variety of experimental conditions.

**Di Toro, D. M. University of Delaware and Carbonaro R. Manhattan College
“Quantitative Structure Activity Relationships for Toxicity and Fate Parameters of Metal and Metal Compounds”**

The purpose of this research project to develop quantitative structure activity relationships (QSARs) for metals for which little or no experimental information exists. The parameters of interest are those required for hazard ranking and ultimately for evaluation using modeling approaches such as the Unit World Model. There are many metal and metalloid compounds for which there is concern with the environmental hazard associated with their release to the environment. It is important that rational methods of evaluating the potential for harm be employed. Unlike the most studied metals, Cd, Cu, Ni, Pb, and Zn, or metals that have recently been of concern, for example Ag, most of the other metals are not well studied, particularly the transition metals in the third and fourth rows and the lanthanides. A method has been developed for estimating metal-ligand formation constants (K_{ML}) utilizing the linear free energy relationship (LFER) $\log K_{ML} = \alpha \log K_{HL} + \beta$ where K_{HL} is the corresponding proton-ligand formation constant. LFERs of this type are presented for 24 different metal ions complexing to negatively-charged oxygen donor atoms. The intercept of all LFERs was nearly zero for all metal ions investigated ($\beta \approx 0$). The magnitude of the slope, α , indicates the relative preference of metal binding to negatively charged oxygen donor atoms and to the proton. This slope is used to estimate the binding constants for metals in versions V and VI of the Windermere Humic Aqueous Model (WHAM).

Di Toro, D. M. University of Delaware and Farley, K. Manhattan College “Developing a Unit World Model for Metals in Aquatic Environments”

The purpose of this project is to build a model – the Unit World Model – for evaluating the environmental fate and hazard associated with the release of metals and metal compounds to the environment. The model includes the major processes that determine the long term fate of metals in an aquatic lake environment: partitioning to suspended particles, and transport to and from the sediment. Toxicological effects of metals in each of these environmental compartments are addressed by the inclusion of the Biotic Ligand Model. The model has been applied to mesocosm studies and selected field sites for model calibration and validation. Based on these results, a screening level model for the transport and fate of metals in an aquatic lake environment including an evaluation of toxicological effects of metals in the water column and sediment compartments. The user defined input for the model includes the metal loading rate, water quality parameters (including pH, hardness, DOC, POC, the sediment dry weight concentration, and percent organic carbon and AVS concentration in the surficial sediment layer), and transport parameters (including surface area, depth, depth / detention time, and settling, resuspension, burial and diffusive exchange rates). Model calculations can also be performed by specifying the free ion activity of the metal or the critical concentration of metal on the biotic ligand and calculating the allowable loading rate of metal to the lake. Calculated critical loadings ($\text{gm/m}^2/\text{yr}$) are in the order: $\text{Cd} < \text{Cu} \sim \text{Zn} < \text{Ni} < \text{Pb}$ and vary by approximately an order of magnitude.

Sondhi, A., Imhoff, P., Allen, H. E., and Dentel, S. K. University of Delaware “Evaluation of Automobile Sources for Metals in Urban Areas”

Automobile brake wear debris have been implicated as major sources of Copper in urban runoff and the South San Francisco Bay. To characterize and understand this source of Coppers emissions, three different types of wear debris were collected from brake pads known to contain Copper and associated with four different types of automobiles. The wear debris were collected following procedures developed by the Brake Pad Partnership (BPP) for Los Angeles City Traffic driving conditions (LACT), by sanding the brake pads (artificial), and by collecting debris from the wheels and hubs of the automobiles (natural). The particle size distribution and chemical composition were determined for the wear debris. The data suggest that these non-airborne or fallout particles contain a significant number of small-size particles that may otherwise be airborne. The chemical composition of the LACT and natural particles indicate contamination by Iron (LACT and natural) and Silica (natural), most likely from the automobile rotors and road dust. Leaching of Copper from debris was studied at pH 4.3 and pH 6.1, which bracket pH conditions for rainwater and urban runoff. A significant fraction of Copper present in natural wear debris was readily leached at low pH, with approximately 90% of the Copper leached from natural brake wear debris at pH 4.3 for all four vehicle types tested over a 15 week leaching period. Dissolution of Copper from brake wear debris was less at pH 6.1, with 35 to 70% leached from the four automobile types. Despite differences in particle size distributions and chemical composition for the wear debris from the four automobiles, the data suggest that artificial particles may be used to make conservative (high) estimates of the leachable fraction of Copper from natural wear debris, although the rate of dissolution is significantly different for these wear debris. Thermodynamic modeling also holds promise for predicting the change in form of metals present in virgin brake pads when released as wear debris.

Sparks, D. and Peltier, E. University of Delaware and van der Lelie, D. Brookhaven National Laboratory “The Impact of Surface Precipitation on Sequestration and Bioavailability of Metals in Soils”

A number of studies have appeared in the literature on the formation of metal (e.g., Co, Ni, and Zn) hydroxide precipitates on mineral and mineral-coated surfaces. These phases occur at surface loadings often below monolayer coverage and at pHs undersaturated with respect to pure metal hydroxide solubility. With time the precipitate phases undergo mineral transformations and metal stability is greatly enhanced. Thus, the formation of these phases in natural materials such as soils could be a significant mode to sequester toxic metals in the environment such that they are less mobile and bioavailable. However, there are limited data on the formation and presence of metal hydroxide surface precipitates in natural systems such as soils. Accordingly, the objectives of this research were to investigate the formation of Ni surface precipitates and subsequent Ni sequestration in soils of differing physicochemical and mineralogical properties over a range of environmental (pH, time) conditions employing macroscopic, molecular, bioavailability, and modeling approaches. Nickel layered double hydroxide (LDH) surface precipitates formed at pH>6.5 on the three soils that were studied, with not only pH but the type of clay mineralogy impacting the type of surface precipitate that was formed. Desorption studies showed that over a 1 year period, the LDH phases were metastable in the soils, which is related to mineral transformations due to increased silication of the interlayers of the LDHs. Thermodynamic and bioavailability data confirmed the effect of LDH formation and interlayer composition on metal stability and bioavailability. A kinetic model was developed that successfully described Ni adsorption/precipitation under different reaction conditions.

Wronkiewicz, D. J., Adams, C. D. and Mendoza, C. University of Missouri-Rolla “Transport Processes of Mining Related Metals in the Black River of Missouri’s New Lead Belt”

Sediment and water samples from the drainage basins of the Big River and the West Fork of the Black River in southeast Missouri were collected and analyzed to determine transport parameters affecting contaminant metal mobility. Metal concentrations vary in the effluent waters from the two tailings piles that we sampled and also in effluent water following rain events. High metal concentrations occur in Elvins Pile (River Mines) effluent water in the Big River basin, with concentrations for most metal contaminants being supersaturated with respect associated metal carbonate mineral phases. Contaminant metals are transported in both soluble and colloidal forms, with a trend towards the former converting to the latter with increasing transport distance. Contaminant metals have a strong tendency to be precipitated as Mn-oxyhydroxide or carbonate phases once the mine effluent waters enter West Fork river system. Weaker associations with Fe-oxyhydroxide and organics (both particulate and DOC fractions) are also found. These metal bearing particles become incorporated into the river bed sediments. The imprint of metals in the mine water effluent discharge is no longer evident at distances of 15 nautical miles or greater in the West Fork. By contrast, the Big River system displays elevated metal contamination levels over the approximately 100 mile distance from which we collected. Contaminant metal associations with Fe and Al are enhanced with transport distance and become even more evident during flood events when suspended sediment loads are highest. Lead appears to remain suspended in the water column during flooding for longer periods relative to Zn. At least a portion of the Pb is associating with low-density particulate organics or clays.

Sulfide minerals containing Pb, Zn, and Fe and other metals are found in Big River sediments at sites up to eight nautical miles downstream of tailings piles. Resistance to combined mechanical and chemical alteration for these phases occurs in the order: galena>sphalerite>pyrite. Sulfides were not found in West Fork sediments. Metals concentrations in sediments collected in cores from Clearwater Lake, a man-made impoundment on the Black River, suggest a doubling of the metal flux of Pb and Zn following the initiation of mining activities in the New Lead Belt. Lead isotopic analyses indicate that the source of the excess lead is from the ore minerals of the New Lead Belt.

Meyer, J. S. University of Wyoming “A Test of the Biotic Ligand Model: Fish Exposed to Time-varying Concentrations of Copper and Zinc”

Research at the University of Wyoming involved two components related to the biotic ligand model (BLM) of the acute toxicity of cationic metals to aquatic organisms: (1) conducting toxicity tests in support of a refined BLM for fathead minnows (FHM; *Pimephales promelas*) exposed to Zn, and (2) linking a FHM Cu BLM with a one-compartment uptake-depuration (OCUD) model of time-variable (pulse) exposures to toxicants. This second component was undertaken because concentrations of metals and other water quality parameters (e.g., pH, dissolved organic carbon (DOC)) often cycle daily in surface waters, thus emphasizing the need to predict the LC50s of dissolved metals during time-variable exposures. Results of the Zn toxicity tests have been incorporated into the parameterization of the current FHM Zn BLM (Version 2.1.1; <http://www.hydroqual.com/blm>). Results of the Cu toxicity tests indicate that one global OCUD equation linked to a re-parameterized FHM Cu BLM can be used to predict the acute toxicity of continuous and pulse exposures of Cu to FHM larvae relatively accurately across the range of combinations of pH, water hardness and DOC concentrations tested in this study. However, the default parameterization of the current FHM Cu BLM (Version 2.1.1) predicts Cu LA50s (median lethal accumulations) that do not fit the generalized form of an OCUD model and thus cannot be used to accurately predict pulse-exposure LC50s of dissolved Cu. Although the accuracy of OCUD-model predictions of the toxicity of pulse exposures of Cu could be improved by incorporating a mechanism to account for the delayed mortality that occurs during recovery periods in pulse-and-recovery exposure cycles, the research conducted at the University of Wyoming demonstrates that linked BLM-OCUD models can be used to predict pulse-exposure toxicity in a variety of situations, potentially including a generalized unit world model for metals and/or site-specific analyses of metal toxicity.

References

- Adams, W.J., B. Conard, G. Ethier, K.V. Brix, P.R. Paquin, D.M. Di Toro. (2000) The Challenges of Hazard Identification and Classification of Insoluble Metals and Metal Substances for the Aquatic Environment. *Human and Ecol. Risk Assessment* 6:1019-1038.
- Ankley, G.T., V. Mattson, E. Leonard, C. West, and J. Bennett. (1993) Predicting the Acute Toxicity of Copper in Freshwater Sediments: Evaluation of the Role of Acid Volatile Sulfide. *Environ. Toxicol. Chem.* 12:312-320.
- Ankley, G.T., D.M. Di Toro, D.J. Hansen, W.J. Berry. (1996) Technical Basis and Proposal for Deriving Sediment Quality Criteria for Metals. *Environ. Toxicol. Chem.* 15:2056-2066.
- Carbonaro, R. (1999) Modeling Metal Sulfide Fluxes from Sediments. MS Thesis. Department of Environmental Engineering. Riverdale, NY, Manhattan College.

- Diamond, M.L., D. Mackay, R.J. Cornett, L.A. Chant. (1990) A Model of the Exchange of Inorganic Chemicals between water and sediments. *Environ. Sci. Technol.* 24:713-722.
- Di Toro, D.M. (2001) *Sediment Flux Modeling*. J. Wiley and Sons, New York. pp 624.
- Di Toro, D.M., J.D. Mahony, D.J. Hansen, K.J. Scott, M.B. Hicks, S.M. Mayr, M.S. Redmond. (1990) Toxicity of Cadmium in Sediments: The Role of Acid Volatile Sulfide. *Environ. Toxicol. Chem.* 9:1487-1502.
- Di Toro, D.M., J.D. Mahony, D.J. Hansen, K.J. Scott, A.R. Carlson, G.T. Ankley. (1992) Acid Volatile Sulfide Predicts the Acute Toxicity of Cadmium and Nickel in Sediments. *Environ. Toxicol. Chem.* 26:96-101.
- Di Toro, D.M., J.D. Mahony, D.J. Hansen, W.J. Berry. (1996) A Model of the Oxidation of Iron and Cadmium Sulfide in Sediments. *Environ. Toxicol. Chem.* 15:2168-2186.
- Di Toro, D.M., H.E. Allen, H.L. Bergman, J.S. Meyer, P.R. Paquin, R.C. Santore. (2001). Biotic Ligand Model of the Acute Toxicity of Metals. I. Technical Basis. *Environ. Toxicol. Chem.* 20:2383-2396.
- EU (1996) Technical Guidance Document in support of commission directive 93/67/EEC on risk assessment for new notified substances and commission regulation (EC) No 1488/94 on risk assessment of existing substances. Part II. Brussels, European Union. ISBN 92-827-8012-0.
- Field, L.J., D.D. Macdonald, S.B. Norton, C.G. Ingersoll, C.G. Severn, D. Smorong, R. Lindskoog. (2002) Predicting Amphipod Toxicity from Sediment Chemistry Using Logistic Regression Models. *Environ. Toxicol. Chem.* 21:1993-2005.
- Hesslein, R.H. (1980) Whole-Lake Model for the Distribution of Sediment-Derived Chemical-Species. *Canadian Journal of Fisheries and Aquatic Sciences* 37(3):552-558.
- Lofts, S., E. Tipping. (1998) An Assemblage Model for Cation Binding by Natural Particulate Matter. *Geochim. Cosmochim. Acta* 62(15):2609-2625.
- Long, E.R., L.G. Morgan. (1991) The Potential for Biological Effects of Sediment-Sorbed Contaminants Tested in the National Status and Trends Program. Seattle, WA, NOAA Tech. Memo. NOS OMA 52.
- Mackay, D. (1979) "Finding Fugacity Feasible." *Environ. Sci. Technol.* 13:1218-1223.
- Mackay, D., (1991) *Multimedia Environmental Models*, Lewis Publishers, Chelsea, MI.
- Mackay, D., S. Paterson, W.Y. Shiu. (1992) "Generic Models for Evaluating the Regional Fate of Chemicals." *Chemosphere* 24:695-717.
- O'Connor, D.J. (1988) "Models of Sorptive Toxic Substances in Freshwater Systems. III: Streams and Rivers." *J. Environ. Engr.* 114:552-574.
- Santschi, P.H., M. Amdurer, D. Adler, P. Ohara, Y.H. Li, P. Doering. (1987) "Relative Mobility of Radioactive Trace Elements Across the Sediment-Water Interface in the MERL Model Ecosystems of Narragansett Bay." *J. Mar. Res.* 45:1007-1048.
- Santore, R.C., D.M. Di Toro, P.R. Paquin, R.C., H.E. Allen, J.S. Meyer. (2001) "A Biotic Ligand Model of the Acute Toxicity of Metals. II. Application to Acute Copper Toxicity in Freshwater Fish and *Daphnia*," *Environ. Toxicol. Chem.* 20:2397-2402.
- Santore, R.C., R. Mathew, P.R. Paquin, D. Di Toro. (2002) "Application of the Biotic Ligand Model to Predicting Zinc Toxicity to Rainbow Trout, Fathead Minnow, and *Daphnia magna*." *Comp. Biochem. Physiology* 133C(1-2):271-285.

- Stephan, C.E., D.I. Mount, D.J. Hansen, J.H. Gentile, G.A. Chapman, W.A. Brungs. (1985) Guidelines for Deriving Numerical National Water Quality Criteria for the Protection of Aquatic Organisms and Their Uses. Springfield VA, National Technical Information Service. PB 85-22-7049.
- Tipping, E. (1994) "WHAM - A Computer Equilibrium Model and Computer Code for Waters, Sediments, and Soils Incorporating a Discrete Site/electrostatic Model of Ion-binding by Humic Substances." *Computers & Geosciences* 20(6):973-1023.
- USEPA, (1986a) "Hazard Evaluation Division, Standard Evaluation Procedure, Ecological Risk Assessment," Office of Pesticide Programs, Washington, DC. EPA 540/9-85-001.
- USEPA (1986b) Quality Criteria for Water 1986. Washington, DC, Environmental Protection Agency. EPA 440/5-86-001.
- USEPA (1996) Water Quality Criteria for Document for the Protection of Aquatic Life in Ambient Water 1995 updates. Washington, DC, Environmental Protection Agency. EPA 820-B-96-001.
- USEPA, (1999) *Integrated Approach to Assessing the Bioavailability and Toxicity of Metals in Surface Waters and Sediments*, a report to the EPA Science Advisory Board, Office of Water, Office of Research and Development, Washington, DC, USEPA-822-E-99-001.
- USEPA, (2000) "An SAB Report: Review of the Biotic Ligand Model of the Acute Toxicity of Metals," prepared by the Ecological Processes and Effects Committee of the Science Advisory Board, EPA-SAB-EPEC-00-0006.

APPENDIX I

Research Project Reports

Ecotoxicology of Mining-Related Metal Oxides in a High Gradient Mountain Stream

James Ranville
Department of Chemistry and Geochemistry
Colorado School of Mines
Golden, CO 80401

Philippe Ross
Department of Environmental Science and Engineering
Colorado School of Mines
Golden, CO 80401

and

Barbara Butler
Department of Environmental Science and Engineering
Colorado School of Mines
Golden, CO 80401

Introduction

This report presents an overview of results obtained in a study of metal transport in the Clear Creek watershed, located near Denver, Colorado. This watershed receives metal-rich inputs from a series of acid mine drainage (AMD) sources. A more detailed presentation of the methods, results, and conclusions can be found in a Colorado School of Mines (CSM) PhD dissertation (Butler, 2005). Several journal articles are currently in press as well.

Background

The Center for the Study of Metals in the Environment (CSME) was created in part to develop a Unit World Model (UWM) to describe the fate and transport of metals in aquatic systems. The term “Unit World” includes both the sediments and water column of a chosen environment. This model will ultimately be linked to the Biotic Ligand Model (a model used to predict toxicity to aquatic organisms) for regulatory purposes. The major components of the UWM for a stream are illustrated in Figure 1. This figure illustrates that fate and transport of metals in aquatic systems, particularly flowing systems, is very complex. Thus, multiple questions have arisen regarding the development of the UWM including: How complex must the model be, how much site-specific data must be available, and can it remain simple enough for ease of use?

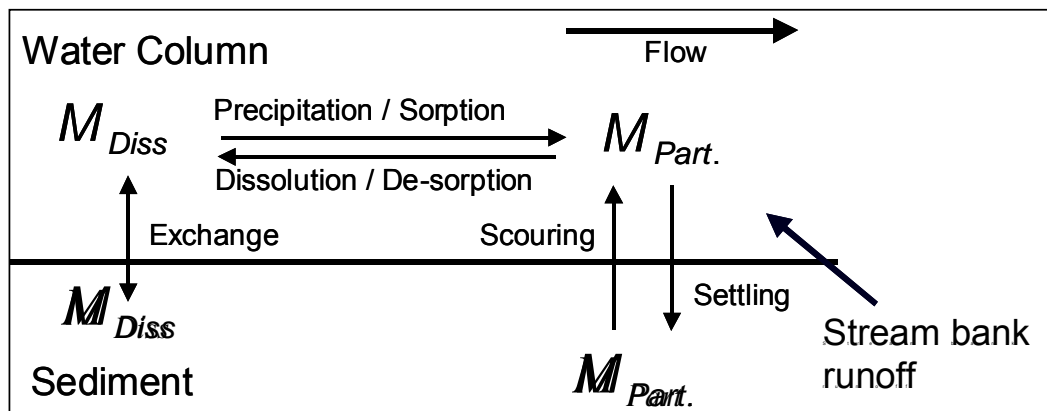


Figure 1. A conceptual model for the transport of metals in streams.

A major-controlling factor for metal transport and bioavailability is the partitioning of metals between the water and sediment phases. This process is particularly relevant for streams that receive metal loads from acid mine drainage (AMD). When AMD enters into a water body of higher pH, oxidation of iron and manganese, dilution of metals and acidity, *in-situ* precipitation of oxide minerals, co-precipitation, and sorption all can occur. Each of these processes contributes to the fate and transport of metals in the water body and must be quantifiable by the model. The process most likely controlling trace element speciation is sorption. With regard to AMD-impacted sites, where there may be multiple sorbent phases, the question arises: Is there a dominant sorbent phase that can be used to describe the fate and transport of metals, or must multiple phases be considered? Most visual observations of the North Fork of Clear Creek (NFCC), which is highly impacted by mining inputs, suggest the presence of abundant hydrous ferric oxide (HFO) precipitates and to a lesser extent hydrous

manganese oxides (HMO). These phases are commonly observed in NFCC (Figure 2) and are known to be important sorbent phases for trace metals.



Figure 2. Two major solvent phases observed in the North Fork of Clear Creek. a.) hydrous ferric oxyhydroxides (HFO), b.) manganese oxide (HFO) coated rocks.

Another question, that must be answered as part of the UWM development, is whether any *currently available* equilibrium based models can accurately describe *real processes* occurring in these AMD-impacted stream systems. Development of the UWM depends in part on the current ability to predict metal sorption in these systems. In this study we examined how well the predictions of metal distribution between dissolved and suspended particulates matched the observations made. We employed the Visual MINTEQ model which utilizes a surface complexation model (SCM) to model sorption processes. Our goal is to determine if the SCM model currently incorporated into this code is sufficient to accurately describe metal association with suspended sediments in the North Fork of Clear Creek over variable hydrologic conditions. The SCM was applied to both field data for suspended sediments and also laboratory investigations of pH-dependant metal sorption to field-collected and laboratory-prepared oxides.

Clear Creek Watershed

One of the challenges in developing a UWM for stream systems is the highly variable nature of hydrologic conditions in streams. Discharge in Clear Creek is dominated by snowmelt that increases streamflow, beginning in late May, and continuing through July (Figure 3). This highly variable flow results in changes in dissolved stream water chemistry and suspended sediment concentrations and particle composition. This provides a challenging test for the SCM predictions of metal speciation.

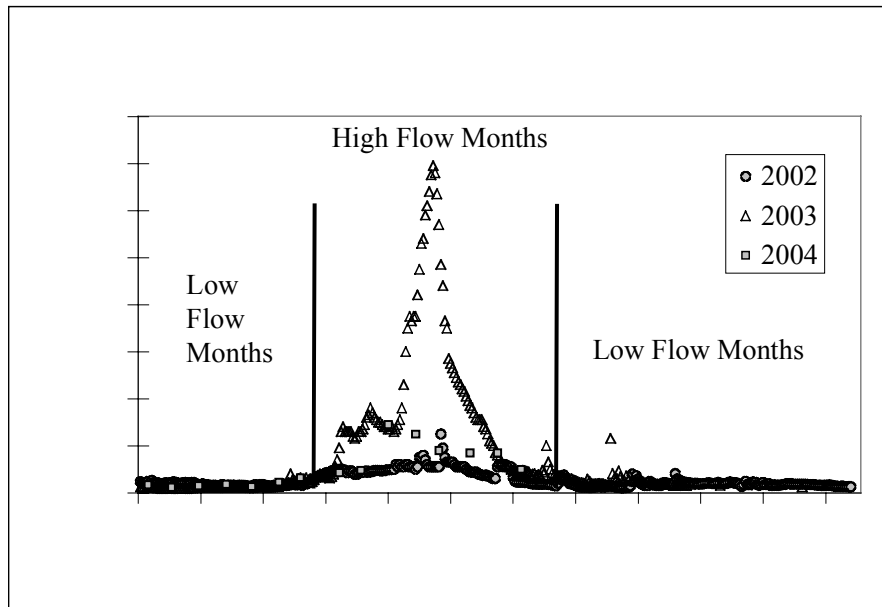


Figure 3. Hydrologic conditions at one sampling site on the North Fork of Clear Creek (NFCC-3) during the three years of the study.

A map of the stream and its confluence with the main stem is shown in Figure 4. Water quality sampling sites are numerically identified using the numbering system of the Colorado Department of Health and Environment (CDPHE), with point-source AMD inputs shown in bold-italic font.

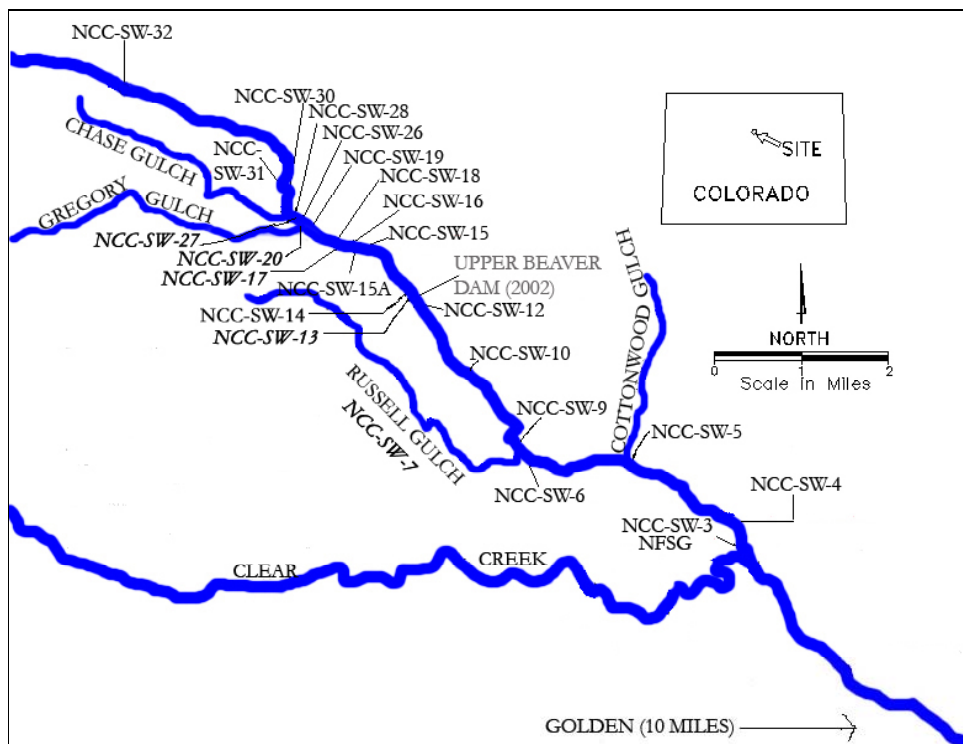


Figure 4. Clear Creek study area showing all sampling locations on North Fork Clear Creek. Two sites (CC-SW-4 & CC-SW-1) on the main stem of Clear Creek are not shown.

AMD enters into NFCC from several point sources and possibly multiple diffuse non-point sources along its reach. The point sources of highest metal input are Gregory Gulch (NCC-SW-27), Gregory Incline (NCC-SW-20), and National Tunnel (NCC-SW-17). Two other known point sources are located further downstream and are the East Williams Mine Adit (NCC-SW-13) and Russell Gulch (NCC-SW-7). Metal input from Gregory and Russell Gulches is through drainage from tailings throughout the gulches. Non-point sources include seepage from waste piles and tailings deposits along the reach of the stream.

Methods

Methods used in this study are given in detail in a CSM PhD dissertation (Butler, 2006) and several journal articles in preparation. A brief discussion of each method follows.

Water and Sediment Sampling

Water samples for total and dissolved (filtered through 0.45 micron) metals, pH, alkalinity, and TOC were collected over twenty-eight months from April 2002 through July 2004. TSS was collected on February 2003 through July 2004 samples. Samples were collected bi-weekly from May 2002 through October 2002, from March 2003 to mid-May 2003, and July 2003 through July 15, 2004; once per month in April 2002 and from November 2002 through February 2003; and weekly from mid-May 2003 through June 2003.

Water samples for inorganic analyses were grab samples collected in high-density polyethylene (HDPE) bottles. Bottles were rinsed three times with the stream water before sample collection. Water collected for total organic carbon (TOC) was collected in pre-burned (at 475 °C) borosilicate amber glass vials. Temperature and pH were measured in the stream. Alkalinity was measured in the bulk raw water sample in the laboratory, using the Hach™ titration method.

Pre-weighed filters that were used in the field for total suspended solids (TSS) were each placed into loosely capped 15-ml tubes and allowed to dry, typically for 48-hours. Once dry, each filter was reweighed on a Mettler™ MT5 balance and the mass of particles determined by subtraction of the original filter mass. A subset of the TSS samples was acid-digested in order to obtain a direct measurement of suspended sediment associated metals.

For the laboratory pH-dependant sorption experiments, black coatings and floc were obtained directly from the field. Coatings were scraped from multiple rocks in the region of NCC-SW-3 on August 26, 2003. Coatings were combined into an HDPE plastic bottle. Also twenty-five gallons of AMD water from the Gregory Incline site (NCC-SW-27) were collected on May 3, 2004 in five gallon plastic buckets. The water was taken back to the laboratory and aerated and the pH was adjusted (to ~ 4.5) to precipitate HFO.

Chemical Analysis

The water sample was prepared for Inductively Coupled Plasma Atomic Emission Spectroscopy (ICP-AES) analyses following a modified EPA Method 200.7 (U.S. EPA 1994a). Briefly, the water was acidified with a few drops of HCl to a pH < 2 and left to equilibrate for a minimum of 24-hours. Prior to analysis on the Perkin Elmer Optima 3000 ICP-AES, the samples were examined for remaining particulate material; if present, additional acid was added to aid in dissolution and the samples were sonicated immediately prior to analysis. ICP-AES

QA/QC included the use of known check standards run after every 20 samples, an internal standard (scandium), and a laboratory standard (a sample collected at National Tunnel, which was included in each instrumental run after every 15 to 20 samples). Samples for total organic carbon were run on a Shimadzu TOC 5000A analyzer following acidification to pH = 3 using HCl.

Solids were characterized by elemental analysis of acid digestions, TOC, FT-IR, and XRD. TOC was analyzed on a UIC CM5014 Coulometrics Solid Phase Total Carbon Analyzer. FT-IR analysis was performed using a Perkin Elmer Paragon 1000PC. XRD analyses on packed powder mounts were run by the Geology Department at the Colorado School of Mines. The analyses were conducted over sixty minutes at one degree per minute. Sequential extractions were performed using a method modified from Tessier et al. (1979).

Sorption Experiments

One-liter volumes of solid-slurry were prepared from field-collected and laboratory precipitated solids and stirred at room temperature for 48 hours to allow for equilibration with the 7 mM ionic strength DI water. Subsamples were adjusted with HCl or NaOH to obtain the desired pH range then were placed on rotary shakers and equilibrated for 48 hours. Following the 48 hours, samples were obtained and filtered from each of the vials and the final pH measured. Filtered samples were acidified to pH < 2 and analyzed for dissolved copper and zinc by ICP-AES. Sorption experiments comprised three differing solid concentrations for Floc, two for the HFO, two for the HMO, and one for the NFCC water (the actual TSS). Triplicate samples of slurries were digested (5 ml slurry plus 1 ml 1:1 HCl / HNO₃, then diluted with 5 ml DI) and the initial total concentrations of iron, manganese, copper, and zinc were determined by ICP-AES. The concentrations of copper and zinc remaining in solution were subtracted from the concentration in the digest plus the known concentration added (where applicable) and the percentage particulate metal was plotted versus the final pH measured for each sample.

Surface Complexation Modeling

Visual-MINTEQ, version 2.30 was downloaded from www.lwr.kth.se/english/OurSoftware/Vminteq (Gustafson, 2001, 2004). Data input to the model included: pH, temperature, alkalinity, and molar concentrations of total Mg²⁺, Na⁺, K⁺, Ca²⁺, Cu²⁺, Zn²⁺, SO₄²⁻, Al³⁺, Mn²⁺, Fe³⁺, and Ni²⁺. The term ‘component’ is used for aqueous elemental inputs to the model. Because the model is a speciation model, total concentrations of components are input and the model partitions the total into dissolved and particulate species and their concentrations. Additionally, the model does not allow the presence of any input solids if alkalinity is specified. This is because the model calculates the total dissolved carbonate concentration assuming no solids exist in the titrated sample for further acid-neutralization (Allison et al. 1991). Thus, a preliminary run (scenario ‘a’), using the measured alkalinity was conducted for each sample to determine the total carbonate concentration (as CO₃²⁻) for subsequent model runs. Reactions included in the sorption modeling, and values for specific parameters are shown in Table 1. The modeling scenarios are given in Table 2.

Table 1. Default equations and parameters included in modeling scenarios and their associated databases (Gustafson 2004; HydroGeoLogic, Inc. and Allison Geoscience Consultants, Inc. 1999) Temporal and Spatial NFCC Visual-MINTEQ modeling scenarios.

Database and Submodels	Species / Equations	LogK	
HFO Surface Complexation	$\equiv\text{Fe}^{\text{s}}\text{OH} + \text{Cu}^{2+} \leftrightarrow \equiv\text{Fe}^{\text{s}}\text{OCu}^+ + \text{H}^+$	2.89 (int)	
	$\equiv\text{Fe}^{\text{s}}\text{OH} + \text{Zn}^{2+} \leftrightarrow \equiv\text{Fe}^{\text{s}}\text{OZn}^+ + \text{H}^+$	0.99 (int)	
	$\equiv\text{Fe}^{\text{w}}\text{OH} + \text{Zn}^{2+} \leftrightarrow \equiv\text{Fe}^{\text{w}}\text{OZn}^+ + \text{H}^+$	-1.99 (int)	
HMO Surface Complexation	$\equiv\text{Mn}^{\text{s}}\text{OH} + \text{Cu}^{2+} \leftrightarrow \equiv\text{Mn}^{\text{s}}\text{OCu}^+ + \text{H}^+$	0.85	
	$\equiv\text{Mn}^{\text{w}}\text{OH} + \text{Cu}^{2+} \leftrightarrow \equiv\text{Mn}^{\text{w}}\text{OCu}^+ + \text{H}^+$	0.86 (see note)	
	$\equiv\text{Mn}^{\text{s}}\text{OH} + \text{CuOH}^+ \leftrightarrow \equiv\text{Mn}^{\text{s}}\text{OCuOH}$	-2.8	
	$\equiv\text{Mn}^{\text{w}}\text{OH} + \text{CuOH}^+ \leftrightarrow \equiv\text{Mn}^{\text{w}}\text{OCuOH}$	-5.7	
	$\equiv\text{Mn}^{\text{s}}\text{OH} + \text{Zn}^{2+} \leftrightarrow \equiv\text{Mn}^{\text{s}}\text{OZn}^+ + \text{H}^+$	-0.01	
	$\equiv\text{Mn}^{\text{s}}\text{OH} + \text{ZnOH}^+ \leftrightarrow \equiv\text{Mn}^{\text{s}}\text{OZnOH}$	-4.4	
Gaussian submodel	$\text{H} + \text{L}_i \leftrightarrow \text{HL}_i$ $\text{Cu}^{2+} + \text{L}_i \leftrightarrow \text{Cu}^+\text{L}_i$ $\text{Zn}^{2+} + \text{L}_i \leftrightarrow \text{Zn}^+\text{L}_i$	Site Densities are solved for iteratively with K's	Solved iteratively (see Chapter 1, Section 1.1.7.2)
NICA-Donnan submodel	/FA-Cu ⁺	Site Densities (mol/g):	0.26
	/FA ₂ -Cu	Weak = 0.00588	8.26
	/FA-Zn ⁺	Strong = 0.00186	-3.84
	/FA ₂ -Zn		-0.73
	/FA-Fe ²⁺		6
	/FA ₂ -Fe ⁺		36
	/FA-Fe ⁺		-1.02
/FA ₂ -Fe		-1.1	
Stockholm Humic submodel	/FA-Cu ⁺	Site Densities (mol/g):	-0.6
	/FA ₂ -Cu	Weak = 0.00702	-5.8
	/FA ₂ -CuOH	Strong = 0.002106	-13.3
	/FA-Zn ⁺		-1.35
	/FA ₂ -Zn		-9
	/FA ₂ Fe ⁺		-0.7
/FA ₂ FeOH		-4.7	

≡ represents a surface; superscript 's' = strong sites; superscript 'w' = weak sites; 'int' = intrinsic constants for ionic strength = 0; L_i = organic ligand; /FA = fulvic acid. Note: In Tonkin et al. (2004) this value is -0.96

Table 2. Temporal and Spatial NFCC Visual-MINTEQ modeling scenarios.

Scenario	Description
a	Measured alkalinity used to set carbonate concentration for remaining scenarios
b	HFO as sole sorbent
c	HFO and HMO sorbents
d	HFO as sole sorbent plus Gaussian model for DOC
e	HFO and HMO sorbents plus Gaussian model for DOC
f	HFO as sole sorbent plus NICA-Donnan model for DOC
g	HFO and HMO sorbents plus NICA-model for DOC
h	HFO as sole sorbent plus Stockholm-Humic for DOC
i	HFO and HMO sorbents plus Stockholm-Humic model for DOC

Results and Discussion

Component 1: Evaluation of methods for the determination of metal distribution between dissolved and particulate phases

Often, published measurements of water quality data include only total and dissolved metal concentrations, with particulate metal concentrations computed as the difference between the two. The accuracy of this assumption for mining influenced waters (MIW) has been addressed for the Clear Creek system by comparing particulate metal data obtained directly through digestion of particles retained on filters with data obtained through subtraction of total and dissolved metal concentrations. Particulate metal content by the difference method was obtained by subtracting the concentration of metal present in the filtered (0.45 μm) water sample from the concentration present in the total (unfiltered) water sample. Particulate metal content from filter digests (TSS method) was determined by calculation of the metal content in the diluted digest sample and conversion back to the concentration present in the known volume of water filtered.

A total of 51 samples were collected at three sites over the study period, including replicates for QA/QC. The concentrations of particulate Al, Cu, Fe, Mn and Zn, obtained by each of the methods at three sites, are shown in Figure 5. For comparison between the methods we arbitrarily chose to use a factor of plus or minus 2 as a means of judging the degree of agreement. The majority of the particulate metal data compared well for the three sites. At the NCC-SW-3 site, there were only excursions from the range for manganese (3 values) and zinc (1 value). Excursions from the range at CC-SW-4 (located 5 km upstream of the confluence of NFCC on the main stem of Clear Creek) included 2 Al values, 1 Cu value, 4 Fe and Mn values, and 3 Zn values. CC-SW-1 (located in Golden) had 1 Al value, 1 Fe value, 2 Mn values, and 4 Zn values that exceeded the range. The results suggest that either method can be used to determine particulate metal reliably.

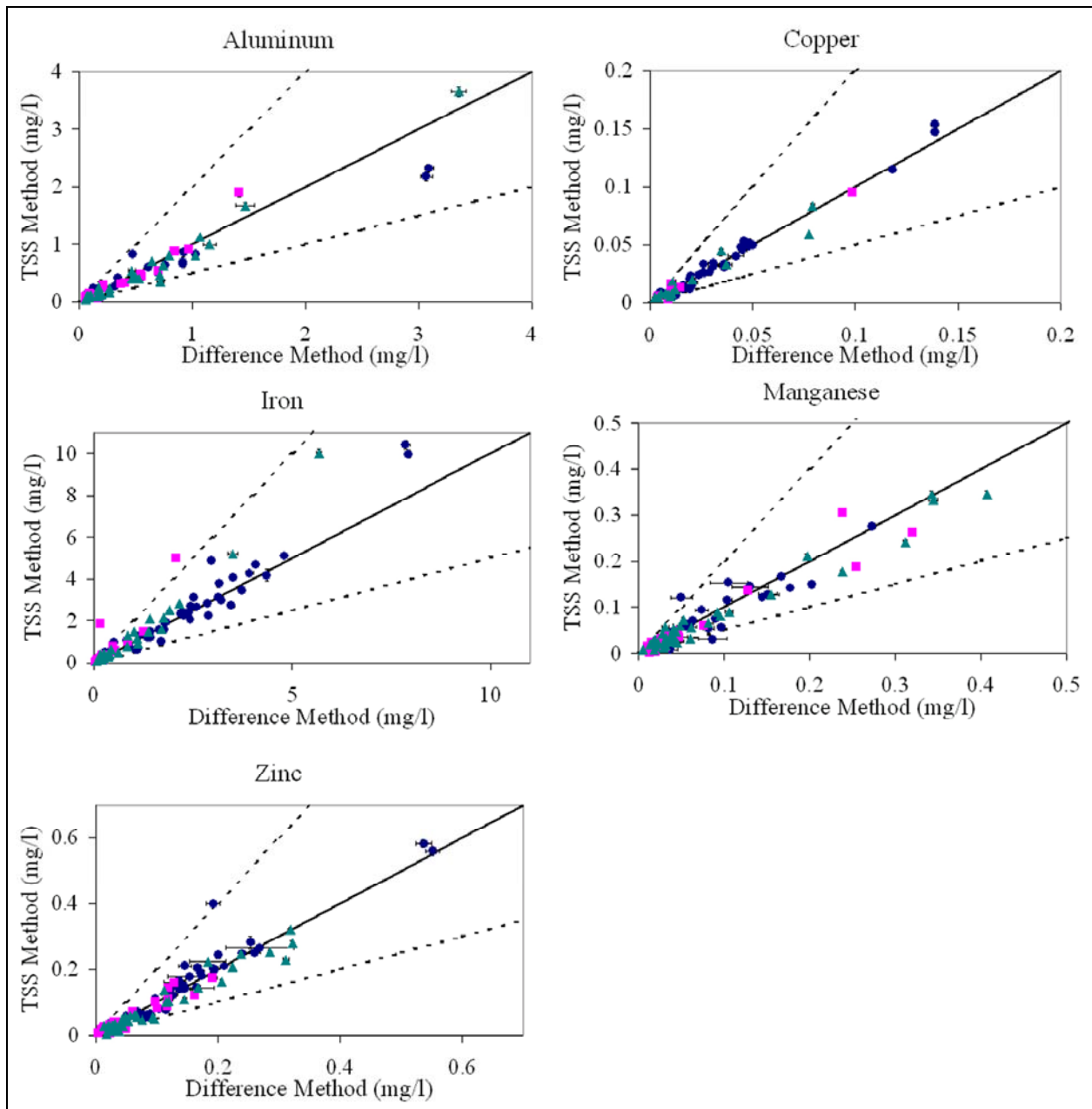


Figure 5. Comparison of two methods for the determination of sediment-associated metals(mg/L). The total suspended sediment method (TSS) uses ICP-AES analysis of acid digestions of sediments retained on filters. The difference method uses acidified samples of unfiltered and filtered water samples.

Component 2: Temporal variations in the geochemistry of Clear Creek

Water samples were collected over two and a half years at three sites. Data for the North Fork Clear Creek site (NFCC-SW-3) are presented in Figures 6 and 7. Seasonal trends related to discharge are obvious for sulfate and the metals predominantly in the dissolved fraction (Mn and Zn), with dilution occurring in high flow and elevated concentrations during lower flows, when the source of stream water is more a result of AMD inputs. Seasonal trends are more difficult to discern in the metals predominantly in the particulate fraction (Fe and Cu), but there is some

evidence of dilution during high flow and gradual increase over base-flow months, when stream water is more affected by AMD. Additionally, particulate Fe and Cu show effects from scouring of bed sediments during increased flow. The small fluctuations observed with all metals during base-flow is likely due to settling and resuspension of both rock coatings and loose flocculated sediments. The UWM may be able to accurately represent metals predominantly found in the dissolved fraction (in this research, Mn, and to a lesser extent, Zn), based on hydrologically driven changes. But, it may be more difficult to relate hydrologic conditions with metals predominantly in the particulate fraction, such as Cu and Fe.

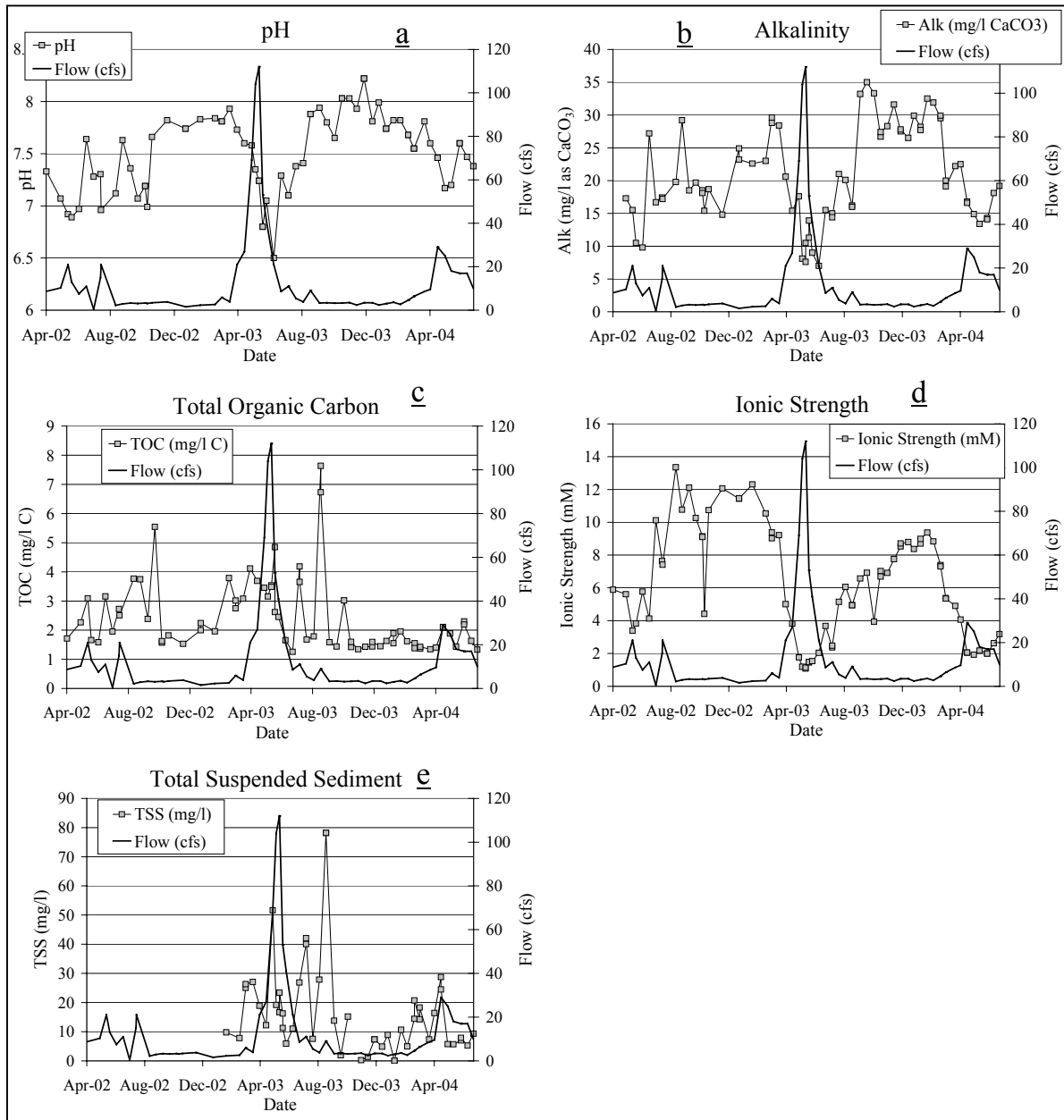


Figure 6. Major water quality parameters and discharge (CFS) in NFCC for 2002-2004 at site NCC-SW-3.

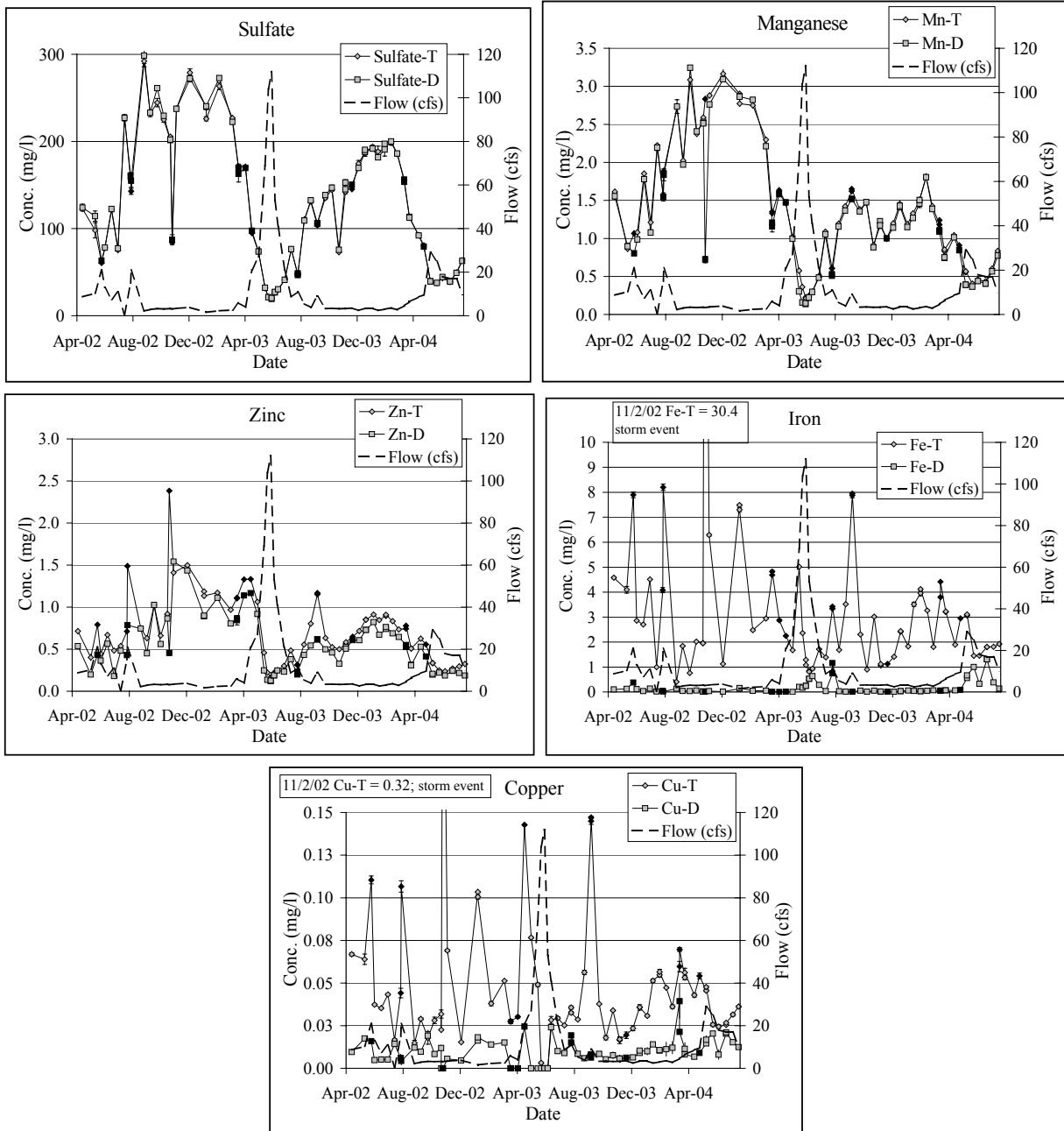


Figure 7. Major species associated with the mine drainage impacts on NFCC for 2002-2004 at site NCC-SW-3.

Strong relationships were observed between particulate Cu and particulate Fe (correlation coefficient of 0.92), particulate Zn and particulate Fe (correlation coefficient of 0.94), dissolved Mn and Zn (correlation coefficient of 0.74), and particulate Zn and particulate Mn (correlation coefficient of 0.86). Seasonal effects are also evident for pH, alkalinity, total organic carbon (TOC), ionic strength, and total suspended solids (TSS). Dilution is not the only process occurring during spring-runoff. Increased input of AMD, which occurs as the abandoned mines are flushed with snowmelt, is somewhat offset by the dilution from uncontaminated snowmelt from the surrounding watershed.

The water chemistry data were used as inputs for Visual M in order to perform calculations of metal partitioning between dissolved and particulate phases. The SCM model parameters are given in Table 1 and modeling scenarios in Table 2. Comparisons between the HFO only and the HFO plus HMO scenarios are shown in Figure 8 for copper and zinc. In each figure, the solid black line represents a 1:1 relationship and the solid gray lines represent plus or minus a factor of two. For copper, the majority of modeled percentage particulate values are within a factor of ± 2 of the observed values, but there is a bias toward over-estimation of model values with both scenarios. This common over-estimate implies that there is a component in the stream that reduces the amount of particulate copper, which is not represented by these model scenarios. Copper is known to form strong complexes with DOC (McLean and Bledsoe 1992), which would reduce the amount of particulate copper. The influence of organic carbon on percentage particulate copper is shown in Figure 9. Inclusion of DOC generally reduced the over-estimation (bias) of percentage particulate copper with solely surface complexation modeling, with the exception of scenarios 'd' and 'e' (Gaussian DOC submodel), which had little to no effect. Data obtained from modeling with the Stockholm-Humic submodel seemed to give the best overall comparison between modeled and observed percentage particulate copper.

The fact that the modeled percentage particulate copper was greatly reduced by the addition of DOC and the comparison between modeled and observed results was improved, seems to indicate that DOC in NFCC does contribute to the control of copper fate and transport and must be considered. The DOC submodels are competitive and thus, complexation of DOC with other components results in an increase in copper available for surface complexation with HFO and HMO. Although scenarios included dissolved iron, which did result in decreased copper complexation with DOC and increased particulate copper, it seems there may be another component in the stream that is complexing with DOC to allow for more particulate copper than predicted by these model scenarios.

Modeled zinc data were less biased toward a maximum than were the copper data for both scenarios 'b' and 'c' (Figure 8). Scenario 'b' resulted in thirty-one data that were under-estimated and below the factor of two range. Inclusion of HMO greatly improved the comparison between modeled and observed percentage particulate zinc, with only twelve of the initial thirty-two data remaining outside of the range of a factor of two. Five of the initial thirty-two data were not modeled with scenario 'c', as there was no particulate manganese present on those dates. The observed under-estimation of percentage particulate zinc for scenario 'c' seems to imply that there is another surface that zinc is sorbing to in the stream, perhaps aluminum oxide, silica, or algae that are known to be present. Slight over-predictions from the 1:1 line may indicate that for a smaller subset of the data, something is keeping more of the zinc in solution than is predicted by simple surface complexation. Although zinc does not form strong dissolved organic complexes (McLean and Bledsoe 1992), the influence of DOC was examined by modeling with each of the three DOC submodels in Visual-MINTEQ. Modeling scenarios for zinc with DOC (Figure 9) indicated DOC had very little effect on the percentage particulate zinc. It does not appear that there is any significant influence of DOC on zinc fate and transport in the stream.

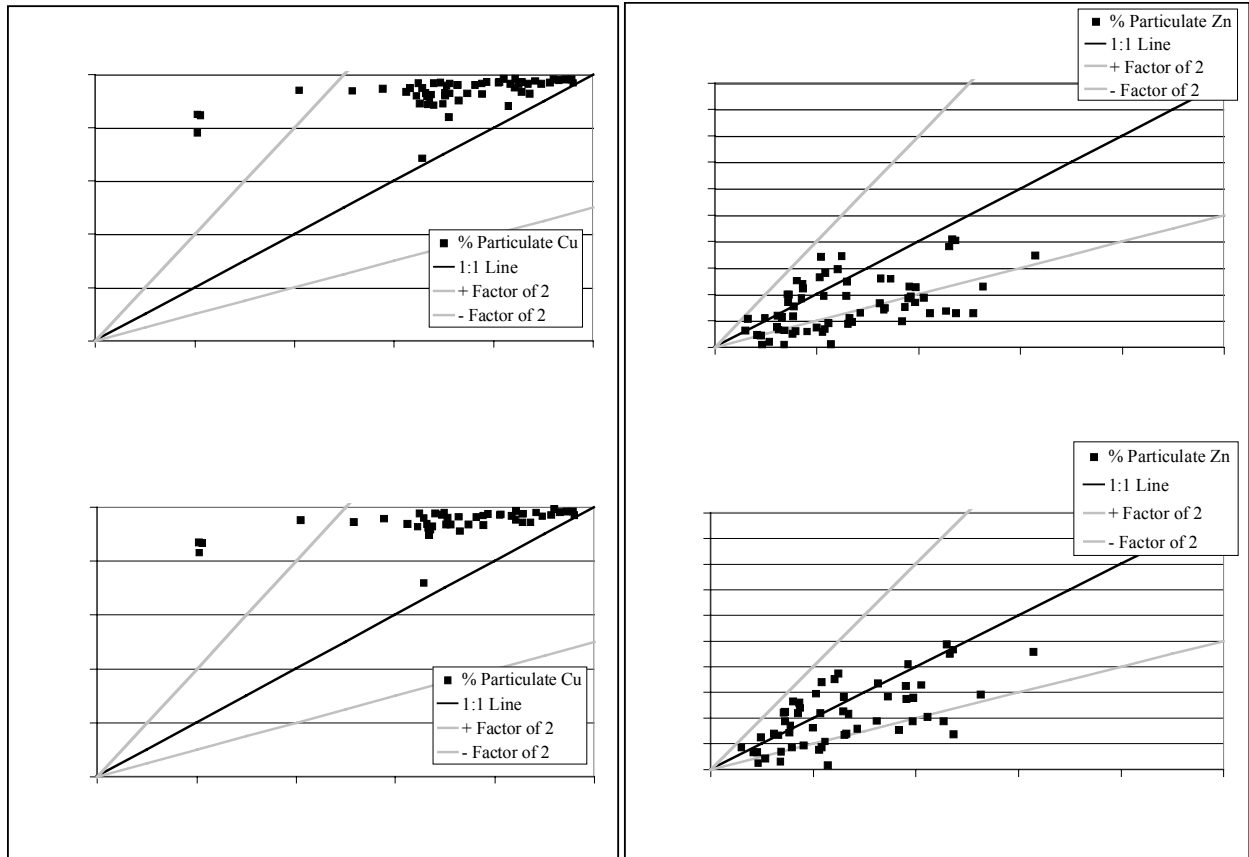


Figure 8. Comparison of the amount of particulate a.) Cu and b.) Zn computed by Visual MINTEQ modeling, versus the measured amount for NFCC. The predictions use one or more oxide phases but ignore dissolved organic carbon (DOC).

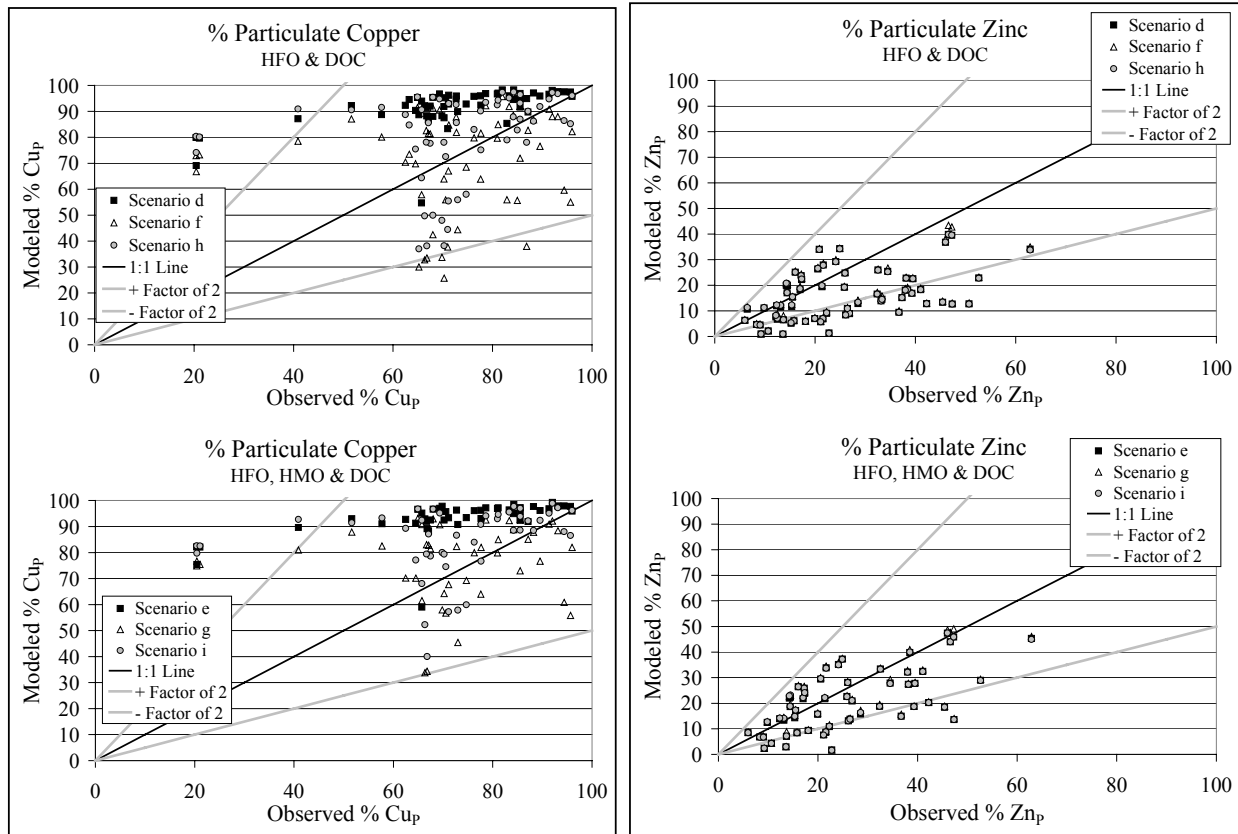


Figure 9. Results of Visual MINTEQ modeling which included DOC in the calculations.

Component 3: Spatial Trends in Stream Geochemistry

Twelve sites on NFCC (NCC-SW-28, 26, 19, 18, 16, 15, 14, 12, 9, 6, 5, and 3), the city of Blackhawk wastewater treatment plant (WWTP; NCC-SW-15A), and four AMD inputs (NCC-SW-27, 20, 17, and 7) were sampled on three dates. Results of observed and Visual Minteq modeled particulate Cu and Zn for the September 14th, 2004, samples are shown in Figures 10 and 11. Input sources are also plotted on the graphs.

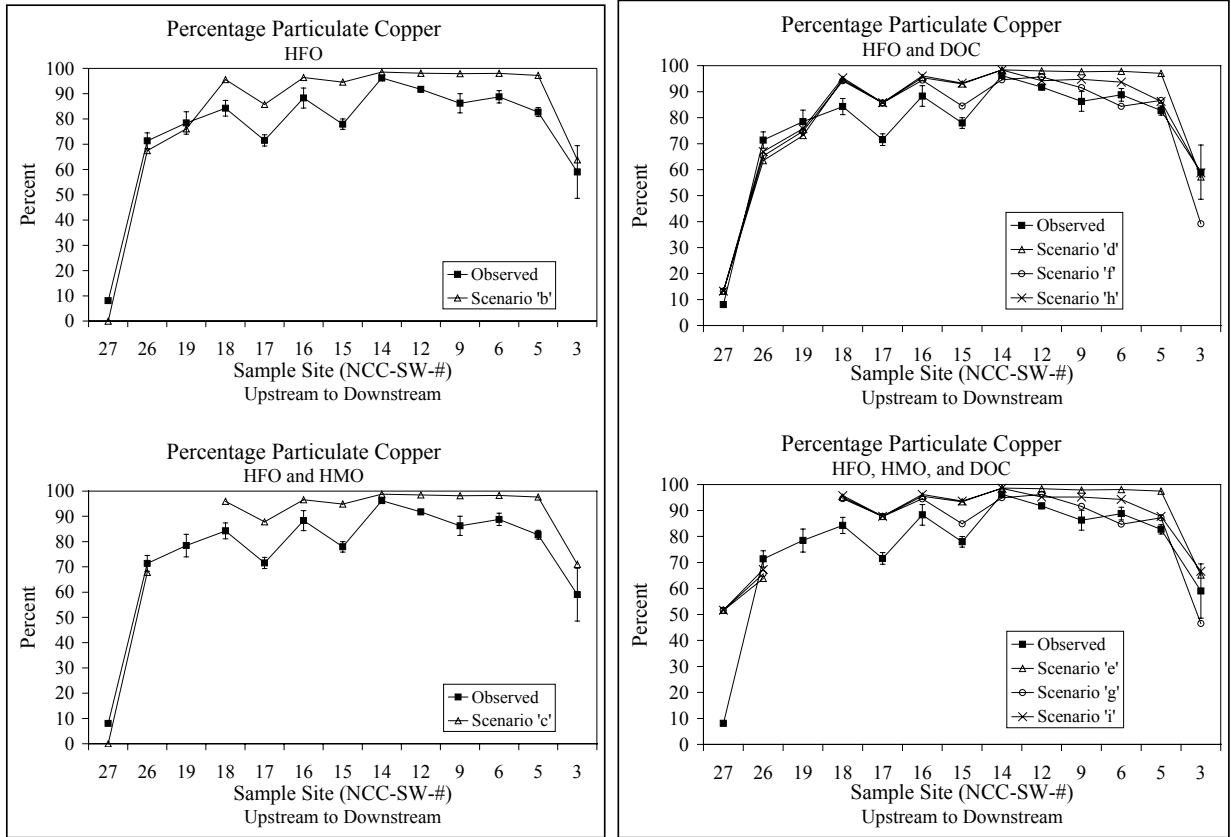


Figure 10. Comparison of SCM modeling and observed percentage particulate Cu for samples collected on September 14th, 2004 along the NFCC.

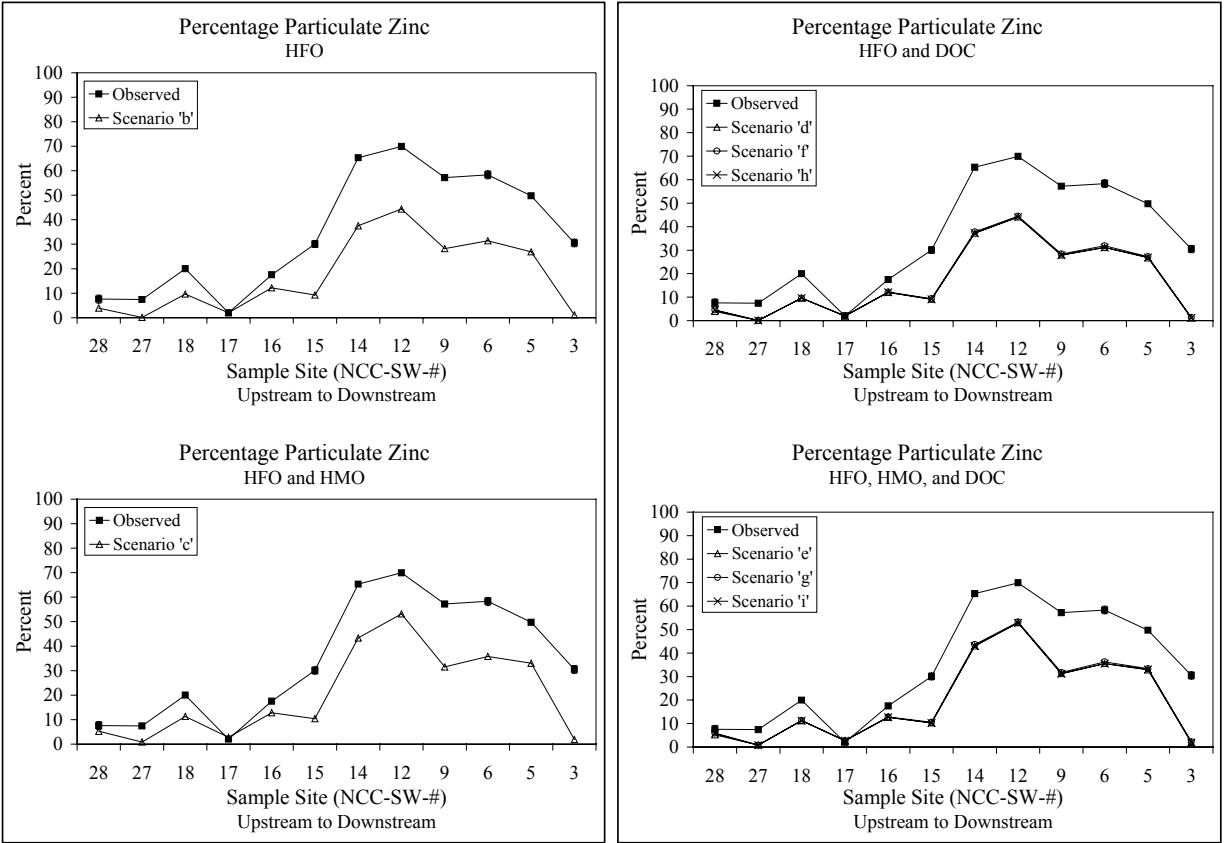


Figure 11. Comparison of SCM modeling and observed percentage particulate Zn for samples collected on September 14th, 2004 along the NFCC.

Percentage particulate copper was over-estimated by scenario ‘b’ for the majority of sites downstream of the major inputs, but was under-predicted at NCC-SW-27 (an AMD input), 26, and 19. Although the model over-estimated the percentage particulate copper, scenario ‘b’ very closely represents the observed data. Addition of HMO slightly increased the deviation from the observed results.

Sites including and upstream from NCC-SW-16 (Figure 11) show a very close comparison between model and observed percentages of particulate zinc. In general, however, scenarios ‘b’ and ‘c’ each under-estimate the percentage particulate zinc, relative to the observed. Scenario ‘c’ gave an exact match for NCC-SW-17 and NCC-SW-28 varied only slightly (2%). Modeling results from sites downstream from NCC-SW-16 show more deviation from the observed percentage particulate zinc.

The influence of DOC is shown in Figures 10 and 11. Figure 10 shows observed and modeled percentage particulate copper over stream distance for scenarios ‘d’, ‘f’, and ‘h’ in the upper graph and observed and modeled percentage particulate copper over stream distance for scenarios ‘e’, ‘g’, and ‘i’ in the lower graph. Figure 11 shows the same for zinc. There are both increases and decreases in modeled percentage particulate copper in the presence of DOC, relative to the observed percentage particulate copper, but all scenarios show good comparison and improvement over scenarios without DOC.

There is no improvement from simple surface complexation versus the models including DOC for percentage particulate zinc. This is expected and similar to the other sampling dates.

Scenario ‘f’ yielded the best comparison between modeled and observed percentage particulate copper, indicating that DOC is likely contributing to the fate and transport of copper in the stream. The best scenarios for zinc were ‘c’ and ‘g’, although there was only minimal improvement of the model including DOC (scenario ‘g’). Since the purpose was to determine the simplest model that most closely represented actual field results, it appears that the addition of HMO along with HFO is the simplest model for representing the spatial zinc data on this date.

Component 4: Laboratory sorption experiments using field-derived materials

It was expected that the most pure solids would more closely fit the model than those containing less of the HMO and HFO. For pH ranges typical in NFCC (range of 5-9), the model using surface complexation onto HFO and HMO fit the experimental sorption onto the HMO rock coatings very well (all had WSOS/DF < 20), as shown in Figure 12. At pH less than 5, the copper and zinc data obtained with the lower total site concentration were not fit as well by the model.

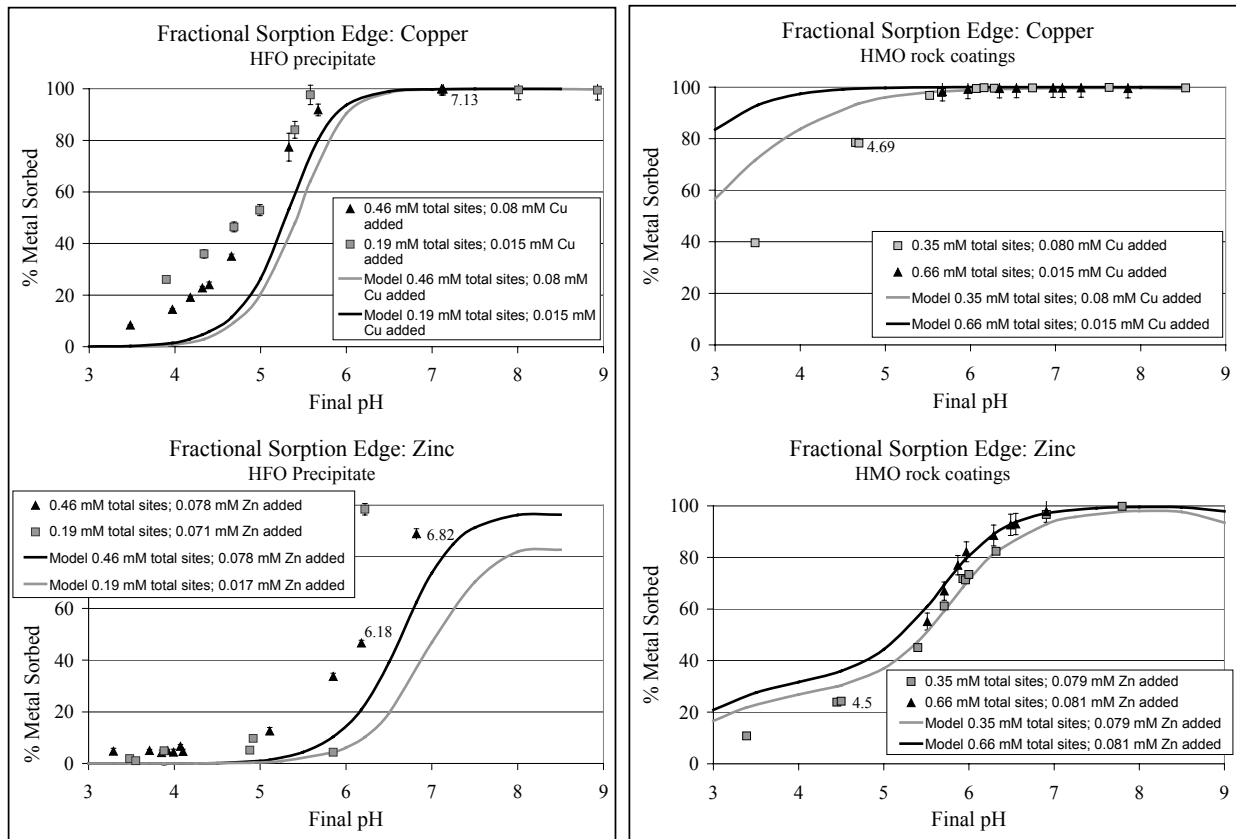


Figure 12. Fractional sorption of Cu and Zn on HFO prepared in the laboratory from water collected from an AMD input and HMO removed from stream bed rocks.

Modeled and observed sorption onto the Floc material (Figure 13) compared the best for the highest total site concentration for both copper and zinc (WSOS/DF = 4 and 52, for copper and zinc, respectively). At pH values typical of NFCC (5 to 9), all experimental and model results for copper onto the Floc material matched well (WSOS/DF ≤ 21). The deviation was more apparent for the zinc than for the copper in all experiments, and the fits were poorer. This

is likely because there are additional solid phases present in the Floc in addition to the HFO and HMO used in modeling, as seen in the FT-IR, XRD, and digestion data, that are affecting actual zinc sorption. Previous chapters have suggested that copper is more strongly associated with the iron oxyhydroxides in NFCC than the zinc. The fact that the model matches extremely well for the copper fractional sorption edges conducted on the Floc material seems to imply that the iron phase present in the stream is predominantly ferrihydrite.

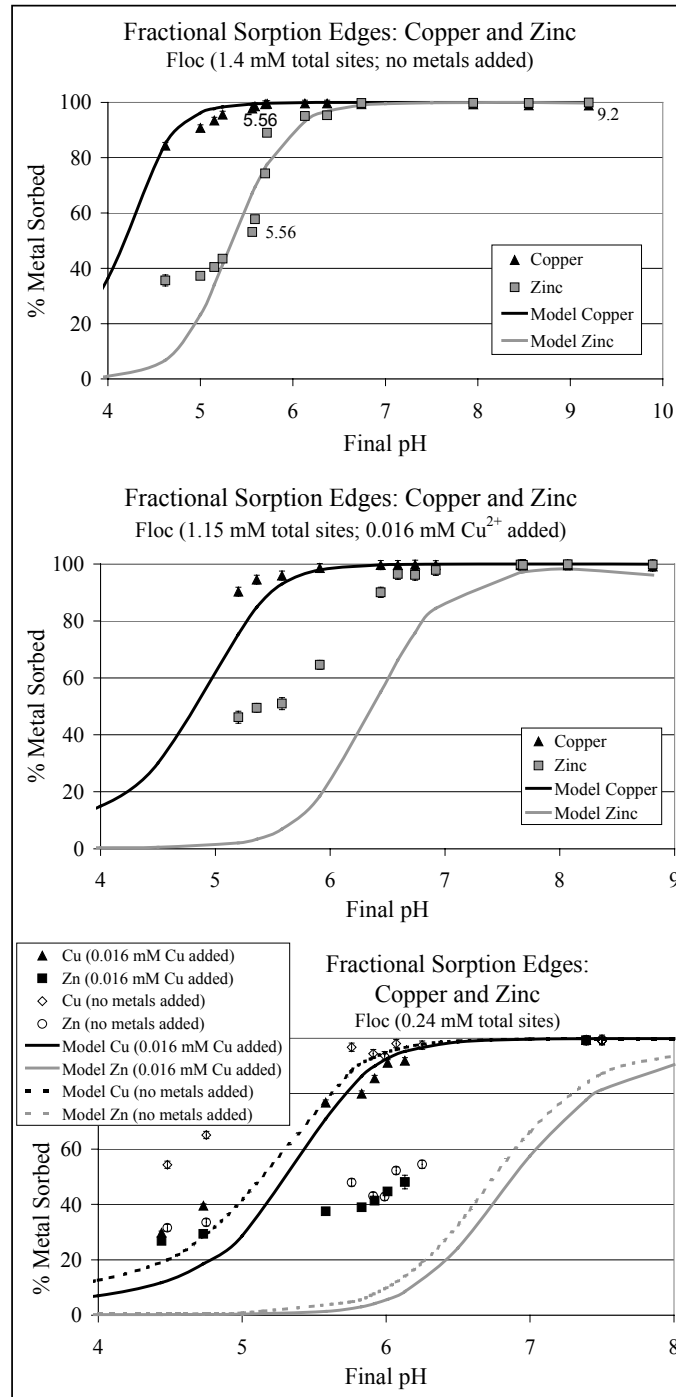


Figure 13. Fractional sorption of Cu and Zn on loose floc collected from the streambed.

The comparison between the HFO AMD-precipitate sorption experiments and the modeled results deviated more than was expected. Although, the experimental and modeled copper sorption with the higher total site concentration were matched well by the model between pH 5 and 9 (WSOS/DF = 15). The surface complexation modeling of the precipitate was based on the assumption that the iron present was ferrihydrite ($\text{Fe}_2\text{O}_3 \cdot \text{H}_2\text{O}$). The laboratory oxidation and precipitation of the HFO material required almost a month for complete conversion of the dissolved Fe^{2+} to the ferric oxyhydroxide mixture. Ferrihydrite forms through rapid oxidation of Fe^{2+} , while goethite is formed from slower oxidation (Cornell and Schwertmann 1996). Thus, the solid ferric oxyhydroxide mixture formed in the laboratory may not be representative of the ferric oxyhydroxide present in the stream (Fe^{2+} is seen to be removed rapidly in the stream system, see Chapter3). Thus, the deviation between observed and modeled results may be due to the mixture of oxyhydroxides formed having sorption characteristics differing from pure ferrihydrite.

Overall, it appears that default parameters based on laboratory-created iron and manganese oxyhydroxides can represent accurately copper sorption onto field-collected oxyhydroxide phases and zinc sorption onto field-collected HMO.

Component 5: Sequential extraction Analysis of Field-derived materials from Clear Creek

Preliminary sequential extraction studies of bed (BS) and suspended sediments (SS) in several size fractions (< 2mm to > 63 μm ; < 63 μm to > 2 μm ; and < 2 μm to > 0.3 μm , for April and May only) at two sites (SW3 and SW4b) and under different hydrologic conditions indicate there are differences between the fractions of metal in each extract-type. As an example, differences in Cu distribution in January and April of 2006 are shown in Figures 14 and 15. In January, Cu is predominantly in the Fe/Mn extracted fraction in all samples. SW3 contains more exchangeable Cu than does SW4b within size groups. The April date shows increases in the organic-extractable Cu, at the expense of the Fe/Mn and exchangeable fractions.

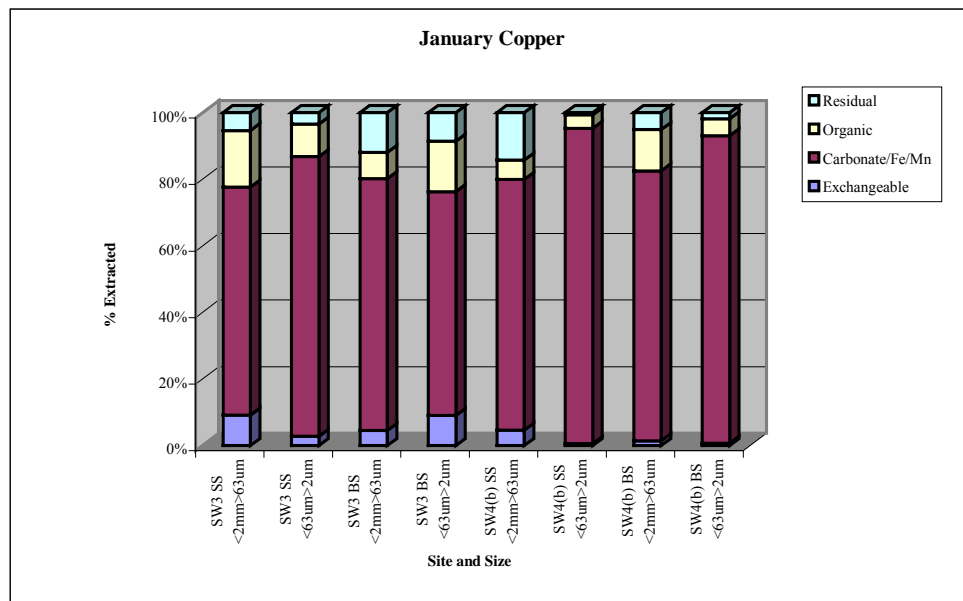


Figure 14. Sequential extraction results for Cu in size fractions of suspended sediment (SS) and bed sediment (BS) collected in January 2006 at two sites along NFCC.

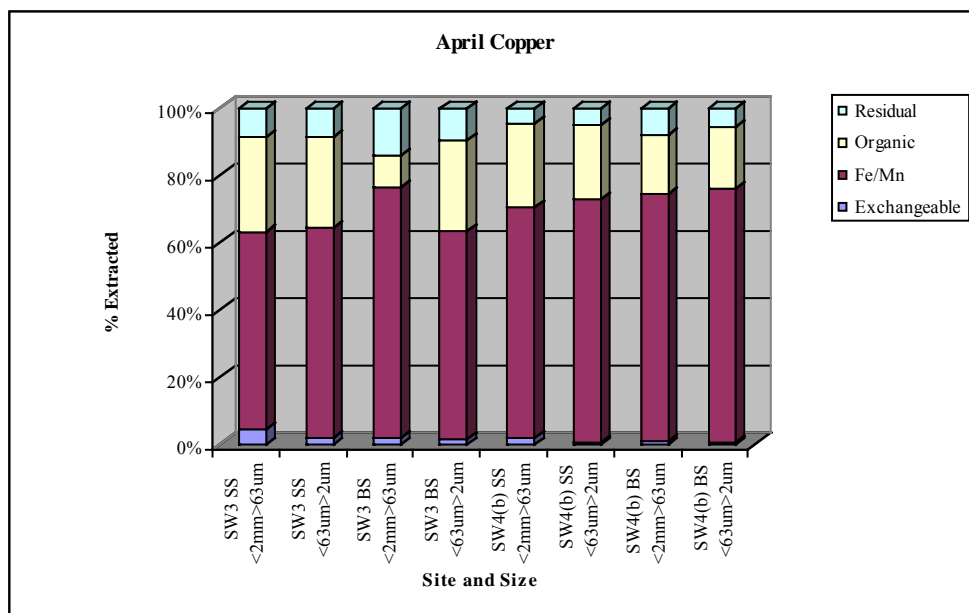


Figure 15. Sequential extraction results for Cu in size fractions of suspended sediment (SS) and bed sediment (BS) collected in April 2006 at two sites along NFCC.

Other results not shown are that Fe is also predominantly in the Fe/Mn extractable phase, but there is a significant amount in the residual phase, especially in the larger size fraction of bed sediment at SW3. The April Fe results show a significant difference with much larger amounts in the residual phase, as well as some in the organic phase. Mn is predominantly associated with the Fe/Mn fraction in both January and April, with the exception that the >63 μ m bed sediment has a large amount associated with the exchangeable fraction. More Zn is associated with the Fe/Mn fraction in April than in January, with decreases in each of the other three fractions.

There is a greater mass of total-extractable Mn and Zn (data not shown) within each of the sampling dates associated with each respective size group at NCC-SW3 compared to SW4b, located about 3 miles upstream of NCC-SW-3. This seems to indicate a removal of these metals from the dissolved phase into the particulate phase in the suspended sediments reaching NCC-SW3, as well as settling occurring further downstream, closer and/or at NCC-SW3. The opposite is true for the Cu and Fe, with more total mass extracted from the upstream site (NCC-SW4) in each of the respective size groups. This suggests that there is a more rapid loss of Fe and Cu from the water column occurring within a shorter distance than for the Mn and Zn. Previous results from the water column studies of particulate and dissolved Cu, Fe, Mn, and Zn indicated Cu is predominantly associated with HFO and Zn is associated with HMO. The sequential extraction observations also support this conclusion.

Overall Summary

The fate and transport of metals in the natural environment are complex issues. Although this study examined only one stream system (North Fork Clear Creek), some generalities about dissolved and particulate metal behavior can be drawn from the extensive database developed from this research. The behavior of manganese, iron, copper, and zinc differ in NFCC. This is

in part due to inherent differences in the chemical properties of the elements and in part due to the characteristics of the NFCC system. The conclusions drawn from this research are likely to be valid for other stream systems receiving metal inputs from mining-related wastes.

Both temporally and spatially, manganese and zinc are predominantly present in the dissolved phase. Strong storm events increase the fraction of these metals transported as particulates, presumably due to scouring of the streambed. Iron and copper are predominantly present in the particulate phase, both temporally and spatially. Strong correlations exist between particulate copper and particulate iron and between particulate zinc and particulate iron and manganese. Both HFO and HMO are known to be strong sorbents for metals. Spatially, it is believed that copper is predominantly controlled by coprecipitation and sorption onto HFO. Precipitation of HFO rapidly occurs in the stream reach close to the AMD inputs. Coprecipitation of copper with the HFO is believed to predominate in the upper reaches of NFCC, where the HFO is actively and rapidly precipitating, while sorption predominates at locations further downstream, when HFO precipitation is complete. Particulate zinc is thought to be controlled by both sorption onto HFO and coprecipitation and/or sorption onto HMO. Partitioning of zinc to the particulate fraction occurs further downstream than does the copper. This indicates that zinc is not coprecipitated with the HFO and that the dominant process for zinc associated with the HFO is via sorption. Zinc association with HMO appears to be a combination of coprecipitation and sorption processes. It is not certain how rapidly the HMO coating is formed on rock surfaces; thus, it is difficult to distinguish between the two processes occurring with respect to zinc.

Hydrologic controls on the fate and transport of metals in NFCC, both temporally and spatially, appear to be significant, with a more obvious relationship observed for metals predominantly in the dissolved form (manganese and zinc). Several strong storm events resulted in statistically significant changes in water-column metal concentrations, relative to non-storm events. In general, dissolved metals are decreased and particulate metals are increased, due to dilution and scouring of the streambed, respectively. During these events, the presence of particulate metals typically not observed in NFCC (titanium, vanadium, and lead) is a useful indicator of particulate input from the watershed. Settling of particulate material to the streambed occurs more readily under lower flow conditions, while higher flows are observed to carry suspended particulate material further downstream. In the NFCC system, and most likely in other mountain streams impacted by AMD, the main water source during base-flow is from AMD-inputs, while the source of water during spring-runoff is predominantly snowmelt.

In the absence of directly obtained particulate metal data, subtraction of measured dissolved and measured total metal is sufficient to quantify suspended sediment transport of metals. There are limitations to both directly and indirectly determined suspended sediment associated metals, but overall, the results are similar for the two methods examined. The subtraction method was utilized for the particulate metals discussed in this research.

Temporal and spatial percentage particulate copper was consistently over-estimated by Visual-MINTEQ modeling, when using surface complexation solely onto HFO, while percentage particulate zinc was both under- and over-estimated. Addition of a second sorbent (HMO) significantly improved the comparison for measured versus model-predicted percentage particulate zinc. Inclusion of dissolved organic carbon (DOC) significantly improved this comparison for percentage particulate copper. Under low-flow conditions, the differences between model predictions and observed percentage particulate copper and zinc were within a factor of two. Under conditions of higher flow, deviations from the modeled and observed

percentage particulate metals increased, more so for the zinc than for the copper. The observed percentage particulate zinc, versus the modeled percentage particulate, appears to have a minor contribution from another sorbent in addition to the HFO and HMO. This additional sorbent may be algae, aluminosilicates, and/or aluminum oxyhydroxides. Each of these is known to strongly sorb metals. Algae have an influence on the oxidation and precipitation of HMO. Zinc is substantially associated with the HMO, and thus, it seems plausible that it is also associated with the algae.

Laboratory sorption experiments onto each of the major types of field solids were conducted to determine if Visual-MINTEQ would more accurately represent sorption of copper and zinc onto these solids, in the absence of the confounding factors present in the field study, such as alkalinity and DOC. Based on elemental, XRD, and FT-IR characterization, it appears the laboratory-created HFO precipitate was a mix of iron oxyhydroxides, dominated by poorly crystalline goethite. The HMO scraped from the rocks was predominantly todokorite and birnessite. The Floc material was a combination of minerals, with a predominance of HFO as ferrihydrite. Models were run with both the HFO (ferrihydrite) and HMO surface complexation submodels. Comparisons of modeled copper and zinc pH sorption edges onto the HMO and the Floc material most closely represented the observed laboratory isotherms. The comparison was poorer with the HFO precipitate created in the laboratory. This might be because the HFO formed is not the same as the HFO present in the Floc material. Rapid precipitation of HFO favors the ferrihydrite or schwertmannite form, while slower precipitation results in goethite (Bingham et al., 1996); rapid formation occurs in the field, but the formation of HFO was slower in the laboratory, requiring about one month. The somewhat poorer comparison between the observed and modeled percentage metal sorbed for the TSS in the NFCC water is most likely due to the presence of other sorbents, such as aluminosilicates, silica, and/or aluminum oxyhydroxides.

Overall, it appears that default parameters based on laboratory-created iron and manganese oxyhydroxides can represent accurately copper sorption onto field-collected oxyhydroxide phases and zinc sorption onto field-collected HMO. In general, Visual-MINTEQ temporal and spatial modeling of both percentage particulate copper and zinc and sorption isotherms did match observed field and laboratory data, within a factor of two (or better in most cases). The question arises then, of how close is close enough? In other words, is it sufficient to have a model which predicts observations to within a factor of two, or should the comparison be better? Additionally, this research used default values supplied by the model, for both simplicity and determination of the model's utility for the layperson. Interestingly, in all model and sorption comparisons (temporal, spatial, and sorption studies), zinc was matched more poorly by modeling than was copper, with a general trend of the model under-estimating observed particulate zinc. It could be that another sorbent present in each of these types of samples, not included in modeling (such as aluminum), has an impact on the observed percentage particulate zinc, or that the default parameters used for sorption of zinc to HFO and/or HMO are not appropriate for natural water and solid samples. Perhaps natural HFO and HMO have a stronger affinity for sorption of zinc than the laboratory created oxyhydroxides used to determine model sorption parameters.

Literature Cited

- Allison, J.D., Brown, D.S., and Novo-Gradac, K.J. (1991) MINTEQA2/PRODEFA2, A Geochemical Assessment Model for Environmental Systems: Version 3.0 User's Manual. Athens, GA: U.S. EPA. EPA/600/3-91/021. pp. 115.
- Bigham, J.M., Schwertmann, U., Traina, S.J., Winland, R.L., and Wolf, M. (1996) Schwertmannite and the Chemical Modeling of Iron in Acid Sulfate Waters. *Geochim. Cosmochim Acta* 60:2111-2121.
- Butler, B.A. (2005).
- Gustafson, J.P. (2001) Modeling the Acid-base Properties and Metal Complexation of Humic Substances with the Stockholm Humic Model. *J. Coll. Inter. Sci.* 244:102-112.
- Gustafson, J.P. (2004) Visual MINTEQ, Version 2.30: A Windows Version of MINTEQA2, Version 4.0 [WWW document]. URL <http://www.lwr.kth.se/english/OurSoftware/Vminteq>.
- McLean, J.E. and Bledsoe, B.E. (1992) Ground Water Issue, Behavior of Metals in Soils. Washington, DC: U.S. Environmental Protection Agency, Office of Solid Waste and Emergency Response. EPA/540/S-92/018.
- Tessier, A., Campbell, P.G.C., and Bisson, M. (1979) Sequential Extraction Procedures for the Speciation of Particulate Trace Metals. *Anal. Chem.* 51:844-851.

Modeling Cu and Zn Desorption Kinetics from Soil Particles

Herbert E. Allen and Zhenqing Shi
Department of Civil and Environmental Engineering
University of Delaware
Newark, DE 19716

Introduction

Metals in the environment occur in several forms: dissolved in surface and ground waters, incorporated in or sorbed on the surface of minerals in rock, sand, and soils or as well as bound to soil organic matter. Cadmium (Cd), copper (Cu), nickel (Ni) and zinc (Zn) are trace metals widely used in industry, transportation, agriculture and are being released into the environment. Cadmium, Cu, Ni, and Zn enter surface waters both in particulate and in dissolved forms from natural and anthropogenic sources. Natural processes contributing trace metals into soils, water and air include soils mineral weathering, water and wind erosion of rocks and soils, volcanic activity, and biological transfer of elements. The major anthropogenic sources of trace metals are mining and smelting, agricultural application of fertilizers, pesticides, and ameliorants containing trace metals, transportation, and municipal and industrial wastes.

Contamination of the environment with trace metals is a serious problem in many regions of the USA and all over the world. Soils can sorb trace metals and provide an important source of trace metals to waters, both in the dissolved form through leaching and in the particulate form through erosion (Bergkvist, 1986; McColl et al., 1986; Rasmussen, 1986; Bergkvist, 1987; Bergkvist et al., 1989). Much of the trace metals entering the surface waters are usually released from contaminated solid particles. The accumulation of the metals in the waters is highly dependent on the weathering of these solid particles. The trace metals leaching out of the soil particles into soil solutions (pore water) can become available to plants and animals in soils.

Both sorption and desorption processes are important for controlling the metal behavior in the soil and solution systems. The sorption process directly affects the metal distribution among different soils components and thus the future desorption from soils. The equilibrium of trace metals partition between soils and solutions has been studied extensively and several equilibrium models have been developed to predict the partitioning of trace metals between solid and solution phases. However, the sorption and desorption of trace metals on the soil particles appear to be a slow process and the equilibrium between solid and solution may not be attained in soils (Sparks, 1989 and 2001). There have been extensive equilibrium studies of metal sorption on soils for many years (Shuman, 1975; McBride and Blasiak, 1979; Zachara et al., 1992; Weng et al., 2001; Gustafsson et al., 2003; Tipping et al., 2003), but many fewer studies have focused on the kinetics of trace metal sorption/desorption on soils (Yin et al., 1997; Strawn and Sparks., 2000; Sukreeyapongse et al., 2002; Zhang et al., 2004).

Knowledge of the kinetic reactions for metals between soils and solutions can be important for predicting metal behavior since an equilibrium assumption may not be appropriate. The kinetic behavior of metals in the field may be affected by different processes including metal reactions between soils and solutions, the mobility of solutions, solution diffusion, or uptake by organisms. The metal reactions between soils and solutions do not achieve equilibrium instantaneously (Yin et al., 1997; Strawn and Sparks, 2000; Zhang et al., 2004). In laboratory column studies, leaching of trace metals from soils is kinetically controlled rather than by instantaneous equilibrium (Kedziorek et al., 1998). However, the importance of this kinetic reaction to control the metal behavior may differ for different chemistry and hydrological conditions (Zhang et al., 1998; Ernstberger et al., 2005; Voegelin et al., 2001). Thus a quantitative understanding of the rates of metal sorption and desorption on different soils at varying solution chemistry would be quite useful for developing models to accurately predict the fate and transport of trace metals in the environment for the levels of contamination present in the soils.

One challenge for the kinetics modeling in the soil system is the heterogeneity of soils, and little progress has been made in previous studies. In soils trace metals are bound to different components including organic matter, clay minerals, and metal oxides-hydroxides to different extents. So, sorption and desorption of the metals may include various chemical reactions proceeding at different time scales with different mechanisms. Taking into account all the main processes controlling the metals sorption and desorption on soils is most important to predict the impact of soil compositions on the metal contamination of surface waters. Based on the data available in the literature (Kabata-Pendias, 2001; Sauvé et al., 2000), metals reactions with soils may depend on metals content, soil organic matter (SOM), iron and manganese oxides-hydroxides and the clay fraction. It is essential to assess the role of different sorbents in soil components to control the reactions of metals with soils at different conditions.

In natural conditions, the solution compositions can be very different. Solution pH, dissolved organic matter (DOM) concentration and other cations (e.g. Ca^{2+} , Al^{3+}) may be the principal solution properties affecting the metals reactions. How these solution parameters affect metal partition equilibrium has been extensively studied, and some speciation models have been developed to calculate the metal speciation at different conditions, such as WHAM (Tipping, 1994). However the understanding of the kinetic effect of solution chemistry is still insufficient. A systematic study on how these factors affect the kinetics of metal sorption and desorption on soils is necessary in order to develop predictive models that can be applied to different solution chemistry conditions.

Another important concept, which has been overlooked by most of the previous studies, is the speciation of metals in the reaction systems. Even in the solutions, the metal speciation can be different at different pH and DOM concentrations. The reactivity of different species may differ greatly. Thus the total dissolved metals may not be a good indicator for the reactive metals in the solutions (Allen et al., 1980). For example, copper availability to plants and animals is found to be related not to total copper concentration in solutions but to the copper ion concentration (Di Toro et al., 2001; McBride, 2001). In the soils, due to their heterogeneity, the metal may be bound by a variety of sorbents and form different metal species. Recently spectroscopic techniques have been used to identify the speciation of metals in soils, which demonstrated that the speciation of metals can vary considerably among soils (Manceau et al., 1996; Roberts et al., 2002). Thus, in the kinetics modeling, the metal speciation should be carefully taken account of since different metal species may have very different kinetic behaviors.

Some kinetics models have been used to describe metal sorption and desorption kinetics in soil systems (Sparks, 1989 and 1999). Briefly, the rates of the reactions on soil constituents have been described using various models, such as ordered models (zero-, first-, and second-order kinetics equations), parabolic diffusion, two-constant rate, Elovich, and differential rate equations. However, the rate constants obtained in these models were not constant but changed with experimental conditions. Most of previous modeling was mainly based on individual curve fitting and then correlation analysis. The mechanisms controlling metal sorption and desorption in these models was not explicit and their usefulness is limited. New kinetics models, which specifically incorporate the reaction chemistry, are needed in order to better predict the metal behavior in the environment.

Furthermore, it has been recognized that the reactivity of different trace metals was different in the environment. The cation properties, such as electron configuration, water exchange rate, and the first hydrolysis constant, etc., vary among metals, which may be the

reasons accounting for their different behaviors. For example the Cu binding to humic substance is nonlinear but Zn binding is very linear. Cu can form strong complexes with DOM but Zn does not. The pH can also affect Cu and Zn binding to humic substances differently. All these factors make kinetics modeling complicated. Robust kinetics models should be able to predict different metal behaviors according to different chemical reactions.

Overall, little progress has been made on the kinetics modeling of trace metals in soil systems compared the extensively used equilibrium models. Predictive kinetics models, which can be used at different solution chemistry and soil compositions, are highly desired. This will improve the existing approaches based on equilibrium assumptions.

The objective of this project was to develop kinetics models to predict trace metals (mainly Cu and Zn) sorption and desorption on soil particles. The effects of soil properties and solution chemistry on kinetics of trace metals sorption and desorption were studied. Key soil and solution properties were selected. The models are based on the minimal number of input parameters that provide reasonable accuracy of model predictions. The developed models will form an important component part of the “Unit World” model of metal behavior in the environment being designed in the Center for the Study of Metals in the Environment, University of Delaware. The results are expected to be critical for the development of soil screening procedures for ecological risk assessment.

Materials and Methods

Six different soils were sampled from the USA and European countries. All soil samples were obtained from the 0-20 cm layer and completely mixed, air-dried, and then sieved using a 2-mm screen. The soils were selected to cover a variety of soil compositions. Selected soil properties are presented in Table 1. These soils have low background trace metal concentrations.

All glassware and bottles used in the experiments were soaked in 10% (v/v) nitric acid for at least 24 hours and then rinsed at least six times with distilled and deionized (DI) water prior to use to prevent trace metal contamination. The 0.1 M $\text{Ca}(\text{NO}_3)_2$ stock solution was prepared from $\text{Ca}(\text{NO}_3)_2$ salt and a 3 mM $\text{Ca}(\text{NO}_3)_2$ solution was made by diluting the stock solution as the background electrolyte for all kinetics experiments. The $\text{Cu}(\text{NO}_3)_2$ and $\text{Zn}(\text{NO}_3)_2$ stock solutions were prepared by dissolving $\text{Cu}(\text{NO}_3)_2$ and $\text{Zn}(\text{NO}_3)_2$ salts into distilled and DI water. The “Better” buffer (Kandegedara and Rorabacher, 1999) MES ([2-(N-morpholino) ethane sulfonic acid]) was purchased from GFS Chemical (Powell, OH), and a 0.1 M metal-free MES buffer solution was prepared with distilled and DI water. Then the buffer stock solution was added to background electrolyte to achieve the desired pH values.

Table 1. Soil properties

Soil type	pH ^a	Particle size composition			Total Organic C ^b	Cation exchange capacity ^c
		Sand	Silt	Clay		
		%			%	cmol, kg
Boonton Bergen County Loam	4.9	60	27	13	3.43	4.2
Boonton Bergen County Loam	4.9	49	35	16	7.15	4.2
Colodorus Soil	6.0	27	45	28	2.51	4.0
Matapeake Silt Loam	6.4	13	63	24	2.32	4.1
Montpellier Loamy Sand	6.4	87	4	9	0.76	2.5
Nottingham Sandy Loam	4.2	64	23	13	5.20	6.7

^a DI H₂O

^b determined with a Variomax CN analyzer

^c at soil pH

Two sets of kinetic experiments were run: (1) desorption of Cu and Zn from the spiked soils; (2) sorption and desorption of Cu and Zn on different soils, which were described as follows.

(1) Desorption of Cu and Zn from the spiked soils. The experiment was carried out using the Matapeake silt loam soil and Codorus clay loam soil (Table 1). Portions of each soil were spiked with Cu (48 mg/kg) and Zn (103 mg/kg) using metal salts. Samples were spiked with 500 mL metal solution to 250 g soil samples. The slurry was mixed for 10 min and allowed to settle for another 2 hours before the supernatant was gently decanted. The moist soil was then mixed and air-dried. The DOM was separated from the water of the Edisto River in South Carolina with a reverse osmosis system. Properties of this DOM can be found elsewhere (Lu and Allen, 2002).

Metals desorption kinetics was studied with a stirred-flow chamber with 6.4-mL reaction volume and the solution was leaching through the soil contained in the chamber (Yin et al., 1997). Soil samples (0.3 g) were leached with 3 mM Ca(NO₃)₂ solution as a background electrolyte. Before leaching, samples were pre-equilibrated in the chamber with the leaching solutions for 20 min. Leaching solution was pumped through the stirred-flow chamber with a peristaltic pump at a flow rate 1 mL/min and the breakthrough solution was collected with a fraction collector. The solutions were analyzed for total Cu and Zn (ICP-AES). DOM concentrations in leaching solutions were changed by adding concentrated DOM solution to the background electrolyte. The DOM concentrations used in our study are close to those observed in surface waters (Tipping, 2002). DOM concentration was measured with a DC-190 Rosemount Total Organic Carbon Analyzer. The pH was kept at desired value using 1 mM MES buffer which does not complex metal ions (Kandegedara and Rorabacher, 1999). Different solution pH (5.5 to 6.5), DOM concentrations (0 to 15 mg/L) and flow rates (0.5 to 4 mL/min) were tested in kinetic experiments.

(2) Sorption and desorption of Cu and Zn on different soils. The soil sample (0.3 g for most experiments) and a Teflon-coated magnetic stirrer were placed into the reaction cell, which

was then filled with the background electrolyte. After sealing the chamber, the suspension in the cell was mixed by the stirrer for 30 min without flow to hydrate the sample. Then the background electrolyte was passed through the cell for another 30 min at the flow rate of 0.9 mL/min to remove most of the soluble organic matter due to SOM dissolution in the chamber. The background electrolyte of the kinetics experiments was 3 mM Ca(NO₃)₂ and pH was kept at the desired value using 3 mM MES buffer. The Zn(NO₃)₂ or Cu(NO₃)₂ stock solution was added to the background electrolyte to reach different concentrations of metal solutions for sorption experiment.

To initiate the sorption experiment, the metal solution was pumped through the chamber at a fixed flow rate. The influent metal concentration was constant during each experiment. After the 3-hour sorption, the desorption was started by passing the background electrolyte through the chamber. The desorption experiment continued for another 4 hours. Effluents were collected with a Spectra/Chrom CF-1 fraction collector using 5-min time intervals for each sample and then analyzed by ICP-MS to determine total metal concentrations. The flow rates were monitored during the experiment and variation of the flow rate within each experiment did not exceed 3%. Different influent Cu and Zn concentrations, different solution pH, from 5.5 to 6.5, and different soil organic carbon (SOC) concentrations, from 0.76% to 7.15%, were tested. The flow rate for all experiments was controlled at 0.9 mL/min. For most of our experiments, the particle concentration was kept constant but a two-fold increase in particle concentration was also tested for the Montpellier and Boonton Union soils.

Model Description

We developed a two-site sorption/desorption kinetics model in this project. Briefly the mass balance equations are derived as follows. Let k_{a1} (L/(g min)), k_{d1} (1/min), and C_{p1} (μg metal/g) be the sorption and, desorption rate coefficients and the particle metal concentration for site 1 respectively, and C_{ion} (μg metal/L) be the solution concentration of ionic metals. Then, we have the kinetic equation for metal reactions with soils on site 1,

$$\frac{dC_{p1}}{dt} = -k_{d1}C_{p1} + k_{a1}C_{ion} \quad (1)$$

and similarly for site 2,

$$\frac{dC_{p2}}{dt} = -k_{d2}C_{p2} + k_{a2}C_{ion} \quad (2)$$

In the flow reactor system, the experimentally observed kinetics was also affected by the mass transport in the reactor. The equation for ionic metal concentration in the solution follows from mass balance

$$\frac{dC_{ion}}{dt} = -k_{a1}mC_{ion} - k_{a2}mC_{ion} + k_{d1}mC_{p1} + k_{d2}mC_{p2} - \frac{Q(C_{ion} - C_{ion,0})}{V} \quad (3)$$

where m (g/L) is soil particle concentration, Q (L/min) is the flow rate, and V (L) is the reaction volume of the reactor. All concentration terms refer to the concentrations in the reactor. Subscript 0 denotes the influent concentration. Because all metal concentrations are expressed as the amount of metal per gram of soil or per liter solution, the above equations still strictly obey the reaction stoichiometry.

The next step is to include the metal-DOM reactions. Total DOM concentration, C_{DOM} (mg C/L), is used to represent total reactive ligand concentration of DOM. The mass balance equations for ionic metal concentration, C_{ion} , and metal-DOM complex concentration, $C_{metal-DOM}$ ($\mu\text{g metal/L}$), are

$$\frac{dC_{ion}}{dt} = -k_{a1}mC_{ion} - k_{a2}mC_{ion} + k_{d1}mC_{p1} + k_{d2}mC_{p2} - \frac{Q(C_{ion} - C_{ion,0})}{V} - k_1C_{ion}C_{DOM} + k_2C_{Me-DOM} \quad (4)$$

$$\frac{dC_{Me-DOM}}{dt} = k_1C_{DOM}C_{ion} - k_2C_{Me-DOM} - \frac{Q(C_{Me-DOM} - C_{Me-DOM,0})}{V} \quad (5)$$

The measured total soluble metal concentration, C_w ($\mu\text{g metal/L}$), equals the sum of the ionic metal concentration and the metal-DOM complex concentration,

$$C_w = C_{ion} + C_{M-DOM} \quad (6)$$

Above equations were derived based on the two-site conceptual model for soil and metal reactions. A special case of the two-site model is the one-site model, in which both sites have the same rate coefficients.

Sorption and desorption reaction rates may be affected by proton competition with metal ions for the binding sites on soils, which can be attributed to the pH dependency of metal equilibrium binding. The pH dependency of metal binding is directly related to the molar proton/metal exchange ratio that is always not integral (Kinniburgh et al., 1999). The pH dependency was incorporated into the sorption rate coefficients not in desorption rate coefficients and is expressed as

$$k_{ai} = a_i[H^+]^{-n_i} \quad (i = 1,2) \quad (7)$$

where a_i is a constant independent on pH and n_i is related to the molar proton/metal exchange ratio in metal equilibrium binding on soils. The relationship of k_{ai} at different pH is

$$\frac{k_{ai,pH1}}{k_{ai,pH2}} = 10^{n_i(pH1-pH2)} \quad (8)$$

Equation (8) is not a pure empirical equation but can be related to metal equilibrium binding under effect of pH. It considers proton competition on the metal sorption rates at different pH, which can be demonstrated through equilibrium isotherm. Equations (1) and (2)

can be solved at steady state corresponding to the batch equilibrium to calculate partition coefficients:

$$K_{p1} = \frac{C_{p1}}{C_{ion}} = \frac{k_{a1}}{k_{d1}} = \frac{a_1}{k_{d1}} [H^+]^{-n_1} \quad (9)$$

and

$$K_{p2} = \frac{C_{p2}}{C_{ion}} = \frac{k_{a2}}{k_{d2}} = \frac{a_2}{k_{d2}} [H^+]^{-n_2} \quad (10)$$

where K_{p1} (L/g) and K_{p2} (L/g) are the partition coefficients for two sites. When n_1 equals n_2 , the pH dependency of partition coefficient K_p (L/g) is expressed as

$$K_p = K_{p1} + K_{p2} = \left(\frac{a_1}{k_{d1}} + \frac{a_2}{k_{d2}} \right) [H^+]^{-n} \quad (11)$$

and in log-log form

$$\log K_p = n(pH) + \log \left(\frac{a_1}{k_{d1}} + \frac{a_2}{k_{d2}} \right) \quad (12)$$

From Equation (12) it is clear the pH dependency parameter in the kinetics models is actually a macroscopic equilibrium parameter, which can be experimentally determined or calculated by an equilibrium model.

The differential equations were solved numerically using an implicit finite difference method. Model parameters were obtained by fitting all breakthrough curves globally with nonlinear regression method using the SOLVER program in Microsoft Excel 2000.

Besides the kinetics model in which a kinetically controlled process was assumed during the model derivation, the model based on the instantaneous equilibrium assumption can also be derived. The instantaneous equilibrium (IE) model was used for comparison. The IE model has a final form as follows,

$$\frac{dC_w}{dt} = \frac{1 + C_{DOM} K_{pDOM}}{1 + C_{DOM} K_{pDOM} + mK_p} \frac{dC_T}{dt} = \frac{Q}{V} \frac{1 + C_{DOM} K_{pDOM}}{(1 + C_{DOM} K_{pDOM} + mK_p)} (C_{w,0} - C_w) \quad (13)$$

Furthermore, we developed a WHAM VI based kinetics model which can account for the nonlinearity of metal binding with SOM. The major difference is the sorption rate coefficient k_a changes with metal loading in soils. Thus, at each time step, k_a was calculated according to the metal loading. The steady state of the kinetics equation gives

$$K_p = \frac{k_a}{k_d} = \frac{C_p}{C_w} \quad (14)$$

If the K_p can be determined at different reaction conditions, it is possible to calculate kinetic rate coefficients based on Equation 14. A version of WHAM VI by Lofts (2005) was used which enabled us to call WHAM VI in an EXCEL spreadsheet. In EXCEL, the VBA functions were programmed to call WHAM VI to execute specific calculations and then return the metal partition coefficient K_p . The model parameters are desorption rate coefficient k_d , which was kept constant for all conditions, and the fraction of active organic matter (f) for each soil.

The WHAM VI input parameters included the solution chemistry composition, including pH, $[Ca^{2+}]$, $[NO_3^-]$, $\{Fe^{3+}\}$, $\{Al^{3+}\}$, and $[Cu^{2+}]$, and SOM, including the particulate [HA] and [FA]. For the solution species, the concentrations were input as exactly used in the experiments. Free Fe^{3+} and Al^{3+} activities were calculated using the method by Tipping et al. (2003).

Results

Kinetics of Cu and Zn desorption from soils

Both one-site and two-site models were used to model kinetics of Zn desorption. The two-site model fits the desorption data for Zn much better than the one-site model. More important, the two-site model can reproduce the stop-flow experimental results but the one-site model cannot (Figure 1a). The model also fit the results of different flow rates very well with the same model parameters (Figure 1b).

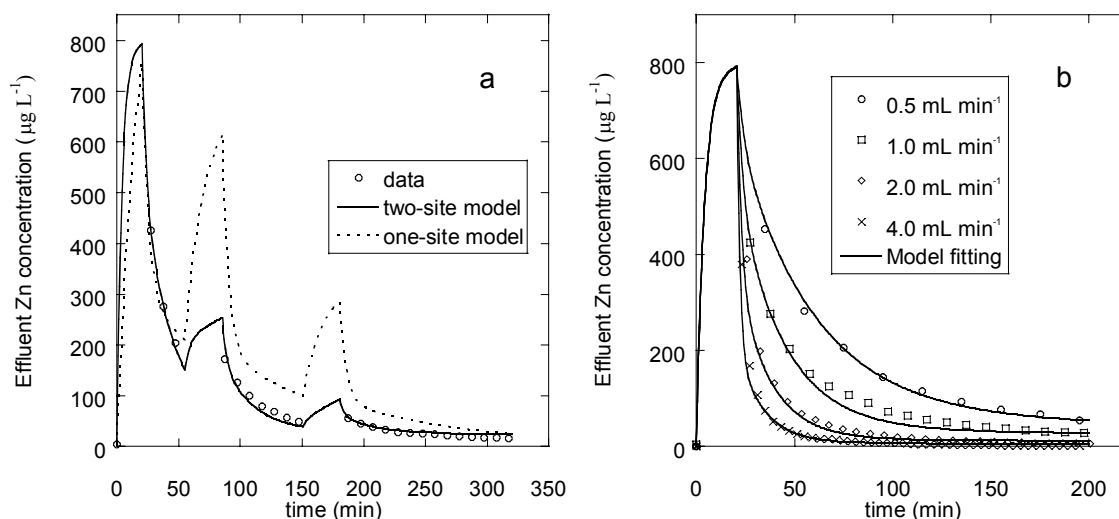


Figure 1. Kinetics of Zn desorption from spiked Matapeake soil at pH 5.5 and $[Ca^{2+}] = 3$ mM. (a) Stop-flow experiment; (b) Different flow rates (values are annotated in the figure). Lines are calculated with the model.

The results for the pH effect are presented in Figure 2 for both soils. Both sites are important for Zn release. The site with larger desorption and adsorption rate coefficients controlled the Zn release during pre-equilibration and fast release periods and the other site with the much lower rate coefficients accounted for the slow Zn release.

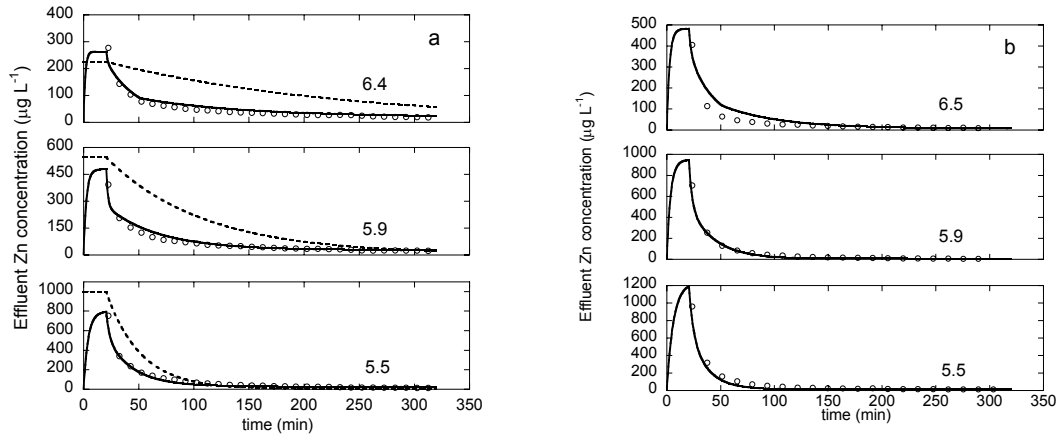


Figure 2. Effect of pH (values are annotated in the figure) on the kinetics of Zn release from spiked (a) Matapeake soil and (b) Codorus soil ($Q = 1 \text{ mL min}^{-1}$). Solid lines are calculated with the two-site kinetics model and dash lines are calculated with the IE model.

Contrary to the Zn results, a one-site model for Cu fit all data as well as a two-site model. A unique set of model parameters fits all the breakthrough curves at different DOM concentrations and flow rates (Figures 3 and 4). Figure 5 presents the effect of pH on Cu release. We can see the model fittings are good.

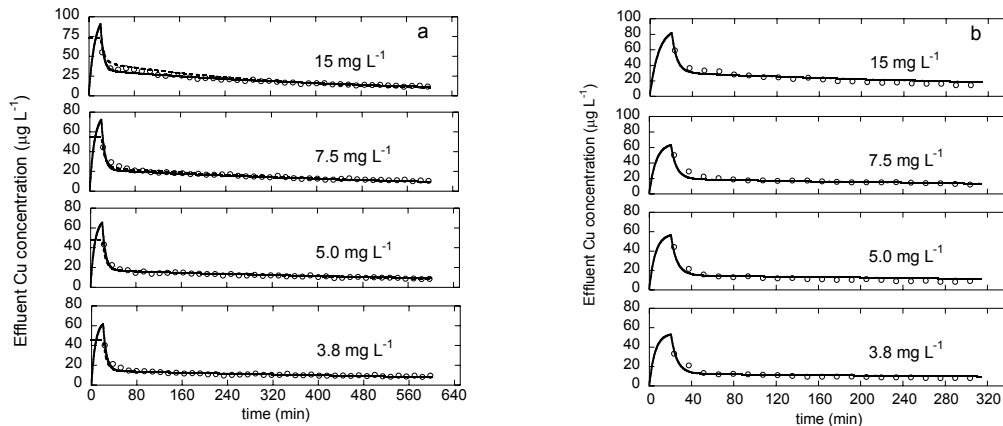


Figure 3. Effect of DOM (values are annotated in the figure) on the kinetics of Cu release from spiked (a) Matapeake soil and (b) Codorus soil ($\text{pH} = 5.5$ and $Q = 1 \text{ mL/min}$). Solid lines are calculated with the kinetics model and dash lines are calculated with the IE model.

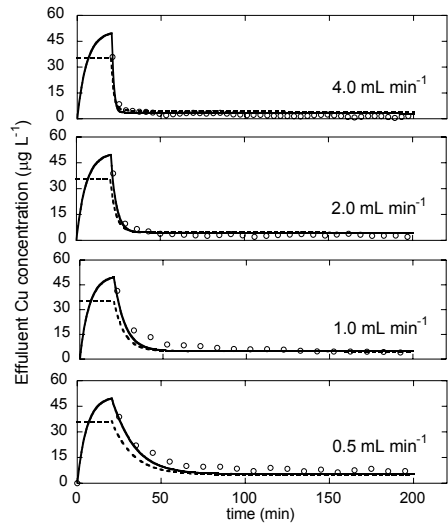


Figure 4. Effect of flow rates (values are annotated in the figure) on the kinetics of Cu release from spiked Matapeake soil (pH = 5.5). Solid lines are calculated with the kinetics model and dash lines are calculated with the IE model.

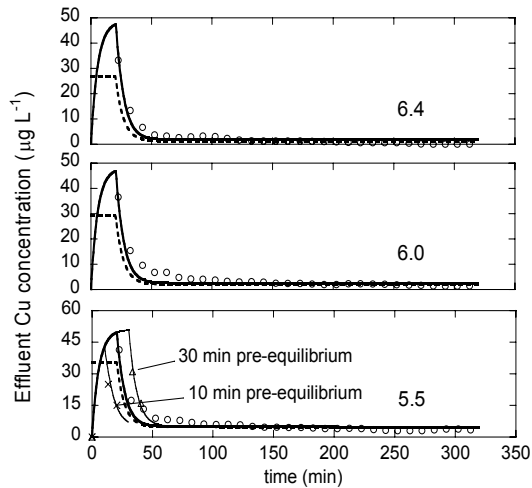


Figure 5. Effect of pH (values are annotated in the figure) on the kinetics of Cu release from spiked Matapeake soil ($Q = 1 \text{ mL/min}$). The effect of different pre-equilibration times is shown on the plot for pH = 5.5. Solid lines are calculated with the kinetics model and dash lines are calculated with the IE model.

The model fitting parameters are listed in Table 2. The Zn desorption rate coefficients are reasonably consistent with those obtained by others (Zhang et al., 2004). Generally we can see the model parameters for these two soils are quite similar which is consistent with the similarity of soil compositions for these two soils.

Table 2. Model fitting parameters for Cu and Zn release kinetics using the kinetics model

Zn							
Matapeake soil							
pH	k_{d1}	k_{a1}	C_{p1}	k_{d2}	k_{a2}	C_{p2}	n
	min^{-1}	$\text{L g}^{-1} \text{min}^{-1}$	$\mu\text{g g}^{-1}$	min^{-1}	$\text{L g}^{-1} \text{min}^{-1}$	$\mu\text{g g}^{-1}$	
5.5	1.02E-1	3.53E-3	43.3	1.79E-3	8.58E-5	60.0	1.0
6.0		1.16E-2*			2.82E-4*		
6.4		3.00E-2*			7.31E-4*		
Codorus soil							
pH	k_{d1}	k_{a1}	C_{p1}	k_{d2}	k_{a2}	C_{p2}	n
	min^{-1}	$\text{L g}^{-1} \text{min}^{-1}$	$\mu\text{g g}^{-1}$	min^{-1}	$\text{L g}^{-1} \text{min}^{-1}$	$\mu\text{g g}^{-1}$	
5.5	1.05E-1	1.39E-3	42.2	4.36E-4	8.39E-6	61.1	1.0
5.9		3.50E-3*			2.11E-5*		
6.5		1.39E-2*			8.39E-5*		
Cu							
	Matapeake soil				Codorus soil		
pH	k_d	k_a	pH	k_d	k_a	n	
	min^{-1}	$\text{L g}^{-1} \text{min}^{-1}$		min^{-1}	$\text{L g}^{-1} \text{min}^{-1}$		
5.5	4.93E-3	8.39E-2	5.5	5.56E-3	1.14E-1	1.3	
6.0		3.97E-1*	5.9		5.61E-1*		
6.4		1.38E-0*	6.5		6.10E-0*		

*recalculated from k_a at pH 5.5 based on Equation 8.

One way to evaluate the obtained kinetics model parameters is to check if the kinetics parameters reflect the reasonable equilibrium conditions. Partition coefficients can be calculated based on the kinetics rate coefficients (Equations 9-11). We can also use WHAM VI to calculate partition coefficients. In addition, an empirical regression model ($\log K_p = 0.62\text{pH} - 0.97$) obtained by statistically analyzing large amounts of literature data (Sauvé et al., 2000) was also used to calculate K_p . The results at the various pH using different approaches are presented in Figure 6. The kinetics rate coefficients obtained K_p are consistent with predicted K_p using WHAM and the regression model. Since these three approaches are completely independent, this consistency supports the validity of our approach and the coefficients we obtained.

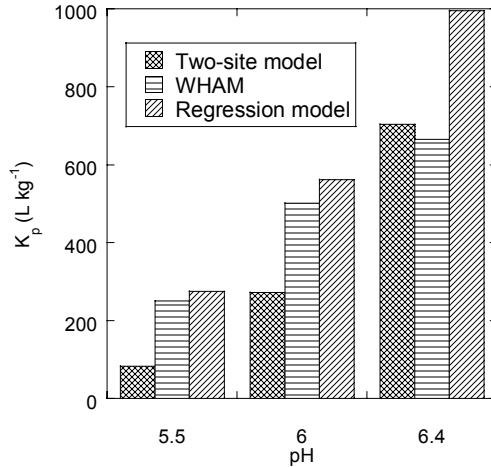


Figure 6. Comparison of Zn partition coefficients calculated from different approaches (indicated in the figure).

Kinetics of Zn sorption on and desorption from soils

We used the previously obtained Zn desorption rate coefficients from the Matapeake soil (Table 2), which remained constant for all soils. Then we obtained the pH dependency n_i and sorption rate coefficients k_{ai} for each soil by globally fitting all experimental data. Generally, the model gave a good fit to the experimental data. Figure 7 presents a sample of the results for three soils containing different amounts of SOM.

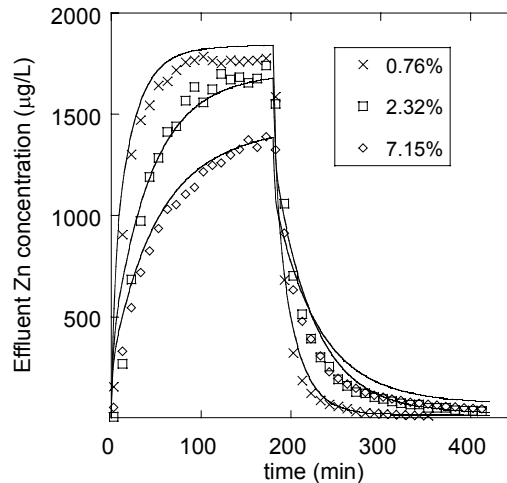


Figure 7. Effect of SOM content on the kinetics of Zn sorption and desorption on different soils (pH = 6.0 and influent [Zn] = 1.78 - 1.90 mg/L). SOC concentrations are presented in the figure. Solid lines are model calculations.

The effect of soil properties on the sorption rate coefficients is examined in Figure 8, a plot of the sorption rate coefficients k_{ai} vs. SOC concentrations for all soils. The sorption rate coefficients are linearly related to the SOC concentrations. We made the linear regressions both with and without a zero intercept. For the slow site (Figure 8(a)), both regressions have high R^2 (0.965 and 0.966 respectively) and the regression with intercept not equal to zero has a very small intercept which is negligible. The fast site (Figure 8(b)) has the lower R^2 (0.713 and 0.841, respectively).

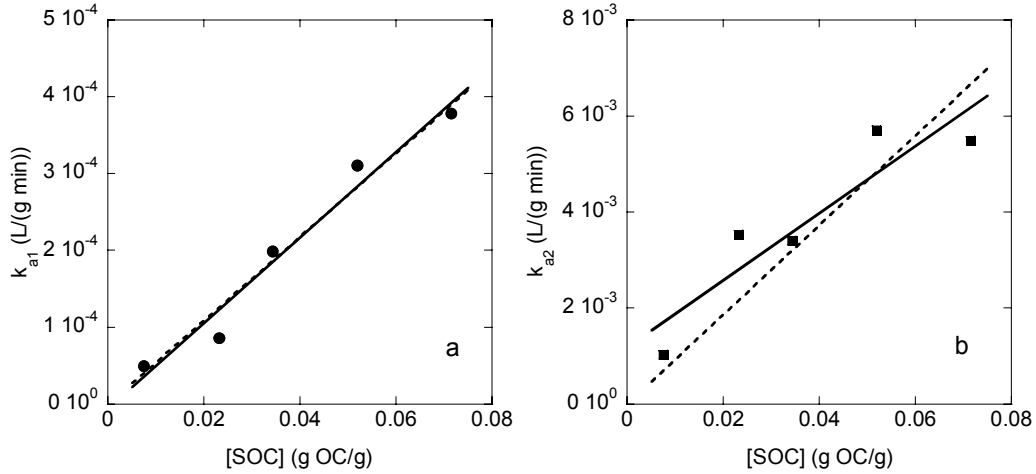


Figure 8. Linear regression of the Zn sorption rate coefficients vs. SOC at pH 5.5. Dashed lines are regressions with zero intercept values and solid lines are regressions with non-zero intercepts. (a) The slow site, (b) the fast site.

We proposed the organic carbon normalized sorption rate coefficients, $k_{ai,OC}$, which should be applicable for Zn sorption on different soils. The relationship between k_{ai} and $k_{ai,OC}$ can be expressed as

$$k_{ai} = k_{ai,OC} f_{OC} \quad (i = 1, 2) \quad (15)$$

where f_{OC} (g OC/g) is the SOC concentration.

Using Equation (15), we globally refit all experimental data to obtain the organic carbon normalized sorption rate coefficients, $k_{ai,OC}$, and pH dependency, n_i , for both sites, which greatly decreased the number of model parameters. Figures 9(a) and 9(b) present the results of kinetics of Zn sorption/desorption on different soils at two pH values, 6.0 and 6.5, and the model results using organic carbon normalized sorption rate coefficients. The model still fit the data reasonably well. Figure 9(c) present the model results for a two fold increase in particle concentrations for two soils at pH 6.0. The ability to handle different soil particle concentrations indicates that the kinetic coefficients are constant for small particle concentration change.

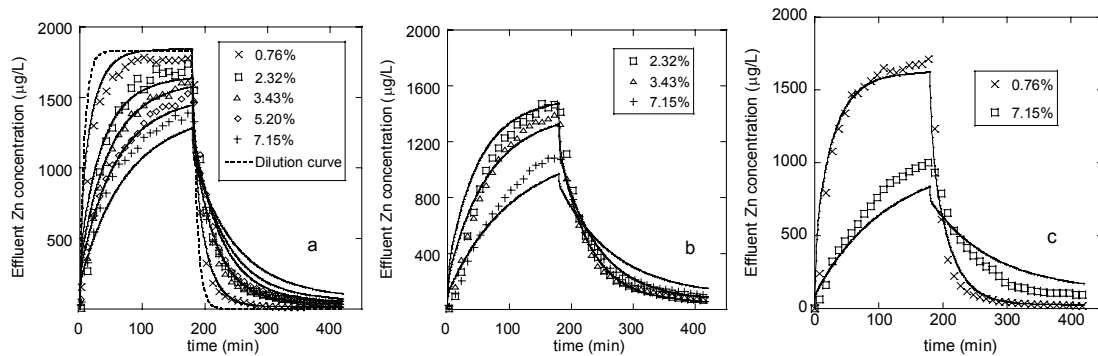


Figure 9. Kinetics of Zn sorption and desorption on different soils at (a) pH = 6.0, (b) pH = 6.5, and (c) pH = 6.0 with double soil particle concentration (Influent [Zn] = 1.70 – 1.90 mg/L). SOC concentrations are presented in the figure. Dilution curve corresponds to the blank experiment without soil particles. Solid lines are model calculations.

The organic carbon normalized the sorption rate coefficients follow the same pH dependency discussed previously. Figure 10 shows the experimental data and model calculations on the effects of Zn concentrations and pH.

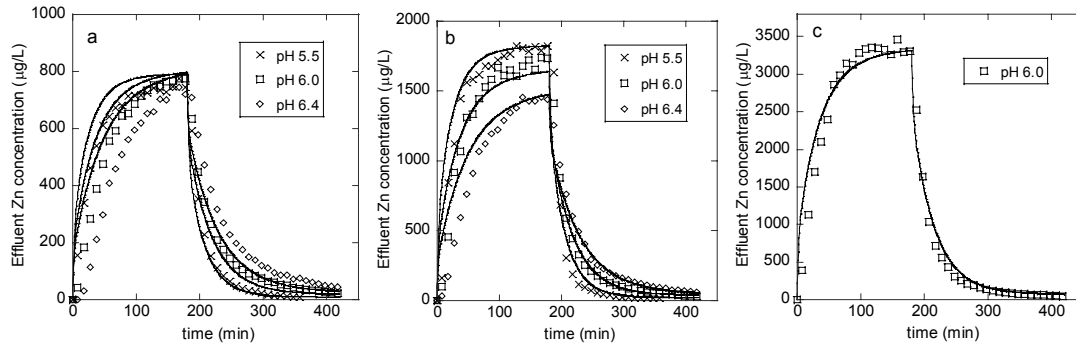


Figure 10. Kinetics of Zn sorption and desorption on the Matapeake soil at different influent Zn concentrations. ([Zn]) and solution pH (pH values are presented in the figure). (a) [Zn] = 0.83 – 0.92 mg/L; (b) [Zn] = 1.73 – 1.91 mg/L; (c) [Zn] = 3.62 mg/L. Solid lines are model calculations.

All model fitting parameters are presented in Table 3 for both individual fitting of all soils and organic carbon normalized fitting.

Table 3. Kinetics model parameters

Model parameters obtained using individual soils					
Soil	Montpellier	Matapeake	Boonton Bergen County	Nottingham	Boonton Union
SOC (g OC/g)	0.0076	0.0232	0.0343	0.052	0.0715
k_{a1}^* (L/(g min))	5.0E-5	8.6E-5	2.0E-4	3.1E-4	3.8E-4
k_{a2}^* (L/(g min))	1.0E-3	3.5E-3	3.4E-3	5.7E-3	5.5E-3
n_1	0.74				
n_2	0.74				
Model parameters obtained using organic carbon normalization					
Parameter	$k_{a1,OC}^*$	$k_{a2,OC}^*$	n_1	n_2	
Unit	L/(g OC min)	L/(g OC min)			
Value	7.9E-3	1.6E-1	0.50	0.53	

* at pH 5.5; $k_{d1} = 1.8 \times 10^{-3}$ 1/min and $k_{d2} = 1.0 \times 10^{-1}$ 1/min.

One way to check the utility of our model parameters is to compare the predicted equilibrium partition coefficients using both kinetics parameters and the equilibrium model, as described previously. Figure 11 presents the comparison of organic carbon normalized partition coefficients at different pH calculated by WHAM VI and our kinetics model.

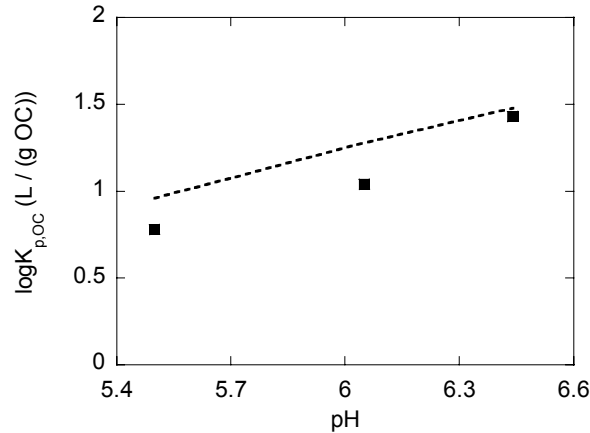


Figure 11. The comparison of organic carbon normalized partition coefficient $K_{p,OC}$ calculated by WHAM VI and the kinetics model (symbols indicate values calculated using the kinetics model; dashed line is the WHAM VI prediction).

WHAM predictions are higher than the values calculated from our kinetics model but they are quite close and almost equal at pH 6.4. The similarity of the results supported our assumption that SOM is the dominant phase in soils to control Zn sorption and desorption.

Figure 12 presents the change of particulate Zn concentration during the sorption and desorption experiment for two soils.

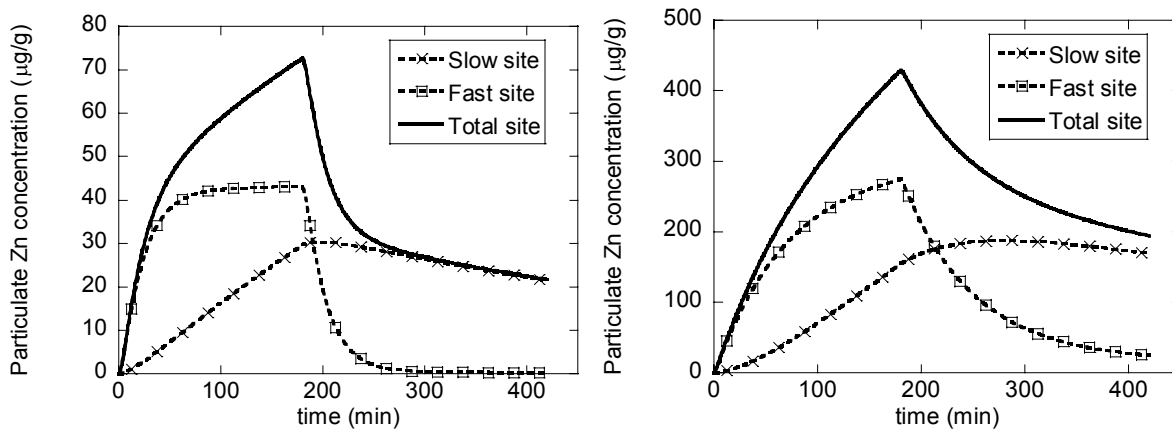


Figure 12. Kinetics of Zn sorption/desorption on two sites with the two-site model simulation at pH 6.0 and $[Zn] = 1.73 - 1.91$ mg/L: (a) $[SOC] = 0.76\%$ and (b) $[SOC] = 7.15\%$.

The importance of the two sites controlling Zn sorption/desorption kinetics can be analyzed in detail with the model calculations for the reaction rates of two sites with time (Figure 12). For the sorption, in the first hour, the fast site can quickly uptake a lot of Zn which dominated the sorption process. After that, the sorption rate of the fast site slowed down and the slow site became more important for the Zn sorption. For the desorption, within the first 2-3 h, the observed desorption kinetics was mainly controlled by the dilution effect and the desorption from the fast site. For the low SOC content (Figure 12(a)), only a small amount of Zn was sorbed (less than 80 $\mu\text{g/g}$). The fast site was saturated quickly in sorption and also depleted quickly in desorption. After one hour the Zn release was mainly controlled by the slow site. For the higher SOC contents (Figure 12(b)), the fast site still has some capacity for sorbing Zn after three hours

sorption and it is important even after four hours desorption. The slow site showed more importance for the high SOC content soils due to higher binding capacity of the slow site.

Kinetics of Cu sorption on and desorption from soils

The WHAM VI based kinetics model was applied to fit Cu sorption and desorption data since Cu sorption shows highly nonlinear behavior with change of Cu concentrations.

Figure 13 presents the results Cu sorption and desorption on the Matapeake soil with different Cu influent concentrations. We can see WHAM VI can handle the effect of Cu loading well.

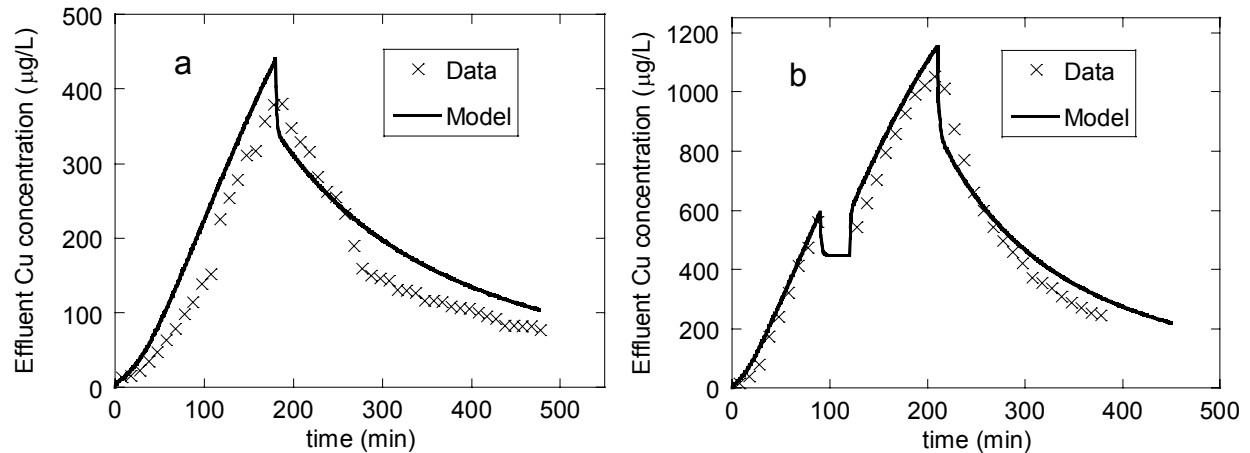


Figure 13. Kinetics of Cu sorption and desorption on the Matapeake soils at pH 5.5: (a) Influent [Cu] = 0.85 mg/L and (b) Influent [Cu] = 1.70 mg/L.

The effect of pH is presented in Figure 14. Together with Figure 13, the increase of pH dramatically decreased Cu sorption, which can be accounted for by WHAM VI without any further model fitting.

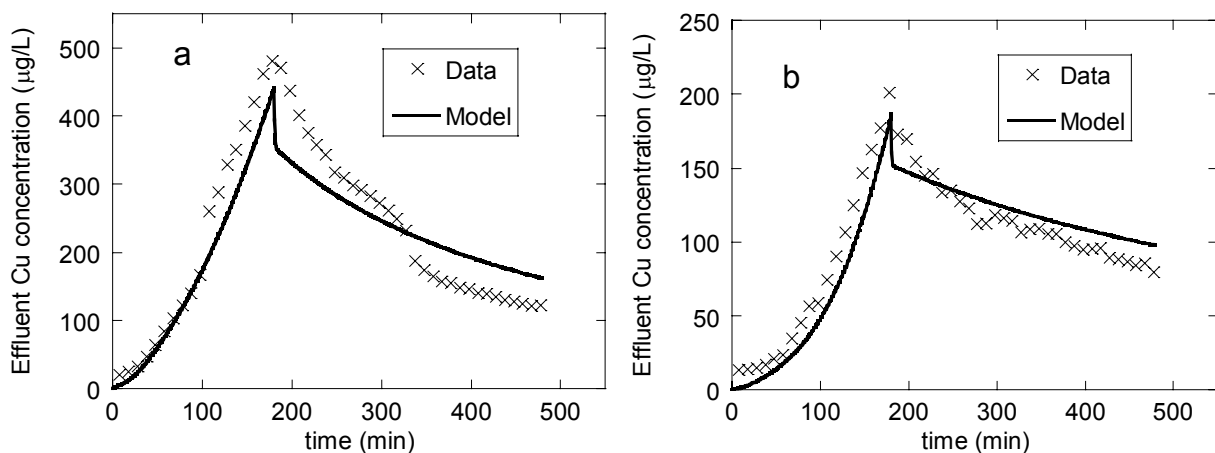


Figure 14. Kinetics of Cu sorption and desorption on the Matapeake soils at (a) pH 6.0 and (b) pH 6.5 (Influent [Cu] = 1.4 - 1.5 mg/L).

For different soils, the amount of active organic matter was optimized by model fitting. Based on the active organic matter, WHAM VI can predict metal partitioning for each soil. The effect of SOM on Cu sorption and desorption kinetics can be explained by the WHAM VI based kinetics model (Figure 15).

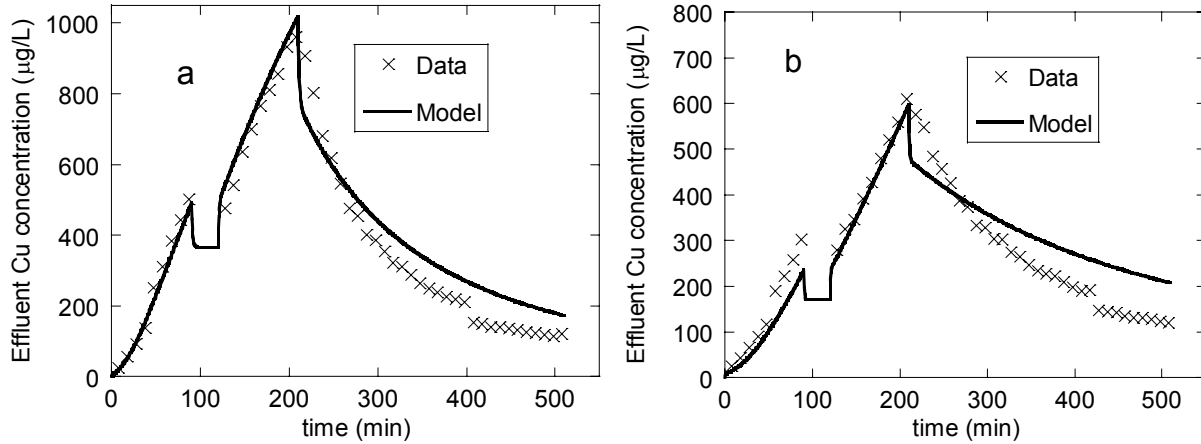


Figure 15. Kinetics of Cu sorption and desorption on (a) the Boonton Bergen soil (influent [Cu] = 1.6 mg/L; [SOC] = 3.43%) and (b) the Boonton Union soil (influent [Cu] = 1.7 mg/L; [SOC] = 7.15%) at pH 5.5.

Generally, WHAM VI based kinetics model gave relatively good fits for all experimental data. It is interesting that the fraction of active organic matter decreased with increase of SOC concentrations (Figure 16(a)). It means with higher SOC concentration, more SOM is inactive. The total mass concentrations of active organic matter increased with SOC concentrations, indicating more reaction sites for higher SOC concentration soils (Figure 16(b)).

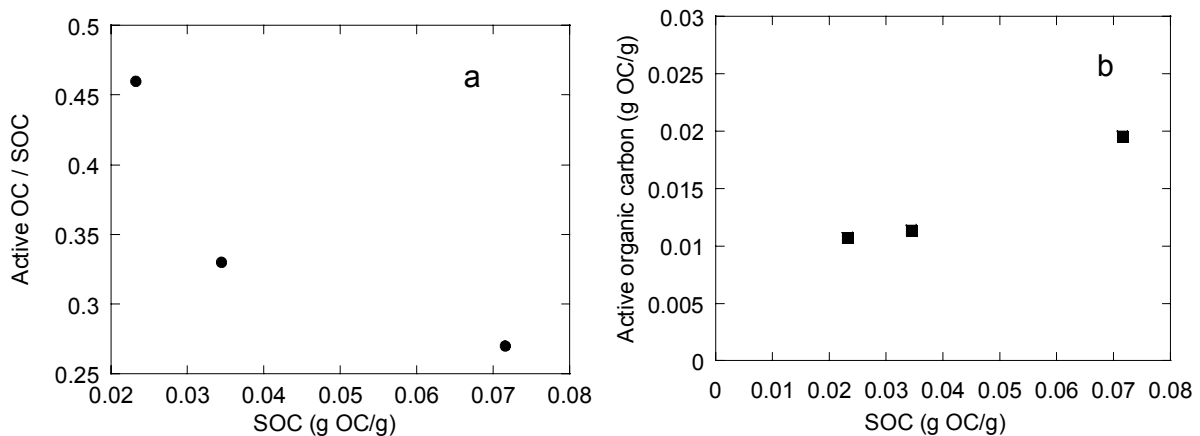


Figure 16. The active organic matter vs. SOC concentration: (a) percentage plot; (b) mass concentration plot.

Table 4 gives WHAM input parameters for the three soils at pH 5.5. The concentrations of HA and FA were automatically recalculated based on the fraction of active organic matter, which was optimized by model fitting. The total Cu concentration was input into WHAM VI at

each time step when calling WHAM VI through the user built VB function. The model parameters for WHAM VI based kinetics model are listed in Table 5.

Table 4. WHAM input parameters at pH 5.5

Parameter	pH	[Ca ²⁺]	[NO ₃ ⁻]	{Fe ³⁺ }	{Al ³⁺ }	[HA]	[FA]
Specie	Fixed	Total	Total	Activity	Activity	Total	Total
Unit		M	M	M	M	g/L	g/L
Matapeake	5.5	0.003	0.006	3.16E-14	1.00E-08	7.55E-01	1.44E-01
Boonton Bergen	5.5	0.003	0.006	3.16E-14	1.00E-08	8.05E-01	1.53E-01
Boonton Union	5.5	0.003	0.006	3.16E-14	1.00E-08	1.39E00	2.64E-01

Table 5. Model fitting parameters for WHAM VI based kinetics model

Kinetics parameter	Fraction of active organic matter (<i>f</i>)		
	Matapeake	Boonton Bergen	Boonton Union
<i>k_d</i> (1/min)			
2.3E-2	0.46	0.33	0.27

Conclusion

The knowledge of kinetics of trace metals sorption and desorption is important for better understanding the reaction mechanisms and developing predictive models for metal behavior in the environment. Previous kinetics models have limited usefulness and predictive models for different metals at various chemistry conditions are needed. This project addressed several questions concerning developing the predictive models for Cu and Zn. A linear sorption isotherm based two-site kinetics model was able to describe the Zn sorption and desorption kinetics at a variety of solution chemistry (different pH, Zn concentrations and flow rates) and soil compositions (mainly different SOC concentrations). The sorption and desorption reactions of Zn with soils were controlled by two sites, one fast and one slow site. The difference of Zn sorption and desorption kinetics for various soils can be explained by the SOC concentrations of different soils. The nonlinear binding behaviors were considered in the Cu kinetics models by using WHAM VI. The WHAM VI based kinetics model is more fundamental and can handle different chemistry conditions.

Two different modeling approaches were used in this study: (a) based on a linear sorption isotherm and (b) based on nonlinear sorption isotherm. The linear sorption isotherm based model can be successfully used to describe Zn sorption/desorption kinetics over a range of solution pH, Zn concentrations, and SOM contents. This is consistent with the observed linear binding behavior of Zn. This model is simple, and can be easily understood and used. The high nonlinearity of Cu binding with soils/humic substance requires a more complex model which is based on a nonlinear sorption isotherm. The kinetics model based on WHAM VI, which predicted the nonlinear sorption isotherm, performed very well to describe the kinetics of Cu sorption and desorption on different soils. The WHAM VI based kinetics model is a more general and fundamental model but it requires more knowledge with the associated equilibrium

model. So these two modeling approaches have different assumptions and their own advantages and disadvantages.

Literature Cited

- Allen, H.E., Hall, R.H. and Brisbin, T.D. (1980) Metal Speciation: Effects on Aquatic Toxicity. *Environ. Sci. Technol.* 14:441-443.
- Bergkvist, B. (1986) Leaching of Metals from a Spruce Forest Soil as Influenced by Experimental Acidification. *Water, Air Soil Pollut.* 31:901-916.
- Bergkvist, B. (1987) Soil Solution Chemistry and Metal Budgets of Spruce Forest Ecosystems in S. Sweden. *Water, Air Soil Pollut.* 33:131-154.
- Bergkvist, B., Folkesson, L. and Berggren, D. (1989) Fluxes of Cu, Zn, Pb, Cd, Cr and Ni in Temperate Forest Ecosystems. A Literature Review. *Water, Air Soil Pollut.* 47:217-286.
- Di Toro, D.M., Allen, H.E., Bergman, H.L, Meyer, J.S., Paquin, P.R. and Santore, R.C. (2001) Biotic Ligand Model of the Acute Toxicity of Metals. 1. Technical basis. *Environ. Toxicol. Chem.* 20:2383-2396.
- Ernstberger, H., Zhang, H., Tye, A., Young, S., and Davison, W. (2005) Desorption Kinetics of Cd, Zn, and Ni Measured in Soils by DGT. *Environ. Sci. Technol.* 39:1591-1597.
- Gustafsson JP, Pechová P, and Berggren D. (2003) Modeling Metal Binding to Soils: The Role of Natural Organic Matter *37:2767-2774*.
- Kabata-Pendias, A. (2001) Trace Elements in Soils and Plants. CRC Press, Boca Raton, Florida.
- Kandedgedara, A., and Rorabacher, D.B. (1999) Noncomplexing Tertiary Amines as "Better" Buffers Covering the Range of pH 3-11. Temperature Dependence of Their Acid Dissociation Constants. *Anal. Chem.* 71:3140-3144.
- Kedziorek, M.A.M., Dupuy, A., Bourg, A.C.M. and Compere, F. (1998) Leaching of Cd and Pb from a Polluted Soil During the Percolation of EDTA: Laboratory Column Experiments Modeled with a Non-equilibrium Solubilization Step. *Environ. Sci. Technol.* 32:1609-1614.
- Kinniburgh, D.G., van Riemsdijk, W.H., Koopal, L.K., Borkovec, M., Benedetti, M.F., and Avena, M.J. (1999) Ion Binding to Natural Organic Matter: Competition, Heterogeneity, Stoichiometry and Thermodynamic Consistency. *Coll. Surf. A* 151:147-166.
- Lofts, S. (2005) A Version of the WHAM program. Personal communication.
- Lu, Y. and Allen, H.E. (2002) Characterization of Copper Complexation with Natural Dissolved Organic Matter (DOM) - Link to Acidic Moieties of DOM and Competition by Ca and Mg. *Water Res.* 36:5083-5101.
- Manceau, A., Boisset, M.C., Sarret, G., Hazemann, J.L., Mench, M., Cambier, P. and Prost, R. (1996) Direct Determination of Lead Speciation in Contaminated Soils by EXAFS Spectroscopy. *Environ. Sci. Technol.* 30:1540-1552.
- McBride, M.B. and Blasiak, J.J. (1979) Zinc and Copper Solubility as a Function of pH in an Acid Soil. *Soil Sci. Soc. Am. J.* 43:866-870.
- McBride, M.B. (2001) Cupric Ion Activity in Peat Soil as a Toxicity Indicator for Maize. *J. Environ. Qual.* 30:78-84.

- McCull, J.G. and Pohlman, A.A. (1986) Soluble Organic Acids and Their Chelating Influence on Al and Other Metal Dissolution from Forest Soils. *Water, Air Soil Pollut.* 31:917-927.
- Rasmussen, L. (1986) Potential Leaching of Elements in Three Danish Spruce Forest Soils. *Water, Air Soil Pollut.* 31:377-383.
- Roberts, D. R., Scheinost, A. C. and Sparks, D. L. (2002) Zinc Speciation in a Smelter-Contaminated Soil Profile Using Bulk and Microspectroscopic Techniques. *Environ. Sci. Technol.* 36:1742-1750.
- Sauvé, S., Hendershot, W. and Allen, H.E. (2000) Solid-solution Partitioning of Metals in Contaminated Soils: Dependence on pH and Total Metal Burden. *Environ. Sci. Technol.* 34:1125-1131.
- Sukreeyapongse, O., Holm, P.E., Strobel, B.W., Panichsakpatana, S., Magid, J. and Hansen, H.C.B. (2002) pH-Dependent Release of Cadmium, Copper and Lead from Natural and Sludge-amended Soils. *J. Environ. Qual.* 31:1901-1909.
- Shuman, L.M. (1975) The Effect of Soil Properties on Zn Adsorption by Soils. *Soil Sci. Soc. Am. J.* 39:455-458.
- Sparks, D.L. (1989) *Kinetics of Soil Chemical Processes*. Academic Press, San Diego, CA.
- Sparks, D.L. (1999) *Soil Physical Chemistry (Second Edition)*. CRC Press, Boca Raton, FL.
- Strawn, D.G. and Sparks, D.L. (2000) Effect of Soil Organic Matter on the Kinetics and Mechanisms of Pb (II) Sorption and Desorption in Soil. *Soil Sci. Soc. Am. J.* 64:144-156.
- Tipping, E. (1994) WHAM – A Chemical Equilibrium Model and Computer Code for Waters, Sediment, and Soils Incorporating a Discrete Site/Electrostatic Model of Ion-binding by Humic Substances. *Computers Geosci.* 20:973-1023.
- Tipping, E. (2002) *Cation Binding by Humic Substances*. Cambridge University Press, Cambridge.
- Tipping, E., Rieuwerts, J., Pan, G., Ashmore, M.R., Lofts, S., Hill, M.T.R., Farago, M.E., Thornton, I.E. (2003). The Solid–solution Partitioning of Heavy Metals (Cu, Zn, Cd, Pb) in Upland Soils of England and Wales. *Environ. Pollut.* 125:213-225.
- Voegelin, A, Vulava, V.M., and Kretzschmar, B. (2001) Reaction-based Model Describing Competitive Sorption and Transport of Cd, Zn, and Ni in an Acidic Soil. *Environ. Sci. Technol.* 35:1651-1657.
- Weng, L.P., Temminghoff, E.J.M., and van Riemsdijk, W.H. (2001) Contribution of Individual Sorbents to the Control of Heavy Metal Activity in Sandy Soil. *Environ. Sci. Technol.* 35:4436-4443.
- Yin, Y., Allen, H.E., Huang, C.P., Sparks, D.L., and Sanders, P.F. (1997) Kinetics of Mercury(II) Adsorption and Desorption on Soil. *Environ. Sci. Technol.* 31:496-503.
- Zachara, J.M., Smith, S.C., Resch, C.T. and Cowan, C.E. (1992) Cadmium Sorption to Soil Separates Contaminating Layer Silicates and Iron and Alumimun-Oxides. *Soil Sci. Soc. Am. J.* 56:1074-1084.
- Zhang, H., Davison, W., Knight, B., and McGrath, S. (1998) In situ Measurement of Solution Concentrations and Fluxes of Trace Metals in Soils Using DGT. *Environ. Sci. Technol.* 32:704-710.

Zhang, H., Lombi, E., Smolders, E., and McGrath, S. (2004) Kinetics of Zn Release in Soils and Prediction of Zn Concentration in Plants Using Diffusive Gradients in Thin Films. *Environ. Sci. Technol.* 38:3608-3613.

Quantitative Structure Activity Relationships for Toxicity and Fate Parameters of Metals and Metal Compounds

Dominic M. Di Toro
Department of Civil and Environmental Engineering
University of Delaware
Newark, DE 19716

and
Richard Carbonaro
Department of Environmental Engineering
Manhattan College
Riverdale, NY 10471

Introduction

The purpose of this research project is to develop quantitative structure activity relationships (QSARs) for metals for which little or no experimental information exists. The parameters of interest are those required for hazard ranking and ultimately for evaluation using modeling approaches such as the Unit World Model. There are many metal and metalloid compounds for which there is concern with the environmental hazard associated with their release to the environment. It is important that rational methods of evaluating the potential for harm be employed. Ranking methods have been suggested for this purpose. Unlike the most studied metals, Cd, Cu, Ni, Pb, and Zn, or metals that have recently been of concern, for example Ag, most of the other metals are not well studied, particularly the transition metals in the third and fourth rows and the lanthanides.

It is not only toxicity that needs to be estimated. Basic environmental chemical parameters are also required. For example the WHAM model has been used to evaluate the extent of metal complexation to dissolved organic carbon. It is part of the Biotic Ligand Model of metal toxicity and is used in the Unit World Model. It requires complexation constants to the strong and weak sites of dissolved organic carbon. It has been shown that there is a correlation between metal-DOC binding constants used in WHAM and the metal binding constant to lactate. It would be very useful if such a relationship could be established for the untested metals and perhaps improved using other predictors. Sorption to particles is also important and data from mesocosm experiments for a variety of metals is available. A QSAR for this parameter would be quite useful as well.

Natural organic matter (NOM) plays an important role in the transport and bioavailability of heavy metals in the environment. Metal binding to NOM can lower free metal ion concentrations in aqueous solution thereby lowering bioavailability and toxic effects to aquatic organisms. For these reasons, quantitative models of metal binding to NOM are a necessary component of metal transport and toxicity models. Unfortunately, the complex and uncertain nature of NOM makes modeling metal-NOM especially challenging.

There have been a number of models that have been developed to predict the extent of metal binding to NOM. They all possess the general feature of proton-metal competition at binding sites. That is, metal binding occurs at the same sites of proton binding, and that both protons and metals compete for these sites. The fundamental differences between metal-NOM models are how they handle the distribution of binding sites: either. They are usually subdivided into the following two groups accordingly: (i) continuous-site distribution models, and (ii) discrete site distribution models (Dudal and Gerard, 2004). Continuous-site distribution models such as the NIC(C)A-Donnan model (Benedetti et al., 1995) assume that pK_a values of carboxylic and phenolic groups of NOM are normally distributed (Benedetti et al., 1995). Discrete site models such as the Windermere Humic Aqueous Models (WHAM, versions V and VI) (Tipping and Hurley, 1992; Tipping et al., 1998) and the Stockholm Humic Model (SHM) (Gustafsson, 2001) employ a relatively small number of discrete binding sites with different pK_a values.

The WHAM models of Tipping and co-workers (Tipping and Hurley, 1992; Tipping, 1998; Tipping, 1994) have gained considerable attention as a result of their general applicability to many metals and the small number of metal-specific fitted parameters. For these reasons, WHAM version V was chosen as the basis for the equilibrium speciation model that is employed in the Biotic Ligand Model (BLM) (Di Toro et al., 2001; Santore et al., 2001) which is used in toxicity assessments. It is also being employed in the "Unit World Model" (currently

under development), which is being used to model fate, transport and toxicity of metals in lakes (Farley, 2006).

Unfortunately, the number of metal cations for which WHAM constants are available is limited by the availability of high quality data sets of metal-NOM binding. Tipping et al (1-3) have employed quantitative structure activity relationships (QSARs) to obtain constants for cationic metals for which experimental data is not available. We have also examined various possibilities for QSARs, and during the development of these relationships it has become apparent that it is also possible to obtain WHAM constants from other chemical information, in particular known relationships between metal-ligand and proton-ligand binding constants as shown below. The purpose of this work is therefore to examine methods for obtaining QSARs for the metal-specific binding parameters that are employed in WHAM version V and VI. These QSARs can then be used to predict WHAM V parameters for metals with no known values for which a value is not known.

Approach

Initially we intended to use modern quantum chemical methods in the development of QSARs. The energetics of gas phase species including main row elements and, to less an extent, transition metals can be evaluated with reasonable accuracy. However, we have discovered a method that is much more accurate and relies on readily available thermodynamic data. The method is presented below and the necessary theory is presented in the metal ligand bonding section.

A assessment is presented of the methods that are available for estimating binding constants for metals in versions V and VI of the Windermere Humic Aqueous Model (WHAM). Both of these models call for specification of one metal-specific binding parameter to calculate the extent of metal complexation by natural organic matter. The required parameters are the $\log K_{\text{MHA}}$ and $\log K_{\text{MA}}$ for WHAM V and WHAM VI respectively. A common approach is to employ linear regressions where known values for these parameters are regressed against the $\log K_{\text{ML}}$ values of a ligand containing negatively-charged oxygen donor atoms (usually a carboxylic acid). The resulting LFER can be then used to estimate $\log K_{\text{MHA}}$ and $\log K_{\text{MA}}$ values for any metal as long as $\log K_{\text{ML}}$ is known. An alternative approach is to use the global tendency of metals to bind with a series of negatively-charged oxygen donor atoms as described by the Irving-Rossotti slope (see metal ligand bonding). The applicability of both methods is compared for WHAM V and WHAM VI.

Lactic Acid LFER for WHAM V

Initially we intended to use modern quantum chemical methods in the development of QSARs. The energetics of gas phase species including main row elements and, to less an extent, transition metals can be evaluated with reasonable accuracy. However, we have discovered a method that is much more accurate and relies on readily available thermodynamic data. The method is presented below and the necessary theory is presented in the metal ligand bonding section.

A LFER based upon the $\log K_{\text{ML}}$ value for metal binding to lactic acid has been used previously to estimate WHAM V $\text{p}K_{\text{MHA}}$ values for which experimental data is not available (Tipping, 1994; Tipping, 1993). This approach is shown in Figure 1 using data from the NIST database and experimentally-derived $\text{p}K_{\text{MHA}}$ for humic and fulvic acid. As pointed out by

Tipping (1993), the resulting relationship appears linear. Linear regression analysis yielded the following equations:

$$pK_{MHA}(HA) = -0.802 \cdot \log K_{ML} + 4.14 \quad r^2 = 0.893 \quad (1)$$

$$pK_{MHA}(FA) = -0.832 \cdot \log K_{ML} + 3.21 \quad r^2 = 0.921 \quad (2)$$

The magnitude of the coefficient of determination (r^2) for both humic and fulvic acid indicate an adequate fit to the data. The residuals for the humic acid regression, however, are not statistically independent, indicating a curvilinear model may be more appropriate (Peters et al., 1974). This is caused by the data point corresponding to Th^{4+} ($\log K_{ML} = 5.5$) which may be exerting undue weight on the regression.

The lactic acid LFER has an inherent weakness in that it is reliant upon the $\log K$ for binding of metals to a single ligand. Thus, availability of thermodynamic data may limit its applicability. For example, Fe^{2+} , Cm^{3+} , Hg^{2+} are not present in Figure 1 because $\log K_{ML}$ data for lactic acid are not available. From a chemical perspective, lactic acid is not an obvious choice for a LFER because it is an α -hydroxycarboxylic acid which usually acts as a bidentate ligand via coordination by the alcohol group (Portanova et al., 2003). In contrast, the WHAM V pK_{MHA} value is used to describe both monodentate and bidentate binding (Tipping and Hurley, 1992). Complications also arise for strong Lewis acids such as Fe^{3+} because the alcohol group of lactic acid deprotonates in the resulting metal-ligand complex. The stoichiometry of the metal-ligand complex is different than the other metals, and so Fe^{3+} is not included in the LFERs shown in Figure 1.

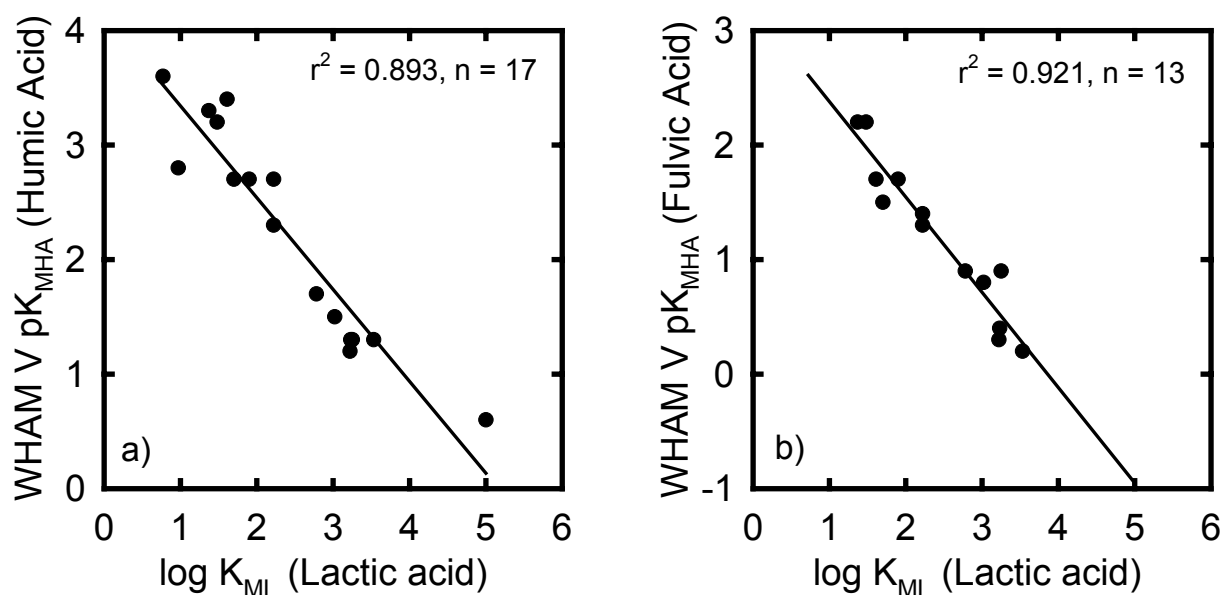


Figure 1. WHAM V pK_{MHA} values versus $\log K_{ML}$ for lactic acid. Each data point corresponds to a metal contained in the WHAM V database that was calibrated by experimental data. Lines are results from linear regression (equations are given in text).

Similar regressions between pK_{MHA} and monodentate carboxylic ligands such as acetate and benzoate appear to be slightly non-linear, or show considerably more scatter (Tipping, 1993). LFERs using acetate is shown in Figure 2a for Humic acid. Comparison of r^2 values between those shown for lactic acid indicates that there is more scatter about the regression line, but residuals do appear statistically independent. Similar analysis using $\log K_1$ for the bidentate ligands malonate is shown in Figure 2b. yield linear regressions that are linear, but contain considerable scatter.

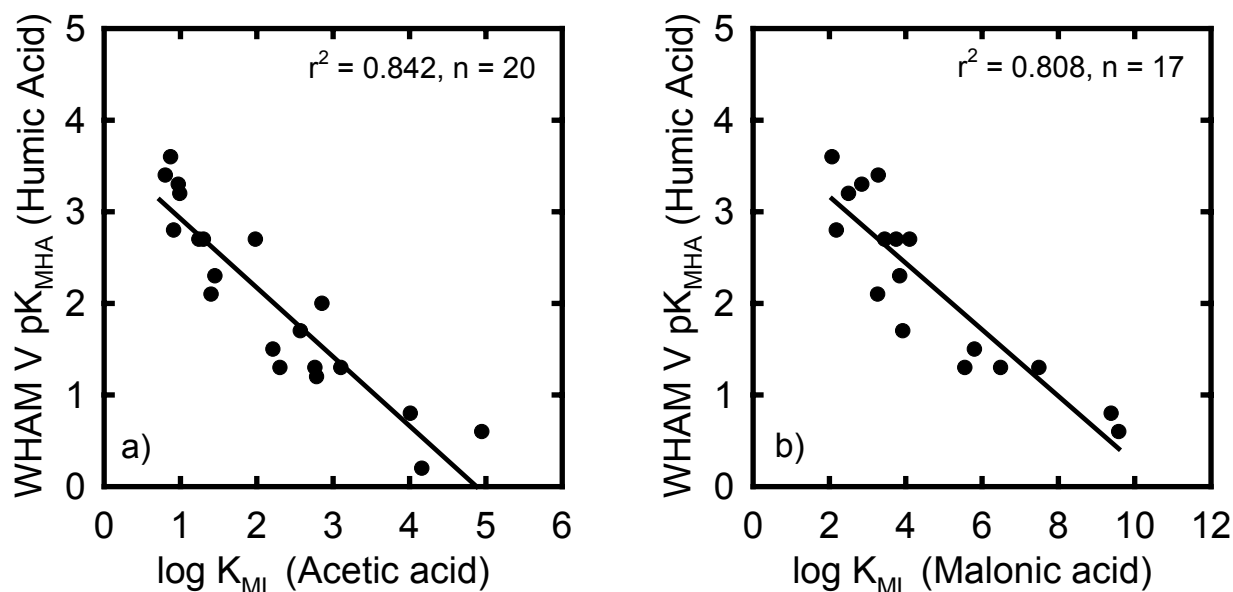


Figure 2. WHAM V pK_{MHA} for humic acid versus $\log K_{\text{ML}}$ for a) acetic acid and b) malonic acid. Solid lines are the results of linear regression analysis.

Irving-Rossotti Slopes

In the our previous paper (Carbonaro and Di Toro, 2006) work, a straight forward method was developed for estimating metal-ligand formation constants for monodentate complexes with negatively-charged oxygen donor atoms (Carbonaro and Di Toro, 2006). Data from the NIST Critical Database (Maretll et al., 2004) was used to develop linear free energy relationships (LFERs) of the form:

$$\log K_{\text{ML}} = \alpha_{\text{O}} \log K_{\text{HL}} + \beta_{\text{O}} \quad (3)$$

where α_{O} and β_{O} are the Irving-Rossotti slope and intercept respectively. The ligands selected for use in these LFERs met the following criteria: (i) they contain negatively-charged oxygen donor atoms (e.g. carboxylic acids and phenols), (ii) they are capable of only monodentate binding to metal ions, (iii) steric hindrances are not expected to influence the extent of metal-ligand binding, and (iv) they are electrically neutral when protonated. The relationship between $\log K_{\text{ML}}$ and $\log K_{\text{HL}}$ is linear for 24 metal ions with near-zero intercepts ($\beta_{\text{O}} = 0$). The magnitude of α_{O} indicates the preference for metal complexation with negatively-charged

oxygen donor atoms. Values for α_O are a good candidate for development of QSARs for metal-NOM binding parameters since NOM is comprised of the same functional groups.

Irving-Rossotti LFERs for WHAM V

In Figure 3, pK_{MHA} for humic and fulvic acid are plotted versus against α_O values taken from our previous work (Carbonaro and Di Toro, 2006). The resulting relationships appear linear. Linear regression analysis yielded the following equations:

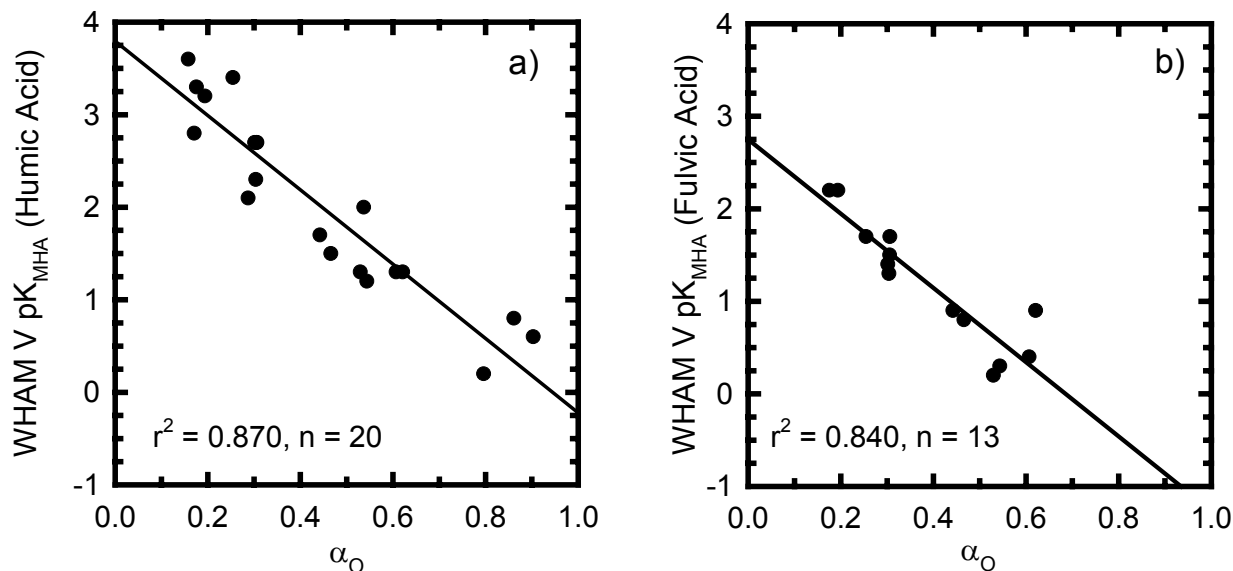


Figure 3. WHAM V pK_{MHA} versus the Irving-Rossotti slope for negatively-charged oxygen donor atoms, α_O . Solid lines are the results of linear regression analysis.

Values for α_O correlate extremely well with the pK_{MHA} value for humic acid and fulvic acid that are used in WHAM V. The advantage of using α_O over $\log K_{\text{ML}}$ for lactic acid is that α_O describes metal complexation with a series of monodentate oxygen donor atoms. While there is somewhat more scatter about the regression lines as compared to the lactic acid LFERs, the residuals appear statistically independent for both humic and fulvic acid.

Equations (4) and (5) were used to obtain estimates for pK_{MHA} for metal ions for in which WHAM V has not been calibrated (Table 1). In general, estimates using the Irving-Rossotti LFER are significantly different than those obtained using the lactic acid LFER.

$$\text{pK}_{\text{MHA}}(\text{HA}) = -4.16\alpha_O + 3.98 \quad r^2 = 0.886 \quad (4)$$

$$\text{pK}_{\text{MHA}}(\text{FA}) = -4.06\alpha_O + 2.88 \quad r^2 = 0.877 \quad (5)$$

Table 1. Published and estimated WHAM V pK_{MHA} values for Humic and Fulvic acid ^(a)

Metal	pK_{MHA} (Humic Acid)		pK_{MHA} (Fulvic Acid)	
	From Tippiig 1993	Estimated ^(b)	From Tipping 1993	Estimated ^(b)
<i>Alkaline Earths</i>				
Be ²⁺	<i>1.7</i>	2.05	<i>0.4</i>	1.01
Mg ²⁺	3.3	–	2.2	–
Ca ²⁺	3.2	–	2.2	–
Ba ²⁺	3.6	–	2.6	2.12
<i>First Row Transition</i>				
Mn ²⁺	3.4	–	1.7	–
Fe ²⁺	2.1	–	1.3	1.60
Co ²⁺	2.7	–	1.7	–
Ni ²⁺	2.7	–	1.4	–
Cu ²⁺	1.5	–	0.8	–
Zn ²⁺	2.3	–	1.3	–
Fe ³⁺	0.8	–	-0.2	-0.70
Cr ³⁺	0.5	0.51	0.1	-0.53
<i>Second Row Transition</i>				
Ag ⁺	–	3.08	–	2.04
Cd ²⁺	2.7	–	1.5	–
<i>Third Row Transition</i>				
Hg ²⁺	0.2	–	-0.3	-0.44
<i>Post-Transition Metals</i>				
Al ³⁺	1.3	–	0.4	–
Pb ²⁺	1.7	–	0.9	–
<i>Lanthanides</i>				
La ³⁺	–	2.13	–	1.09
Ce ³⁺	1.8	1.98	0.8	0.94
Eu ³⁺	1.3	–	0.2	–
<i>Actinides</i>				
Am ³⁺	1.2	–	0.3	0.57
Th ⁴⁺	0.6	–	-0.4	-0.87
UO ₂ ²⁺	1.3	–	0.9	–
Am ³⁺	1.2	–	0.3	–
Cm ³⁺	2.0	–	1.6	0.60

^(a)Values in bold were determined by calibration to experimental data; values in italics were estimated using regressions described in Tipping, 1993.

^(b)Estimated using equations (4) and (5).

Estimating Metal-Ligand Binding

Relationships between the coordinating tendencies of Lewis acids (metal ions) and Lewis bases (ligands) provide insight into the factors that govern metal-ligand complex formation.

Ahrland et al. (1958) classified metal ions as either Class A or B depending upon whether they formed their most stable complexes with the first ligand atom of each group of the Periodic Table. For example, Class A metal ions tended to prefer complex formation with oxygen as opposed to sulfur, and F^- as opposed to Cl^- , while Class B metal ions preferred the opposite. Pearson (1963) concluded that combinations of “like” acids and bases give the most effective interaction. “Hard” acids and bases were defined as those which are highly electronegative, have low polarization of valence electrons, and are most effective in electrostatic bonding (thus displaying class A behavior). “Soft” acids and bases were defined as those having large dipoles, are easily polarized and effectively form covalent bonds (thus displaying Class B behavior). While these relationships are very instructive and form the basis of many of our ideas about the coordination of Lewis acid and bases, their obvious shortcoming is their qualitative nature (Drago and Wayland, 1965).

Pre-dating the work of Ahrland and Pearson, Edwards (1954) formulated these ideas in quantitative terms. Using an extension of the Swain-Scott (1953) linear free energy relationship (LFER), Edwards used a “double-basicity” scale to relate the logarithm of the formation constant for metal-ligand complexation, K_1 , to the basicity and nucleophilicity of the Lewis Base:

$$\log \left(\frac{K_1}{K_0} \right) = \alpha E_n + \beta H \quad (6)$$

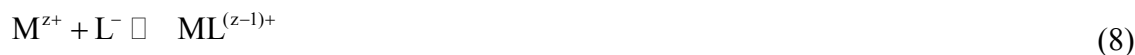
where K_0 is the reference formation constant for metal ligand complexation, E_n is a nucleophilic constant characteristic of an electron donor, H is the relative basicity of the donor to protons and is equal to the ligand $pK_a + \log 55.5$. The constants α and β are substrate constants that were parameterized for Cu^{2+} , Ag^+ , Au^+ , Zn^{2+} , Cd^{2+} , Hg^{2+} , In^{3+} , Pb^{2+} and Fe^{3+} . Using the Edwards equation, $\log K_1$ can be predicted for a series of monodentate ligands to within approximately 1 log unit.

Hancock and Marsicano (1978; 1980) building on the work of Pearson (1963; 1968), Edwards (1954), and Drago (1965; 1971), developed the following equation to calculate $\log K_1$ for metal ions with monodentate ligands.

$$\log K_1 = E_A^{aq} E_B^{aq} + C_A^{aq} C_B^{aq} - D_A D_B \quad (7)$$

where E_A^{aq} and E_B^{aq} represents the ionic contribution to the metal-ligand bond for the acid (A) and the base (B), C_A^{aq} and C_B^{aq} represents the covalent contribution to the metal-ligand bond for the acid (A) and the base (B), and D_A and D_B are a measure of steric hindrance to bond formation (Hancock and Marsciano, 1978; 1980). The 6 model parameters in Equation (7) were obtained via parameterization using literature data of $\log K_1$. E_A^{aq} , C_A^{aq} and D_A are available for 32 Lewis acids while values of E_B^{aq} , C_B^{aq} and D_B are available for 18 Lewis bases. Examples of Lewis bases included in the original parameterization include oxygen donor atoms (hydroxide ion, acetate), nitrogen donor atoms (ammonia, pyridine, azide) and halogens (chloride, fluoride, bromide, iodide ions). Equation (7) has excellent predictive capabilities as it is usually accurate to within 0.2 log units for alkaline earth and first row transition metals. In general, it appears to be slightly less accurate for second and third row transition metals, lanthanides and actinides.

A simpler method of predicting metal-binding constants can be made utilizing relationships between $\log K_1$ and the corresponding ligand pK_a (Martell and Hancock, 1996). For the following metal-ligand and proton-ligand binding reactions:



the corresponding mass action laws are

$$K_{\text{HL}} = \frac{\{\text{HL}\}}{\{\text{H}^+\} \{\text{L}^-\}} \quad (10)$$

$$K_{\text{ML}} = \frac{\{\text{ML}^{z-1}\}}{\{\text{M}^{z+}\} \{\text{L}^-\}} \quad (11)$$

where K_{HL} is the formation constant for protonation of a monodentate ligand and K_{ML} is the formation constant for the formation of a metal ligand complex with a 1:1 stoichiometry. Note that K_{ML} and K_{HL} are used in place of K_1 to avoid ambiguity between metal and proton complexation and that $\log K_{\text{HL}}$ is the equivalent of the ligand pK_a . Larsson (1934) was the first to make quantitative comparisons of $\log K_{\text{ML}}$ and $\log K_{\text{HL}}$, noting that the ratio of $\log K_{\text{ML}}$ to $\log K_{\text{HL}}$ was approximately a constant value of 0.3 for Ag^+ complexes with various amines. Calvin and Wilson (1945) examined Cu^{2+} complexes with β -diketone derivatives (e.g. acetylacetonate ion) in 50% dioxane-water mixtures, also noting a constant ratio between $\log K_{\text{ML}}$ and $\log K_{\text{HL}}$.

Irving and Rossotti (1956), after reviewing most of the previous literature on relationships between $\log K_{\text{ML}}$ and $\log K_{\text{HL}}$, noted that these linear free energy relationships (LFERs) have the following empirical form:

$$\log K_{\text{ML}} = \alpha \log K_{\text{HL}} + \beta \quad (12)$$

where α is the slope, and the intercept, β . A thorough thermodynamic treatment of this LFER is given by Irving and Rossotti (1956) and it is appropriate to refer to α as the Irving-Rossotti slope. Martell and Hancock (1996) showed that plots of $\log K_{\text{ML}}$ versus $\log K_{\text{HL}}$ for Fe^{3+} and UO_2^{2+} binding to monodentate ligand donor atoms with negatively charged oxygen donor atoms (substituted-phenols, carboxylic acids, hydroxide ion) are linear with intercept nearly equal to zero ($\beta \approx 0$) (1996). Thus, the magnitude of the formation constant for metal ligand complexation scales linearly with the basicity of the negatively charged oxygen donor atom (i.e. the $\log K_{\text{HL}}$ value of the ligand). According to Martell and Hancock (1996), this relationship is not derivable in any strict thermodynamic way, and is therefore best described as an “extra-thermodynamic relationship.”

Although the Hancock-Marsicano equation (Equation 7) is currently the most accurate and robust method for predicting metal complexation constants with monodentate ligands, it currently cannot be used for ligands which have not been included in its original parameterization. The Martell-Hancock LFER (Equation 12), however, does not suffer from this

limitation because $\log K_{HL}$ is known accurately for nearly all monodentate ligands of interest. The purpose of this paper is to examine the Martell-Hancock LFER for a large set of metal ions and assess its capabilities for estimating metal complexation constants with monodentate ligands, starting with ligands containing negatively-charged oxygen donor atoms, since data for these are the most abundant in the literature.

Analysis Methods

Thermodynamic Constant Selection Criteria and Ionic Strength Corrections

All thermodynamic constants were taken from NIST Critical Database (Martell et al., 2004), where metal-ligand and proton-ligand complexation reactions are described according to Equations (10) and (11). All K_{HL} and K_{ML} values were corrected to an ionic strength of $\mu = 0.0$ mol/L using the Davies Equation (1962) with $b = 0.3$. The Davies equation does an adequate job of correcting equilibrium constants to zero ionic strength for $\mu < 0.5$ mol/L (Morel and Hering, 1993). In many cases, however, constants from the NIST database were only available at $\mu = 1.0$ mol/L. For lack of a better method, the Davies equation was also used to correct these values. Constants listed at ionic strengths greater than 1.0 mol/L were not included in the analysis. The majority of the constants used in developing LFERs were listed at 25°C. However constants between 20°C to 30°C were used without correction. Constants outside of this range were not employed. A table of all the thermodynamic data is included in the Supplementary Information.

Regression Analysis

One-parameter (slope is fitted, intercept is set equal to zero) and two-parameter (slope and intercept are both fitted) linear regression analyses were performed using analytical solutions resulting from traditional minimization of least-squares approaches (Acton, 1966). In all cases, the number of data points used in the regression, n , is reported. Coefficient of determination (r^2) values are reported for one-parameter regressions when $n \geq 3$, and for two-parameter regressions when $n \geq 4$. Error estimates on slopes and intercepts from linear regression analysis represent 95% confidence intervals (Peters et al., 1974). Visual Basic for Applications (VBA) code was written so that all results from regression and statistical analyses could be calculating using Microsoft EXCEL. A copy of this code is available in Supplemental Information.

Results and Discussions

Martell-Hancock LFERs

Data for $\log K_{ML}$ was plotted versus the corresponding $\log K_{HL}$ of monodentate ligands containing negatively-charged oxygen donor atoms. In total, 24 metal ions were selected based upon availability of $\log K_{ML}$ data in the NIST database. One-parameter linear regressions of $\log K_{ML}$ versus $\log K_{HL}$ data was performed for each metal. The resulting Martell-Hancock LFER for Co^{2+} is shown in Figure 4. The Irving-Rossotti slope of the best-fit line was $\alpha = 0.304 \pm 0.013$ ($n = 9$), with $r^2 = 0.987$. The ligands used in the LFER are hydroxide ion, and the conjugate bases of substituted-carboxylic acids, nitrous acid, and phenol.

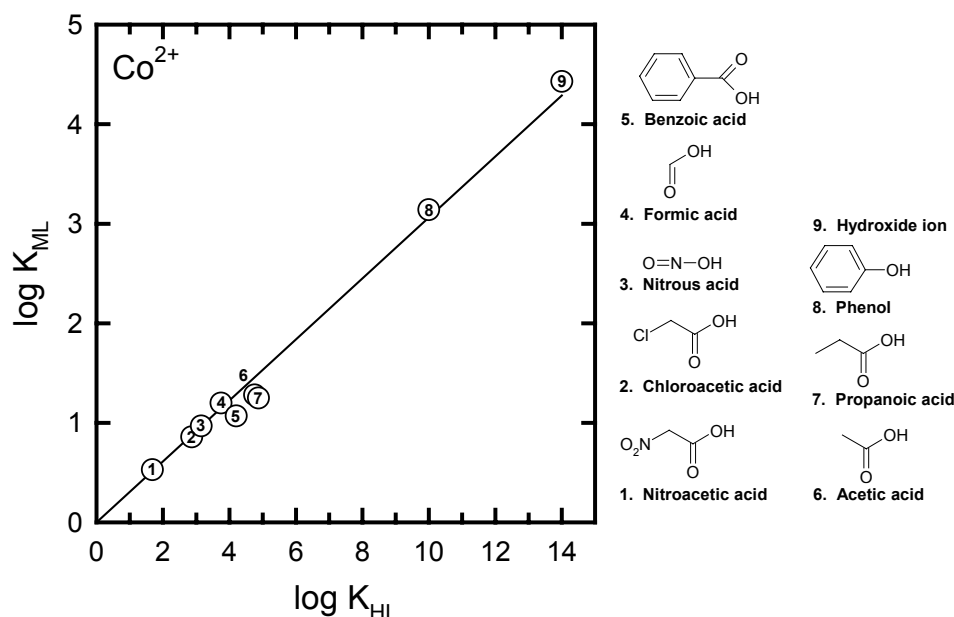


Figure 4. Plot of $\log K_{ML}$ for Co^{2+} versus the corresponding $\log K_{HL}$ for a series of monodentate ligands containing negatively-charged oxygen donor atoms. The solid line represents results from linear regression analysis with the intercept forced through zero (slope = 0.306 ± 0.017 , $r^2 = 0.987$).

The ligands employed in all LFERs were carefully selected such that they met the following four criteria: (i) they contain negatively-charged oxygen donor atoms with $\log K_{HL}$ values between 1 and 14, (ii) they are capable of forming only monodentate complexes with metal ions, (iii) steric hindrances to metal binding not expected to influence the extent of metal-ligand complexation, and (iv) the negatively-charged oxygen donor atom is the only functional group that imparts charge. These criteria were imposed to minimize contributions from other physical and chemical factors which may decrease or increase the extent of metal binding.

Ligands such as α -hydroxycarboxylic acids (e.g. lactic acid, glycolic acid), α -keto carboxylic acids (e.g. glyoxylic acid) were not included in LFERs. Despite the fact that the database reports one $\log K_{HL}$ value, they violate criteria (ii) because they are capable of forming bidentate complexes through the use of alcohol or carbonyl oxygen atoms (Portanova et al., 2003). Substituted-phenols with alkyl or halogen functional groups at ortho positions were excluded because they likely possess a steric hindrance to metal complexation thus violating criteria (iii). Ligands which possess acidic functional groups which impart negative charge (such as sulfonate groups) were excluded because they violate criteria (iv). The increased molecular charge contributed by these functional groups results in greater electrostatic attraction to metal ions which likely affects the value of $\log K_{ML}$ (Wilkins, 1962). Ligands with negatively charged oxygen donor atoms that meet the four criteria fall into the following four categories: substituted-aliphatic carboxylic acids (henceforth designated as R-COOH), substituted-benzoic acids (Ar-COOH), substituted-phenols (Ar-OH), and inorganic hydroxides (henceforth designated as Inorg-OH). A complete listing of these ligands is shown in Table 1, together with their value of $\log K_{HL}$ and NIST database ID.

If it is assumed for Co^{2+} that β is equal to zero in Equation (12), the slope resulting from the LFER shown in Figure 1 is the ratio of $\log K_{\text{ML}}$ to $\log K_{\text{HL}}$:

$$\alpha = \frac{\log K_{\text{ML}}}{\log K_{\text{HL}}} = \frac{\Delta G_{\text{ML}}^0}{\Delta G_{\text{HL}}^0} \quad (13)$$

Since the Irving-Rossotti slope α (Equation (13)) is independent of the ligand identity, metal to metal comparisons of α indicate the relative binding preference of a metal towards complexation with monodentate ligands containing negatively-charged oxygen donor atoms.

The zero intercept is an extremely convenient feature of these LFERs because only one metal-specific parameter (α) is required to estimate the metal-ligand formation constant for a monodentate ligand containing negatively-charged oxygen donor atoms. As previously mentioned (Hancock and Marsciano, 1980), a non-zero intercept results from these LFERs if units other than molarity are chosen to express concentration, or if equilibrium constants are written in terms of mole fractions. Since there was no obvious reason to transform equilibrium constants in this manner, the molar units were retained.

For consistency with the other acids listed in Table 2, it might be suspected that water should be placed on a molar concentration scale instead of a mole fraction scale. This would change $\log K_{\text{HL}}$ for water from 14.00 to 15.74 to account for the molarity of water in aqueous solution (55.5 M). As indicated in Figure 1, this modification was not made and a value of 14.00 was employed. Had a value of 15.74 been used, water would appear an outlier on all LFERs. Retaining $\log K_{\text{HL}}$ for water equal to 14.00 can be rationalized by converting $\log K_{\text{ML}}$ and $\log K_{\text{HL}}$ to their corresponding free energy changes, ΔG_{ML}^0 and ΔG_{HL}^0 . This effectively eliminates difficulties resulting from choice of standard and reference states. Plotting ΔG_{ML}^0 versus ΔG_{HL}^0 results in LFERs similar to those shown in Figure 4 with water falling on the regression line.

Table 2. Acid forms of the monodentate ligands used in LFERs

Name of acid	NIST ID	Functional Group	$\log K_{\text{HL}}^{(a)}$
Formic acid	3042	R-COOH	3.744
Acetic acid	3043	R-COOH	4.757
Propanoic acid	3045	R-COOH	4.874
Butanoic acid (Butyric acid)	3046	R-COOH	4.818
Pentanoic acid (Valeric acid)	3047	R-COOH	4.843
Caprioic acid	3048	R-COOH	4.857
Isobutyric acid	3051	R-COOH	4.849
Isovaleric acid	3057	R-COOH	4.781
Isohexanoic acid	3059	R-COOH	4.845
Isoheptanoic acid	3060	R-COOH	4.900
Isooctanoic acid	3061	R-COOH	4.930
Pivalic acid	3062	R-COOH	5.032
Allylacetic acid	3089	R-COOH	4.677
Hex-5-enoic acid	3091	R-COOH	4.719
Hept-6-enoic acid	3093	R-COOH	4.780
Phenylacetic acid	3099	R-COOH	4.31

^(c)At $\mu = 0.0$, $T = 25$ °C.

Table 2. Continued - Acid forms of the monodentate ligands used in LFERs

Name of acid	NIST ID	Functional Group	log K_{HL}^(a)
3-Phenylpropanoic acid	3101	R-COOH	4.664
4-Phenylbutanoic acid	3102	R-COOH	4.757
5-Phenylbutanoic acid	3103	R-COOH	4.860
6-Phenylbutanoic acid	3104	R-COOH	4.680
Chloroacetic acid	3136	R-COOH	2.862
Dichloroacetic acid	3137	R-COOH	1.10
3-Chloropropanoic acid	3144	R-COOH	4.11
Bromoacetic acid	3146	R-COOH	2.902
2-Bromobutanoic acid	3148	R-COOH	2.97
2-Bromopentanoic acid	3149	R-COOH	3.054
Iodoacetic acid	3154	R-COOH	3.175
3-Iodopropanoic acid	3156	R-COOH	4.10
Nitroacetic acid	3189	R-COOH	1.68
Cyanoacetic acid	3199	R-COOH	2.472
Benzoic acid	3098	Ar-COOH	4.202
3-Fluorobenzoic acid	3160	Ar-COOH	3.863
4-Fluorobenzoic acid	3161	Ar-COOH	4.131
3-Nitrobenzoic acid	3192	Ar-COOH	3.449
4-Nitrobenzoic acid	3193	Ar-COOH	3.442
Phenol	3806	Ar-OH	9.997
m-Cresol	3808	Ar-OH	10.095
p-Cresol	3809	Ar-OH	10.269
3-Fluorophenol	3827	Ar-OH	9.206
4-Fluorophenol	3828	Ar-OH	9.908
3-Chlorophenol	3832	Ar-OH	9.125
4-Chlorophenol	3833	Ar-OH	9.426
3-Bromophenol	3843	Ar-OH	9.031
4-Bromophenol	3844	Ar-OH	9.347
3-Iodophenol	3847	Ar-OH	9.033
4-Iodophenol	3848	Ar-OH	9.332
3-Nitrophenol	3851	Ar-OH	8.36
4-Nitrophenol	3852	Ar-OH	7.15
3-Cyanophenol	3865	Ar-OH	8.57
4-Cyanophenol	3866	Ar-OH	7.97
3-Hydroxybenzaldehyde	3910	Ar-OH	8.988
4-Hydroxybenzaldehyde	3911	Ar-OH	7.616
3-Acetylphenol	3924	Ar-OH	9.25
4-Acetylphenol	3925	Ar-OH	8.05
Boric acid	4721	Inorg-OH	9.236
Nitrous acid	4740	Inorg-OH	3.15
Chlorous acid	4797	Inorg-OH	1.96
Water	4708	Inorg-OH	14.00

^(c)At $\mu = 0.0$, $T = 25$ °C.

Irving-Rossotti Slopes for Negatively-Charged Oxygen Donor Atoms

The Martell-Hancock LFERs for 24 metal ions are shown in Figures 5 and 6. In all cases, the linear regression analyses were performed with the intercept forced through the origin. For some metal ions, data points exhibited undue weight on the best fit line and were excluded from the regression analysis. These are indicated with open circles and will be discussed later in more detail. Irving-Rossotti slopes, α_o , for all 24 metal ions and their 95% confidence intervals are reported in Table 3. Since slopes can also be obtained for other ligand donor atoms (e.g. nitrogen, sulfur), a subscript has been adopted to denote the ligand donor identity.

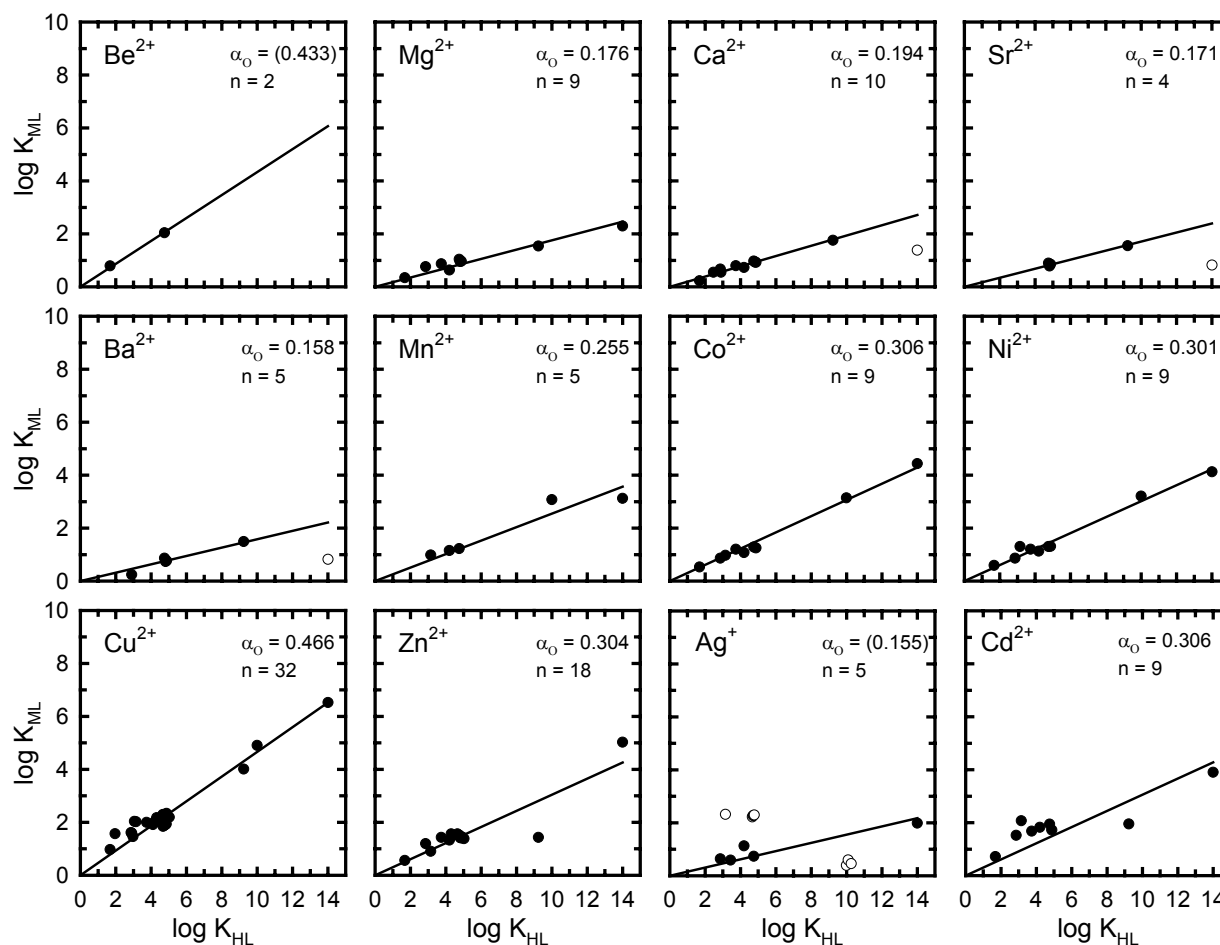


Figure 5. Plots of $\log K_{ML}$ for metal complex formation versus the corresponding ligand $\log K_{HL}$ for a series of monodentate ligands with oxygen donor atoms. Metals include alkaline earths, divalent first row transition metals, and second row transition metals. Solid lines represent results from linear regression with intercepts forced through zero. Irving-Rossotti slopes and the number of data points, n , are indicated on each plot.

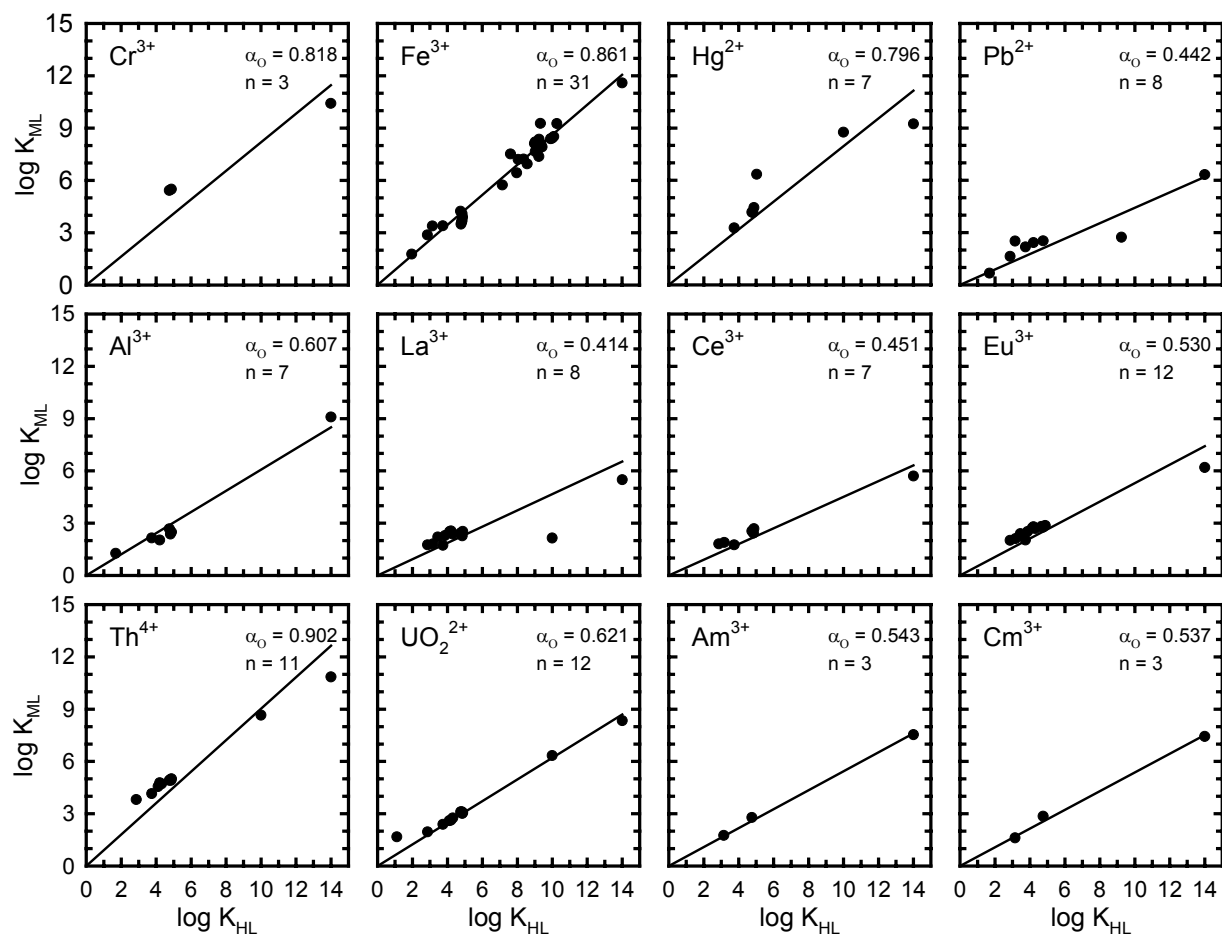


Figure 6. Plots of $\log K_{ML}$ for metal complex formation versus the corresponding ligand $\log K_{HL}$ for a series of monodentate ligands with oxygen donor atoms. Metals include trivalent first row transition metals, third row transition metals, aluminum, lanthanides and actinides. Solid lines represent results from linear regression with intercepts forced through zero. Irving-Rossotti slopes and the number of data points, n , are indicated on each plot.

Table 3. Oxygen Irving-Rossotti Slopes for metal cations

Metal	Irving-Rossotti Slope ^(a) , α_O	n	r^2
<i>Alkaline Earths</i>			
Be ²⁺	(0.433)	2	-
Mg ²⁺	0.176 ± 0.019	9	0.915
Ca ^{2+(b)}	0.194 ± 0.039	10	0.970
Sr ^{2+(b)}	0.171 ± 0.014	4	0.977
Ba ^{2+(b)}	0.158 ± 0.059	5	0.923
<i>First Row Transition</i>			
Mn ²⁺	0.255 ± 0.053	5	0.892
Fe ^{2+(c)}	(0.287)	1	-
Co ²⁺	0.306 ± 0.017	9	0.987
Ni ²⁺	0.301 ± 0.020	9	0.978
Cu ²⁺	0.466 ± 0.017	32	0.936
Zn ²⁺	0.304 ± 0.035	18	0.796
Fe ³⁺	0.861 ± 0.021	31	0.965
Cr ³⁺	0.818 ± 0.466	3	0.652
<i>Second Row Transition</i>			
Ag ⁺	(0.177)	5	-
Cd ²⁺	0.306 ± 0.078	9	0.390
<i>Third Row Transition</i>			
Hg ²⁺	0.796 ± 0.160	7	0.699
<i>Post-Transition Metals</i>			
Al ³⁺	0.607 ± 0.065	7	0.970
Pb ²⁺	0.442 ± 0.095	8	0.787
<i>Lanthanides</i>			
La ³⁺	0.467 ± 0.058	8	0.735
Ce ³⁺	0.451 ± 0.066	7	0.886
Eu ³⁺	0.530 ± 0.064	12	0.742
<i>Actinides</i>			
Am ³⁺	0.543 ± 0.043	3	0.998
Th ⁴⁺	0.902 ± 0.099	11	0.802
UO ₂ ²⁺	0.621 ± 0.034	12	0.971
Cm ³⁺	0.537 ± 0.064	3	0.995

^(a)Values in parenthesis are approximate.

^(b)K_{ML} for hydroxide ion omitted from this regression (see text for discussion).

^(c)Estimated via interpolation (see text for discussion).

First Row Transition Metals

Data for many of the common oxidation states of the first row transition metals (Mn²⁺, Co²⁺, Ni²⁺, Cu²⁺, Zn²⁺, Fe³⁺) were abundant, and one-parameter regression of data for log K_{ML} versus log K_{HL} yielded high r^2 values and small confidence intervals. The α_O value for Fe³⁺ that was obtained ($\alpha_O = 0.861 \pm 0.021$, $n = 31$) is nearly identical to that reported by Martell and

Hancock ($\alpha = 0.85$, $n = 13$) (Martell and Hancock, 1996), while using far more data. The α_O value for Cr^{3+} (0.812 ± 0.476) had a large confidence interval because only three $\log K_{\text{ML}}$ values were available in the database ($n = 3$). A LFER was not developed for Fe^{2+} because the ligand and thermodynamic selection criteria were met only by one ligand (hydroxide ion) in the database.

Across the first row transition metals with +2 charges, α_O values follow the following trend: $\text{Mn}^{2+} < \text{Co}^{2+} \approx \text{Ni}^{2+} < \text{Cu}^{2+} > \text{Zn}^{2+}$. Since α_O describes the overall binding strength of a metal with a series of negatively-charged oxygen donor ligands, it is logical that α_O values calculated here follow the Irving-Williams series (Schalfer and Gliemann, 1969). To estimate the α_O value for Fe^{2+} , it was assumed that its value was between that of Mn^{2+} and Co^{2+} , based on the Irving-Williams ordering. A method utilizing linear interpolation of $\log K_{\text{ML}}$ values of bidentate ligands containing negatively-charged oxygen donor atoms was used to estimate an α_O value of 0.287 for Fe^{2+} . This procedure is described in detail in the Supplementary Information.

Alkaline Earth Metals

Compared to some of the other metal ions surveyed, data for alkaline earth metals were far more limited. Most notably, there were only two ligands for Be^{2+} , which met the selection criteria. Furthermore, data for alkaline earth metal complexation with substituted-phenols was completely lacking from the database. Preliminary linear regressions of the data that were available revealed that the hydroxide ion $\log K_{\text{ML}}$ for Ca^{2+} , Sr^{2+} and Ba^{2+} exhibited undue weight on the regression line. As a result, $\log K_{\text{ML}}$ for hydroxide ion was excluded from the final regression analyses. Values of α_O for alkaline earth metals decreased with increasing ionic radii according to the following: $\text{Be}^{2+} \gg \text{Mg}^{2+} \approx \text{Ca}^{2+} > \text{Sr}^{2+} > \text{Ba}^{2+}$.

Despite differences in coordination number and geometry, the alkaline earth metals exist as +2 metal ions in aqueous solution, and tend to form complexes with a large degree of ionic character as a result of their low electronegativity (Richens, 1997). Ionic bonding is usually described as resulting from electrostatic attractive forces between opposite charges, which increase with decreasing separation distance between ions. Thus, the trend of increasing α_O with decreasing ionic radii supports the importance of ionic bonding for alkaline earth metals. Be^{2+} is slightly different from the rest of the of the alkaline earth metals in that its ionic radii is considerable smaller. It is far more electronegative than its heavier counterparts and therefore engages in significant covalent bonding (Richens, 1997). This is exemplified by its α_O value which is far larger than the rest of the alkaline earth metals.

Lanthanides and Actinides

Three lanthanides (La^{3+} , Ce^{3+} , Eu^{3+}) and four actinides (Th^{4+} , UO_2^{2+} , Am^{3+} , Cm^{3+}) were selected to determine if the Martell-Hancock approach can be extended to f-block metal ions. In general, plots of $\log K_{\text{ML}}$ versus $\log K_{\text{HL}}$ were highly linear, and one-parameter linear regressions yielded adequate fits to the data. The resulting value of α_O for UO_2^{2+} (0.621 ± 0.034 , $n = 13$) is nearly identical to that reported by Martell and Hancock (0.63). The α_O values for the lanthanides increased with increasing atomic number such that $\text{La}^{3+} < \text{Ce}^{3+} < \text{Eu}^{3+}$. Th^{4+} had the largest α_O value (0.902) of all metal ion surveyed.

The uranyl ion, UO_2^{2+} , is the stable form of the +VI oxidation state of uranium. It is unlike any of the other metal ions surveyed in that the “aqua ion” contains ligands other than water. It is coordinated by two oxygen atoms in the axial direction, but readily adds 4 to 6 ligand donor atoms in its equatorial plane (Richens, 1997). When coordinated only to water molecules,

there are five water molecules in the equatorial plane, and it is usually written as $[\text{UO}_2(\text{H}_2\text{O})_5]^{2+}$ (Richens, 1997). Despite these differences, it readily forms complexes with Lewis bases in aqueous solution and the LFER presented in Figure 4 represents an excellent fit to the $\log K_{\text{ML}}$ versus $\log K_{\text{HL}}$ data.

It is well known that metal ions within the lanthanide series possess similar chemical properties. Since the three lanthanides had the same ionic charge, it is not surprising that their α_{O} values had only slight differences in value. Lanthanide ions are weakly electronegative, engaging in primarily ionic bonding (Richens, 1997). Moving from left to right across the period, the ionic radius of each lanthanide trivalent ion steadily decreases, a phenomenon known as “lanthanide contraction.” Their increasing α_{O} values across the period can be explained on the basis of the lanthanide contraction which results in increasing electrostatic attraction and larger $\log K_{\text{ML}}$ values.

Other Metal Ions

Plots of $\log K_{\text{ML}}$ versus $\log K_{\text{HL}}$ for Cd^{2+} (a second-row transition metal), Hg^{2+} (a third-row transition metal), Al^{3+} and Pb^{2+} (post-transition metals) showed linear relationships. However, there was considerable error about the regression line for Cd^{2+} and Hg^{2+} which resulted in lower r^2 values and larger confidence intervals than that observed for the metal ions discussed previously. There was considerable scatter in the data for Ag^+ , which prevented the development of a reliable LFER. For Ag^+ the data for allylacetic acid, hex-5-enoic acid, hept-6-enoic acid, phenol, m-cresol, and p-cresol was not used in the LFER. Justification is provided in the Supporting Information. The resulting value of α_{O} for Ag^+ was 0.177. In addition, $\log K_{\text{ML}}$ for nitrous acid is extremely large compared to the substituted carboxylic acids possessing similar $\log K_{\text{HL}}$ values, and may possibly be considered an outlier. Removing nitrous acid from the regression yielded a slope equal to 0.155.

Relationship of Proton and Metal Ligand Complexes

The values for α_{O} from all 24 LFERs were all less than 1.0, ranging from 0.158 for Ba^{2+} to 0.902 for Th^{4+} . A simple combination of Equations (10) – (12) results in the following relationship (assuming $\beta = 0$):

$$\log \frac{\{\text{ML}^{z-1}\}}{\{\text{HL}^0\}} = (1 - \alpha) \log K_{\text{HL}} + \log \frac{\{\text{M}^{z+}\}}{\{\text{H}^+\}} \quad (14)$$

Given equivalent metal ion and proton activities, this equation reduces to:

$$\log \frac{\{\text{ML}^{z-1}\}}{\{\text{HL}^0\}} = (1 - \alpha) \log K_{\text{HL}} \quad (15)$$

Since $\alpha < 1.0$, the right-hand side of Equation (14) will always be negative, and therefore $\{\text{ML}^{z-1}\}$ is always less than $\{\text{HL}^0\}$. This indicates that protons will always out-compete metal ions for complexation of monodentate ligands given equal activities of free metal ion and hydrogen ion (i.e. when $\{\text{M}^{z+}\} = \{\text{H}^+\}$). Logically, this is not true for multidentate ligands where chelation leads to significantly larger $\log K_{\text{ML}}$ values than those for monodentate ligands.

Correspondingly, plots of $\log K_{ML}$ versus $\log K_{HL}$ for a chelating ligands such as derivatives of 8-hydroxyquinoline yields slopes greater than 1.0 (Irving and Rossotti, 1954).

Relationship Between the Irving-Rossotti Slope and C_A^{aq}

As a result of the zero intercept, the Martell-Hancock LFER is closely related to the parameterization developed by Hancock and Marsicano (1978; 1980). Since Equation (7) is underdetermined, C_A^{aq} was defined as $\log K_1$ (hydroxide) divided by 14.0 (the ion product for water, $\log K_w$) (Hancock and Marsicano 1978). Dividing by $\log K_w$ was done to give numbers of a more convenient size (Hancock and Marsicano 1978). This effectively sets E_B^{aq} and D_B^{aq} equal to zero, and C_B^{aq} equal to 14.00. This can be seen by examining Eq. (2) for proton (A) binding to hydroxide (B). For metal binding to hydroxide ion, Equation (7) reduces to the following:

$$\log K_1 = C_A^{aq} C_B^{aq} \quad (\text{since } E_B^{aq} \text{ and } D_B^{aq} = 0) \quad (16)$$

Equating Equation (12) (assuming $\beta = 0$) and Equation (16) we obtain:

$$\alpha_O \log K_{HL} = C_A^{aq} C_B^{aq} \quad (17)$$

and since $C_B^{aq} = \log K_{HL} = 14.00$,

$$\alpha_O = C_A^{aq} \quad (18)$$

Thus, the Hancock and Marsicano C_A^{aq} parameter is the equivalent of the Irving-Rossotti slope for negatively-charged oxygen donor atoms. A plot of C_A^{aq} versus α_O for 16 metal ions is shown in Figure 7. The data fall very close to the 1:1 line, confirming the result obtained from Equation (18). Note that one of the data points falling furthest from the 1:1 line is Ca^{2+} . As discussed earlier, for alkaline earth metals values of $\log K_{ML}$ for hydroxide ion are lower than what would be predicted by the Martell-Hancock LFER. Thus, C_A^{aq} (and Equation (16)) does not adequately describe the overall coordination tendency of heavier alkaline earth metals (Ca^{2+} , Sr^{2+} , Ba^{2+}) with oxygen donor atoms. Equations (16)-18) show that the Hancock and Marsicano approach can be extended for monodentate negatively-charged oxygen containing ligands that were not included in its original parameterization.

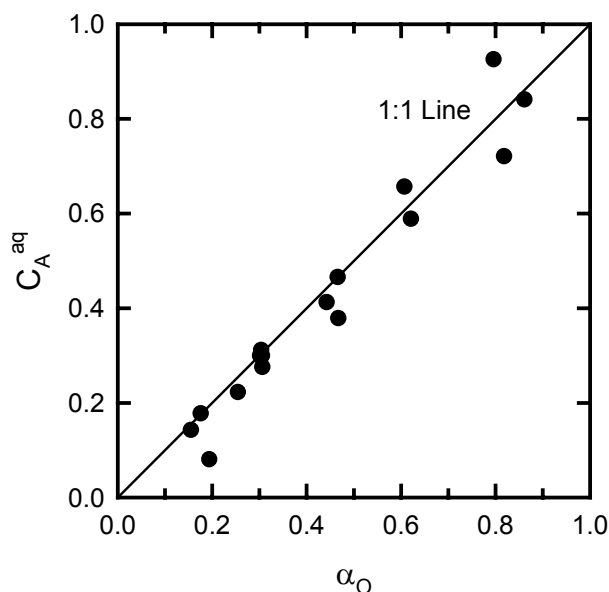


Figure 7. Plot of the Hancock-Marsicano parameter, C_A^{aq} , versus the Irving-Rossotti slope for oxygen donor atoms, α_O , for all metal ions for which both parameters have been determined.

It is also apparent that the approximate 1:1 ratio between C_A^{aq} and α_O can be used to estimate α_O for metals where there is not sufficient data in the database to construct Martell-Hancock LFERs. For example, C_A^{aq} values have been determined for Na^+ , Li^+ , Au^+ , Cu^+ , CH_3Hg^+ , Sn^{2+} , Pd^{2+} , Tl^{3+} , In^{3+} , Bi^{3+} , $\text{V}^{\text{VI}}\text{O}^{2+}$, Ga^{3+} , Lu^{3+} , Y^{3+} , U^{4+} , and Pu^{4+} . Formation constants for complexation of these metal ions with monodentate ligands containing negatively-charged oxygen atoms can therefore be estimated using combination of Equations (12) and (18).

Applications for Irving-Rossotti Slopes

The most obvious application of Irving-Rossotti slopes is estimation of metal complexation constants with monodentate ligands for which experimental data does not exist. Since, only the $\log K_{\text{HL}}$ is required, calculation of $\log K_{\text{ML}}$ is straightforward. An extension of this approach to multidentate ligands is also possible as will be discussed in a future paper. In addition, the information provided by the Irving-Rossotti slopes α is directly applicable to metal binding to natural organic matter (NOM). Since NOM consists of various different types of oxygen and nitrogen containing functional groups, relationships between $\log K_{\text{HL}}$ and $\log K_{\text{ML}}$ will likely be useful in modeling metal ion complexation by NOM.

At the present time, availability of data for metal complexation with monodentate ligands hinders further extension of these LFERs. Use of α_O values for some of the metal ions presented here must be done with caution because of the lack of thermodynamic data. Surprisingly, data for some of the environmentally important metal ions (most notably Fe^{2+} and Cr^{3+}) is mostly lacking for ligands containing negatively-charged oxygen donor atoms.

Conclusions

The method presented above, equations (4) and (5), are superior to previously available QSARs for WHAM parameters. They are based on a more fundamental relationship between the proton and metal binding constants to oxygen containing ligands. They rely only on the pKa of the ligand, and for NOM, they are the starting point for any modern model of metal-NOM partitioning. Finally they can be used to provide estimates of other important parameters, such as the WHAM VI partitioning parameters. This is the subject of a forthcoming paper.

Literature Cited

- Acton, F. (1966) *Analysis of Straight Line Data*; Dover Publications, Inc.: New York, NY.
- Arhland, S., Chatt, J., and Davies, N. (1958) *Quarterly Reviews of the Chemical Society* 12:265-276.
- Benedetti, M.F., Milne, C.J., Kinniburgh, D.G., Vanriemsdijk, W.H., and Koopal, L.K. (1995) *Environ. Sci. Technol.* 29:446-457.
- Calvin, M. and Wilson, K.W. (1945) *J. American Chemical Society* 67:2003-2007.
- Carbonaro, R.F., and Di Toro, D.M. (2006) *Estimating Metal Ligand Binding Section* (this report).
- Davies, C.W. (1962) *Ion association*; Butterworths: Washington D.C.
- Di Toro, D.M., Allen, H.E., Bergman, H.L., Meyer, J.S., Paquin, P.R., and Santore, R.C. (2001) *Environ. Toxicol. Chem.* 20:2383-2396.
- Drago, R.S.; Vogel, G.C.; and Needham, T.E. (1971) *J. American Chemical Society* 93:6014-6026.
- Drago, R.S.; and Wayland, B.B. (1965) *J. American Chemical Society* 87:3571-5577.
- Dudal, Y., and Gerard, F. (2004) *Earth-Science Reviews* 66:199-216.
- Edwards, J.O. (1954) *J. of the American Chemical Society* 76:1540-1547.
- Farley, K.J. (2006).
- Gustafsson, J.P. (2001) *J. Coll. Inter. Sci.* 244:102-112.
- Hancock, R.D., and Marsciano, F. (1978) *Inorg. Chem.* 17:560-564.
- Hancock, R.D., and Marsciano, F. (1980) *Inorg. Chem.* 19:2709-2714.
- Irving, H. and Rossotti, H. (1956) *Acta Chemica Scandinavica* 10:72-93.
- Irving, H. and Rossotti, H.S. (1954) *J. American Chemical Society* 76:2910-2918.
- Larsson, E.Z. (1934) *Phys. Chem., A* 169:215.
- Martell, A.E.; and Hancock, R.D. (1996) *Metal Complexes in Aqueous Solution*; Plenum Press: New York.
- Martell, A.E.; Smith, R.M.; and Motekaitis, R.J. (2004) 8.0 Edition.; NIST.
- Morel, F.M.M.; and Hering, J.G. (1993) *Principles and Applications of Aquatic Chemistry*; J. Wiley & Sons, Inc.: New York.
- Pearson, R.G. (1968) *J. Chemical Education* 45(9):581-&.
- Pearson, R.G. (1963) *J. American Chemical Society* 85(22):3533-&.

- Peters, D.G.; Hieftje, G.M.; and Hayes, J.M. (1974) *Chemical Separations and Measurements: Theory and Practice of Analytical Chemistry*; Saunders College Publishing: Philadelphia, PA.
- Portanova, R.; Lajunen, L.H.J.; Tolazzi, M.; and Piispanen, (2003) *J. Pure and Applied Chemistry* 75:495-540.
- Richens, D.T. (1997) *The Chemistry of Aqua Ions*; John Wiley & Sons: West Sussex, England.
- Santore, R.C.; Di Toro, D.M.; Paquin, P.R.; Allen, H.E.; and Meyer, J.S. (2001) *Environ. Toxicol. Chem.* 20:2397-2402.
- Schalfer, H.L. and Gliemann, G. (1969) *Basic Principles of Ligand Field Theory*; Wiley-Interscience: New York.
- Swain, C.G.; and Scott, C.B. (1953) *J. American Chemical Society* 75(1):141-147.
- Tipping, E. (1998) *Aquat. Geochem.* 4:3-48.
- Tipping, E. (1994) *Comput. Geosci.* 20:973-1023.
- Tipping, E., and Hurley, M. (1992) *Geochim. Cosmochim. Acta* 56:3627-3641.
- Tipping, E., Lofts, S., and Lawlor, A.J. (1998) *Sci. Tot. Environ.* 210:63-77.
- Wilkins, R.G. (1962) *Quarterly Reviews* 16:316-342.

Developing a Unit World Model for Metals in Aquatic Environments

Dominic M. Di Toro
Department of Civil and Environmental Engineering
University of Delaware
Newark, DE 19716

George W. Luther III
College of Marine and Earth Studies
University of Delaware
Lewes, DE 19958

and

Kevin J. Farley
Department of Environmental Engineering
Manhattan College
Riverdale, NY 10471

Introduction

There has been, and continues to be, interest in developing methods for evaluating the environmental hazard associated with the release of metals and metal compounds to the environment (Adams et al., 2000). These procedures should include the major processes that affect the fate of metals. However, existing methods (e.g. Mackay, 1992) were developed for organic chemicals and ignore many of the processes that determine the long-term fate of metals in the environment. Furthermore, unlike most organic chemicals, the total metal concentration is not the bioavailable fraction. There is a clear need for a more comprehensive approach to estimating the persistence, bioaccumulation, and toxicity of metals and metal compounds that takes into account these metal specific processes. The purpose of this project is to build such a model – the Unit World Model.

Approach

Environmental fate and transport models have been used to conduct exposure assessments for metals (e.g. O'Connor, 1988; Diamond, 1990; Di Toro et al., 1991). However these models did not address the specific issues of persistence, bioaccumulation, and toxicity of metals. To be useful the model should include the major processes that determine the long term fate of metals in an aquatic environment. These include partitioning to suspended particles, and transport to and from the sediment. The bioaccumulation and toxicological effects of metals in each of these environmental compartments would be addressed by the addition of suitable representations of metal bioavailability and bioaccumulation. This model would represent a standard aquatic environment, a “unit world”. The general concept of a unit world modeling approach is not new. It has previously been applied in various forms to pesticides (USEPA, 1986) and industrial organic chemicals (Mackay, 1991; Mackay et al., 1992, European Commission, 1996).

The model is designed to represent the major processes that determine the fate and transport of metals in the aquatic environment. In the water column these processes include solubilization, complexation with dissolved ligands, and partitioning to suspended particles. The Biotic Ligand Model (BLM) has recently been developed (USEPA, 1999, 2000; Di Toro, et al., 2000; Santore et al., 2000, Paquin et al., 2002) and can be used to compute the complexation of metals to dissolved ligands. A particle sorption model SCAMP (Lofts and Tipping, 1998) has also recently become available as part of the WHAM 6 program (Tipping, 1998). The sorption of metals to particulate matter leads to the transfer of the metal to the bottom sediments. Hence, sediments are the ultimate repository of metals in aquatic settings. It is for this reason that an approach for evaluating the fate, bioavailability, and toxicity of metals in the sediments is important. For metals, EPA has developed sediment quality guidelines that are based on the relative magnitudes of acid volatile sulfide AVS and simultaneously extractable metal SEM, and organic carbon (Di Toro et al., 1990, 1992; Ankley et al., 1993, 1996; USEPA, 2000). A number of sediment models have been developed that successfully predicts levels of AVS and SEM in sediments and resulting fluxes of dissolved metal from the sediments to the overlying water column (Di Toro, 1996; Carbanaro, 1999; Di Toro, 2001). Therefore the frameworks exist, for at least most of the processes in various stages of development, for the water column and sediment compartments.

In order to produce a unit world, it is necessary to synthesize these components into a unified modeling framework, and then to test the model with laboratory and field data for a

variety of metals. The model has been applied to mesocosm studies and selected field sites for model calibration and validation. Based on these results, a screening level model for the transport and fate of metals in aquatic systems has been developed for an intact aquatic environment; i.e., a “Unit World.” Toxicological effects of metals in the water column and sediment compartments are included by the addition of suitable representations of metal bioavailability.

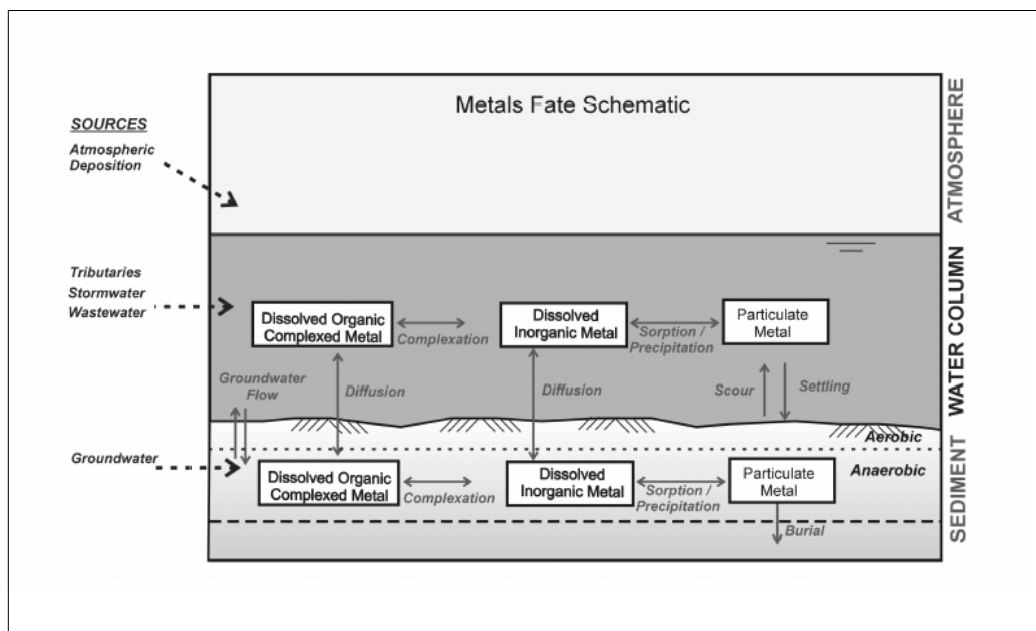


Figure 1. Schematic diagram for the fate of metals in aquatic environments

A conceptual model framework for the transport and fate of metals in aquatic systems is given in Figure 1. In this diagram, metals enter the aquatic environment via surface runoff, storm water flow, groundwater inflow, atmospheric deposition, and direct discharges of wastewater. In the water column and sediments, the metals are distributed among the dissolved inorganic phase (which can include both the ionic form and inorganic complexes of the metal), the dissolved organically complexed phase, and the particulate phase (which can include sorbed metal, newly precipitated metal, and stable mineral phases). The specific distribution of metals will depend on chemistry in the water column and the sediments. For example, the pH, hardness, salinity, total dissolved solids, and dissolved organic carbon impact the distribution of metals in the water column, and particulate concentration of metal in anaerobic sediments typically include significant levels of metal sulfides. The transfer of metal between the water column and the sediment is dependent on the physics of the system (which controls the movement of water and particles), and on the chemistry (which controls the distribution of metal among dissolved and particulate phases).

Review of Current Models for Metal Speciation and Organic Carbon Cycling

Although simple partitioning models are useful for preliminary evaluations of field data, these models do not provide a predictive method for determining distributions among the various metal phases, or ultimately, the transport, fate and bioavailability of metals in aquatic

environments. In addition, simple partitioning models do not provide any information on how water chemistry may change in time or space (e.g., seasonal variations in organic carbon cycling and redox chemistry that are associated with phytoplankton growth and organic matter decomposition). A number of models have previously been developed to address issues of metal speciation and bioavailability, and organic carbon cycling and redox chemistry in aquatic systems. A brief review of the models used in the development of the “unit world” model for metals is given below.

Windermere Humic Aqueous Model (WHAM, Model V) (Tipping, 1994)

WHAM V describes the binding of metals to natural organic matter by considering a distribution of eight monodentate and twelve bidentate site types on humic and fulvic acids. In the model, metal binding to specific site types is a function of intrinsic binding constants and electrostatic interactions at humic and fulvic acid surfaces. Accumulation of counterions in the Donnan layer is also considered. The intrinsic binding constants in WHAM V are based on a generalized description of metal binding to the various site types, and have been calibrated to a large number of published data sets. More recently, the model has been extended to include tridentate metal complexes and a more specific (i.e., less generalized) description of metal binding to the various site types (WHAM VI, Tipping, 1998).

SEM-AVS (Di Toro et al. 1990; Di Toro et al. 1992)

The SEM-AVS method has been shown to be a useful approach for evaluating toxicity of Cd, Cu, Ni, Pb, Zn in sediments. In this approach, acid volatile sulfide (AVS) serves as a reliable indicator of bioavailable metal concentrations in sediment pore water. The rationale is that AVS, which is present in sediment as FeS(s), will react with the SEM (i.e., the concentration of Cd, Cu, Ni, Pb, Zn that are simultaneously extracted with sulfide) and form insoluble metal sulfides that are relatively non-available for uptake by benthic organisms. Accordingly, if the AVS is greater than the SEM (i.e., $SEM / AVS < 1$ or $SEM - AVS < 0$), excess AVS exists and all the metals are present as insoluble non-toxic metal sulfides. The lack of toxicity for $SEM / AVS < 1$ has been confirmed in spiked and field contaminated sediments (Berry et al. 1996, Hansen et al. 1996). Because the SEM-AVS method does not explicitly consider other sediment phases that can influence pore water concentrations, the method is appropriate for predicting the lack of toxicity for the $SEM / AVS < 1$ condition.

Biotic Ligand Model (BLM) (Di Toro et al. 2001)

The concept of the BLM is based on the gill surface interaction model for trace metal toxicity to fish (Pagenkopf, 1983), and the finding of Playle et al. (1993) who showed through laboratory study that the toxicity of the dissolved metal is proportional to the accumulation of the metal on the gill. In the BLM, the concentration of metal accumulating on the gill surface is described by (1) the free metal ion activity which is dependent on metal binding to inorganic and organic ligands in solution, and (2) competition of metals and major cations for sites on the gill surface. In extending this construct from fish to all aquatic organisms, the more general term "biotic ligand" is used to denote the site of action for metal binding. In the BLM, WHAM V (Tipping, 1994) is used to describe metal binding to dissolved organic carbon (DOC) and other ligands in the solution phase. The binding of metals and major ions to the gill surface as proposed by Playle et al. (1993) are described by equilibrium constants given in Di Toro et al. (2001). Preliminary results also show the potential utility of extending the BLM for predicting

metal toxicity in sediment (Di Toro 2005). More complete descriptions of WHAM, SEM-AVS, and BLM, are given in Euras (2005).

Sediment Flux Model (Di Toro, 2001). The sediment flux model quantifies the processes in sediments that determine the extent to which materials that settle to the sediment are recycled to the water column. It is the flux of materials to and from the water column that is the primary focus. The substances considered are the nutrients: ammonia, nitrate, phosphate, and silica; dissolved oxygen and the metals: calcium, manganese, iron, and cadmium. They were chosen primarily because of their importance in water quality problems: eutrophication and its consequences (N, P, Si), low dissolved oxygen with its attendant severe biological impacts□ excessive concentrations of toxic metals (Mn, Cd), and for their importance to other processes (Ca, Fe).

Of most importance to the development of the Unit World model is the treatment of organic matter diagenesis and the production of AVS since both organic carbon and AVS greatly affect the distribution of metals in the sediment and their toxicity and are required for the SEM-AVS model of sediment toxicity.

Preliminary Modeling Studies

A simple description for the transport and fate of metals in lakes, which is based on previous models for hydrophobic organic contaminants like PCBs, PAHs and pesticides (Di Toro et al., 1984; O'Connor 1988a,b; Mackay, 1991; Mackay and Paterson, 1992), is described schematically in Figure 2. In this approach, metals can enter the lake via surface runoff, storm water flow, groundwater inflow, atmospheric deposition, and / or direct discharges. In the water column and the surficial sediment layer, metals are distributed between the dissolved phase (which can include the ionic form of the metal, as well as dissolved inorganic and organic complexes) and the particulate phase (which can include metal sorbed to particulate organic matter, hydrous iron oxides, manganese oxides, clays, etc., newly precipitated metal, and stable mineral phases).

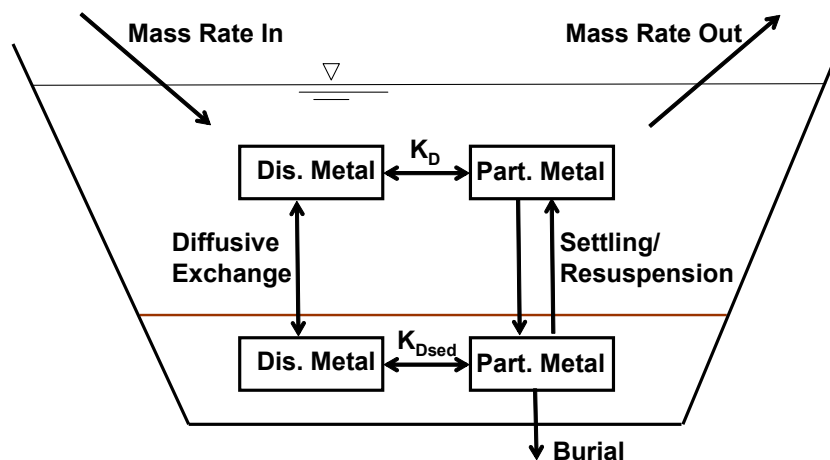


Figure 2. Simple partitioning (K_D) model for metals in lakes.

The specific distribution of metals between the dissolved and particulate phases depends on water chemistry. For example, pH, hardness, DOC, POC, and AVS will affect the

distribution of metals between dissolved and particulate phases in the water column and in the surficial sediment layer. The transfer of dissolved and particulate phase metal between the water column and the surficial sediment layer is controlled by diffusive exchange and settling / resuspension rates. Loss of metal from the lake is associated with the outflow of dissolved and particulate metal from the lake, and from burial of metal to the deeper sediments.

For preliminary model evaluations, the distribution of metal between the dissolved and particulate phases can be assumed to be in dynamic equilibrium and described by an equilibrium partition coefficient (K_D). A time-variable version of this simple partitioning model was constructed in Visual Basic for Applications (VBA) for EXCEL to examine field data from enclosures in Perch Lake (a Canadian soft water lake) and Lake Baldegg (a Swiss hard water lake) as described below.

Perch Lake, Canada

Spike additions of several radio-labeled metals including ^{57}Co , ^{59}Fe , ^{65}Zn , and ^{203}Hg , were added to enclosures in Perch Lake (Diamond et al., 1990). The enclosures were 0.78 m diameter and 2 m deep, and were sealed to prevent inflow of ambient lake water. Concentrations of the metals were monitored over a period of twenty one days to examine the rate of metal loss to the underlying sediments. After twenty one days, the overlying waters in some enclosures were flushed for three days, a new enclosure was placed above the contaminated sediment, and the overlying waters were monitored for an additional fifty days to examine the release of radio-labeled metal from the contaminated sediments.

For model evaluations, partition coefficients for metal in the overlying water and the surficial sediment layer were adjusted separately to match observed water column concentrations. All other model parameters and coefficients were taken directly from Diamond et al. (1990) and are summarized in Table 1.

A comparison of model and observed concentrations for zinc (^{65}Zn) in the overlying water are shown in Figure 3. Results show that the simple K_D partitioning model overall provides a good description of metal concentrations in the enclosures with a consistent set of K_D 's for both the initial twenty one day contamination period and the subsequent release of zinc from sediments. A deviation in model results and observations is apparent at the end of the study and may be related to leakage from the enclosure or binding of metal to the enclosure wall. In addition, lower K_D values for the surficial sediment layer were obtained for all metals examined. Based on our assumption that organic carbon is likely to be the dominant metal binding phase in Perch Lake water column and the underlying aerobic sediments, this result is consistent with expectations for lower organic carbon fractions in sediments compared to overlying waters.

Table 1. Summary of Model Inputs for Lake Enclosures

	Perch Lake ^a	Lake Baldegg ^b
Diameter (m)	0.78	12
Surface Area (m ²)	0.5	113
Water Depth (m)	2	10
Flow (m ³ / day)	0	11.5
Suspended Solids (mg / L)	2	1.4
Active Sediment Depth (cm)	1	1.5
Sediment Porosity	0.95	0.7
Bulk Density of Sediment (kg / L)	1.025	
Sediment Solids (mg / L)	75000	750000
Settling Velocity (m / day)	0.3	0.4
Resuspension (m / day)	0	4 x 10 ⁻⁷
Water Column - Pore Water Diffusive Exchange Coefficient (cm / day)	5	5
Radioactive Half Life (days)	⁵⁷ Co: 271.8 ⁵⁹ Fe: 44.5 ²⁰³ Hg: 46.6 ⁶⁵ Zn: 244.2	
Incoming Concentration (µg / L)		Cd: 5.1 Cu: 11.4 Hg: 1.0 Pb: 49.7 Zn: 209
Initial Metal Concentrations (µg / L)		Cd: 0.067 Cu: 1.27 Hg: 0.0 Pb: 0.21 Zn: 6.5

^aFrom Diamond et al. 1990

^bFrom Gatcher and Mares, 1979

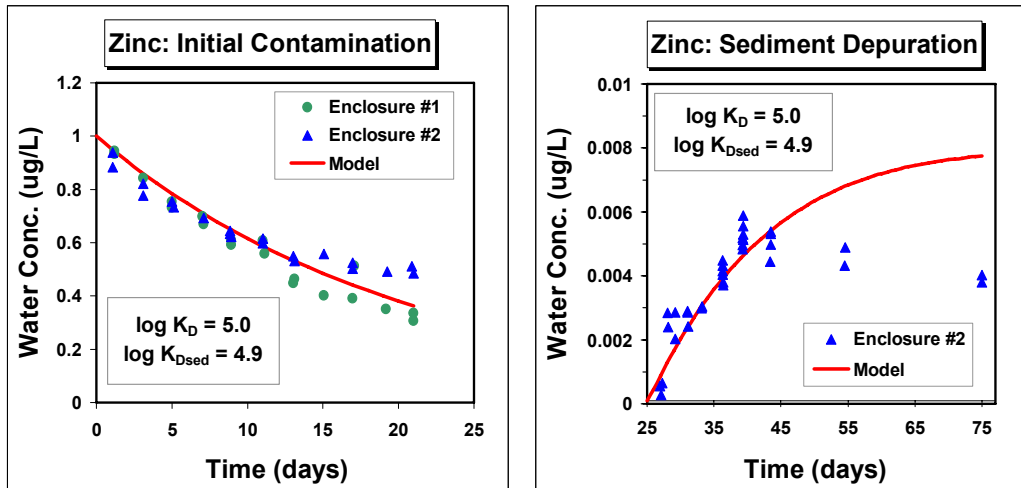


Figure 3. Comparison of model and observed concentrations of zinc (^{66}Zn) in Perch Lake enclosure studies. (Data from Diamond et al., 1990).

Lake Baldegg, Switzerland

Continuous additions of several metals including Cd, Zn, Pb, Cu and Hg were added to large enclosures (limno-corals) in Lake Baldegg for a period of 430 days as part of the Metal LIMological EXperiment (MELIMEX) (Gachter and Mares, 1979). The enclosures were 12 m in diameter and 10 m deep. Total and dissolved concentrations of metals were measured in the water column as a function of time. For model evaluations, partition coefficients for metal in the overlying water were adjusted to match observed water column concentrations. All other model parameters and coefficients were taken directly from Gachter and Mares (1979) and are summarized in Table 1.

A comparison of model and observed concentrations for total and dissolved copper (Cu) in the overlying water are shown in Figure 4. Results show that the simple K_D partitioning model again provides a good description of total and dissolved metal concentrations over the study period. A summary of water column K_D values that were obtained using the simple partitioning model for the Lake Baldegg and Perch Lake studies are given in Table 2.

Table 2. Summary of $\log K_D$ Values for the Water Column in Perch Lake and Lake Baldegg Enclosure Studies

	Perch Lake	Lake Baldegg
Cadmium		5.3
Cobalt	6.5	
Copper		5.1
Lead		5.9
Zinc	5.3	4
Iron	5.4	
Mercury	5.2	6

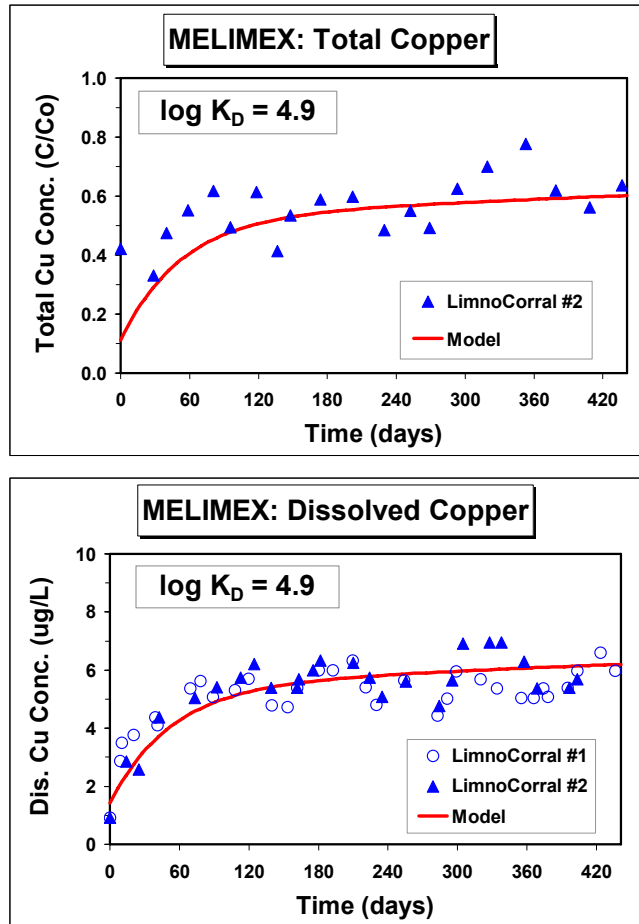


Figure 4. Comparison of model and observed concentrations of total and dissolved copper in Lake Baldegg enclosures. (Data from Gatcher and Mares, 1979.).

WHAM V Calculations for K_D

Although the simple partitioning (K_D) model provides a good description of metal behavior in both the Perch Lake and Lake Baldegg studies, the results show that K_D values for a particular metal can vary by as much as an order of magnitude between the two lakes. The simple partitioning model alone therefore does not provide a predictive method for evaluating metal behavior in lakes with varying water chemistry. The utility of WHAM V in predicting the partitioning of metals was therefore examined.

Based on information in Diamond et al. (1990), Perch Lake was modeled as a soft water lake with a hardness of approximately 50 mg/L as CaCO_3 and a pH of 7. The average DOC concentration is given as 10 mg/L; the average total suspended solids (TSS) concentration is given as 2 mg/L; and the organic carbon content of the TSS was assumed to be 20% resulting in a POC concentration of 0.4 mg/L. For model calculations, POC is considered to be composed of WHAM humic acid, and DOC is considered to be composed of WHAM fulvic acid. K_D values that were obtained from the simple partitioning evaluation of the enclosure data (triangles) are compared to WHAM V calculated K_D values (asterisks with connecting solid line) in Figure 5. As shown, derived K_D 's for Zn, Fe and Hg from the enclosure studies fall within a factor of two (dashed lines) of the WHAM V calculated K_D values. The higher K_D value for cobalt (Co) that was obtained from the enclosure data may indicate that precipitation, co-precipitation, or

possibly the sorption to oxide surfaces may be more important than binding of cobalt to organic matter.

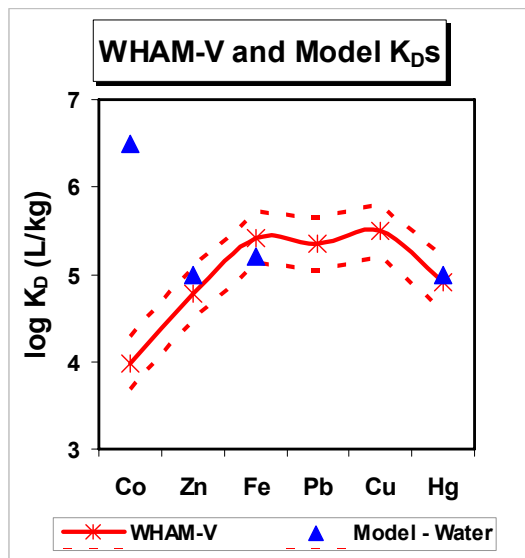


Figure 5. Comparison of K_D values from simple partition model evaluations of Perch Lake enclosure studies (triangles) and WHAM V calculated K_D values (asterisks with connecting solid lines). (Dashed lines represent plus or minus a factor of two.).

A similar analysis of WHAM V calculated K_D values was performed for Lake Baldegg. Based on information in Gachter and Mares (1979), Lake Baldegg was modeled as a hard water lake with a hardness of approximately 250 mg/L as CaCO_3 and an average pH of 8.8. The average DOC concentration is given as 2 mg/L; the average TSS is given as 2 mg/L; and the organic carbon content of the TSS was again assumed to be 20% resulting in a POC concentration of 0.4 mg/L. The POC is again considered to be composed of WHAM V humic acid and the DOC is considered to be composed of WHAM V fulvic acid. K_D values that were obtained from the simple partitioning evaluation of the Lake Baldegg enclosure data (triangles) are compared to WHAM V calculated K_D values (asterisks with connecting solid line) in Figure 6. As shown, derived K_D 's for Zn and Cu from the enclosure studies fall within a factor of two (dashed lines) of the WHAM V calculated K_D values. The higher K_D value for Cd, Pb and Hg that were obtained from the enclosure data are likely the result of carbonate precipitation in the hard water, alkaline Swiss lake. An examination of solubility products for the various metal carbonate (Table 3) are consistent with our finding that Hg, Cd and Pb are more likely to precipitate as carbonates in the alkaline waters of Lake Baldegg than either Zn or Cu.

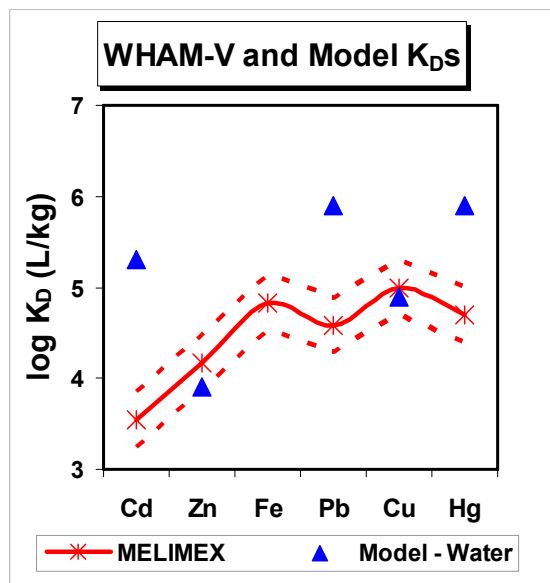


Figure 6. Comparison of K_D values from simple partition model evaluations of Lake Baldegg enclosure studies (triangles) and WHAM V calculated K_D values (asterisks with connecting solid lines). (Dashed lines represent plus or minus a factor of two.).

Table 3. Solubility Products for Various Metal Carbonates

	$\log K_{sp}^{(a)}$
$HgCO_3(s)$	-16.1
$CdCO_3(s)$	-13.7
$PbCO_3(s)$	-13.1
$ZnCO_3(s)$	-10
$CuCO_3(s)$	-9.6

^(a)Values from Morel and Hering, 1993

A summary of the K_D results from the simple partitioning model evaluations of the enclosure data and the WHAM V calculated K_D values are shown in Figure 7. As shown, the K_D 's for Perch Lake and Lake Baldegg studies are adequately described using WHAM V for most metals. The use of the simple partitioning model with WHAM-derived K_D 's however is still missing key aspects that are critical in evaluating the long-term fate and effects of metals in lakes.

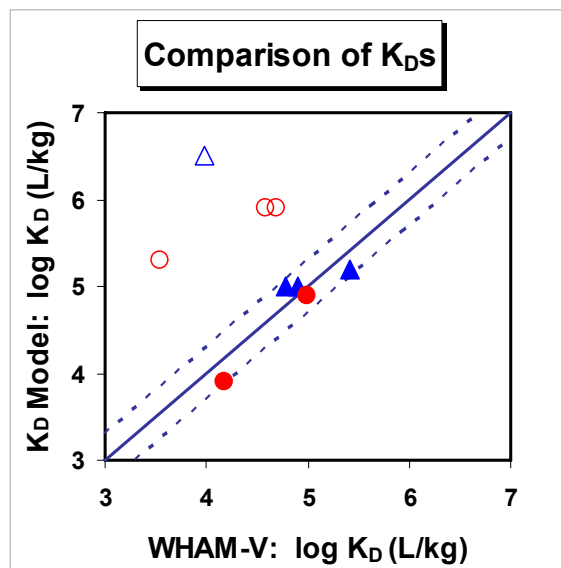


Figure 7. Summary of K_D results from simple partitioning model evaluations of lake enclosure studies and WHAM V calculated K_D value. Results for Perch Lake and Lake Baldegg are denoted by triangles and circles, respectively. (Filled symbols are used to denote metals where partitioning is expected to be controlled by binding to organic carbon. Open symbols are used to denote metals where partitioning is likely to be controlled by precipitation reactions.).

These include:

- Organic carbon cycling
- Sulfide production and oxidation in sediments
- Metal precipitation (particularly to sulfides in sediments and carbonates in alkaline lakes)
- Metal toxicity evaluation (e.g., by considering metal binding to the biotic ligand).

Development of UWM: Tier 1 Model for Metals in Lakes

The goal in our development of a Tier 1 Model for Metals in Lakes is to combine dissolved and particulate phase transport (as described in the simple partitioning (K_D) model) with: (1) metal speciation calculations (using information from WHAM V and MINEQL+ databases); (2) organic carbon cycling and AVS production, and (3) metal toxicity evaluation (using the BLM) into a unified model to determine the long-term fate and effects of metals in lakes.

Steady-state concentrations of metal in the water column and surficial sediment layer are then obtained by simultaneous solution of the chemical speciation and transport equations. The solution is based on a simplified version of the Tableau Input Coupled Kinetic Equilibrium Transport (TICKET) model algorithm (Miller, 1997, Miller et al., 2006). Conceptually, the modeling approach follows the chemical equilibrium tableau of Morel and Hering (1993) where chemical components are written across the top of the tableau and chemical species are written down the side (see top of Table 4). Mobility factors are also considered to include the effect of various transport processes (i.e., outflow, diffusive exchange, settling, resuspension, and burial) on each chemical species. Based on this information, a steady-state, flux balance equation is

written for each chemical component in the water column and the active sediment layer following equations given in the bottom of Table 4. Since an equilibrium mass action equation is required for each chemical species and a flux balance equation is required for each chemical component, the final solution involves a total of approximately 550 equilibrium mass action equations and 100 flux balance equations. These equations are simultaneously solved using a Newton-Raphson iteration technique following the approach outlined in Westall et al. (1976). The modeling algorithms are written in Visual Basic for Applications (VBA) for EXCEL. Appropriate adjustments in the code (e.g., by recalculating the total component concentrations or mass input fluxes, and modifying specific terms in the Jacobian matrix) are made to handle electrostatic corrections, accumulation of counterions in the Donnan layer.

Table 4. TICKET Input Tableau for Chemical Equilibrium and Kinetic Reactions

	X _{h,1}	X _{h,2}	• • •		Mq	Me	Mw
<u>Species</u>				<u>log K</u>			
C _{h,1}	a _{1,1}	a _{1,2}	• • •	K ₁	Mq ₁	Me ₁	Mw ₁
C _{h,2}	a _{2,1}	a _{2,2}		K ₂	Mq ₂	Me ₂	Mw ₂
•	•			•	•		
•	•			•	•		
•	•			•	•		
	Input _{h,1}	Input _{h,1}	• • •				

Note: h is used in multi-cell problems as the cell index.

Water Column (h = 1)

$$V_{1,j} \frac{d(TOTX_{1,j})}{dt} = Inputs - Q_{out} \sum_i^m Mq_i \cdot a_{i,j} \cdot C_{h,i} - w_{settling} \cdot A_{sed} \sum_i^m Mw_i \cdot a_{i,j} \cdot C_{1,i} + k_f \cdot A_{sed} \cdot \left[\sum_i^m Me_i \cdot a_{i,j} \cdot C_{2,i} - \sum_i^m Me_i \cdot a_{i,j} \cdot C_{1,i} \right] + w_{resuspension} \cdot A_{sed} \sum_i^m Mw_i \cdot a_{i,j} \cdot C_{2,i}$$

Sediment (h = 2)

$$V_{2,j} \frac{d(TOTX_{2,j})}{dt} = k_f \cdot A_{sed} \cdot \left[\sum_i^m Me_i \cdot a_{i,j} \cdot C_{1,i} - \sum_i^m Me_i \cdot a_{i,j} \cdot C_{2,i} \right] + w_{settling} \cdot A_{sed} \sum_i^m Mw_i \cdot a_{i,j} \cdot C_{1,i} - (w_{burial} + w_{resusp}) \cdot A_{sed} \sum_i^m Mw_i \cdot a_{i,j} \cdot C_{2,i}$$

Tier 1 Model Applications

Although the construction of the Tier 1 Model for Metals in Lakes is rather complex, use of model input is straightforward. The user defined input for the model includes the metal loading rate, water quality parameters (including pH, hardness, DOC, POC, the sediment dry weight concentration, and percent organic carbon and AVS concentration in the surficial

sediment layer), and transport parameters (including surface area, depth, depth / detention time, and settling, resuspension, burial and diffusive exchange rates). Model calculations can also be performed by specifying the free ion activity of the metal or the critical concentration of metal on the biotic ligand and calculating the allowable loading rate of metal to the lake.

For our initial calculations, a pH of 7 was specified in the overlying water and the surficial sediment layer; the hardness was given as 50 mg / L as CaCO₃ for a soft water lake; the POC and DOC were selected as typical field values of 1 mg / L and 3 mg / L, respectively. The sediment dry weight concentration, the percent organic carbon and AVS concentrations in the surficial sediment layer were specified as 400 g / L, 2.5% and 20 μmole AVS / g (dry wt). For unit loading calculations, the surface area of the lake was set at 1 m². The depth and depth / detention time of the lake were specified as 10 m and 10 m / yr, respectively based on an average lake from surveys by Vollenweider (1975, 1976). The net settling rate for POC was taken as 60 m / yr based on early lake eutrophication studies. The resuspension and burial rates were specified as 0 and 0.2 cm / yr, respectively, and the diffusive exchange rate was set at 1 cm / day. Based on input values given above, POC and AVS cycling in the lake are calculated internally in the modeling code.

A summary of the steady-state POC and AVS fluxes that are considered in the initial Tier 1 model calculations presented below are given in Figure 8. Other information for chemical reaction stoichiometry, chemical equilibrium constants, and WHAM V coefficients for electrostatic corrections and Donnan layer accumulation, and biotic ligand parameters that are required for running the Tier 1 Model are included in the model database. The model is executed directly in EXCEL using VBA programmed macros. A user's guide for running the model is available (Farley et al., 2005).

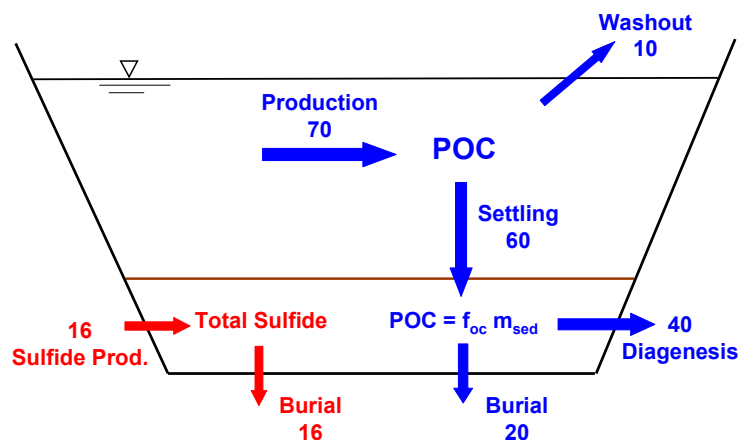


Figure 8. Steady-state POC and AVS fluxes considered in initial Tier 1 model applications. (POC fluxes are given in gC/m² /day and AVS fluxes are given in mmoles AVS/m²/yr.).

Model Results

Model calculations were initially performed by specifying various metal loading rates and calculating the speciation and concentrations of metals in the water column and the surficial sediment layer. Sample results for the free ion activity, dissolved concentration and concentration of metal on the biotic ligand in the water column and the surficial sediment layer

are given for copper in Figure 9. As expected, copper concentrations in the lake increase with increasing loading rate. The responses however are highly non-linear due to the sequential binding of copper to various sites (ranging from high affinity to low affinity sites) on POC and DOC and to the binding of copper to AVS in sediments.

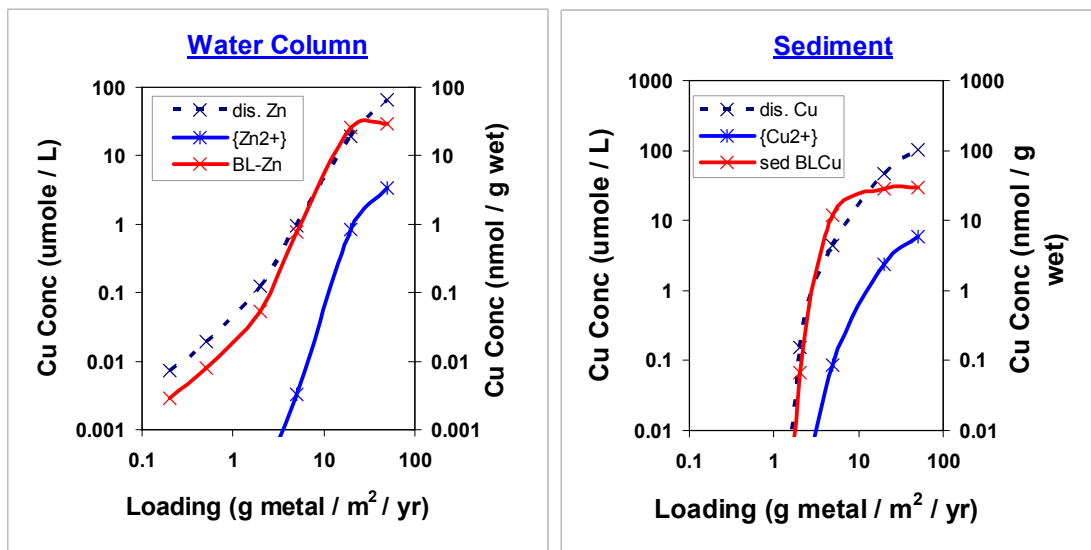


Figure 9. Sample results for the free ion activity, dissolved metal concentration and metal concentration on the biotic ligand for water column and sediment.

Subsequent model calculations were performed to determine allowable loads of Cd, Cu, Ni, Pb, Zn based on critical concentrations of metal on the biotic ligand in the water column. For this calculation, critical concentrations on the biotic ligand were specified based on acute toxicity values for *Daphnia magna* as given in Di Toro et al. (2005). The model results for critical loading rates are given in Figure 10. As shown, critical loading rates vary from 1.6 g metal / m² / yr for Cd to 21 g metal / m² / yr for Pb.

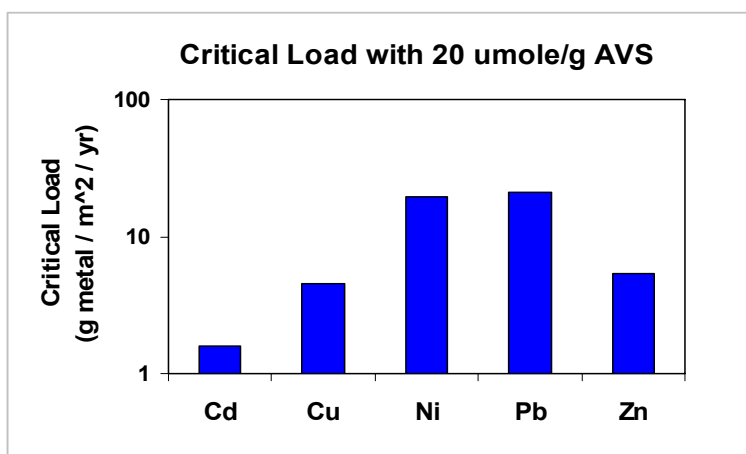


Figure 10. Critical loading rates for Cd, Cu, Ni, Pb and Zn in an idealized, circum-neutral, soft water lake (pH 7; hardness 50 mg / L as CaCO₃).

Differences in calculated loading rates for the various metals are dependent not only on critical concentrations on the biotic ligand, but also on the affinity of the metal to bind to organic carbon, the transfer of metal to sediment by settling and diffusive exchange, and the binding of metal to AVS in sediment. For example, Cu, which has a much lower critical concentration on the biotic ligand than Cd, is calculated to have a higher allowable loading rate. This occurs because Cu has a strong affinity to bind to organic carbon, which results in Cu being effectively removed from the water column by settling on POC and ultimately being removed from the lake by burial of POC-bound and AVS-bound Cu. This is contrasted by Cd, which has a relatively low affinity to bind to organic carbon, is not effectively removed to sediments, remains largely in the water column in its ionic form (Cd^{2+}), and as a result, builds up to high concentrations on the biotic ligand. Thus the unit world model is capable of ranking the persistence and toxicity of metals that accounts for their varying properties.

A user friendly version of the unit world model has been developed (Farley et al., 2005) with support from the International Council of Mining and Metals (ICMM).

Unit World Model for Streams and Rivers

The Unit World Model is intended to be used for both lake and stream settings. Since there appears to be very little suitable stream data in the literature, two center projects are sampling metal impacted streams.

An analysis of the results of one of the projects (Colorado School of Mines) is presented below. The sampling stations in Clear Creek CO are shown in Figure 11.

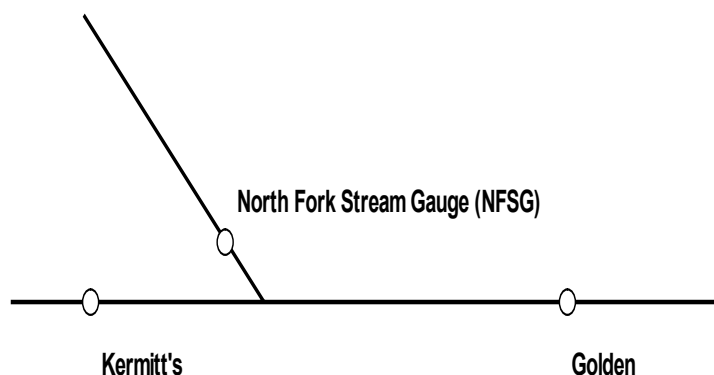


Figure 11. Sampling locations in the North Fork Clear Creek and in the main stem of the Clear Creek. (Butler, personal communication, Colorado School of Mines).

Probabilistic Dilution Modeling

A probabilistic dilution analysis (Di Toro, 1984) was conducted for several of the constituents from the data set listed above. It was assumed for this investigation that chemical species examined were conservative (i.e. settling or resuspension of particulate metal was not considered). Two upstream locations in the main stem and a tributary (Kermits and NFSG) flow into the downstream station at Golden. The concentration at Golden can be computed as the flow weighted concentrations from the two upstream stations as shown in Figure 11. This computation assumes that there are no sources or sinks of metal in the reaches between the upstream and downstream stations. The probability distribution of sodium, which is expected to be a conservative tracer, at Golden is described very well by the model (Figure 12). However, for both zinc and copper the model over predicts the downstream concentration distributions.

This suggests that these species are being removed from the water column by sorption to particulate material and settling. Oxyhydroxides of iron and manganese are visible in the North Fork of the Clear Creek and represent potential sorbent species for zinc and copper. These results indicate that the probabilistic dilution model for Clear Creek must be modified to include the partitioning of metals to particulate species and settling of these particulate species.

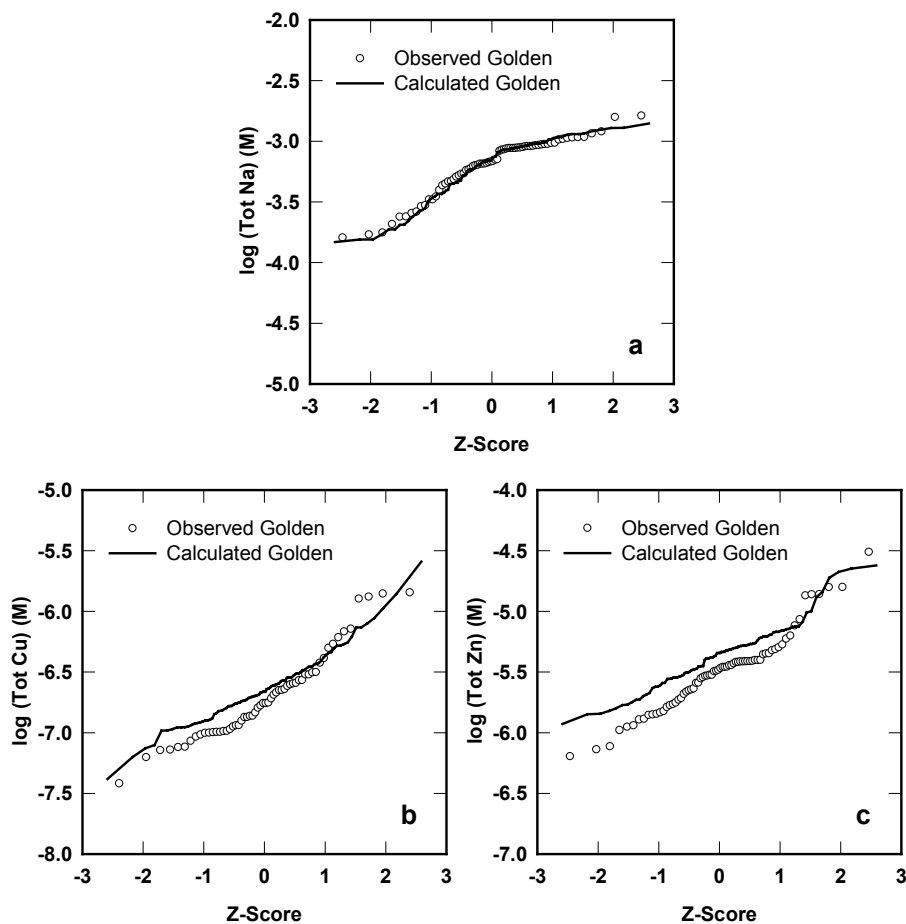


Figure 12. Probabilistic dilution model analysis for the Clear Creek at Golden, Colorado. Results for a) sodium, b) copper, and c) zinc are shown.

Metal Partitioning Analysis

Preliminary chemical speciation analysis was conducted on the Clear Creek data set to determine if the available models described above could adequately simulate partitioning of zinc and copper to particulate phases. Data from the three sampling locations depicted in Figure 12 were included. For these calculations three potential sorbent phases were considered: iron oxide, manganese oxide, and particulate organic carbon (POC). Particulate iron, obtained by subtracting dissolved iron concentrations from total iron concentrations, was assumed to be hydrous ferric oxide (HFO). Similarly particulate manganese, obtained by subtracting dissolved manganese concentrations from total manganese concentrations, was assumed to be hydrous manganese oxide (HMO). Estimates of POC concentrations were made using TSS and VSS values from a data set collected by the Upper Clear Creek Watershed Association (UCCWA)

(Butler, personal communication,) assuming that VSS is 40% organic carbon. Measured values of pH, temperature, magnesium, sodium, potassium, calcium, sulfate, aluminum, nickel, and DOC were included in the calculations. Initial calculations were made on dissolved data to determine the activity of zinc and copper in the aqueous phase. These activity values were then used in subsequent calculations to speciate the two metals in the presence of the various particulate phases.

WHAM6 Results

Initial WHAM6 (Tipping, 1998; Lofts and Tipping, 1998) results for zinc and copper in the presence of various sorbent configurations are shown in Figure 13. The WHAM 6 analysis considers the system in the presence of HFO and HMO with DOC included (top two panels in Figure 13). The particulate values for both zinc and copper are under predicted in the WHAM 6 analysis. If HFO and HMO are omitted from the calculation and POC is included (middle two panels in Figure 13), a general improvement in accuracy is observed. However, both the particulate zinc and copper predictions for the NFSG data are still remain low indicating that HFO and HMO must be included. When all three potential particulate sorbent phases are included (bottom two panels in Figure 13), a reasonable fit to the observed data is achieved.

The WHAM6 results suggest that POC is required to fully describe zinc and copper partitioning in the Clear Creek. It is possible that consideration of additional particulate sorbent phases, such as aluminum oxides, could further improve the agreement between the calculated and observed values. The results also indicate that the relative importance of different particulate phases may vary at different locations in the same system. Both analyses indicate the importance of including a speciation model that considers multiple particulate sorbent phases in the UWM for streams and rivers.

Sorption to Algae

The WHAM V model is intended for modeling metal sorption to humic and fulvic acids. It also appears that it can be applied to non-living particulate organic carbon (POC). However, in many situations the primary form of particulate organic matter in the water column is algal biomass. Therefore, it is necessary to have a modeling framework that can be applied to the algal component of POC.

We have assembled a substantial quantity of algal sorption data from the literature as a starting point for the model development. The usual model applied to algal sorption is a surface complexation model, usually a single site model. Since we have a multi-site model available (WHAM V), we applied it to the algal sorption data. The algal data is normalized as metal sorbed per unit algal organic carbon, in order to be consistent with the WHAM formulation. An example of the results are presented in Figure 14 (Kieffer et al., 1997). The top panels are pH vs acid/base added, i.e. potentiometric titrations. The bottom panels are isotherm plots, the concentration of sorbed metal per unit algal organic carbon versus $-\log_{10}(\text{metal activity})$. The metal activity is either reported by the authors, or it is computed from the aqueous chemistry data reported by the authors. The parameters for the proton binding spectrum have been adjusted from those for humic acid in order to fit the titration data (Table 5). However no adjustments have been made to the proton-metal replacement parameters since they are intrinsic properties of the metals.

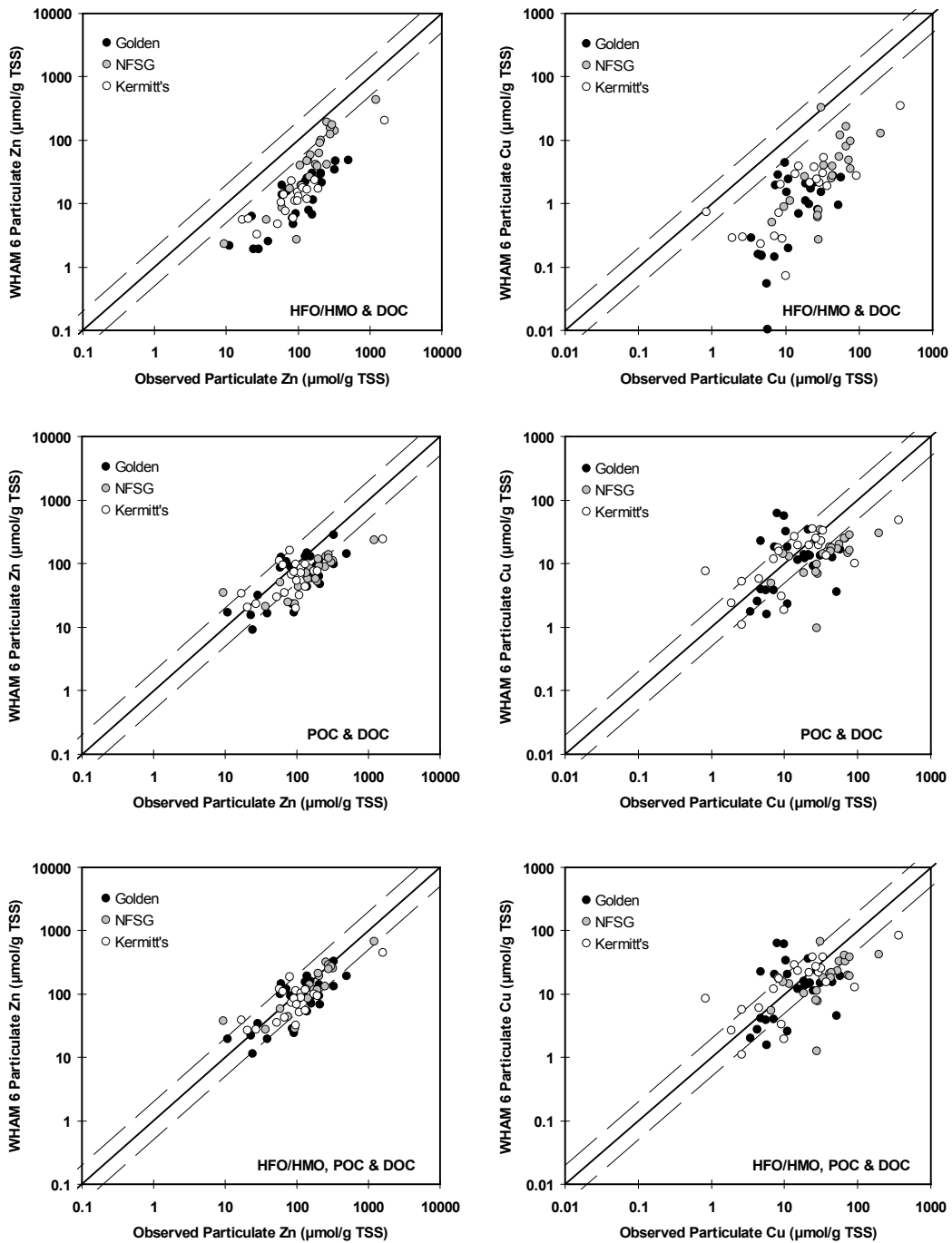


Figure 13. Comparison of predicted and calculated particulate zinc and copper. Data from three sample stations—Golden, NFSG, and Kermitt’s—are included. Predicted values were calculated using the Windermere Humic Aqueous Model VI (Tipping, 1998). Three distinct scenarios are presented: 1) hydrous ferric oxide (HFO) and hydrous manganese oxide (HMO) with dissolved organic carbon (DOC) included, 2) particulate organic carbon (POC) with DOC included, and 3) both oxide species and POC with DOC included.

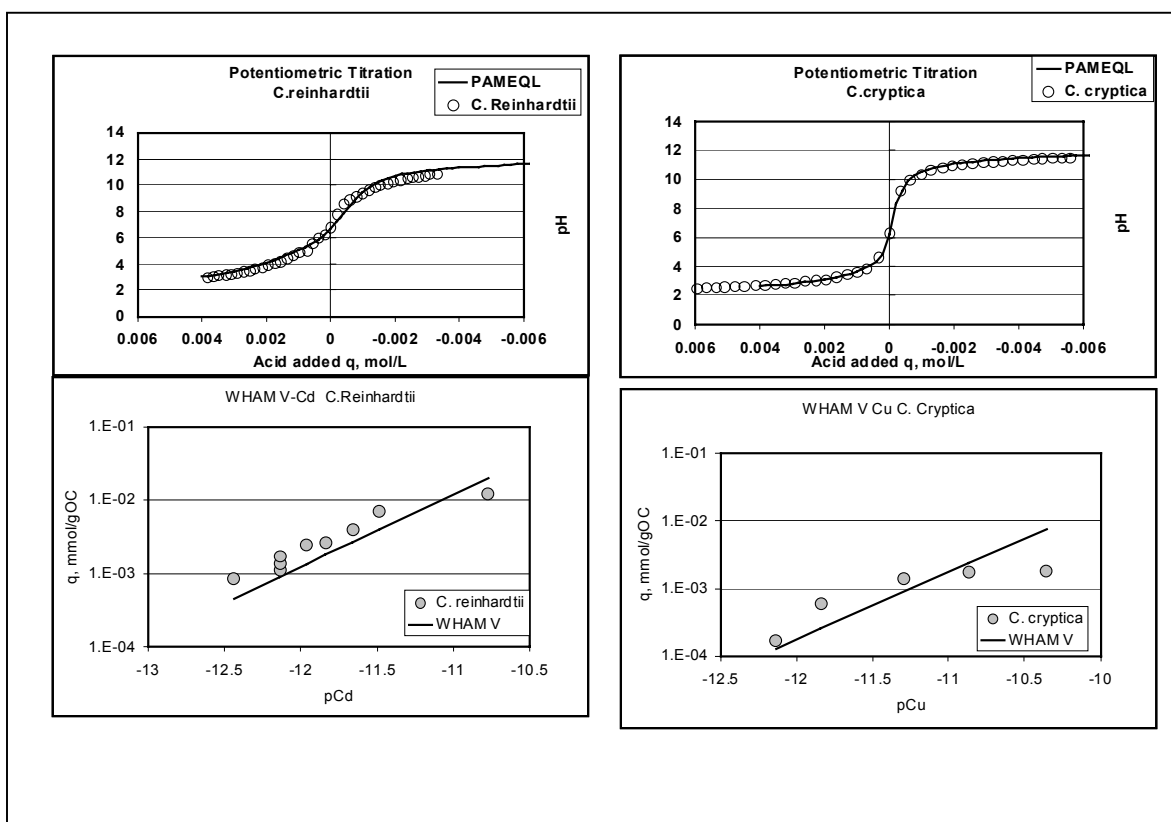


Figure 14. Comparison of WHAM V prediction for potentiometric titrations and observed metal sorption to algae, normalized by algal organic carbon content (Kieffer et al., 1997).

Table 5. WHAM V Parameters

Variable	C.reinhardtii	C.cryptica
nA (mol/gOC)	1.9e-3	9.1e-4
PKA	3.5	3.0
ΔpKA	1.78	1.78
PKB	7.9	9.0
ΔpKB	3.43	3.43
I (M)	0.01	0.01
P	374	748

The results are certainly encouraging. For most of the data the WHAM V model is within a factor of two of the observations at the lower concentrations. There is a deviation at the higher concentrations.

We anticipate that additional data will be analyzed in this manner and that a consensus set of algal proton spectrum parameters will be developed, in the same spirit as the WHAM humic and fulvic acid constants.

Delaware Bay Chemical Speciation

Some additional preliminary speciation work has been performed with a data set from the Delaware Bay Database a portion of which was collected by Church et al as part of the Center's research, as well as additional data (Culberson 1988). This data set includes both dissolved and particulate measurements for manganese, iron, cobalt, nickel, copper, zinc, lead, and cadmium. Other species and parameters such as major cations and anions, DOC, POC, alkalinity, pH, salinity, and temperature were quantified as well. In short, the database provides all the required information with which to test the accuracy of WHAM6 speciation calculations. What makes this data set particularly appealing is the fact that salinity for the samples ranges from less than 0.1 ppt to more than 30 ppt.

For the WHAM6 speciation calculation the following particulate sorbents were included: POC, HFO, and HMO. In addition, DOC was included. The results of the initial speciation calculation for the six trace metals are shown in Figure 3.5. With the exception of copper, WHAM6 general under predicts the log K_D .

Residual plots comparing the prediction error against the log of the salinity values are shown in Figure 3.6. The under prediction of log K_D generally increases as the salinity increases (except for the case of copper). This suggests that the deviation of the WHAM6 prediction from the observations might be caused by ionic strength effects, cation competition for binding sites on POC, HFO, and/or HMO, or overestimation of the solubilizing effects of aqueous phase organic and inorganic ligands.

The divalent cations calcium and magnesium compete with metals for binding sites on DOC, POC, and metal oxides (Dzombak et al. 1990, Lofts et al. 1998, Tipping 1998, Lofts et al. 2000, and Tipping 2002). To investigate the competition effect of cations, the concentrations of calcium and magnesium were omitted from the WHAM6 calculation. The WHAM6 output from this calculation is shown in Figure 3.7. For most metals considered, this dramatically improves the WHAM6 fit to the observations. This suggests that the manner in which WHAM6 addresses competition may need to be reassessed. However at this point, one cannot rule out the possibility of WHAM6 errors stemming from ionic strength effects and/or inaccurate quantification of the solubilizing effects of aqueous phase organic and inorganic ligands.

Literature Cited

- Adams, W.J., Conard, B., Ethier, G., Brix, K.V., Paquin, P.R., and Di Toro, D.M. (2000) The Challenges of Hazard Identification and Classification of Insoluble Metals and Metal Substances for the Aquatic Environment. *Human and Ecol. Risk Assessment*. 6(6):1019-1038.
- Ankley, G.T., Mattson, V., Leonard, E., West, C., and Bennett, J. (1993) Predicting the Acute Toxicity of Copper in Freshwater Sediments: Evaluation of the Role of Acid Volatile Sulfide. *Environ. Toxicol. Chem.* 12:312-320.
- Ankley, G.T., Di Toro, D.M., Hansen, D.J., and Berry, W.J. (1996) Technical Basis and Proposal for Deriving Sediment Quality Criteria for Metals. *Environ. Toxicol. Chem.* 15:2056-2066.
- Berry, W.J., Hansen, D.J., Mahony, J.D., Robson, D.L., Di Toro, D.M., Shipley, B.P., Corbin, J.M., and Boothman, W.S. (1996) Predicting the Toxicity of Metals-Spiked Laboratory Sediments Using Acid-Volatile Sulfide and Interstitial Water Normalization. *Environ. Toxicol. Chem.* 15:2067-2079.

- Carbanaro, R. (1999) Modeling Metal Sulfide Fluxes from Sediments. MS Thesis. Department of Environmental Engineering. Riverdale, NY, Manhattan College.
- Diamond, M.L., Mackay, D., Cornett, R.J., and Chant, L.A. (1990) A Model of the Exchange of Inorganic Chemicals Between Water and Sediments. *Environ. Sci. Technol.* 24(4):713-722.
- Di Toro, D.M. (1984) Probability Model of Stream Quality Due to Runoff. *J. Environ. Engr. ASCE.* 110:607-628.
- Di Toro, D.M., and Paquin, P.R. (1984) Time Variable Model of the Fate of DDE and Lindane in a Quarry. *Environ. Toxicol. Chem.* 3:335-353.
- Di Toro, D.M., Mahony, J.D., Hansen, D.J., Scott, K.J., Hicks, M.B., Mayr, S.M., and Redmond, M.S. (1990) Toxicity of Cadmium in Sediments: The Role of Acid Volatile Sulfide. *Environ. Toxicol. Chem.* 9:1487-1502.
- Di Toro, D.M., Hallden, J.A., and Plafkin J.L. (1991) Modeling Ceriodaphnia Toxicity in the Naugatuck River. II. Copper, Hardness and Effluent Interactions. *Environ. Toxicol. Chem.* 10:261-274.
- Di Toro, D.M., Mahony, J.D., Hansen, D.J., Scott, K.J., Carlson, A.R., and Ankley, G.T. (1992) Acid Volatile Sulfide Predicts the Acute Toxicity of Cadmium and Nickel in Sediments. *Environ. Toxicol. Chem.* 26:96-101.
- Di Toro, D.M., Mahony, J.D., Hansen, D.J., and Berry, W.J. (1996) A Model of the Oxidation of Iron and Cadmium Sulfide in Sediments. *Environ. Toxicol. Chem.* 15:2168-2186.
- Di Toro, D.M., Allen, H.E., Bergman, H.L., Meyer, J.S., Paquin, P.R., and Santore, R.C. (2001) Biotic Ligand Model of the Acute Toxicity of Metals. I. Technical Basis. *Environ. Toxicol. Chem.* 20(10):2383-2396.
- Di Toro, D.M. (2001) Sediment Flux Modeling. J. Wiley and Sons, New York. pp 624.
- Di Toro, D.M., McGrath, J.M., Hansen, D.J., Berry, W.J., Paquin, P.R., Mathew, R., Wu, K.B., and Santore, R.C. (2005) Predicting Sediment Metal Toxicity Using a Sediment Biotic Ligand Model: Methodology and Initial Application. *Environ. Toxicol. Chem.* 24(10):2410-2427.
- Effler, S.W., Litten, S., Field, S.D., Tong-Ngork, T., Hale, F., Meyer M., and Quirk, M. (1980) Whole Lake Responses to Low Level Copper Sulfate Treatment. *Water Research* 14:1489-1499.
- European Commission, (1996) EUSES Documentation – The European Union System for the Evaluation of Substances. National Institute of Public Health and the Environment (RIVM), the Netherlands.
- Farley, K.J., Carbonaro, R.F., and Di Toro, D.M. (2005) Unit World Model Tier 1 Model for Metals in Lakes: Users Guide Manhattan College, Riverdale NY.
- Gachter, R., Imboden, D.M., Eid, B.S.F., Joller, T., Schurter, M., Wetzel, J., Hohl, H., Vagenknecht, A., Baccini, P., Ruchti, J., Wanner, O., Grieder, E., Mares, A., Urech, J., Bossard, P., Lang, C., Lang-Dobler, B., Geiger, W., and Suter, U. (1979) MELIMEX, An Experimental Heavy Metal Pollution Study. *Swiss J. Hydrol.* 41(2):165-314.
- Gustafsson, J.P. (2001) Modeling the Acid-Base Properties and Metal Complexation of Humic Substances with the Stockholm Humic Model. *J. Colloid Interface Sci.* 244:102-112.

- Hansen, D.J., Berry, W.J., Mahony, J.D., Boothman, W.S., Di Toro, D.M., Robson, D.L., Ankley, G.T., Ma, D., Yan, Q., and Pesch, C.E. (1996) Predicting the Toxicity of Metals-Contaminated Field Sediments Using Interstitial Concentrations of Metal and Acid Volatile Sulfide Normalizations. *Environ. Toxicol. Chem.* 15(12):2080-2094.
- Kieffer, E., Sigg, L., and Schosseler, P. (1997) Chemical and Spectroscopic Characterization of Algae Surfaces. *Environ. Sci. Tech.* 31:759-764.
- Lofts, S., and Tipping, E. (1998) An Assemblage Model for Cation Binding by Natural Particulate Matter. *Geochim. Cosmochim. Acta* 62(15):2609-2625.
- Mackay, D. (1991) *Multimedia Environmental Models*, Lewis Publishers, Chelsea, MI.
- Mackay, D., Paterson, S., and Shiu, W.Y. (1992) Generic Models for Evaluating the Regional Fate of Chemicals. *Chemosphere* 24:695-717.
- Miller, B.E. (1997) Development of a General Aquatic Multi-Component Reactive Transport Computer Model, with Application to a Wetland Sediment. Doctoral, Clemson University, Clemson, SC.
- Miller, B.E., Rader, K.J., and Farley, K.J. (2006) Tableau Input Coupled Kinetic Equilibrium Transport (TICKET) Model. *Environmental Sci Tech.* (Submitted).
- Morel, F.M.M., and Hering, J.G. (1993) *Principles and Applications of Aquatic Chemistry*. John Wiley & Sons, New York, NY.
- O'Connor, D.J. (1988a) Models of Sorptive Toxic Substances in Freshwater Systems. I: Basic Equations. *J. Environ. Engr.* 114(3):507-532.
- O'Connor, D.J. (1988b) Models of Sorptive Toxic Substances in Freshwater Systems. II: Lakes and Reservoirs. *J. Environ. Engr.* 114(3):533-551.
- O'Connor, D.J. (1988c) Models of Sorptive Toxic Substances in Freshwater Systems. III: Streams and Rivers. *J. Environ. Engr.* 114 (3):552-574.
- Pagenkopf, G.K. (1983) Gill Surface Interaction Model for Trace Metal Toxicity to Fishes: Role of Complexation, pH, and Water Hardness. *Environ. Sci. Technol.* 17:343-347.
- Paquin, P.R., Gorsuch, J.W., Apte, S., Batley, G.E., Bowles, K.C., Campbell, P.G.C., Delos, C.G., Di Toro, D.M., Dwyer, R.L., Galvez, F., Gensemer, R.W., Goss, G.G., Hogstrand, C., Janssen, C.R., McGeer, J.C., Naddy, R.B., Playle, R.C., Santore, R.C., Schneider, U., Stubblefield, W.A., Wood, C.M., and Wu, K.B. (2002) The Biotic Ligand Model: A Historical Overview. *Comp. Biochem. Physiol. C-Tox. Pharm.* 133(1-2):3-35.
- Playle, R.C., Dixon, D.G., and Burnison, K. (1993) Copper and Cadmium Binding to Fish Gills: Estimates of Metal-gill Stability Constants and Modeling of Metal Accumulation. *Can. J. Fish. Aquatic Sci.* 51:2678-2687.
- Santore, R.C., Di Toro, D.M., and Paquin, P.R. (2000) A Biotic Ligand Model of the Acute Toxicity of Metals. II. Application to Acute Copper Toxicity in Freshwater Fish and Daphnia. *Environ. Toxicol. Chem.* 20(10):2397-2402.
- Tipping, E. (1994) WHAM-A Chemical Equilibrium Model and Computer Code for Waters, Sediments, and Soils Incorporating a Discrete Site/Electrostatic Model of Ion-Binding by Humic Substances. *Comput. Geosci.* 20(6):973-1023.
- Tipping, E. (1998) Humic Ion-Binding Model Model VI: An Improved Description of the Interactions of Protons and Metal Ions with Humic Substances. *Aquat. Geochem.* 4:3-48.

- USEPA, (1986) Hazard Evaluation Division, Standard Evaluation Procedure, Ecological Risk Assessment. Office of Pesticide Programs, Washington, DC. EPA 540/9-85-001.
- USEPA, (1999) Integrated Approach to Assessing the Bioavailability and Toxicity of Metals in Surface Waters and Sediments, a report to the EPA Science Advisory Board, Office of Water, Office of Research and Development, Washington, DC, USEPA-822-E-99-001.
- USEPA, (2000) An SAB Report: Review of the Biotic Ligand Model of the Acute Toxicity of Metals. prepared by the Ecological Processes and Effects Committee of the Science Advisory Board, EPA-SAB-EPEC-00-0006.
- Vollenweider, R.A. (1975) Input-Output Models with Special Reference to the Phosphorus Loading Concept in Limnology. *Schweiz. Z. Hydrol.* 37:53-83.
- Vollenweider, R.A. (1976) Advances in Defining Critical Loading Levels for Phosphorus in Lake Eutrophication. *Mem. 1st Ital. Idrobiol.* 33:53-83.
- Westall, J.C., Zachary, J.L., and Morel, F.M.M. (1976) MINEQL: A Computer Program for the Calculation of Chemical Equilibrium Composition of Aqueous Systems. Technical Note No. 18, MIT, Cambridge, MA.

Evaluation of Automobile sources for Metals in Urban Areas

Akash Sondhi, Paul T. Imhoff, Herbert E. Allen and Steven, K. Dentel
Department of Civil and Environmental Engineering
University of Delaware
Newark, DE 19716

This report summarizes results of the project “Evaluation of Automobile Brake Pads for Metal Emissions in Urban Areas.” The objectives of the study were to

- compare the natural brake wear debris released in the urban environment with two types of laboratory-generated debris: those generated with a dynamometer using the Los Angeles City Traffic protocol (LACT particles), and those generated using a belt sander (artificial particles);
- evaluate particle size distribution of wear debris, which affects the fate and transport of particles in the environment;
- study Copper dissolution from wear debris over long time periods, on the order of 15 weeks;
- study the effect of pH on the dissolution behavior of Copper from these wear debris;
- characterize wear debris density;
- evaluate the variability of Copper leaching characteristics (rate and amount) across four representative automobile types; and
- evaluate the utility of using artificially generated brake wear debris to estimate or bound Copper leaching characteristics from naturally generated debris.

Important findings from the work can be summarized as follows:

Lab generated LACT brake wear debris differ significantly from natural brake wear debris released in the environment. The average size of natural brake wear debris released in the environment is three to ten times larger than LACT debris for the two automobile types tested.

Leaching from natural wear debris occurred at two different rates - a rapid rate for the first 10 hours, followed by a slow rate that lasted an additional 15 weeks.

A significant fraction of Copper present in natural brake wear debris is readily leachable at low pH, with approximately 90% of the Copper leached from natural brake wear debris at pH 4.3 for all four vehicle types tested over a 15 week leaching period.

Dissolution of Copper from brake wear debris is significantly influenced by pH, with 35 to 70% Copper leached from the four automobile types at pH 6.1 but approximately 90% of Copper leached at pH 4.3.

Artificial wear debris may be used to make conservative (high) estimates of the leachable fraction of Copper from natural wear debris, at least for the automobile types and conditions tested thus far in this study.

Thermodynamic modeling holds promise for predicting the change in form of metals present in virgin brake pads when released as wear debris.

Introduction

Total and dissolved concentrations of Copper in urban runoff often exceed U.S. EPA criteria for fresh and marine waters (USEPA, 2002). Recent studies of urban runoff have shown dissolved Copper concentrations as high as 380 µg/l, one to two orders of magnitude above discharge criteria to surface water (Sansalone and Buchberger, 1997). This Copper-laden runoff ultimately enters natural water bodies. High concentrations of metals, such as Copper, in the

aquatic environment have been shown to have deleterious effects on aquatic and marine life (Pitt et al., 1995; Soucek, et al., 2003).

Of the various sources of metals that exist in the urban environment, a recent study indicated that vehicle brake emissions are among the most important sources of Copper in urban stormwater runoff (Davis, et al., 2001). Estimates show that 55% of all Copper discharged to South San Francisco Bay comes from urban runoff (Santa Clara Valley Pollution Prevention Program, 1997). Brake pad sources have been estimated to account for 47% of Copper in an urban residential neighborhood in Maryland (Davis et al., 2001). Brake pads have also been implicated as a major source of Copper to the environment of California, where brake emissions were estimated to contribute 80% of Copper in the urban stormwater runoff leading to the South San Francisco Bay (Santa Clara Valley Runoff Pollution Prevention Program, 1997).

The dissolution of Copper contained in particles is influenced by various factors. Particle size and surface area, solution pH, concentrations of natural organic matter (NOM), concentrations and types of Copper complexing ligands, and the hydrodynamics of the system are some of the important factors that control the dissolution of Copper from brake wear debris in natural systems. The influence of several of these factors on Copper dissolution were elucidated in earlier studies for a set of wear debris from one automobile (Hur et al., 2003; Hur et al., 2004). More recently, the Brake Pad Partnership (BPP) supported similar leaching studies on a composite sample of wear debris collected from three brake pads that comprised greater than 90% of the Copper usage in original equipment manufacturer automobile brake pads for the 2002 model year (Schlautman and Haselden, 2005).

While the results from these laboratory dissolution studies illustrate the influence of various factors on Copper leaching, open questions remain. These include (1) what are particle size distributions and the Copper leaching characteristics of wear debris generated from automobiles under *actual driving conditions*, as opposed to Copper leaching from debris generated in the laboratory; (2) how does the rate and amount of Copper leaching differ between different brake pad formulations found on different types of automobiles; and (3) is it possible to use artificial wear debris generated by inexpensive measures to predict or bound Copper emissions from natural debris. A major objective of this work is to answer these three questions.

Material and Methods

Break Pad Wear Debris

automobiles known to use semi-metallic brake pads: Nissan Sentra 1997, Honda Civic 1998, Honda Accord 2000, and Toyota Camry 2000. These automobiles were selected because they were known to use copper-containing brake pads, and they were driven in Newark, Delaware and thus were exposed to similar environmental conditions. Two different sets of brake pad wear debris were collected from each brake pad for the four automobile types: natural brake wear debris, which were taken from the wheels/hubs of the automobile; and artificial brake wear debris, which were sanded off of the brake pads in the laboratory using a belt sander.

In addition to these two types of debris collected from the brake pads, an additional type was collected from brake pads associated with the Honda Accord 2000 and the Honda Civic 1998. Here, procedures developed by the BPP were followed to generate wear debris using a dynamometer (Trainor, 2001; Trainor et al., 2002). The same brake pads that were used to generate the natural and artificial wear debris were used here, and the Los Angeles City Traffic protocol was followed. Debris were generated at Link Testing Laboratories, Detroit MI, the

same laboratory used by the BPP. Two types of brake wear debris were collected from these tests: fallout particles that collect on the ductwork surrounding the dynamometer and airborne particles that collect on filter paper which screens the air. The fallout particles were compared with similar particles collected on the wheels and hubs of automobiles (natural particles), as well as the artificial particles generated from the same two automobile types. The characterization of airborne brake wear debris is underway using supplemental funding from the University of Delaware.

Leaching Solution and Chemical Reagents

A non metal complexing organic buffer solution 10 mM PIPBS buffer and 10 mM MOPS buffer obtained from GFS chemicals Inc, Ohio were used as leaching solutions. The buffer solutions were prepared by dissolving the buffer in distilled de-ionized water (DDW) having a resistivity >18 M-ohm cm. The buffer solutions were then titrated with NaOH to adjust the pH to 4.3 (PIPBS) and 6.1 (MOPS), respectively.

The study used trace metal grade or analytical grade hydrochloric acid (HCl, 30%), nitric acid (HNO₃, 70%), sodium chloride (NaCl, analytical grade), and hydrogen peroxide (H₂O₂, 30%) (Fisher Scientific, NJ).

Analytical Equipment

Metal concentrations in leached samples were measured using an inductively coupled plasma spectrophotometer (ICP) (Spectro Flame-EOP, Spectro Analytical Instruments). A digital pH meter (Orion Research Inc.) with a glass pH electrode (Orion Research Inc.) was used for the measurement of pH. Density measurements were carried out using AccuPyc 1330 Pycnometer (Micromeritics Ins. Corp, GA). A Beckman Coulter LS230 (Coulter Corp. Sci. Ins., FL) at Dupont Inc. was used to obtain particle size distributions.

Experimental Design

Representative elementary mass

A representative elementary mass (REM) of brake wear debris was determined for assessing the minimize mass of wear debris that could yield representative data. A series of natural particles from Honda Civic 1998 with increasing masses 5, 15, 25, 35, 45 mg were each digested in 10 mL of acid solution (HNO₃:HCl:H₂O₂ ::1:3:0.5, by volume) (Schlautman, 2002, SC Report). Total Copper in the samples was determined using microwave assisted digestion. The smallest sample mass above which no change in the fraction of Copper per unit mass of particles was observed was selected as the REM, in this case 25 mg. This REM was used as the sample masses in all tests performed in this study.

Total metal content

The natural, artificial, and LACT particles collected were analyzed for total metals using the microwave assisted acid digestion method. Automated microwave-assisted acid digestion was conducted in a commercial microwave sample preparation system.

A REM of brake wear debris was taken and placed into a Teflon microwave digestion vessel. A digesting solution (Sec. 2.4.1) was used in place of the conventional nitric acid solution. A controlled volume (10 mL) of digesting solution was then added to the vessel, and the contents were gently swirled to ensure complete contact of the brake pad particles and digesting solution. The Teflon vessel was then sealed with its Teflon cover and placed into the

microwave for digestion. The consecutive digestion time and temperature program based on EPA Method – 3051 were, 100°C –5 min, 120°C –5min, 160°C –5min and 100°C – 5min. Pure Copper metal and Copper oxide were also digested to check the efficacy of the digestion procedure.

Dissolution/leaching of copper

The leaching experiments were designed to determine the dissolution of metals and other elements from natural and artificial brake wear debris. These experiments were conducted at two pH conditions: pH 4.3 and 6.1, which are representative of rainwater and urban runoff, respectively (Sansalone and Buchberger, 1997).

Batch reactors 250 ml in size were used for the dissolution experiments. A blank reactor served as control. Each reactor was filled with 250 ml of leaching solution with an initial pH 4.3. A solid to liquid ratio of 1:1x10⁴ was selected. The batch reactors were shaken in a horizontal shaker at a uniform speed (200 RPM) throughout the study. The pH of the samples was monitored and 3ml samples were withdrawn from each reactor with time for a period of 15 weeks and 10 weeks, for artificial and natural brake wear debris, respectively. Samples were passed through 0.45-micron filters and then acidified with 0.5% HNO₃ before analysis with ICP. The total Copper in each set of wear debris was determined by summing the mass of Copper leached during the course of experiment and that obtained from digesting the remaining particles at the end of experiment using microwave assisted digestion. The total Copper was used to normalize the dissolution data.

A dissolution study was also conducted at pH 6.1 to observe the effect of pH on dissolution, following the same procedures described above. The reactors were operated for only 120 hrs at the higher pH. The dissolution data collected at this pH were normalized using an independent measurement of total Copper in the brake wear debris: the total Copper in the brake pad wear debris was determined by digesting a subset of the brake wear debris using concentrated nitric acid solution. The procedure described in Sec. 2.4.2 was used for the digestion of particles.

Particle distribution

To understand the fate of Copper in the environment, it is important to determine the size distribution of the Copper-containing particles. The particle size distribution was measured on samples from artificial and natural brake wear debris for all four automobiles studied in this research. The particle size distributions of LACT brake wear debris generated from Honda Accord 2000 and Honda Civic 1998 were also characterized.

A representative sample (25mg) of brake wear debris from each automobile was dispersed and homogenized in 10 ml acetone solution. The suspension was analyzed using Beckman Coulter LS230 to obtain the particle size distribution. The particle size distribution in this instrument is obtained on the basis of the Coulter principle (Jillavenkatesha et al., 2001; Khalili et al.,).

Specific surface areas

A Micromeritics Accelerated Surface Area and Porosimetry System (ASAP) 2010 was used to perform surface area analysis. Specific surface areas of the brake wear debris were determined using an eight-point Brunauer, Emmet and Teller (BET) krypton gas adsorption method. A standard operating procedure using Nitrogen gas was used for the measurement. A

sample mass greater than the REM was used for all analyses. Each sample was accurately weighed and degassed prior to measurement to minimize error.

Results

Total Metal Content and Important Elements in Brake Wear Debris

The mean Copper content of artificial and natural brake wear debris is shown in Table 1, with artificial debris containing significantly more Copper than natural debris. The difference in Copper content suggests entrainment of contaminants from other non-Copper sources in the natural debris, or the preferential loss of Copper in the airborne fraction when the natural debris were generated. The airborne particles were not collected in this study but were emitted into the environment and may have had a higher mass fraction of Copper than the fallout particles collected on the wheels and hubs of the automobiles.

Copper recoveries were $99.8 + 0.006SE\%$ (SE = one standard error) and $94.1 + 0.087SE\%$ for Copper metal and Copper oxide samples, respectively, based on three samples tested with microwave assisted acid digestion. Thus, the efficiency of Copper extraction in the brake pad wear debris was expected to be high.

A greater fraction of Fe was observed in artificial as compared to natural debris for all four automobile types (see Table 1). The higher fraction of Fe was as a result of rotor wear particles generated by abrasion of brake pads against the rotor. It was also observed that different brake pads vary significantly in elemental composition. Copper contents differed among particle type (artificial versus natural) depending on the vehicle, with differences ranging from 40% to a factor of 10, with Copper content always higher for the artificial particles than the natural particles.

Table 1. Total elemental content (percent) in artificial and natural debris

Automobile	Particle Type	Iron (Fe)	Barium (Ba)	Calcium (Ca)	Sulphur (S)	Copper (Cu)
Honda Accord	Artificial	0.92+/- 0.1561	11.60+/- 0.5433	3.35 +/- 0.00258	3.57 +/- 0.1637	30.16 +/- 2.69
	Natural	16.65 +/- 1.3938	5.93 +/- 0.4816	3.18 +/- 0.0908	1.96 +/- 0.1604	6.1698 +/- 0.151
Honda Civic	Artificial	1.2	10.51+/- 1.6322	3.21+/-0.4672	3.12 +/- 0.5767	33.38+/-4.8790
	Natural	3.99+/-0.9674	2.19+/-0.0073	6.44+/-0.0676	0.66+/-0.0439	1.1217+/-0.0583
Toyota Camry	Artificial	13.73+/- 0.5112	11.24+/-0.0318	1.86+/-0.0370	3.58+/-0.05423	8.42+/-0.1395
	Natural	38.56	6.96	1.85	2.15	1.68
Nissan Sentra	Artificial	0	14.19+/-0.3832	2.06+/-0.0331	4.29+/-0.2461	24.44+/-0.535
	Natural	23.43+/- 3.3543	8.38+/- 0.1563	1.95+/-0.1161	2.53+/-0.0696	7.94+/-0.0331

Values reported above are (Mean+/-1SE) based on duplicate samples, SE = one standard error

The amount of Copper in LACT brake wear debris was smaller than that in artificial brake wear debris but larger than natural brake wear debris (Table 2). The difference in Copper content between LACT and artificial particles might be due to the loss of Copper mass in the airborne fraction of wear debris and/or addition of Iron from rotor.

Table 2. Total Copper content (percent) in natural, artificial, and LACT brake wear debris from Honda Accord and Honda Civic

	LACT brake wear debris	Natural brake wear debris	Artificial brake wear debris
Honda Accord 2000	17.32 +/- 0.38	6.097 +/- 0.631	30.16 +/- 2.69
Honda Civic 1998	14.29 +/- 0.95	1.1217 +/- 0.0583	33.38 +/- 4.8790

Values reported above are (Mean+/-1SE) based on duplicate samples, SE = one standard error

Surface Area of Natural and Artificial Brake Wear Debris

Specific surface determined using the BET isotherm differed between the artificial and natural particles. Surface areas for brake wear debris from the four automobile types are shown in Figure 1. Specific surface areas differed by as little as 30% and up to a factor of 10 between artificial and natural particles, depending on the vehicle type. There was no consistent trend in the data, with specific surface areas for the artificial particles sometimes larger and sometimes smaller than the corresponding areas for natural particles.

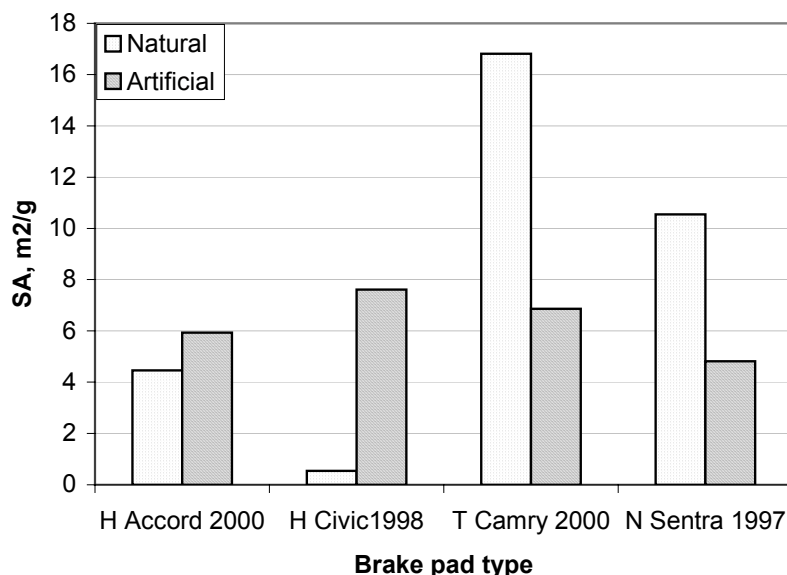


Figure 1. Surface area of artificial and natural brake wear debris.

Distribution of Copper in Artificial and Natural Wear Debris

Artificial and natural brake wear debris were observed under a scanning electron microscope (SEM) to examine the size and morphology of brake wear debris. X-ray energy dispersive spectroscopy (XEDS) was simultaneously performed to examine the distribution of copper and other important elements on debris surfaces. Figures 2-a and 2-b. show the SEM and XEDS of artificial and natural brake wear debris from Honda Accord 2000. The artificial and natural particles were found to range from 1-10 μm in size. Although similar in size, the natural particles were more spherical compared to the artificial which were more angular.

A significant difference was observed in the distribution of Copper in the debris. For the artificial debris, the Copper was primarily associated with the large particles and was found in a few large “clumps.” For the natural debris, on the other hand, the Copper was associated with all

sizes of particles, and no large clumps of Copper were observed in the data. This suggests that the braking process distributes copper more evenly among the wear debris, as opposed to debris generated from sanding the brake pad. This observation was confirmed for all the automobiles tested.

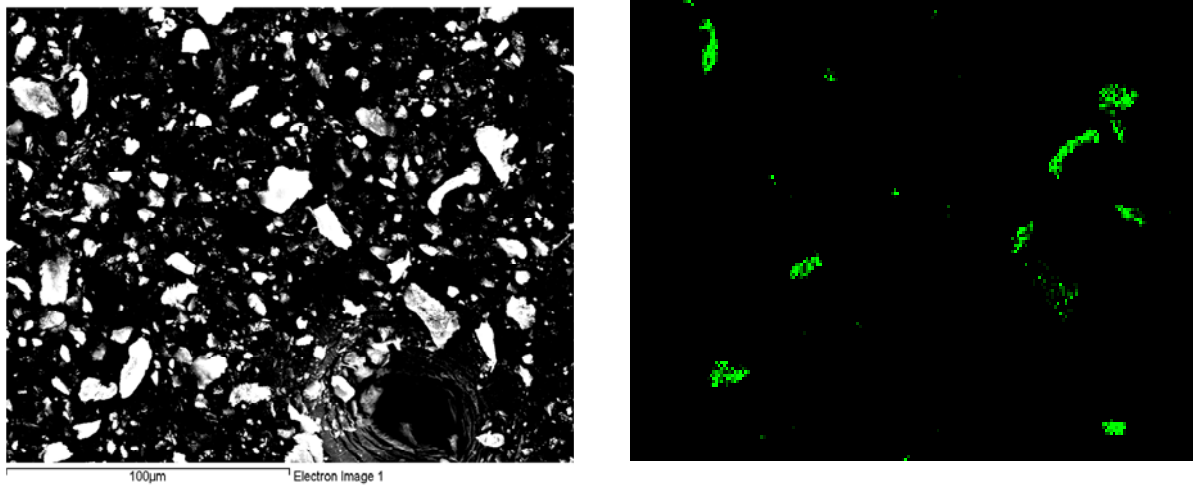


Figure 2a. Scanning micrograph (left) and Copper distribution (right) in artificial brake wear debris from the Honda Accord 2000. The bright spots in the right represent Copper.

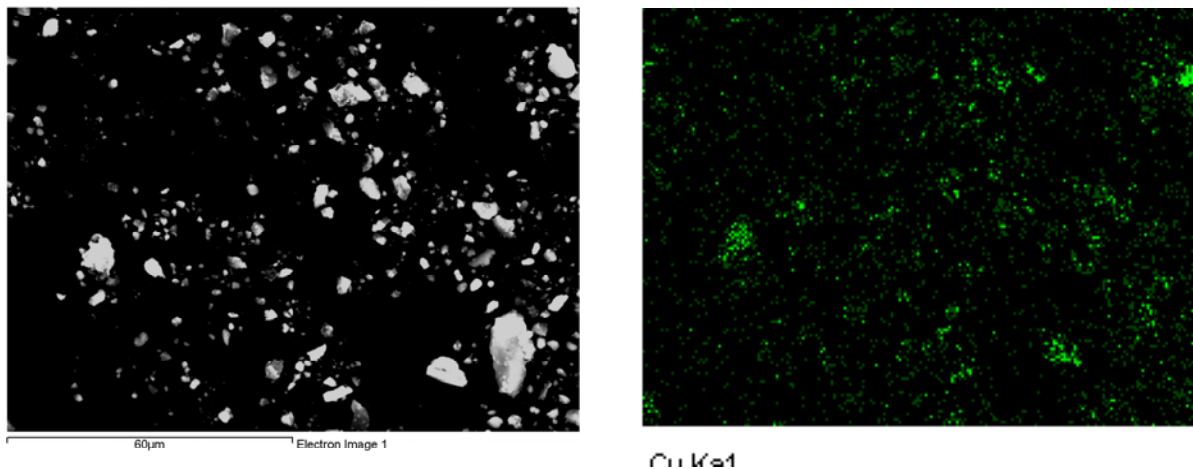


Figure 2b. Scanning micrograph (left) and Copper distribution (right) in artificial brake wear debris from the Honda Accord 2000. The bright spots in the right represent Copper.

Density Measurement

Another important physical parameter for brake wear debris that influences the transport of debris in the environment is particle density. The average densities of artificial and natural brake wear debris for the four automobile types are shown in Table 3. The particle densities showed little variation among automobile types, with the exception of wear debris from the

Honda Civic 1998, where artificial wear debris were significantly more dense than natural debris.

Table 3. Density of artificial and natural brake wear debris

Vehicle Type	Density g/cm ³	
	Artificial wear debris	Natural wear debris
Honda Accord 2000	3.3713±0.0009	3.6128±0.0019
Honda Civic 1998	3.4913±0.0014	2.5±0.0013
Toyota Camry 2000	3.4191±0.0016	3.5115±0.0008
Nissan Sentra 1997	3.5895±0.0018	3.7038±0.0008

Reported +/- values represent one estimated standard error of the mean based on three measurements

Dissolution/Leaching of Metals and Elements at pH 4.3

Figures 3, 4 and 5 show the long-term dissolution study at pH 4.3 with natural and artificial brake wear debris. The results from the long-term study suggest that about 90% of the Copper was leached from natural brake wear debris for all except one vehicle type, the Toyota Camry 2000 (see Figure 3). For the Toyota Camry 2000 about 80% of the Copper was leached over this time period. Dissolution of artificial brake wear debris showed that similar portions of the Copper (90-95%) were leached during the period of this study (2532hrs or 15 weeks) for the different automobile types (see Figure 5).

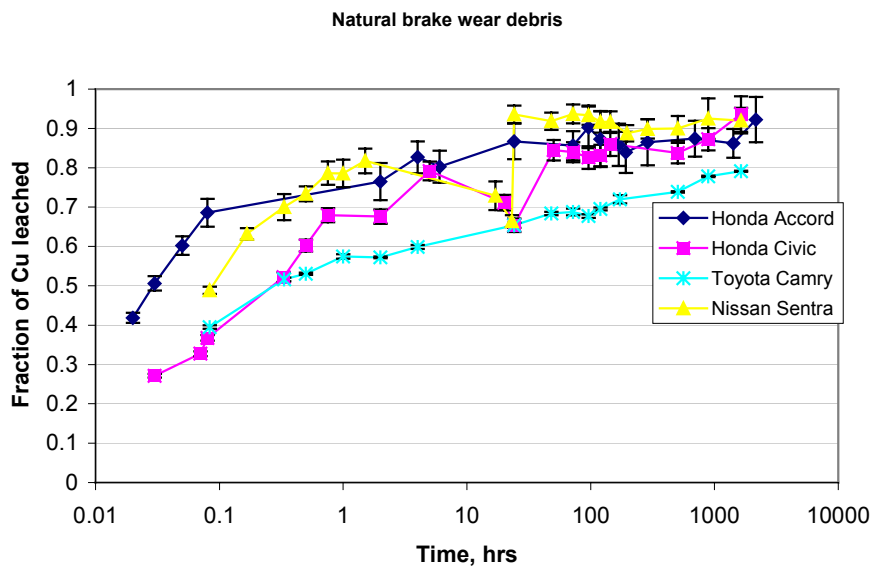


Figure 3. Mass of Cu leached normalized to total Cu content in natural brake wear debris at pH 4.3.

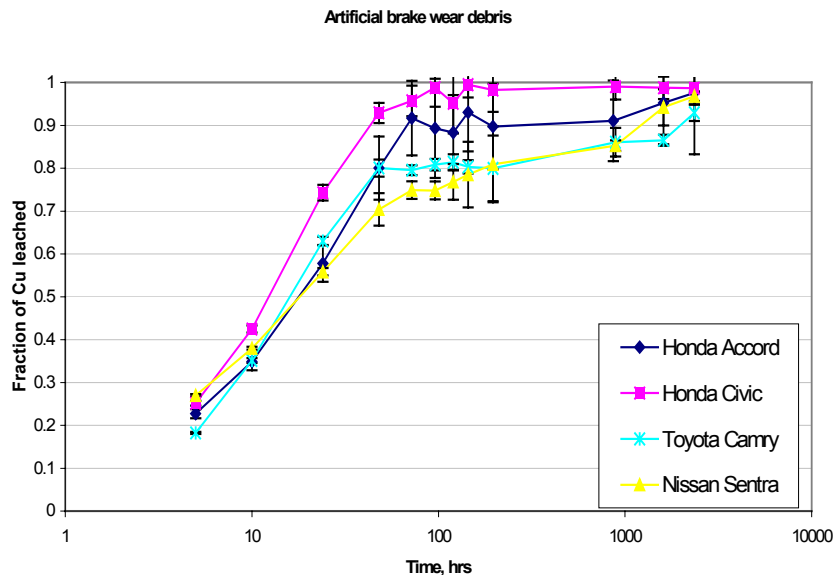


Figure 4. Mass of Cu leached normalized to total Cu content in artificial brake wear debris at pH 4.3.

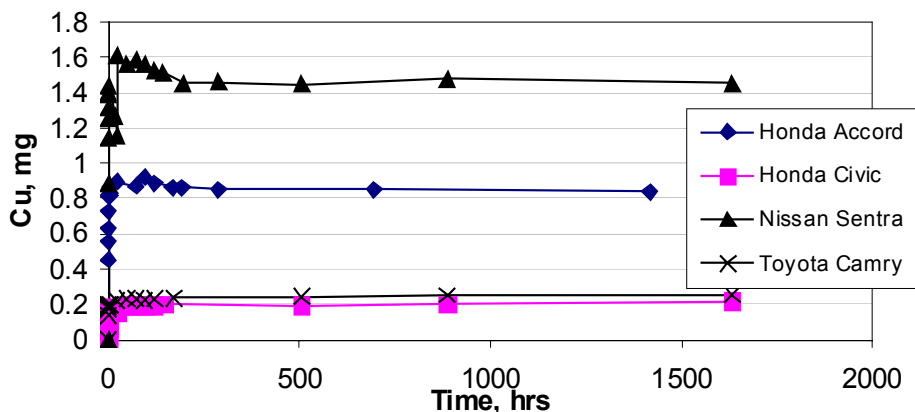


Figure 5. Mass of Copper leached from natural brake wear debris.

While the fraction of the Copper leached from the four automobile types were quite similar at pH 4.3, the aqueous concentrations of Copper were dramatically different between the four automobile types. This can be readily seen in Figure 5, where significant differences in the mass of Copper leached from each set of natural debris collected from the different automobiles was observed. Since an identical solution volume was used in each experiment, the corresponding aqueous phase concentrations at the completion of each experiment differed by up to a factor of 7. Similar results were found for the artificial particles. Dissolution was more rapid (compare Figures 3 and 4) and aqueous Copper concentrations lower in the natural wear debris as compared to artificial debris. Despite these differences, normalizing the data to the mass of Copper in the particles resulted in similar fractions of Copper leached across all automobile types and for both types of particles. This is an important observation that suggests

that dissolution of Copper from artificial wear debris, which is relatively easy to obtain, may be used to estimate Copper dissolution from more naturally generated debris.

Dissolution/Leaching of Metals and Elements at pH 6.1

Figures 6 and 7 show the dissolution data from natural and artificial brake wear debris at pH 6.1. Though equilibrium appears to have been reached for natural brake wear debris at ~ 24 hrs, equilibrium was not reached even at 120 hrs for artificial brake wear debris. The rates of Copper dissolution from artificial and natural brake wear debris showed a marked difference, with much slower rates of dissolution for artificial versus natural particles. This observation is consistent with observations at pH 4.3 (see Figures 3 and 4). The higher rate of Copper dissolution in natural brake wear debris was due to more homogenous and uniform distribution of Copper in debris (Sec 3.3) and possibly higher surface areas associated with smaller particles.

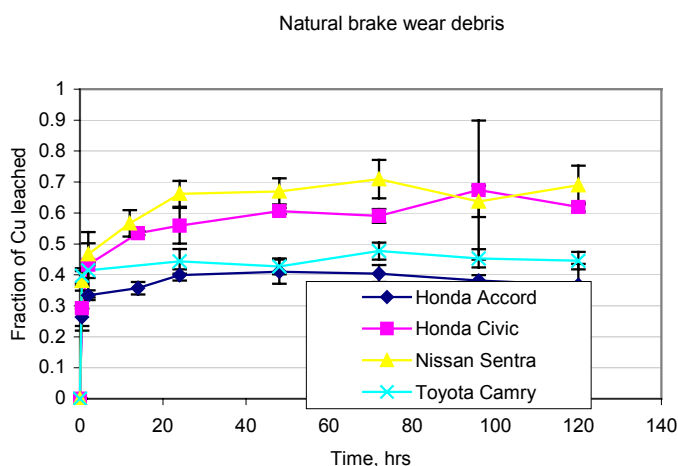


Figure 6. Mass of Copper leached normalized to total Copper content in artificial brake wear debris at pH 6.1.

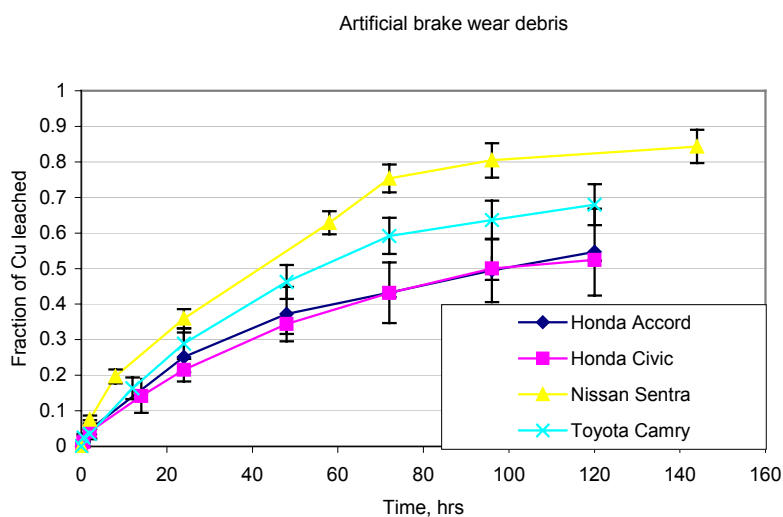


Figure 7. Mass of Copper leached normalized to total Copper content in artificial brake wear debris at pH 6.1.

Comparison of Dissolution at pH 4.3 and 6.1

The total Copper leached from natural brake wear debris at 120 hrs is compared for pH 4.3 and pH 6.1 in Figure 8. The amount of Copper leached at pH 6.1 is smaller than at pH 4.3. The percent of Copper leached at pH 6.1 vs pH 4.3 was 70% vs 92% for Nissan Sentra, 45% vs 69% for Toyota Camry, 37% vs 88% for Honda Accord, and 62% vs 83% for Honda Civic, respectively. The effect of pH on dissolution may be due to proton competition. At low pH the high proton (H^+) activity results in greater leaching of Copper in the solution due to proton displacement. In comparison, at high pH the low proton (H^+) activity results in smaller leaching of Copper in the solution. It should be noted that the comparisons of Copper leached were performed at 120 hrs from the initiation of the experiments. The total amount of Copper that can be readily leached can only be known by conducting the experiments for longer times (e.g., see Nissan Sentra data in Figure 3.).

In addition to the pH effect, the data suggested different trends in the amount of Copper leached from the four vehicle types. For example, the fraction of Copper leached from the brake wear debris of the Honda Accord 2000 at high pH was smallest among the four vehicle types, whereas at the low pH the amount of Copper leached was similar to two of the other three vehicle types. This suggests that leaching of Copper from natural brake wear debris behaves differently at different pH conditions for the various automobile types. This in turn suggests that the forms of Copper in the brake wear debris is likely different for the different automobile types.

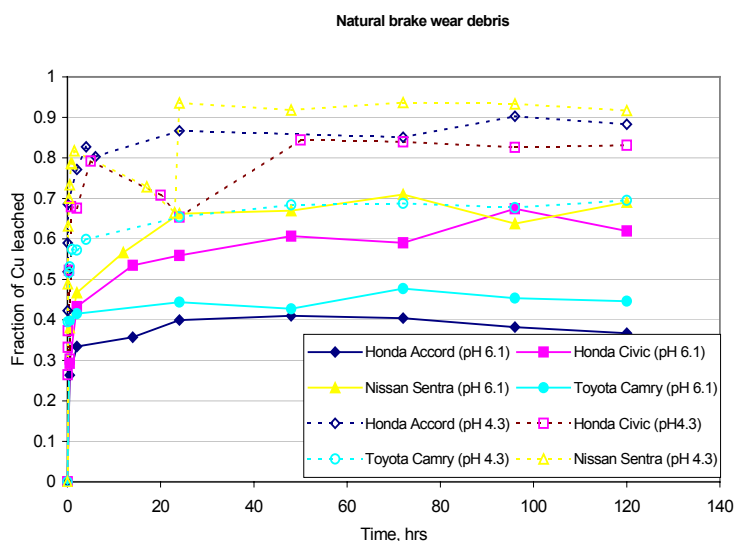


Figure 8. Fraction of Copper leached from natural brake wear debris at pH 4.3 and pH 6.1. Solid and open symbols represent pH 6.1 and 4.3 respectively.

Estimating Copper Emissions from Natural Wear Debris with Artificial Wear Debris

A comparison of the percent Copper leached from artificial and natural brake wear debris at 1600 hrs (pH 4.3) and 120 hrs (pH 6.1) is shown in Table 4. The error associated with prediction of Copper leached from natural brake wear debris using artificial brake wear debris is also shown. At pH 4.3 where the experiments were carried out for a longer time, the artificial wear debris gives a conservative (high) estimate of the amount of Copper leached from natural

brake wear debris. The error associated with the prediction of Copper leached ranged from 2 to 9%.

Table 4. Prediction of leached Copper from natural wear debris using artificial wear debris

Brake Pad	Copper leached (%) at 1600 hrs (pH 4.3)			Copper leached (%) at 120 hrs (pH 6.1)		
	Artificial wear debris	Natural wear debris	Error in prediction	Artificial wear debris	Natural wear debris	Error in prediction
Nissan Sentra	94.21	92.5	1.85	84.33	69.03	22.16
Toyota Camry	86.5	79.12	9.33	67.98	44.59	52.46
Honda Accord	98.73	93.63	5.45	54.66	36.72	48.86
Honda Civic	95.22	92.22	3.25	52.44	61.92	-15.31

At pH 6.1 the error associated with the prediction of Copper leached from natural brake wear debris using data from artificial debris varied from -15 to 52%. Thus, at this pH using artificial wear debris to predict Copper emission from natural debris would result in significant error. However, emissions from artificial debris are *larger* than corresponding emissions from natural debris for all but one vehicle type. Thus, artificial wear debris might be used to make conservative (high) estimates of the fraction of leachable Copper from natural wear debris for many automobile types.

Particle Size Distribution of Artificial, Natural and LACT Brake Wear Debris

The artificial brake wear debris collected from four automobiles were analyzed for particle size distribution. Figures 9 and 10 shows the distribution of particles for the four automobile types for the artificial and natural wear debris, respectively. The distribution of particles found in the artificial wear debris were found to be similar for all automobiles.

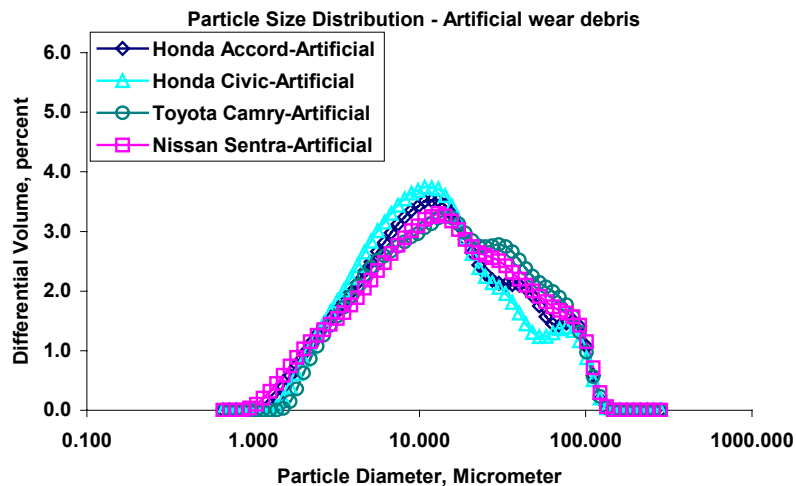


Figure 9. Particle size distribution of artificial brake wear debris.

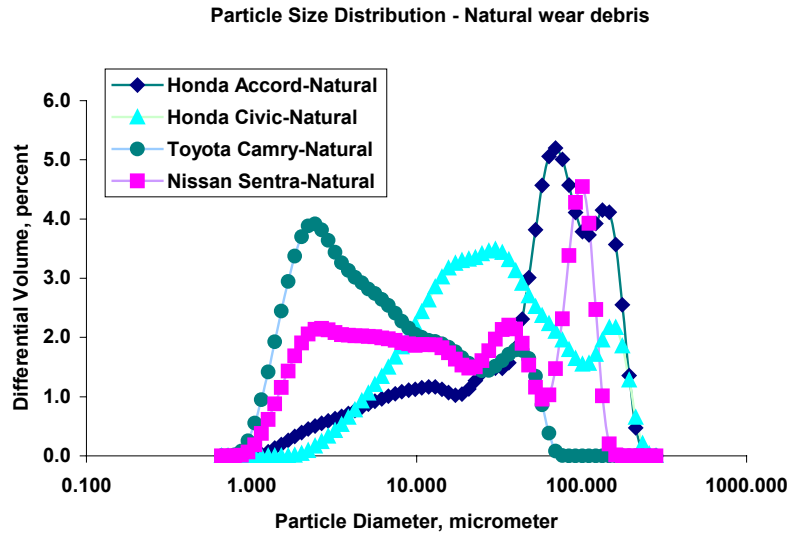


Figure 10. Particle size distribution of natural brake wear debris.

In contrast to artificial wear debris, significant differences were found in natural brake wear debris. The distribution of particles was different within the four automobiles and across the two particle classes (artificial and natural).

The mean particle size for artificial and natural wear debris for the four automobiles tested is shown in Table 5. The mean particle sizes in artificial wear debris were similar with mean particle size ranging from approximately 12 to 15 microns. The mean particle size for natural wear debris varied by up to a factor of 13 for the four automobile types (Table 5). The artificial and natural wear debris differed with each other by as little as 6% to as much as a factor of 5. These variations in the size of natural wear debris might be due to the entrainment of particles such as Silica and Iron from external sources, which are absent in artificial wear debris. Differences in particle size distributions between the natural wear debris collected from the four automobile types might also be associated with differences in driving behavior of the owners of these automobiles.

Table 5. Mean particle size (volume distribution) for artificial natural and LACT wear debris

Automobile	Artificial wear debris	Natural wear debris	LACT wear debris
Honda Accord	12.68 +/- 0.73	65.21 +/- 0.37	9.25 +/- 0.009
Honda Civic	11.89 +/- 0.44	28.62 +/- 0.66	8.11 +/- 0.134
Toyota Camry	15.40 +/- 0.58	5.00 +/- 0.47	-NA-
Nissan Sentra	14.1254 +/- 0.44	15.03 +/- 0.79	-NA-

Reported +/- values represent one estimated standard error of the mean based on three measurements.

Particle size distributions for the LACT particles from Honda Accord 2000 and Honda Civic 1998 suggested deviations from the other two classes of particles tested. The distribution of LACT particles are compared with the natural particles in Figure 11. The two classes of particles (LACT and natural) varied significantly from each other, with mean particle size 3 to 7 times smaller for the LACT than the natural particles (Table 5). The reason for these significant

differences are unknown, but undoubtedly due to the difference in the methodologies used to generate the two types of particles. Figure 12 shows the cumulative distribution of LACT and natural particles for the two automobiles.

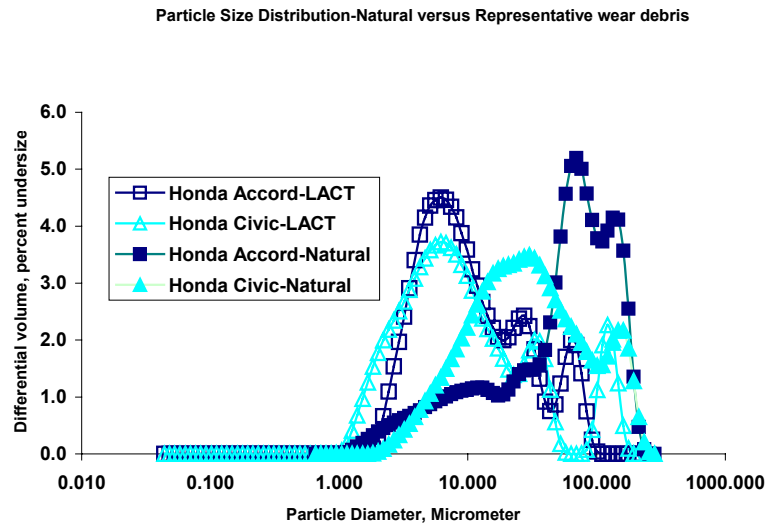


Figure 11. Particle size distribution of natural versus LACT wear debris.

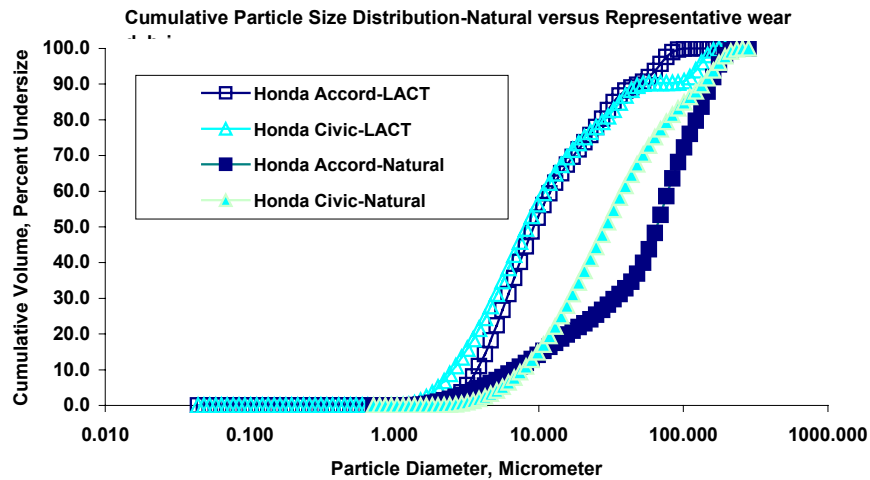


Figure 12. Cumulative particle size distribution of natural versus LACT wear debris.

Prediction and confirmation of bimetallic oxides

The braking process results in rise in temperature at the surface of brake pads and rotor. The braking process results in rise in temperature at the surface of brake pads and rotor. Studies performed in the past have measured elevated ambient temperatures around the brake pads in laboratory (Zaidi and Senouci, 1999; Bettge and Starcevic, 2002). Also it has been predicted that the actual temperature at the brake pad-rotor surface can increase to as high as 500°C. Brake pads are composed of various compounds. The important elements in brake pad formulation are Copper, Iron, Barium, Sulfur, Aluminum and organics. This rise in temperature may result in

reactions of the various products added in the brake pad formulation to form other species/compounds. In an attempt to characterize the species formed during the braking process, thermodynamic modeling software was used. Interactions between the compounds were modeled using FACTSAGE 5.2 (Bale et al., 2002).

Barium and Aluminum compounds were found to be stable under the conditions observed in braking. However an important reaction was observed with the interaction of Oxygen with Copper and Iron. The reaction will be significantly affected by the amount of Oxygen (partial pressure) present in the region of interest.

Figure 13 shows the output from FACTSAGE for the reactions between Oxygen, Iron, and Copper. The input values selected for the modeling were Iron (mole ratio) = 0.5, Temperature range = 250 – 2000 K and Oxygen (partial pressure) range = 10^{-20} – 10^{-8} . These input values bound the conditions that are expected to occur during the braking process. The FACTSAGE model predicts the formation of bimetallic oxides; $\text{Cu}_2\text{Fe}_2\text{O}_4$ and CuFe_2O_4 at temperatures as low as 633 K for varying partial pressures of oxygen. Thus, the formation of these bi-metallic compounds seems quite likely in the braking process.

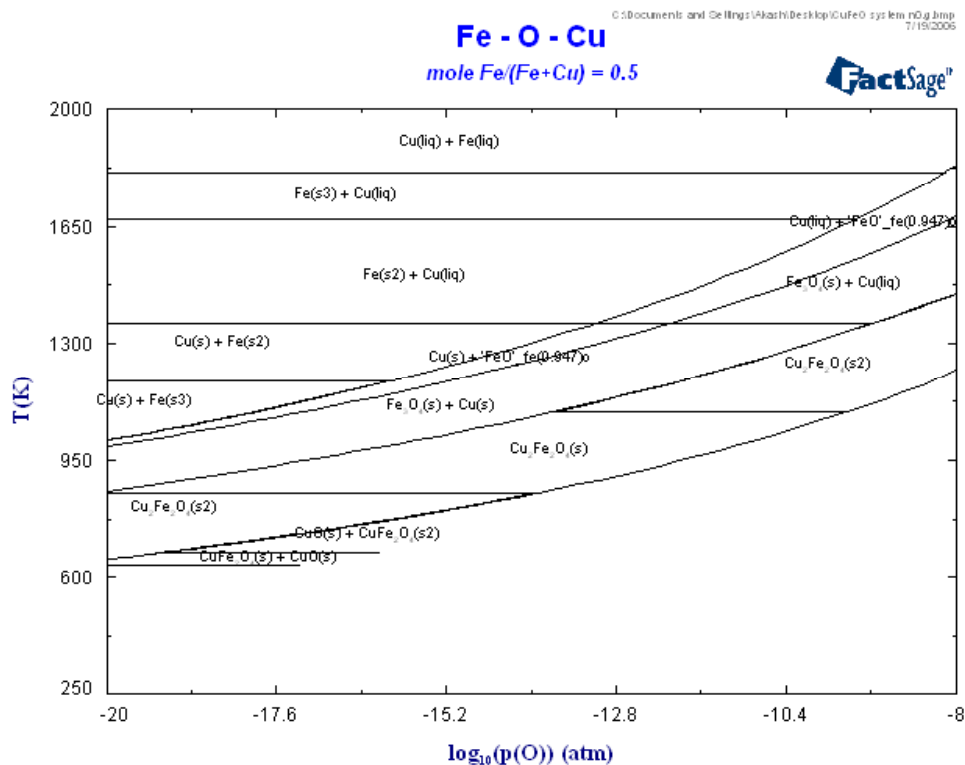


Figure 13. Prediction from Thermodynamic modeling software FACTSAGE-5.2.

Figure 14a and 14b shows elemental maps from of Iron and Copper for artificial and natural brake wear debris, respectively, from Honda Accord 2000. The black dots represent Iron and Copper on the particle surfaces. Consistent with analyses reported earlier, Copper is more uniform in natural brake wear debris while it is preferentially associated with large particles in artificial brake wear debris. Iron and Copper are also observed to coexist in the natural brake wear debris whereas the two elements are found at different spatial locations in artificial particles. Similar observations were noted for the other brake wear debris from other

automobiles. The co-occurrence of Copper and Iron at the same spatial locations supports predictions from the thermodynamic modeling. These results will be quantified in ongoing work by performing a spatial correlation analysis between the two elements for these wear debris.

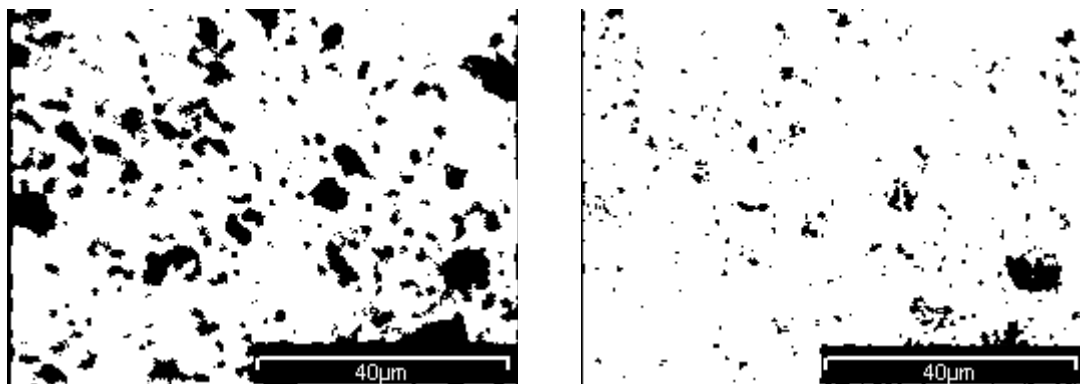


Figure 14a. Elemental map of Iron and Copper from one spatial location within natural brake wear debris for Honda Accord 2000. “Black” regions indicate spatial locations of the element in question.

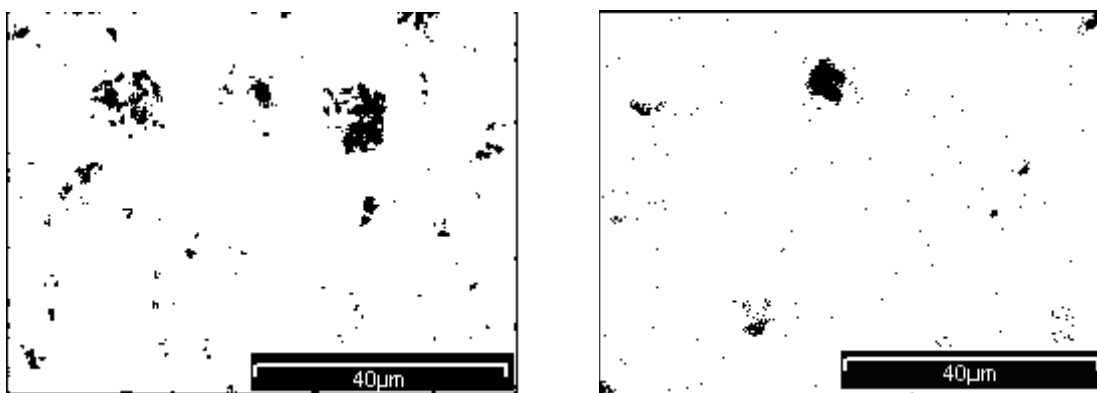


Figure 14b. Elemental map of Iron and Copper from one spatial location within artificial brake wear debris for Honda Accord 2000. “Black” regions indicate spatial locations of the element in question.

Discussion

The fate of brake wear debris in the environment depends on the chemical composition of brake particles released during braking. The two categories of particles generated in the lab - artificial and LACT - were compared with natural particles to assess and predict the fate of Copper from brake wear debris. The elemental analysis performed on the artificial, LACT and natural particles suggest that substantial amounts of material are added to brake wear debris before it enters the environment. Most notably, this includes Iron from the automobile rotors. Significant amounts of Silica were also observed in XEDS analyses of natural wear debris (data not presented in this report).

The composition of LACT particles differed from natural brake wear debris. The only possible source of interference in LACT particles was the rotor wear debris, while the natural particles were contaminated by both Iron and Silica. As a result of this interference (Iron from rotors and Silica from road dust) the chemical fingerprint of brake wear debris released in the

environment will be different than that of abraded brake wear particles generated under laboratory conditions. While this statement clearly holds for the fallout particles analyzed here, it may not hold for airborne particles. In ongoing work the airborne particles generated from the LACT test will be analyzed and compared with natural, artificial and the LACT fallout particles.

The pH conditions (4.3 and 6.1) used for the dissolution study bracket the typical pH conditions reported for rainfall and stormwater runoff (Sansalone and Buchberger, 1997). The mass fraction of Copper leached varied significantly between these two pH conditions, suggesting a wide range of Copper leaching characteristics from wear debris exposed to different environmental conditions.

The final Copper concentrations in the leaching solutions for natural and artificial wear debris were dramatically different between automobile types at both pH conditions (e.g., Figure 5). However, when the dissolution data were normalized with the total Copper content of the particles, the fraction of the Copper dissolved was quite similar for the four automobile types tested at pH 4.3, with approximately 90% of the Copper contained in the natural particles leached for three automobile types while for the fourth (Toyota Camry 2000) approximately 80% was leached. The normalized data also suggests that the amount of leachable Copper from natural brake wear debris might be predicted based on the Copper leached from artificial brake wear debris with an error that ranged between 2 to 9% for the four automobiles. When the same analysis was repeated with data at pH 6.1, the differences in leachable Copper between artificial and natural wear debris were more significant (-15 to 52%), but again the artificial debris resulted in higher Copper fractions leached than natural debris for all but one automobile type. Thus, artificial wear debris might be used to make conservative (high) estimates of the leachable Copper from natural wear debris, although further analysis of particles from other automobile types and in other leaching solutions is needed to substantiate this.

At both pH conditions the natural wear debris showed a fast rate of Copper dissolution at early time followed by a slow rate of leaching. The data also indicate a significant pH effect with more Copper leached at pH 4.3 than at pH 6.1. Both findings are consistent with the results reported in recent studies of Copper dissolution from wear debris collected from an unknown brake pad (Hur et al., 2004) and from a composite of representative brake pads (Schlautman and Haselden, 2006). The amount of Copper leached over the first 18 hours into the solution with pH 6.1 ranged between 35 –55% for the four automobile types. This result, though, is significantly greater than the 18% Copper leached over the same time period from an unknown brake pad into distilled deionized water with a final pH of 6.0 (Hur et al., 2004). This difference between the two studies is likely due to differences in the forms of Copper in the brake pads tested.

For Copper dissolution from natural particles at pH 6.1 there was greater variability among the automobile types in the fraction leached than at pH 4.3. The dissolution data at pH 6.1 versus pH 4.3 also suggest different trends in the amount of Copper leached from the four vehicle types. For example, the fraction of Copper leached from the brake wear debris of the Honda Accord 2000 at pH 6.1 was smallest among the four vehicle types, whereas at pH 4.3 the amount of Copper leached for this automobile was high and similar to two of the other three vehicle types. The leaching of Copper from natural brake wear debris thus behaves differently at different pH conditions. This suggests that the predominant form of the leachable Copper in the natural brake wear debris may be different between the four automobile types tested.

Due to high temperatures at the brake pad surfaces, chemical reactions likely occur during the braking process. Thermodynamic modeling (using FactSage 5.2) was used to predict the change in composition of brake pad materials during braking, which should provide insight

into the forms of Copper that might exist in wear debris. This analysis, when combined with spectroscopy data and leaching studies, may provide a means to predict the forms of Copper in brake pad wear debris for brake pad formulations that are not a part of our testing materials, and the corresponding Copper leaching characteristics associated with these wear debris. The results of this analysis presented here suggest that bimetallic elements will form in the braking process, which was supported with the data from one automobile type. Thus, thermodynamic modeling may hold promise for assessing the impact of new formulations of brake pads on the chemical composition of wear debris.

The particle size distribution data suggest that a substantial fraction of particles in natural brake wear debris were less than 10 microns in size. This data is similar to the mass mean diameter of the airborne brake wear debris, which was reported to be 2.7 microns (Haselden et al., 2006), 6 microns (Sanders et al., 2003), and 0.5-2.5 microns (Garg et al., 2003). These observations suggest that the natural brake wear debris collected in this study contain particles that might otherwise be airborne.

The average size of natural brake wear debris released in the environment was three to ten times larger than LACT debris for the two automobile types tested. The deviations in particle sizes suggest that dissolution rates of Copper from LACT particles will be different from natural wear debris, which will be tested in ongoing work at the University of Delaware.

To better understand the fate of Copper leached from brake wear debris and the influence of environmental conditions, additional experimental, modeling and spectroscopic analyses are underway using supplemental funding from the University of Delaware. The experiments will be used to assess Copper leaching under different environmental conditions, and to further evaluate the utility of using artificial wear debris for estimating. Copper leaching from natural particles will be performed in the presence of dissolved organic matter, which may enhance the rate of leaching but reduce the amount of free Copper in solution. The dissolution of Copper from the airborne and non-airborne fraction of LACT particles will also be studied at pH 4.3 and pH 6.1.

Literature Cited

- Bale, C.W., Chartrand, P., Degterov, S.A., Eriksson, G., Hack, K., Mahfoud, R.B., Melancon, J., Pelton, A.D. and Petersen, S. (2002) FactSage Thermochemical Software and Databases. *Calphad*. 26(2):189-228.
- Bettge, D., and Starcevic, J. (2002) Topographic properties of the contact zones of wear surfaces in disc brakes. *Wear*. 254:195-202.
- Davis, A. P., Shokouhian, M., and Ni, S. (2001) Loading Estimates of Lead Copper, Cadmium, and Zinc in Urban Runoff from Specific Sources. *Chemosphere* 44:997-1009.
- Garg, B.D., Cadle, S.H., Mulawa, P.A., Groblicki, P.J., Laroo, C. and Parr, G.A. (2000) Brake wear particulate matter emissions. *Environ. Sci. Technol.* 34:4463-4469.
- Haselden, A., Christoforou, C., and Schlautman, M. (2006) Characterization of airborne brake wear debris. Final Report to the Association of Bay Area Governments, San Francisco Estuary Project. CA, downloaded from <http://www.suscon.org/brakepad/documents.asp>.
- Hur, J., Yim, S., and Schlautman, M. (2003) Copper leaching from brake wear debris in standard extraction solutions. *J. Environ. Monit.* 5(5):837-843.

- Hur, J., Schlautman, M. A., and Yim, S. 2004. Effect of Organic Ligands and pH on the Leaching of Copper from Brake Pad Wear Debris in Model Environmental Solutions. *J. Environ. Monit.* 6:89-94.
- Jillavenkatesha, A., Dapkunas, S.J., and Lum, L.H. (2001) Particle Size Characterization – Practice Guide. Special Publication 960-1. N.I.S.T.
- Khalili, M.A., Solimeo, H.T., and Hockman, J.N., An Investigation for Optimizing Sample Preparation and Measurement Conditions for a TiO₂ Powder for Measuring Particle Size Distribution by Beckman Coulter LS230, Dupont Company, DE, downloaded from <http://www.beckmancoulter.com/literature/Bioresearch/ar-407.pdf>
- Pitt, R., Field, R., Lalor, M., and Brown, M. (1995) Urban Stormwater Toxic Pollutants: Assessment, Sources, And Treatability. *Water Environment Research* 67(3):260-275.
- Santa Clara Valley Regional Pollution Prevention Program, 1997. Evaluation of Nine Metals of Concern, Volume II, , San Jose, CA.
- Sanders, P.G., Xu, N., Dalka T.M. and Maricq, M. (2003) Airborne Brake Wear Debris: Size Distributions, Composition, and a Comparison of Dynamometer and Vehicle Tests. *Environ. Sci. Technol.* 37:4060-4069.
- Sansalone, J.J., and Buchberger, S.G. (1997) Partitioning and First Flush of Metals in Urban Roadway Stormwater. *J. Environ. Eng.* 123(2):134-143.
- Schlautman, M.A. and Haselden, A., (2006) Chemical Characterization of the Nonairborne Fraction of the Representative Brake Pad Wear Debris Sample, Report to the Association of Bay Area Governments, San Francisco Estuary Project, CA, downloaded from <http://www.suscon.org/brakepad/documents.asp>
- Soucek, D.J., Cherry, D.S., and Zipper, C.E. (2003) Impacts of Mine Drainage and Other Nonpoint Source Pollutants on Aquatic Biota in the Upper Powell River System, Virginia. *Human and Ecological Risk Assessment*, 9(4):1059-1073.
- Trainor, J.T., (2001) Disc Brake Wear Debris Generation and Characterization: A Dynamometer Based Protocol for Generating and Collecting Vehicle Disc Brake Wear Debris, Prepared by the Brake Manufacturers Council Product Environmental Committee in Collaboration with the Brake Pad Partnership.
- Trainor, J.; Duncan, T.; and Mangan, R., (2002) Disc Brake Wear Debris Generation and Collection, 2002-01-2595, SAE Technical Paper Series, SAE International, Warrendale, PA, 2002. (available for purchase at www.sae.org/servlets/productDetail?PROD_TYP=PAPER&PROD_CD=2002-01-2595).
- USEPA. 2002. National Section 303(d) List Fact Sheet.
- Zaidi, H., and Senouci, A. (1999) Thermal Tribological Behavior of Composite Carbon Metal/Steel Brake. *Applied Surface Science* 144-145:265-271

The Impact of Surface Precipitation on Sequestration and Bioavailability of Metals in Soils

Donald L. Sparks and Edward Peltier, Zhenqing Shi
Department of Plant and Soil Sciences
University of Delaware
Newark, DE 19716

and
Danial van der Lelie
Biology Department
Brookhaven National Laboratory
Upton, NY 11973

Objectives and Background Information

The objectives of this study are to investigate the formation and residence time of metal precipitate phases, particularly metal hydroxides, in contaminated soils under a range of environmental conditions and the effect this formation has on metal availability and sequestration in field contaminated soils. Sorption, sequestration, and precipitation of metals within the soil matrix are critical processes affecting contaminant speciation, toxicity, transport and bioavailability. Unfortunately, there is a lack of fundamental understanding of these processes in natural soil systems at a molecular, mechanistic level. In order to improve the decision making process for metal contaminated sites and develop reliable risk assessment methods, it is necessary to acquire a more thorough understanding of the processes controlling metal mobility, speciation and bioavailability in contaminated soils.

An important sorption mechanism for metal retention in natural system is the formation of polynuclear metal hydroxide complexes and surface precipitates. A number of investigators, using in-situ x-ray absorption fine structure spectroscopy (XAFS), have shown that metal (Co, Cr, Cu, Ni, Pb, and Zn) hydroxide complexes and surface precipitates can form on the surfaces of important soil components such as clay minerals and metal oxides (Chisholm-Brause et al., 1990; Charlet and Manceau, 1992; Fendorf et al., 1994; O'Day et al., 1994; Scheidegger et al., 1997; Towle et al., 1997; Scheidegger et al., 1998; Ford et al., 1999; Thompson et al., 1999; Ford and Sparks, 2000). The formation of these precipitates occurs at pHs undersaturated with respect to pure metal hydroxide solubility and at submonolayer surface loadings. In many cases, the surface precipitates occur on time scales of minutes (Scheidegger et al., 1998; Roberts et al., 1999). Moreover, research from our group at the University of Delaware, using X-ray absorption fine structure spectroscopy (XAFS) and diffuse reflectance spectroscopy (DRS), has precisely shown that metal (Ni and Zn) sorption on Al-bearing clay minerals, metal oxides, and soils results in the formation of mixed metal-Al hydroxide precipitates while metal hydroxide precipitates form on non-Al bearing minerals Ford et al., 1999; Roberts et al., 1999; Scheinost et al., 1999). Co-Al hydroxide surface precipitates have been noted by Towle et al. (1997) and Thompson et al. (1999). These precipitate phases share structural features common to the hydroxalite group of minerals and the layered double hydroxides (LDH) observed in catalyst synthesis. The LDH structure is built up of stacked sheets of edge-sharing metal octahedra containing divalent (e.g., Mg(II), Ni(II), Co(II), Zn(II), Mn(II)) and trivalent (e.g., Al(III), Fe(III), and Cr(III)) metal ions separated by anions between the interlayer spaces. The LDH structure exhibits a net positive charge, x , per formula unit (e.g., when Al(III) would substitute for a divalent metal in the octahedral layer) which is balanced by an equal negative charge from interlayer anions. While mixed Co-Al, Ni-Al and Zn-Al hydroxide surface precipitates form on Al-bearing metal oxides and phyllosilicates, which appears to be related to the similar size of Co(II), Ni(II), and Zn(II) to Al(III) such that substitutions could occur, such phases have not been observed with Pb(II). This could be related to the mismatch in size between Pb(II) and Al(III), preventing substitution.

As these surface precipitates age, metal retention is greatly enhanced. Several studies document that, as LDH-type precipitates that have formed on a pyrophyllite clay mineral substrate age, Ni release is greatly impeded (Scheckel et al., 2000; Scheckel and Sparks, 2001). With increased aging time the mixed Ni-Al surface precipitate on the pyrophyllite surface was transformed to a precursor mixed Ni-Al phyllosilicate surface precipitate phase, greatly enhancing the stability of Ni. The increased stability is due to a combination of factors, depending on sorbent structure, but includes enhanced silication of the interlayers of the LDH

phases and Ostwald ripening (Ford et al., 1999; Scheckel et al., 2000). In short, the formation of metal hydroxide surface precipitates could be an important way that metals could be sequestered in soils, greatly diminishing their mobility and bioavailability.

However, questions remain as to whether such phases occur in soils, what environmental conditions (e.g., pH, time, metal loadings, competitive ions and sorbents) affect metal precipitate formation, and how precipitate formation and residence time affects metal sequestration/release from field contaminated soils. Some preliminary data collected by our group suggests that metal hydroxide surface precipitates can form in soils. Studies by Roberts et al. (1999) found that mixed metal-Al surface precipitates formed on the clay fraction of a Matapeake silt loam soil from Delaware and the whole soil when reacted with Ni in the laboratory (a Ni concentration of 3 mM and a reaction pH of 7.5). The intensity of the precipitate formation was enhanced as time increased. Precipitates also formed at pH 6.8, but not at pH 6 under similar reaction conditions. It is hypothesized that under soil pH conditions of 6.5 and higher and at relatively high metal loadings, which would be the case for some contaminated soils, metal surface precipitates form and they could significantly sequester the metal so that it is less mobile and bioavailable. More recently, Nachtegaal et al. (2005) have shown that both mixed metal-Al and metal phyllosilicate phases occur in Zn-contaminated and remediated soils, respectively, from Belgium. In order to establish the importance of these soils under field contamination conditions and to develop predictive models incorporating these phases where appropriate, a better understanding of precipitate formation and stability under field soil conditions is required.

Besides the direct identification of Ni speciation in soils, a more quantitative understanding of Ni reaction kinetics is important for predicting Ni behavior in soils. Both solution chemistry (e.g. pH and Ni concentration) and soil composition can affect Ni reaction kinetics. Ni can form surface complexes with soil organic matter (SOM) and also precipitate on mineral phases at higher pH. Accounting for all these variables and various species in kinetics models is essential for developing predictive models.

The nonlinearity of sorption reactions in soils has been accounted for by using either Langmuir or Freundlich isotherms (Amacher et al., 1988; Schlebaum, et al., 1999). However, both Langmuir and Freundlich isotherms are empirical and application of model parameters from one condition to other conditions is limited. Recently, some mechanistic equilibrium models have been developed and successfully used to describe metal partitioning between soils and solutions such as the Windermere Humic Aqueous Model (WHAM) (Tipping, 1994; Tipping *et al.*, 2003). It has been recognized that, in kinetics models, the kinetic rate coefficients are not independent with each other but constrained by the reaction equilibrium status (Shi et al., 2005). For example, the adsorption and desorption rate coefficients are constrained by the equilibrium partition coefficient. The kinetics models based on the well-calibrated mechanistic equilibrium model are promising for predicting metal reaction rates in soils at various reaction conditions.

The formation of Ni layered double hydroxides (LDH) is dependent on solution pH, Ni concentrations and the substrate where the Al can be released into the solutions. The Ni-LDH phase is thermodynamically stable (Peltier et al., 2006) and may be an important species in sequestering Ni in soils. Although the kinetic reactions for Ni-LDH have been investigated by multiple studies (Scheidegger et al., 1998; Roberts et al., 1999; Scheckel et al., 2000; Scheckel and Sparks, 2001; Nachtegaal and Sparks, 2003), there is an absence of quantitative calculations of Ni-LDH precipitation and dissolution rates especially due to SOM complexation of Ni in soils.

With the aid of X-ray Absorption Spectroscopy (XAS), it is possible to determine Ni speciation at different reaction conditions. The quick-scanning x-ray absorption spectroscopy (QEXAFS) enables us to quickly collect the data on Ni speciation on the soil surface during the initial stages of Ni sorption onto the soil surface. XAS measurements provide direct speciation and reaction mechanism information for kinetics modeling.

Approach

The specific hypotheses being tested in this research are:

1. The formation of polynuclear metal hydroxide complexes and surface precipitates, particularly layered double hydroxides, could play a significant role in trace metal speciation and sequestration in contaminated soils with pH levels ≥ 6.5 .
2. Formation of these precipitates sequesters metals into stable phases of low bioavailability, reducing their toxicity to the surrounding ecosystem.

In order to test these hypotheses, our experimental approach has focused on assessing metal speciation in laboratory contaminated soils and soil parameters controlling the formation of layered double hydroxide (LDH) phases. We have also examined interaction between precipitate formation, metal retention and bioavailability and modeled Ni sorption and desorption kinetics on the soils. Studies using soils reacted with Ni in the laboratory under conditions representative of those found in field contaminated soils have demonstrated the formation of Ni LDH precipitates at $\text{pH} \geq 7$ when the appropriate aluminum bearing clay substrates are present. Kinetic studies show that these phases form rapidly, within 4-24 hours after the addition of Ni. BIOMET analysis of metal bioavailability in these soils has also been carried out to determine the effect of precipitate formation on metal sequestration and toxicity to nickel-sensitive microbial species. Concurrent thermodynamic analyses of the formation and stability of these LDH precipitate phases has allowed us to begin to predict the conditions allowing for their formation in other systems based on a few controlling variables, primarily the soil clay mineralogy, pH, and organic matter content. While the experimental and modeling work in this study focuses exclusively on nickel speciation and precipitation, the use of thermodynamic and kinetic analysis methods provides an avenue for extrapolating these results to other metals capable of forming mixed metal-aluminum hydroxides, including cobalt and zinc. Further experimental details are given below.

Precipitate Formation in Ni Amended Laboratory Soils

In order to investigate the role of organic matter and soil mineralogical properties on metal precipitate formation under more controlled circumstances, three distinct soils were reacted with Ni in the laboratory under conditions identical to those used in previous studies (Roberts, et al., 1999), i.e. 3 mM Ni and 0.1 M NaNO_3 , at various pHs. The three soils used are described in Table 1 below. The Matapeake and Berryland soils are typical Delaware agricultural soils, while the Fort Ellis soil is a reference soil with high clay content. Soil samples were reacted with an aqueous solution of $\text{Ni}(\text{NO}_3)_2$ at 3 mM Ni and 12 g/L soil under a N_2 atmosphere using CO_2 free reagents in order to minimize the potential formation of NiCO_3 phases. Samples were reacted with constant stirring for periods of up to 30 days at pH 6.0 and 7.5, and for 24-72 hours at pH 6.0, 7.0 and 7.5 to examine both the short term and longer term characteristics of Ni sorption. A portion of the 30 day reacted soils were then aged for up to one year in contact with

the Ni solution in order to examine the effects of precipitate aging and silicate substitution on Ni release.

Table 1. Soil Properties

	Matapeake	Berryland	Fort Ellis
pH	5.7	4.5	5.3
Sand-Silt-Clay %	30-58-12	65-16-19	21-42-37
Mineralogy	K,V	V	M
Organic Matter %	2	8	5
ECEC (meq/100 g)	5.3	4.1	26.2

K= Kaolinite, V=Chloritized Vermiculite, M= Montmorillonite

Metal Speciation

Metal speciation studies using XAS analysis were carried out to determine the nickel phases (adsorbed, metal precipitates, mineral) present in the soils. Determination of the bulk Ni speciation was primarily carried out at beamline X-11A at the National Synchrotron Light Source (NSLS) at Brookhaven National Laboratory (BNL). Samples were run under ambient conditions using an unfocussed beam under conditions described in previous papers published by our research group (Ford et al., 1999; Roberts et al., 2002). Data were collected in fluorescence mode using a Stern-Heald type (Lytle) detector filled with Ar gas and equipped with a filter. Depending on metal concentrations in the individual sample, three or more scans were collected for each sample and averaged to produce a single spectrum. Spatially resolved micro-XANES (x-ray absorption near edge structure) and micro-EXAFS (extended x-ray absorption fine structure) and micro-X-ray fluorescence (XRF) spectroscopic analyses of the metal-contaminated soils after 1 month of contact with the Ni solution were determined at beamline X-26A at beamline 10.3.2 at the Advanced Light Source (ALS) at Lawrence Berkeley National Laboratory (LBNL). EXAFS data were extracted from the raw spectra using the Athena software for background removal and χ extraction.

Determination of the identity of metal precipitate phases has been accomplished using both empirical and theoretical analyses of the χ -extracted and Fourier transformed data. A wide range of EXAFS spectra for nickel-containing mineral phases, aqueous species and organic complexes, as well as Ni sorbed to various clay minerals (kaolinite, vermiculite, pyrophyllite and montmorillonite) under controlled conditions, were also collected during the course of this project. A principle component analysis/target transformation method was used to identify the reference phases that made significant contributions to the spectra of the Ni spiked soils, and least squares fitting of the appropriate reference spectra was then carried out using the linear combination fitting module of the freely available Sixpack software suite. For details of this general approach, see Nachtegaal et al. (2005). Theoretical fitting has been carried out using FEFF 7 and the Artemis software package, along with a wavelet analysis of second shell identity, as described in Vespa et al. (2006).

Metal Desorption/Dissolution Studies

To determine the effect of precipitate formation and aging on metal sequestration and release, a series of desorption/dissolution experiments were conducted using two distinct desorbing agents: 1 mM EDTA at pH 7.5 and 0.1 mM HNO₃ at pH 4.0 after Scheckel and Sparks (2001). Studies were conducted in the replenishment mode, with the desorbing solution changed

every 24 hours for a period of 11-14 days. Desorption experiments were conducted on soils after 1, 6, and 12 months contact with the 3 mM Ni spiking solution at pH 6.0 and 7.5 for all three of the soils studied. Similar dissolution studies were conducted on pure phase Ni(OH)₂, Ni-LDH, and Ni-phyllosilicate phases prepared as part of the thermodynamic study described below.

Thermodynamic Analysis

In order to develop models of metal speciation that incorporate the potential formation of LDH-type surface precipitates, thermodynamic information on the formation and stability of these phases must be obtained. A number of model Ni-LDH phases were prepared at environmentally relevant conditions (25 °C and pH 6.9) from solutions containing 2:1 and 10:1 aqueous Ni to Al ratios with a range of interlayer anions (NO₃⁻, SO₄²⁻, CO₃²⁻). These phases were prepared by titration of a Ni- Al solution to pH 6.9 following the method described by Taylor (1984), and their identities confirmed by both XRD and EXAFS analysis as described in Peltier et al. (2005). Enthalpies of formation for these compounds were determined using high temperature oxide-melt calorimetry as described in Navrotsky (1997). Using this information, it was possible to calculate solubility product constants for the analogous surface precipitate phases under our experimental conditions. Additionally, the effect of substituting silicate into the anion interlayer on LDH stability was studied using a CO₃ interlayer LDH phase reacted with an H₄SiO₄ solution for a period of two weeks.

Nickel Bioavailability

Samples of the Ni-amended soils reacted for 1 month at pH 6.0 and 7.5 were analyzed using the BIOMET test procedure published by Corbisier et al (1999). The bacterial biosensor strain *Ralstonia metallidurans* AE2515, which produces a luminescent signal in the presence of Ni, was used to assess Ni bioavailability in the soil samples. Soil suspensions were prepared at various dilutions and added to reconstituted cells. Light production from the biosensor was then monitored every 30 minutes over a 12 hour period. Standard and blank assays were also prepared, and a constitutively light producing strain, *R. metallidurns* AE864, was used to correct for toxicity of the sample or quenching of light. The induction of bioluminescence (presented as the signal to noise (S/N) ratio) was calculated as the light production value (S) found for the soils tested, divided by the light production value found for the uncontaminated control soil (N). A S/N value below 0.8 indicates toxicity, while a value above 0.8 indicates the presence of bioavailable metals. An induction is considered as significant when a S/N ratio of at least 2 is found. With a calibration curve set up for the specific heavy metal, these ratios allow one to calculate the amount of bioavailable metal (mg equivalent/ kg soil). For further details of the method, see Tibazarwa et al. (2001).

Modeling Ni Sorption and Desorption Kinetics

The kinetics model for Ni adsorption and desorption reactions is based on the modeling method presented by Shi et al. (2005). The adsorption and desorption reactions can be formulated as

$$\frac{dC_p}{dt} = -k_d C_p + k_a C_w \quad (1)$$

and

$$\frac{dC_w}{dt} = -k_a m C_w + k_d m C_p \quad (2)$$

where k_a (L/(g min)), k_d (1/min), and C_p ($\mu\text{g Ni/g}$) are the adsorption and desorption rate coefficients and particulate Ni concentration, respectively, C_w ($\mu\text{g Ni/L}$) is the solution concentration of ionic Ni, and m (g/L) is soil particle concentration. All Ni species concentrations are expressed as the amount of Ni per gram of soil or per liter of solution.

Due to the high concentration of Ni used in this study, the linear sorption isotherm is not suitable. We used WHAM VI to account for nonlinear Ni binding and the effect of reaction chemistry, such as the variation of pH effect and SOM concentrations. The reaction chemistry is incorporated into the adsorption reaction and, for the desorption reaction, it is assumed that the desorption rate coefficient k_d is constant irrespective the reaction conditions (Shi et al., 2005). At the specific metal concentration in soils, if the reaction reaches equilibrium, we have

$$k_a C_w = k_d C_p \quad (3)$$

and

$$k_a = k_d C_p / C_w \quad (4)$$

Thus at the specific particulate Ni concentration in soils, the adsorption rate coefficient can be calculated based on the adsorption isotherm which can be predicted by WHAM VI at different reaction conditions. The only kinetic model parameter is the desorption rate coefficient.

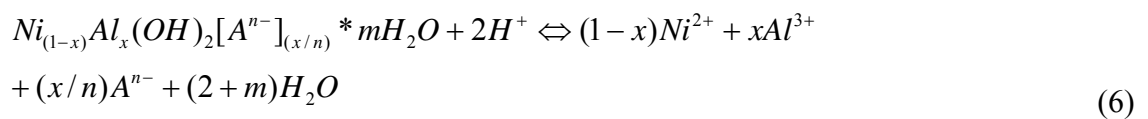
In our experimental conditions, either precipitation or dissolution reactions are far away from equilibrium. Thus the precipitation and dissolution rate constants could be determined independently.

The Ni removal due to precipitation in the first few hours is negligible compared with Ni complexation with SOM since precipitation is a much slower reaction. The type of anions (e.g. NO_3^- or CO_3^{2-}) may affect the reaction rate. We used a model Ni-LDH phase when NO_3^- is the major anion, $\text{Ni}_{0.67}\text{Al}_{0.33}(\text{OH})_2(\text{NO}_3)_{0.33} \cdot 0.505\text{H}_2\text{O}$, with $\text{Log}K_{\text{sp}} 5.85$ (Peltier et al., 2006). Since the pH and NO_3^- concentrations were constant, we formulated the precipitation rate as

$$R_p = k_1 [\text{Ni}]^n \quad (5)$$

where R_p is the precipitation rate, k_1 is the rate constant and n is the reaction order. The n value was set as 0.67.

For the dissolution reaction, the proton promoted dissolution reaction is considered which can be formulated as (Peltier et al., 2006),



Scheckel and Sparks (2000, 2001) have demonstrated that during the dissolution process the chemistry of Ni precipitates did not change. Thus the Ni-LDH solid activity can be treated as a constant during the dissolution process. Considering two protons will replace one Ni cation, the dissolution rate can be formulated as.

$$R_d = k_2[H^+]^2 \quad (7)$$

where R_d is the dissolution rate and k_2 is the rate constant.

Results

Thermodynamic Stability of Ni LDH Precipitate Phases

The full results of the thermodynamic study portion of this work are available in Peltier et al. (2006). Briefly, model LDH phases created from starting solutions with 2:1 and 10:1 Ni to Al ratios resulted in precipitate phases with solid phase Ni to Al ratio between 1.8 to 3.3. Standard enthalpies of formation (ΔH_f^0) for Ni LDH phases containing sulfate, carbonate and nitrate anion interlayers ranged from -900 to -1000 kJ/mol. Differences in the identity of the anion interlayer resulted in substantial changes in the enthalpies of formation of the LDH phases, in the order of increasing enthalpy $\text{CO}_3 < \text{SO}_4 < \text{NO}_3$. Estimations of solubility product constant (K_{sp}) values from these data revealed that Ni-LDH are six to eight orders of magnitude less soluble than pure phase nickel hydroxides. Substitution of silicate ions into the interlayer of a carbonate-LDH phase resulted in a further decrease in standard enthalpy (to -1130 kJ/mol) at only 40% substitution of silicate for carbonate. This confirms previous suggestions that interlayer silication is the likely reason for the increased stability of LDH precipitates as they age (Ford et al., 1999). Using the K_{sp} values generated from this study, we were able to estimate the equilibrium distribution of Ni species on various clay surfaces at the conditions of our spiking study (3 mM Ni, 0.1 M NaNO_3 ~10 g/L solid), assuming that all CO_3 has been removed by the N_2 degassing and ignoring the effects of competing sorption reactions and Ni complexation with soil organic matter. These models predict little to no Ni precipitate formation at pH 6.0, and that Ni-LDH phases will predominate in kaolinite soils such as the Matapeake and Berryland samples, at higher pH. In smectitic soils, such as the Fort Ellis samples, Ni speciation at pH 7-7.5 is expected to be a mixture of Ni-LDH and Ni(OH)_2 , with Ni-LDH phases favored if solution Ni concentrations decrease due to competing sorption of complexation reactions. Under the conditions of the soil spiking studies, Ni-LDH phases should be thermodynamically stable above pH 6.5 for all three soils.

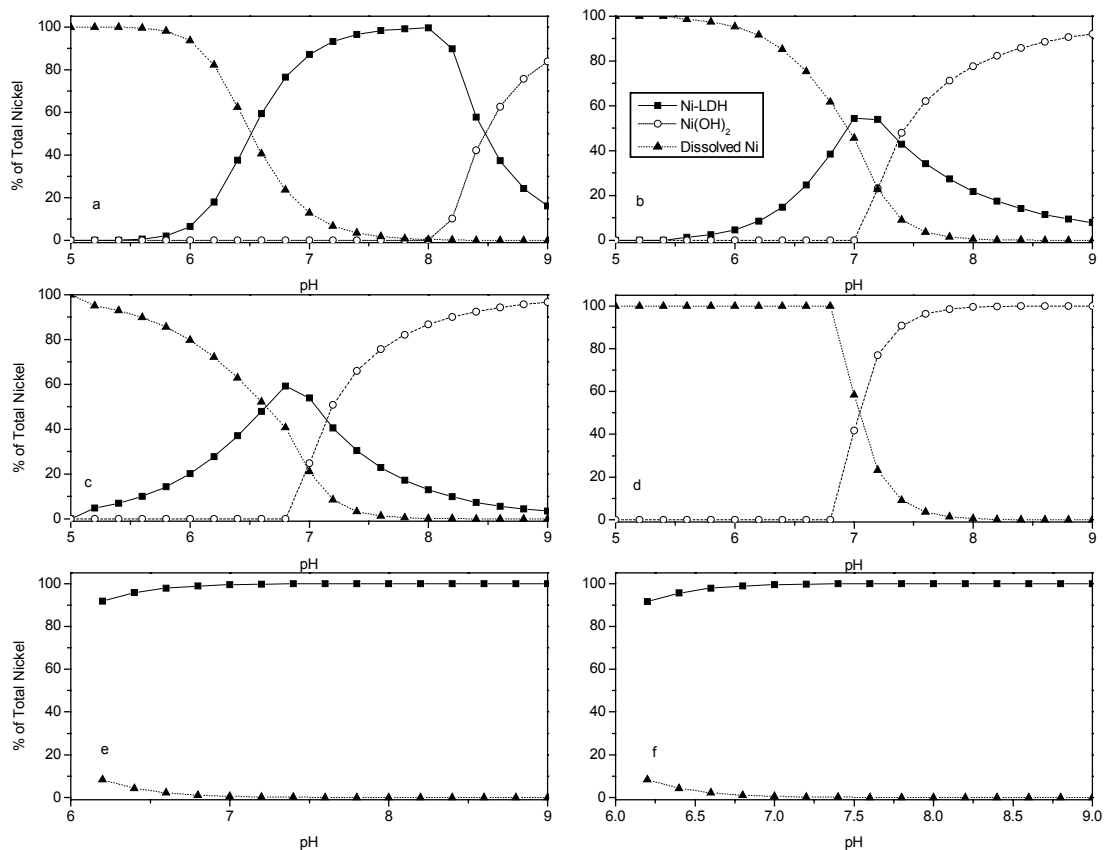


Figure 1. Calculated Ni speciation for 3 mM Ni solution in equilibrium with 10 g/L of a.) kaolinite b.) pyrophyllite c.) montmorillonite d.) silica e.) gibbsite and f.) mixture of 60% silica and 40% gibbsite in a N₂ atmosphere.

Precipitate Formation on Laboratory Contaminated Soils

As expected, Ni loading increased with increasing pH for all soils. At pH 6, almost all Ni sorption on the Fort Ellis and Matapeake soils, and approximately 65% of Ni sorption on the Berryland soil, is complete after 24 hours. At pH 7.5, however, Ni sorption continues in all three soils throughout the 30 days of the experiment. By 30 days, Ni concentrations in solution have dropped to less than 10% of the original value in the Berryland and Fort Ellis samples, and 25% in the Matapeake sample. At the end of the 30 day experiments, Ni concentrations in the Matapeake soil were 1,800 mg/L at pH 6.0 and 9,000 mg/L at pH 7.5, while the Berryland and Fort Ellis soils had concentrations around 4,000 mg/L and 12,000 mg/L at pH 6.0 and 7.5, respectively. Samples aged beyond 30 days were no longer stirred to maintain good soil-solution contact, and soil Ni loadings at 6 and 12 months show no significant change from the 30 day samples.

XAS analysis of the bulk soil samples show no precipitate formation in any of the pH 6 samples even after 1 year. This suggests that, as predicted by thermodynamic modeling, Ni LDH and hydroxide precipitate phases are not stable at this pH. Bulk XAS analyses of the pH 7.5

samples at 1 month indicate that Ni-LDH phases are present in both the Matapeake and Berryland samples. In the Fort Ellis soil, however, Ni surface precipitates appear to be primarily composed of either Ni(OH)₂ or Ni-phyllsilicate phases. The use of μ -scale x-ray imaging and XAS confirms that there are LDH precipitates in both the Berryland and Matapeake soils. This is consistent with previous laboratory studies confirming that LDH phases can form on kaolinite surfaces. Some regions of the Matapeake soil, however, also appear to contain Ni(OH)₂ precipitates. This may be due to the presence of chloritized vermiculite particles in the Matapeake soil. μ -XAS of Ni hot spots in the Fort Ellis sample, however, indicates a mixture of numerous different Ni species, including Ni sorption complexes and both LDH and non-LDH type precipitates. In general, montmorillonite does not appear to support the formation of LDH surface precipitates, possibly due to the lower solubility of Al from these phases (Scheinost and Sparks, 2000).

At 6 and 12 months after Ni addition, Ni speciation in the Matapeake and Berryland soils remains dominated by LDH phases (Figure 2). Empirical fitting of EXAFS spectra from these soils was performed with the SixPack software using a set of reference standards including Ni-LDH phases, α and β -Ni(OH)₂, Ni₃Si₄O₁₀(OH)₂ (a nickel-phyllsilicate phase), NiCO₃, Ni(H₂O)₆²⁺, Ni complexed with humic acid, and Ni sorbed onto a variety of clay substrates. For both soils, more than 75% of the sorbed Ni is accounted for by Ni-LDH precipitates. This value increases to > 85% after 12 months. These results suggest that the LDH surface precipitates are stable under these conditions. Thus, while silicate substitution into the LDH interlayer may indeed be occurring, there is no evidence to suggest a rapid transformation of these phases to Ni phyllsilicate structures, despite the much greater thermodynamic stability of the phyllsilicate phases.

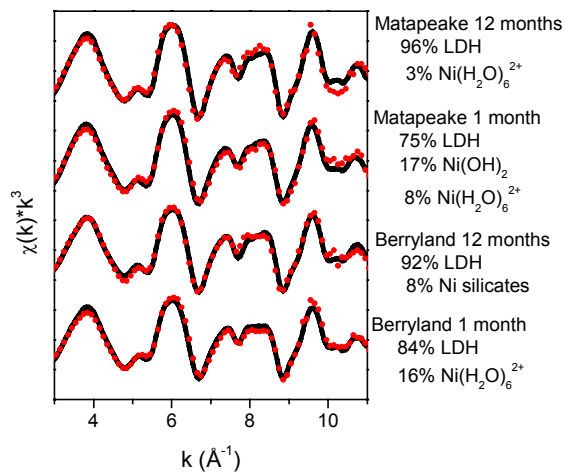


Figure 2. Results of linear least-squares fitting to Matapeake and Berryland EXAFS spectra at 1 and 12 months. The black line represents the best fit line to the actual data points.

Given the uncertainty in the potential Ni sorption phases present in the heterogeneous soil mixture, empirical fitting cannot be taken as full proof of the presence of LDH phases in the two Delaware soils. Further analysis of the EXAFS spectra from these soils at 1 and 12 months, however, reveals further evidence of the presence of these surface precipitates. Single shell

fitting of the 2nd nearest neighbor Ni or Al shell cannot resolve the presence or absence of Al because of the much lower contribution to the spectrum of the lighter Al ion (Scheinost and Sparks, 2000). However, the presence of LDH type Ni precipitate phases on clay substrates can be identified by a characteristic dampening in the chi-transformed EXAFS data at 7.5-8 Å⁻¹ when compared with Ni(OH)₂ or Ni phyllosilicate phases. In order to amplify and isolate this effect, we filtered the data through a Fourier transformation of the χ -extracted data over 2.3-11.9 Å⁻¹, followed by a back transformation from 1.0-6.3 Å. This process helps to highlight the contribution of surface precipitate phases over that of the sorbed Ni also present. The dampening in the soil samples (Figure 2) is the result of multiple scattering effects between the 2nd and 4th shell Ni and/or Al atoms. Theoretical fitting using single shell and multiple scattering paths calculated by FEFF give a best fit with an Al substitution ratio of ~ 0.22 for the Matapeake and Berryland samples (Table 2), consistent with the substitution patterns of Ni-LDHs, and show a greatly reduced coordination number for 2nd shell Ni when Al is excluded from the fit. By contrast, the values for the Fort Ellis soil are lower and not always significantly different from zero, providing further evidence that there is little LDH formation in the soil. Further analysis of these data using wavelet analysis has recently been undertaken in order to further distinguish the presence or absence of Al in the Ni surface precipitates.

Table 2. Theoretical Fitting Parameters for Bulk Soil Samples

	N _{Ni}	R _{Ni-Ni}	σ^2	$x = (N_{Al}/(N_{Ni}+N_{Al}))$
Matapeake 1 month	5.3	3.08	0.010	0.22 ± 0.11
Matapeake 12 months	5.5	3.07	0.009	0.23 ± 0.16
Berrylans 1 month	4.7	3.06	0.010	0.22 ± 0.10
Berryland 12 months	5.3	3.07	0.010	0.25 ± 0.13
Fort Ellis 1 month	5.4	3.07	0.010	0.15 ± 0.13
Fort Ellis 12 months	5.6	3.08	0.009	0.13 ± 0.17

N represents the number of second neighbor Ni atoms and R is the Ni-Ni bond distance

Short term kinetics of Ni precipitate formation

Ni speciation was determined in all three soils within the first 72 hours after Ni addition using a continuous scanning XAS technique that allowed us to gain time-resolved EXAFS spectra at 1.5-2 hour intervals. At pH 7.5, both of the Delaware soils showed the onset of Ni precipitate formation within 9-12 hours after Ni addition. At pH 7, Ni speciation in the Matapeake soil followed a similar pattern, but the Berryland soil showed little precipitate formation until 48 hours after Ni addition. These results suggest that soil organic matter can retard the formation of surface precipitate phases, most likely by forming organic Ni complexes. We did not observe the inhibitory effect seen in previous studies (Nachtegaal and Sparks, 2003), however, the Ni precipitates did eventually form at longer times. Precipitate formation in the Fort Ellis soil was slower (24-48 hours) and less influenced by pH. At pH 6.0, no precipitate formation was seen even after 72 hours. The amount of dissolved aluminum in solution was substantially lower than in Ni-free blank solutions after Ni addition, except in the Fort Ellis soil slurries.

Identification of the Ni precipitates formed in these short term studies was performed using bulk XAS analysis of soils freeze-dried after 24 hours reaction time. Principle component analysis and target transformation on the full set of 15 samples from each soil (at pH 7.0 and 7.5 combined) indicate that Ni-LDH was the best reference phase of the precipitate standards,

indicating that LDH phases are present in these soils. While there is some indication that small amounts of Ni-LDH precipitates are present in the Fort Ellis soil, it is impossible to fully distinguish the identity of Ni surface precipitates in this soil from the kinetic data alone. Based on the results of the 1 month bulk studies, it appears that the slower kinetics of Al release from the montmorillonite substrate in the Fort Ellis soil results in minimal formation of LDH surface precipitates in this soil. While Al release over the long term might eventually result in LDH formation as the Fort Ellis slurries approach equilibrium, Ni(OH)₂ formation occurs instead, locking up the sorbed nickel into alternate surface precipitates.

Ni desorption from aged soils

Distinct differences were seen in the desorption patterns of Ni from the Matapeake and Berryland soils as a function of sorption solution pH. For samples spiked at pH 6.0, extraction into 0.1 mM HNO₃ resulted in recovery of >60% of the sorbed Ni in both soils. For samples spiked at pH 7.5, the recovery of Ni was 20-30% for the Matapeake soil and 20% for the Berryland soil. Only the Matapeake sample spiked at pH 7.5 showed signs of any consistent change in Ni recovery with increased soil age. For all samples, Ni recovery in the EDTA desorption experiments approached 100%. The lack of increased Ni retention with aging in these experiments deviates from results seen using pure substrate materials. It appears that the LDH phases formed in these soils are less resistant to dissolution than those formed under similar conditions on the clay substrates.

Nickel desorption from the Fort Ellis soil using the 0.1 mM HNO₃ solution was less than 15% of total sorbed Ni at both pH 6 and 7.5, indicating the formation of strong Ni sorption complexes on the smectite clay. Diffusion of Ni into the layered clay structure over time may have also inhibited Ni recovery. Ni recovery in the 1 mM EDTA desorption experiment was 80% for the pH 6 spiked soil, but only 60% in the pH 7.5 spiked soil. The increased resistance of Ni to desorption in the pH 7.5 sample suggests that the Ni surface precipitates formed in this soil may include Ni silicate phases, which are more resistant to dissolution than the nickel hydroxide phases. Again, there was no consistent trend observed for nickel release with increased soil aging.

Metal bioavailability

Results of the BIOMET tests on these soils show a substantial effect of Ni surface precipitate formation on nickel bioavailability. While the overall concentrations of bioavailable nickel are somewhat higher in the Matapeake and Berryland soils spiked at pH 7.5 (Table 1), the percentage of sorbed nickel that is bioavailable drops from 70-90% in the soils spiked at pH 6 (where no precipitation occurred) to 25% in the precipitate influenced samples.

Table 3. Ni surface precipitate on Nickel bioavailability spiked at (pH 6.0) or spiked at (pH 7.5)

	pH 6.0		pH 7.5	
	Bioavailable Ni (mg/kg)	% of Total	Bioavailable Ni (mg/kg)	% of Total
Matapeake	1640	90	2447	27
Berryland	2606	70	3492	27
Fort Ellis	3027	74	3020	25

Modeling Ni Sorption and Desorption Kinetics

We focused our modeling efforts on the sorption and desorption kinetics of the Matapeake and Berryland soils, both of which have relatively low clay contents. At pH 6.0, Ni sorption experiments were run up to 26 days. No precipitates were observed during the sorption process based on XAS measurements for both the Matapeake and Berryland soils. Thus adsorption and desorption reactions are proposed as the main mechanisms controlling observed kinetics.

The only fitting parameter in this adsorption/desorption model is the desorption rate coefficient k_d . At pH 4.0, the desorption reaction controls the observed Ni release kinetics and the Ni re-adsorption back to soil particles is minimal due to the small partition coefficient at pH 4.0. Thus, the k_d was obtained from the desorption data at pH 4.0 by minimizing the sum of square errors between model calculations and experimental data using the SOLVER program in Microsoft Office EXCEL 2003. After obtaining k_d , it was directly used to predict adsorption kinetics.

Figures 3(a) and 3(b) presents the modeling results of the desorption experiment for both soils. For the first two replenishments, samples were collected every 12 hours. After that the samples were collected every 24 hours. We can see the solution Ni concentration was initially low for the shorter sampling time. After the first two replenishments, solution Ni concentration decreased with the number of replenishments, which was attributed to the decrease of particulate Ni concentration in soils. The model fittings are relatively good for both soils.

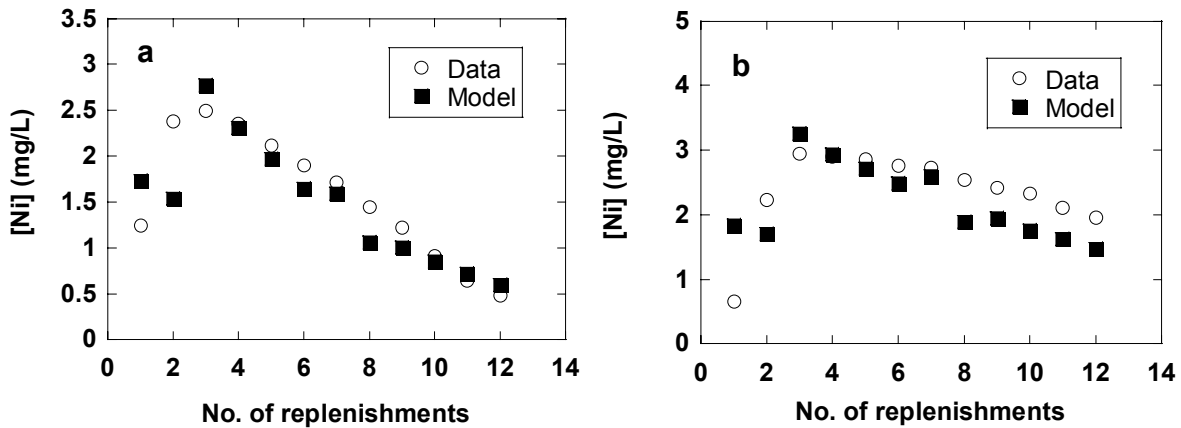


Figure 3. Kinetics of Ni desorption from the spiked (a) Matapeake and (b) Berryland soils with 0.1 mM HNO₃ after Zn sorption at pH 6.0 (Open symbols are experimental data and filled symbols are model calculations).

The percentage of Ni removal versus the number of replenishments is presented in Figure 4 for both soils.

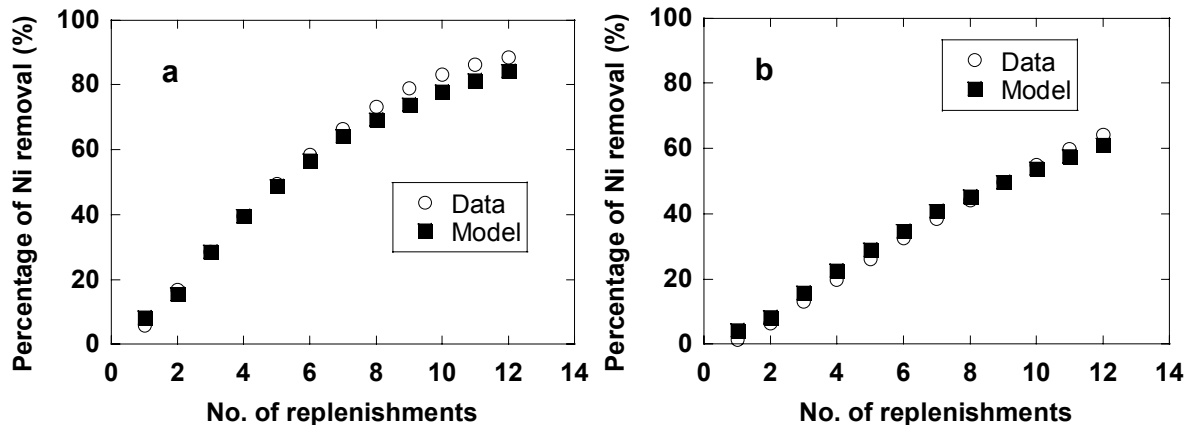


Figure 4. The percentage of Ni removal from the spiked (a) Matapeake and (b) Berryland soils during the replenishment experiment with 0.1 mM HNO₃ (Open symbols are data calculated based on mass balance and filled symbols are model calculations).

Using the desorption rate coefficients obtained from the desorption data, the adsorption kinetics can be predicted without any model fitting. Figure 5 presents the model predictions of adsorption kinetics together with the experimental data for both soils. Generally the model predictions followed a similar trend as the experimental data, a fast adsorption within 24 hours followed by a slower adsorption up to a few days. The applicability of desorption rate coefficient obtained from desorption kinetics to adsorption kinetics supports the validity of our kinetics model.

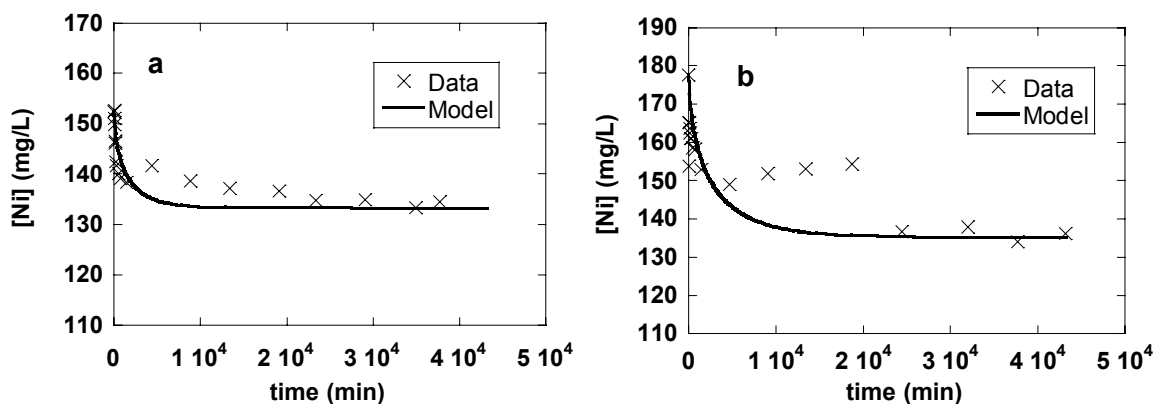


Figure 5. Kinetics of Ni adsorption on the (a) Matapeake and (b) Berryland soils (pH = 6.0 and [Ni]₀ = 178 mg/L).

The Ni desorption rate coefficients obtained from this study are close to the values reported by other researchers (Ernstberger, et al., 2002; 2005).

At pH 7.0, only short-term (48 h) sorption experiments were run. In the XAS study, Ni precipitates are observed after 6 hours. Meanwhile, an increase in pH also increases the complexation of Ni by SOM. Considering the slow precipitate formation, it is likely that adsorption is the main process in the short-term. We used the desorption rate coefficients obtained at pH 6.0 for each soil to predict Ni adsorption kinetics at pH 7.0.

Figure 6 presents the results of Ni adsorption for both soils at pH 7.0. We can see that the k_d can be applied to different pHs and reasonably predicts Ni adsorption kinetics.

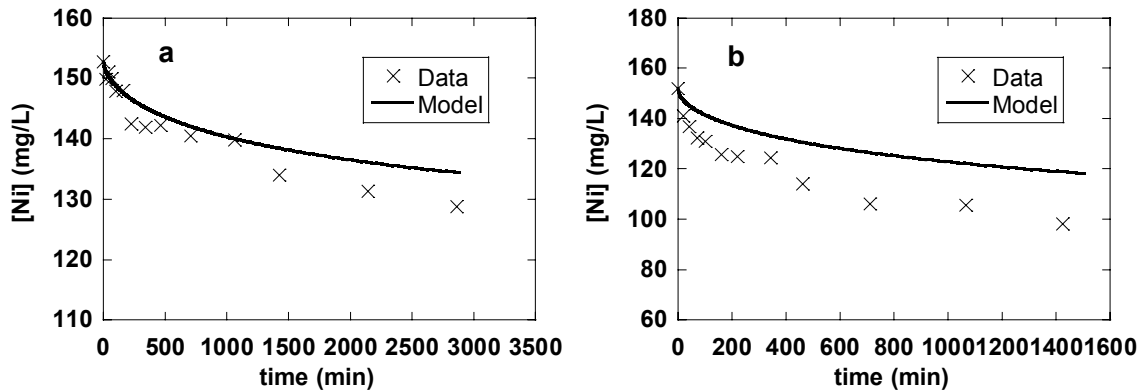


Figure 6. Kinetics of Ni adsorption on the (a) Matapeake and (b) Berryland soils (pH = 7.0 and $[Ni]_0 = 178$ mg/L).

At pH 7.5, Ni-LDH precipitates were formed after a few hours in the sorption experiment. Either precipitation or dissolution processes are far from equilibrium under our experimental conditions. Thus, the precipitation and dissolution rate constants can be determined independently.

In the short-term (less than 48 h), Ni adsorption by the soil controlled the Ni removal from the solution. With increases in time, adsorption slowed down, and the precipitation became dominant. The model parameters for adsorption/desorption reactions are the same as those at pH 6.0 and 7.0. The only fitting parameter for Ni sorption at pH 7.5 is the precipitation rate constant k_l . The k_l was obtained from the sorption data at pH 7.5 by minimizing the sum of square errors between model calculations and experimental data using the SOLVER program in Microsoft Office EXCEL 2003.

Figure 7 presents the Ni sorption results at pH 7.5 for both soils. Similar to results at pH 6.0 and 7.0, the short-term Ni adsorption kinetics can be described by the adsorption/desorption reactions. At longer time, the precipitation reaction can account for the steady and slow Ni uptake from solution.

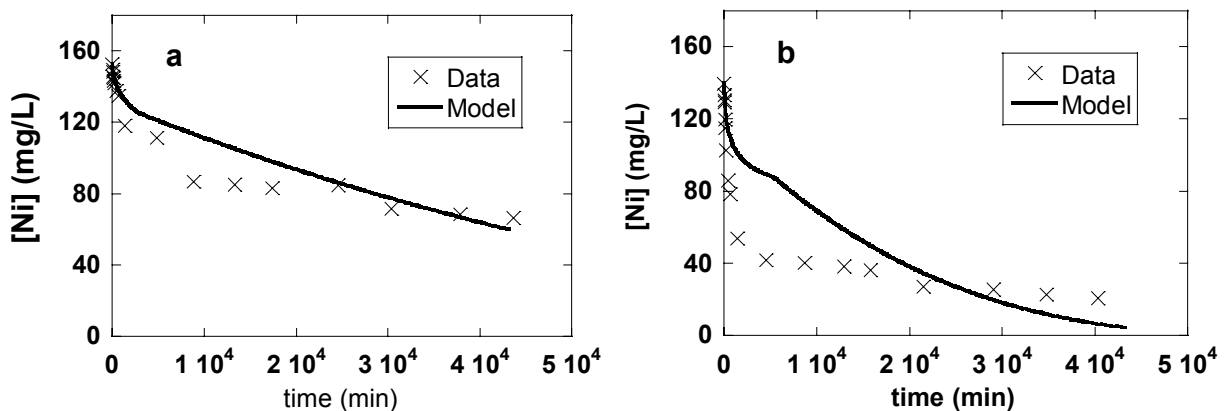


Figure 7. Kinetics of Ni adsorption/precipitation on the (a) Matapeake and (b) Berryland soils (pH = 7.5 and $[Ni]_0 = 178$ mg/L).

For Ni dissolution, the k_2 was obtained from the desorption data at pH 4.0 by minimizing the sum of square errors between model calculations and experimental data using the SOLVER program in Microsoft Office EXCEL 2003. Figure 8 presents the modeling results for both soils. We can see that the model calculations are quite close to the experimental data.

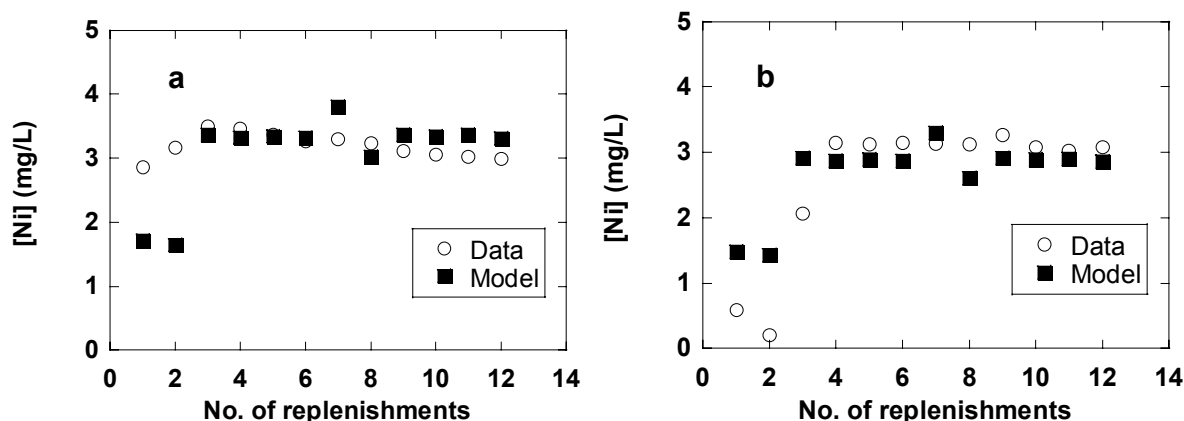


Figure 8. Kinetics of Ni desorption from the spiked (a) Matapeake and (b) Berryland soil with 0.1 mM HNO₃ after Zn sorption at pH 7.5 (Open symbols are experimental data and filled symbols are model calculations).

The WHAM VI input parameters and the kinetics model fitting parameters are listed in Table 4 for both soils.

Table 4. Model parameters

WHAM VI parameters						Kinetic parameters		
[HA]	[FA]	pK _{s0} (Al)	pK _{s0} (Fe(III))	[Na]	[NO ₃]	k _d	k ₁	k ₂
g/L	g/L			M	M	1/min		
Matapeake soil								
0.238	0.061	6	3	0.1	0.1	1.20E-4	2.27E-6	4.07
Berryland soil								
0.607	0.133	6	3	0.1	0.1	6.12E-5	5.39E-6	3.52

Summary and Conclusions

The formation of Ni layered double hydroxide type surface precipitate phases is possible in contaminated soils containing kaolinite (and likely pyrophyllite) at pH ≥ 6.5 , despite some competition from soil organic matter. The primary factors affecting LDH precipitate formation appear to be the soil pH and clay mineralogy, which controls the total solubilizable aluminum present in the soil matrix. Thus, in soils containing smectitic clays, the slower release of Al from the substrate matrix appears to act to inhibit Ni-LDH formation, resulting instead in Ni(OH)₂ and/or Ni-phyllsilicate phases. The presence or absence of LDH phases in pure substrate studies is therefore a reasonable surrogate for predicting Ni behavior in whole soils, provided that the soils are not extremely high in soil organic matter (in which case Ni-organic complexation may

become much more significant), or Ni sorption to the Al bearing phases is not too much slower than to non-Al bearing phases (as has happened in mixed gibbsite/SiO₂ systems). The thermodynamic models developed from enthalpy data generated in this experiment may be capable of predicting when LDH saturation occurs in kaolinite type soils, but cannot be used for smectitic soils due to the effect of Al solubilization kinetics on the final form of the Ni precipitate. Desorption studies indicate that the soil LDH phases formed here are less stable, and show fewer aging effects, than those formed on pure clay substrates in previous experiments. Over at least 1 year, these LDH phases are metastable in the soil, and any transformation to Ni-phyllosilicate phases may not occur except on very long timescales. At the same time, Ni-LDH formation can substantially increase Ni retention and decrease Ni bioavailability compared to estimates from sorption only models, and should be considered in assessing the fate of Ni in contaminated soils. The kinetics of Ni adsorption/desorption reactions with soils were successfully described using a WHAM VI based model. The nonlinearity of Ni binding, effects of solution pH and Ni concentration, and variation of SOM concentrations were well accounted for by this kinetics model. The Ni precipitation/dissolution kinetics can be described by the formation of a model Ni-LDH phase and proton promoted dissolution process. Our model can quantitatively calculate the formation and dissolution of Ni precipitates on different soils. The Ni and SOM complexation seems to control the overall Ni reaction in the short term (less than 48 h) and Ni precipitates are important for controlling the long term Ni reactions at high pH. The kinetics model presented in this project, which considers Ni chemical reactions based on Ni speciation measurement using XAS, provides the basis for further developing a predictive model for Ni reactions with soils.

Acknowledgements

Funding for this work was provided by the US Environmental Protection Agency through the Center for the Studies of Metal in the Environment and by the Unidel Foundation. X-ray absorption spectroscopy results experiments were carried out at beamline X-11A of the National Synchrotron Light Source, Brookhaven National Laboratory, beamline 10.3.2 of the Advanced Light Source, Lawrence Berkley National Laboratory, and at DND-CAT, Sector 5 of the Advanced Photon Source at Argonne National Laboratories.

Literature Cited

- Amacher, M.C., Selim, H.M., and Iskandar, I.K. (1988) Kinetics of Chromium(VI) and Cadmium Retention in Soils; A Nonlinear Multireaction Model. *Soil Sci. Soc. Am. J.* 52:398-408.
- Charlet, L., and Manceau, A.A. (1992) X-ray Absorption Spectroscopic Study of the Sorption of Cr(III) at the Oxide-Water Interface 2. Adsorption, Coprecipitation, and Surface Precipitation on Hydrous Ferric-Oxide. *J. Coll. Inter. Sci.* 148:443-458.
- Chisholm-Brause, C.J., O'Day, P.A., Brown, J.G.E. and Parks, G.A. (1990) Evidence for Multinuclear Metal-Ion Complexes at Solid Water Interfaces from X-ray Absorption Spectroscopy. *Nature* 348:528-531.
- Corbisier, P., van der Lelie, D., Borremans, B., Provoost, A., de Lorenzo, V., Brown, N.L., Lloyd, J., Hobman, J.L., Csöregi, E., Johansson, G. and Mattiasson, B. (1999) Whole Cell

- and Protein Based Biosensors for the Detection of Bioavailable Heavy Metals in Environmental Samples. *Analytica Chimica Acta* 387:235-244.
- Ernstberger, H., Davison, W., Zhang, H., Tye, A., and Young, S. (2002) Measurement and Dynamic Modeling of Trace Metal Mobilization in Soils Using DGT and DIFS. *Environ. Sci. Technol.* 36:349-354.
- Ernstberger, H., Zhang, H., Tye, A., Young, S., and Davison, W. (2005) Desorption Kinetics of Cd, Zn, and Ni Measured in Soils by DGT. *Environ. Sci. Technol.* 39:1591-1597.
- Fendorf, S.E., Lamble, G.M., Stapleton, M.G., Kelley, M.J., and Sparks, D.L. (1994) Mechanisms of Chromium(III) Sorption on Silica. 1. Cr(III) Surface-Structure Derived by Extended X-ray Absorption Fine Structure Spectroscopy. *Environ. Sci. Technol.* 28:284-289.
- Ford, R.G., Scheinost, A.C., Scheckel, K.G., and Sparks, D.L. (1999) The Link Between Clay Mineral Weathering and the Stabilization of Ni Surface Precipitates. *Environ. Sci. Technol.* 33(18):3140-3144.
- Ford, R.G., and Sparks, D.L. (2000) The Nature of Zn Precipitates Formed in the Presence of Pyrophyllite. *Environ. Sci. Technol.* 34:2479-2483.
- Nachtegaal, M., Marcus, M. A., Sonke, J.E., Vangronsveld, J., Livi, K.J.T., van der Lelie, D., and Sparks, D. L. (2005) Effects of In-situ Remediation on the Speciation and Bioavailability of Zinc in a Smelter Contaminated Soil. *Geochim. Cosmochim. Acta* 69:4649-4664.
- Nachtegaal, M., and Sparks, D.L. (2003) Nickel Sequestration in a Kaolinite-Humic Acid Complex. *Environ. Sci. Technol.* 37:529-534.
- Navrotsky, A. (1997) Progress and New Directions in High Temperature Calorimetry Revisited. *Physical Chemistry of Minerals* 24(3):222-241.
- O'Day, P.A., Parks, G.A., and Brown, J.G.E. (1994) Molecular-Structure and Binding-Sites of Cobalt(II) Surface Complexes on Kaolinite from X-ray Absorption Spectroscopy. *Clays and Clay Minerals* 42:337-355.
- Peltier, E.F., Allarda, R., Navrotsky, A., and Sparks, D.L. (2006) Nickel Solubility and Precipitation in soils: A Thermodynamic Study. *Clay and Clay Minerals* 54:153-163.
- Roberts, D.R., Scheidegger, A.M., and Sparks, D.L. (1999) Kinetics of Mixed Ni-Al Precipitate Formation on a Soil Clay Fraction. *Environ. Sci. Technol.* 33: 3749-3754.
- Roberts, D.R., Scheinost, A.C., and Sparks, D.L. (2002) Zinc Speciation in a Smelter-Contaminated Soil Profile Using Bulk and Microspectroscopic Techniques. *Environ. Sci. Technol.* 36:1742-1750.
- Scheckel, K.G., and Sparks, D.L. (2001) Dissolution Kinetics of Nickel Surface Precipitates on Clay Mineral and Oxide Surface. *Soil Sci. Soc. Am. J.* 65:685-694.
- Scheckel, K.G., Scheinost, A.C., Ford, R.G., and Sparks, D.L. (2001) Stability of Layered Ni Hydroxide Surface Precipitates – A Dissolution Kinetics Study. *Geochim. Cosmochim. Acta* 64:2727-2735.
- Scheidegger, A.M., Lamble, G., and Sparks, D.L. (1997) Spectroscopic Evidence for the Formation of Mixed-cation Hydroxide Phases Upon Metal Sorption on Clays and Aluminum Oxides. *J. Coll. Inter. Sci.* 186:118-128.

- Scheidegger, A. M., Strawn, D.G., Lamble, G.M., and Sparks, D.L. (1998) The Kinetics of Mixed Ni-Al Hydroxide Formation on Clay and Aluminum Oxide Minerals: A Time-Resolved XAFS Study. *Geochim. Cosmochim. Acta* 62:2233-2245.
- Scheinost, A.C., Ford, R.G., and Sparks, D.L. (1999). The Role of Al in the Formation of Secondary Ni Precipitates on Pyrophyllite, Gibbsite, Talc, and Amorphous Silica: A DRS Study. *Geochim. Cosmochim. Acta* 63:3193-3203.
- Scheinost, A.C., and Sparks, D.L. (2000) Formation of Layered Single and Double Metal Hydroxide Precipitates at the mineral/Water Interface: A Multiple-Scattering XAFS Analysis. *J. Coll. Inter. Sci.* 223:167-178.
- Schlebaum, W., Schraa, G. and van Riemsdijk, W.H. (1999) Influence of Nonlinear Sorption Kinetics on the Slow-Desorbing Organic Contaminant Fraction in Soil. *Environ. Sci. Technol.* 33:1413-1417.
- Shi, Z., Di Toro, D.M., Allen, H.E., and Ponizovsky, A.A. (2005) Modeling Kinetics of Cu and Zn Release from Soils. *Environ. Sci. Technol.* 39:4562-4568.
- Taylor, R.M. (1984) The Rapid Formation of Crystalline Double Hydroxy Salts and Other Compounds by Controlled Hydrolysis. *Clay Minerals* 19:591-603.
- Thompson, H.A., Parks, G.A., and Brown, G.E. (1999) Dynamic Interactions of Dissolution, Surface Adsorption, and Precipitation in an Aging Cobalt(II)-Clay-Water System. *Geochim. Cosmochim. Acta* 63(11-12):1767-1779.
- Tibazarwa, C., Corbisier, P., Mench, M., Bossus, A., Solda, P., Mergeay, M., Wyns, L., and van der Lelie, D. (2001) A Microbial Biosensor to Predict Nickel in Soil and Its Transfer to Plants. *Environ. Pollut.* 113:19-26.
- Tipping, E. (1994) WHAM – A Chemical Equilibrium Model and Computer Code for Waters, Sediment, and Soils Incorporating A Discrete Site/Electrostatic Model of Ion-Binding by Humic Substances. *Computers Geosci.* 20:973-1023.
- Tipping, E., Rieuwerts, J., Pan, G., Ashmore, M.R., Lofts, S., Hill, M.T.R., Farago, M.E., and Thornton, I. (2003) The Solid-solution Partitioning of Heavy Metals (Cu, Zn, Cd, Pb) in Upland Soils of England and Wales. *Environ. Pollut.* 125:213-225.
- Towle, S.N., Bargar, J.R., Brown, J.G.E., and Parks, G.A. (1997) Surface Precipitation of Co(II)(aq) on Al₂O₃. *J. Coll. Inter. Sci.* 187:62-68.
- Vespa, M., Dähn, R., Grolimund, D., Wieland, E., and Scheidegger, A.M. (2006) Spectroscopic Investigation of Ni Speciation in Hardened Cement. *Environ. Sci. Technol.* 40:2275-2282

Transport Processes of Mining Related Metals in the Black River of Missouri's New Lead Belt

David J. Wronkiewicz

Environmental Research Center for Emerging Contaminants and Environmental Engineering
Department of Geology and Geophysics
University of Missouri - Rolla
Rolla, MO 65409
and

Craig D. Adams and Cesar Mendosa

Environmental Research Center for Emerging Contaminants and Environmental Engineering
Department of Environmental Engineering
University of Missouri - Rolla
Rolla, MO 65409

Introduction

Objectives

Researchers at the University of Missouri - Rolla have conducted a metals fate and transport study on two adjacent river systems in southeastern Missouri; the Big River and the West Fork of the Black River. Both watersheds are located in the St. Francois Mountains, approximately 50 to 80 miles (80 to 130 km.) south-southwest of Saint Louis. Each river transects a world-class sized Pb-Zn mining district with ores hosted in carbonate bedrock. This study will provide an opportunity to characterize specific contributions of metals from mining discharges, determine how these metals are transported, provide information on how water and sediment quality has changed over time, and characterize how hydrologic and geochemical factors affect transport of metals in the water column and sediment load.

Background

There have been four previous investigations involving metal mobility in the Big and Black Rivers. The first included an investigation of water, sediment, and various biota at six sites occurring within the West Fork drainage basin and was conducted before some of the mines in the New Lead Belt began production (Bolter et al., 1977). Elevated metal contents were observed in the water column during flooding and metals were found to be associated with organics. An investigation conducted by Schmitt and Finger (1982) contrasted with the study by Bolter et al. in determining that Pb was evenly distributed between five fractions of sediment: the exchangeable, carbonate, Fe- and Mn-oxide, organic, and residual fractions. Zinc was primarily associated with the residual fraction, though significant amounts were also correlated with the oxides and carbonates. A third study conducted by the United States Geological Survey (USGS) found extensive contamination levels throughout a wide stretch of the Big River system (Smith and Schumacher, 1991). A fourth study, also conducted by the USGS, investigated water quality parameters throughout the Ozark Plateau including ten mine impacted and background (control) sites along the West Fork (Peterson, 1998). Results from this final study indicate that there were higher levels of trace metals in the mine impacted sediment and clam tissues relative to background sites, however, river water concentrations did not usually exceed federal drinking water, human health, or aquatic life standards.

Regional Geology and Geography

Nearly 300 years of mining in Missouri's Old Lead Belt, and 45 years in the New Lead Belt, have collectively resulted in the accumulation of approximately 500 million tons of waste tailings. Small scale mining activity began in Old Lead Belt region in 1701. Industrial scale mining techniques were first employed in the early 1860s and continued nearly uninterrupted until the last mines were closed in 1972. The New Lead Belt, or Viburnum Trend ore district, mirrors the size and productivity of the Old Lead Belt. Initial discoveries of subsurface ore deposits were made in 1955 and ore production began in 1960. The district is still active today and is one of the largest lead producing districts in the world.

Ore zones in both the Old and New Lead Belt Districts are primarily hosted in Cambrian-aged dolomite [$\text{CaMg}(\text{CO}_3)_2$] of the Bonneterre Formation. Ore minerals include galena (PbS), sphalerite (ZnS), and chalcopyrite (CuFeS_2); with variable amounts of Co, Ni, Ag, Cd, and As also occurring as trace components in primary sulfide minerals and/or in accessory mineral phases. Contaminant metals in unrecovered sulfide grains may be released from the waste tailings piles and discharged into the river basin by the chemical dissolution of sulfide minerals

and their secondary weathering products, or the physical erosion of tailings pile particles by the action of wind or water. The dolomite in the tailings piles has a profound effect on the chemistry of weathering fluids. Sulfuric acid produced during the oxidative dissolution of sulfide minerals is rapidly neutralized through reactions with the dolomite. Interaction of meteoric water with the regional carbonate geologic strata also results in a slightly alkaline pH and high dissolved bicarbonate content in the West Fork and Big Rivers. Two operational smelters are also located in this region for both the processing of ore (Glover Facility) and reprocessing of scrap lead (e.g., batteries; Buick facility) and represent potential sources of air-borne particulate metals. Other potential metal sources include automotive lead accumulated in soils (derived prior to the phase-out of leaded gasoline), naturally high metal background in rocks affected by regional metallization episode(s), recreational activities (e.g., lead-based hunting projectiles or boating), urban pollution, etc.

The West Fork of the Black River emerges from its headwaters and flows approximately 11 nautical miles in an easterly direction until it intersects the north-south trending New Lead Belt district (Figure 1). Over the next 16 miles, the river receives drainage from three mine tailings piles: the West Fork Mine which started production in 1986 (ASARCO, 1996), Brushy Creek which started in 1973 (Wharton et al., 1975), and Fletcher which started in 1967 (Warner and Rickmar, 1970). The river flowage continues an additional 28 miles until it empties into Clearwater Lake, a man-made impoundment built in 1948. Along the way, the West Fork merges with the Center Fork which receives drainage from two additional New Lead Belt Mines. In our primary sampling region, the West Fork falls at a relatively steep gradient of 11.2 feet per nautical mile. The character of the river sediments reflect this gradient, being dominated by cobble, pebble, and sand-sized particles. The majority of the West Fork watershed can be characterized as forested wilderness, with limited agriculture and livestock grazing. Water clarity is generally very high as a result of the coarse sediments and limited urban and agricultural activity.

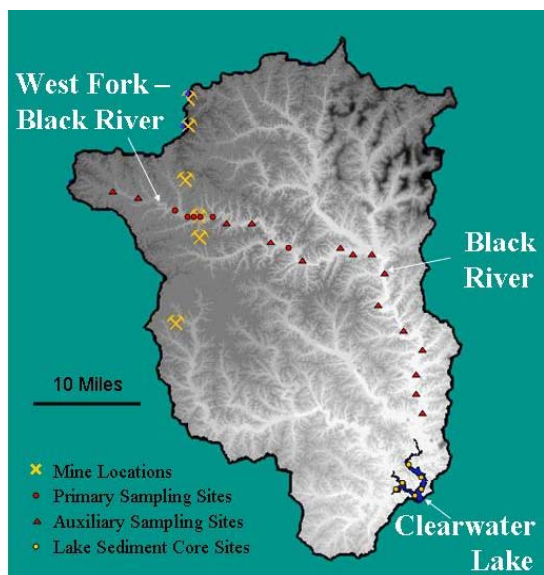


Figure 1. Location map for the Black River watershed showing locations of six primary and sixteen secondary sampling sites, six locations for New Lead Belt mines located within the Clearwater Lake drainage basin, and the Clearwater Lake impoundment with associated locations noted for collection of sediment cores. The general river flow direction is from north (top of photo) to south.

The Big River watershed drains all mines from the Old Lead Belt and Washington County Barite (BaSO_4) District to the north. The Big River flows approximately 138 nautical miles from its headwaters in the St. Francois Mountains until it merges with the Meramec River southwest of St. Louis, Missouri (Figure 2). Stream gradients near the mines are relatively gentle, ranging from approximately two to four feet per mile. The sediments reflect this gentle gradient, being dominated by sand- and silt-sized particles. Land usage adjacent in the Big River basin is characterized by pasture, minor row cropping, and small urban centers.

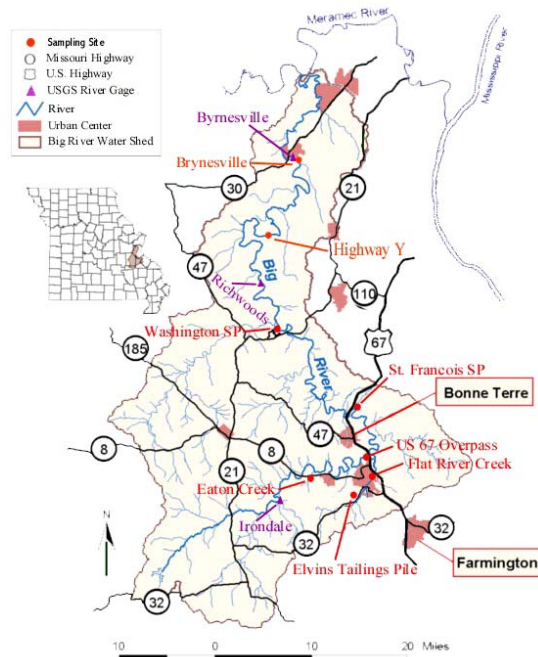


Figure 2. Location map for the Big River watershed showing locations of eight primary sampling sites, urban centers, major highways, and three river gauging stations operated by the U.S. Geological Survey. Our ninth sampling site is located at the Irondale gage station. The general river flow direction is from south to north.

Experimental Procedures

Site Selection, Sampling Dates and Locations

Six West Fork and eight Big River locations were selected as primary sampling sites for this study (Figures 1 and 2). Primary sites were selected based upon accessibility, proximity to known mine tailings piles, and correspondence to sampling locations of previous investigations. Sampling sites were also located upstream of all bridges and boat launch sites to avoid potential contamination from these features, and were located far enough downstream of tributaries to ensure homogenization of mixing tributary waters. Twenty locations on the Big River and sixteen on the Black River were selected as secondary sites to be sampled on a limited basis.

Sediment and water samples were collected on the West Fork of the Black River during ten sampling trips over the course of our study between 2002 and 2005 (Table 1). Water samples were collected during each visit while sediment samples were collected during five of the

sampling trips. Two of these events (2/21/03 and 6/11/03) captured levels of higher water flow and increased turbidity following rain events. The 6/11/03 event included both a sampling of the river during normal flow and a subsequent rise in the river level following a summer rain storm. The remaining eight sampling periods captured normal flow events; however, our 8/23/02 sampling inadvertently coincided with a gravel collection and low-water bridge reconstruction episode occurring approximately 1.4 miles upstream from our uppermost sampling site.

Table 1. Flow conditions of the Big River during sampling events.

Date	Conditions	USGS Gage Richwoods	River Water Temp. °C
3/09/02	-Moderate flood stage high turbidity water	4040 ft ³ /sec Gage hgt. 8.77	10.4 – 11.5
6/09/02	Water slightly above normal seasonal flow	440 ft ³ /sec Gage hgt. 3.57'	22.9 – 24.5
9/08/02	Water slightly above normal seasonal flow	188 ft ³ /sec Gage hgt. 2.77	24.8 – 26.2
12/19/02	-Minor flooding of Flat River Creek	1050 ft ³ /sec Gage hgt. n/a	8.4 – 10.6
10/23/04	Minor flooding rise, increase turbidity	290 ft ³ /sec	16.2 – 19.7
01/15/05 & 01/07/05	Major flood stage high turbidity high turbidity water	13000 ft ³ /sec Gage hgt. n/a	4.8 – 9.7

The Clearwater Lake impoundment, constructed in 1948, is located approximately 55 nautical miles downstream of the West Fork Mine tailings pile (Figure 1). This lake receives drainage from six of the ten mines in the New Lead Belt, with three of the mines located in the West Fork drainage, two in the Center Fork, and the sixth in the separate Logan Creek system. An analysis of six vertical sediment piston cores collected from Clearwater Lake in 2002 are used to provide a record of anthropogenic metal delivery rates to the basin, including potential contributions from New Lead Belt mining district. The sediments were analyzed for their Pb isotopic compositions, ¹³⁷Cs, and trace element metal concentrations. The Clearwater Lake study is ongoing, and is being supported jointly by the USGS and the University of Missouri-Rolla (Gary Krizanich Ph.D. student).

On the Big River system, sediment and water samples were collected from eight primary sites, five on the Big River itself and three on connected tributary systems. Water samples were collected during six separate trips and sediments during four trips between March 2002 and January 2005 (Table 2). Our January 2005 sampling captured a major river flood event, with eighteen water sample collected from nine sites over a three-day interval (1/05-1/07/05). These included repeat collections at some locations where both rising and falling river flow rate events were captured. The January 2005 flood was the highest of the year and the third highest event in

the previous six years. Three additional minor flood events were captured on the Big River (3/09/02, 12/19/02, and 10/23/04).

Table 2. Flow conditions of the West Fork of the Black River during sampling events.

Date	Conditions	Calculated Flow Site D	River Water Temp. °C
5/28/02	low flow, high water clarity	135 ft ³ /s	17.3 - 18.6
8/23/02	low flow, high water clarity County gravel operation disturbance	57 ft ³ /s	24.1 - 26.1
11/23/02	low flow, high water clarity	35 ft ³ /s	6.9 - 11.3
2/21/03	water high from previous rain light rain throughout the day	293 ft ³ /s	5.1 - 6.7
6/11/03	Flood rise and increasing turbidity multiple samples collected during rise	28 ft ³ /s (low)	17.7 - 19.5
9/16/03	low flow, high water clarity	40 ft ³ /s	19.6 - 23.7
02/08/04	low flow, high water clarity	92 ft ³ /s	0.4 - 4.0
11/07/04	low flow, high water clarity	92 ft ³ /s	12.3 - 15.2
6/29/05 & 07/09/05	low flow, high water clarity	72 ft ³ /s	22.1 - 26.7

Sampling and analytical procedures

Water samples were collected by submerging a pre-cleaned polyethylene bottle just below the river water surface in a manner that avoid collecting sediment particles moving near the river bottom or particulate material floating at the water surface. Four different water aliquots were field processed using disposable plastic syringes and filters: 1) unfiltered water, 2) 5.0 µm nylon filter, 3) 0.45 µm cellulose acetate filter, and 4) 0.02 µm alumina filter samples. A 0.45 µm acetate filtered sample was also collected for anion analysis, while 0.45 µm glass-filtered organic carbon samples were processed in the field into amber glass bottles and cold-stored until analyzed. Total suspended solids (TSS) and total dissolved solids (TDS) determinations were made by filtering and evaporating, respectively, between 200 and 1000 mL of river water upon return to the laboratory. Water hardness, alkalinity, and turbidity measurements were performed in the field using portable analytical kits, while conductivity, pH, Eh, and temperature readings were measured *in situ*. Conductivity and pH meters were calibrated in the field using standards, while Eh measurements were conducted without calibration.

Representative sediment samples were collected from the river bed by combining equal volume proportions of pool and riffle sediments from the top one or two inches of the river bed and wet sieving samples in the field using stainless steel sampling sieves and river water to collect -10 to +80 mesh (coarse to medium sand), -80 to +230 mesh (medium to fine sand), and

–230 mesh (silt + clay) sediment fractions. Additional sediment particles were processed in the field using a plastic gold pan to concentrate high density particles from the river bed. These particles were examined using a combination of Scanning Electron Microscopy/Energy Dispersive Spectroscopy (SEM/EDS), optical microscopy, and X-ray diffraction (XRD) techniques. The EDS determinations were made without using calibration standards, and thus provide only semi-quantitative values.

Batch metal adsorption tests were initiated by adding the following potential adsorptive phases to pre-cleaned one liter polyethylene bottles: 1) organic particulate material collected from the West Fork upstream of all mining locations, 2) hematite (Fe_2O_3), or 3) hausmannite (Mn_2O_3). A fourth control vessel was prepared without the addition of solid phases. Unfiltered effluent water from the West Fork tailings pile was collected from a concrete drainage channel at the point where it pours into the West Fork channel and added into each bottle to initiate the tests. Each test was run in a batch mode with sequential 30 ml water aliquots being periodically withdrawn using a syringe and 0.45 μm cellulose acetate filter. These aliquots were collected after 0.25, 0.5, 1, 2, 4, 8, 16, 24, 48, 96, 192, 384, and 768 hours. The atmospheric headspace in each test vessel progressively increased as a result of the successive sampling. No attempt was made to control the volume or composition of this headspace other than the immediate closing the vessels after each sampling interval.

All water samples for ICP/MS or ICP/OES analysis were acidified with ultra-pure HNO_3 to a pH of ~ 2.0 upon return to the laboratory. Filtered river water samples without any visible particulate material were analyzed without any further processing. Sediment samples and river water samples containing visible particulate material were digested following the EPA Method 200.2 prior to chemical analysis. Appropriate sample blanks, spikes, and standards were run as prescribed in the procedure. For the sediment samples the EPA 200.2 procedure was modified slightly in that samples were gently disaggregated in an agate mortar and pestle rather than crushing in an impact grinder. This alteration allowed us to more directly sample the ions adsorbed to the surfaces of the particles and limited the potential for cross-contamination of samples during pulverization. The sequential extraction procedure followed the method described by Tessier et al. (1979), which allowed for the determination of five separate metal fractions: 1) exchangeable, 2) bound to carbonates, 3) bound to Fe-Mn oxides, 4) bound to organic matter, and 5) residual.

Analytical Precision and Accuracy

Cation analyses for all solution samples and sediment digestions were analyzed by Inductively Coupled Plasma/Mass Spectroscopy (ICP/MS) (EPA Procedure 200.8) and Inductively Coupled Plasma/Optical Emission Spectroscopy (ICP/OES). Anions were determined by Ion Chromatography and Organic Carbon using a Dohrman total carbon analyzer. Analytical errors for water and sediment samples using ICP-MS and ICP-OES were calculated using reference standards. Water sample accuracies were better than 5% for Cr, Mn, Co, Ni, Cu, Zn, As, Se, Mo, Ag, Cd, Sb, Ba, and Pb. Accuracies for Mg, Al, Ca, and Fe lie between 5 and 10%, while Si accuracy was between 10-15%. Sediment samples displayed accuracies of better than 5% except for Na, which has an error of $\sim 10\%$.

Results and Discussion

Regional Sediments – Background Metal Concentrations

Local background metal values for river sediments were determined by collecting sieved samples at our designated control Site A on the West Fork of the Black River during five separate collection dates. Site A is located 2.2 miles south of the Brushy Creek Mine and 2.2 miles west of the West Fork Mine, however, this site does not receive any direct surface drainage from any of the New Lead Belt Mines (Figure 1). Because of Site A's proximity to two mines, we were concerned that sediments at this location may have enriched metal contents resulting from elevated background concentrations associated with the original formation of the ore deposits, addition of wind blown tailings pile material, and/or subsurface drainage from mines or tailings through a karsted geologic bedrock terrain. Due to these concerns, Sites X and W, which are located an additional 4.9 and 6.9 nautical miles, respectively, upstream and east of control Site A were added to our sampling array.

Metal concentrations in the sediments increased with decreasing particle size, with the -230 mesh grain size (silt and clay-sized) fraction containing the highest metal contents. The following discussion will focus on this fine grained fraction. Average and one standard deviation values for the sediments from Site A in $\mu\text{g/g}$ were Pb 48.8 \pm 20.0, Zn 171 \pm 239, Cu 36.7 \pm 18.4, Cd 0.88 \pm 0.45, Co 13.9 \pm 1.5, Ni 25.2 \pm 11.0, As 2.46 \pm 0.75, and Ba 127 \pm 13. One of the samples contained an anomalously high Zn concentration of 597 $\mu\text{g/g}$ Zn. When this one sample was removed from the total, the remaining four samples averaged 64.0 \pm 20.3 $\mu\text{g/g}$ for Zn. Concentrations of Pb, Zn, and Cd in the -230 mesh fraction at Sites X and W are notably lower than those at Site A. Values for Cu, Co, Ag, and As are also lower; however, the differences are within one standard deviation of the mean value for Site A.

The influence of mining related activities on the West Fork and Big Rivers can be seen in both water and sediment samples collected downstream from points of mine tailings effluent input. Contaminant metals (Pb, Zn, Cu, Co, Ni, Cd, etc.) may potentially enter the river as dissolved ions, suspended colloidal particles, sulfide mineral grains, or alteration phases produced during the weathering of tailings pile material. Rivers and streams are inherently dynamic systems with physio-chemical conditions that may change as a result of natural interactive parameters such as seasonal and diel temperature changes, amount and degradation state of organic material, biological activity, and meteoric water influx. The exposure of mine tailings waste material to atmospheric weathering processes may induce additional perturbations upon these river systems including sulfuric acid production and a decrease in the pH of the tailings waters.

West Fork Sediments – Mineralogy

An analysis of the bulk West Fork sediment material by XRD analysis indicates that the mineral composition of all size fractions is dominated by quartz. The character of the sediments in the West Fork visibly changes, however, from the clean light-colored quartz sand grains with minimal surface coatings at Site A to the darker in color grains noted downstream of the mine tailings piles (Sites D and E; Figure 3). Heavy mineral fractions of sediment that were examined by SEM/EDS investigations also confirmed that the red, orange, to black colored coatings and individual grains were composed of Mn and Fe oxide, hydroxide, or mixed oxide-hydroxide phases; herein referred to as "oxyhydroxides". Metal sulfides were not detected in any of the West Fork sediments. Dolomite grains were occasionally found, reflecting minor contributions from the surrounding carbonate bedrock geology and/or dolomite from the mine waste tailings.

Coarse grained organic material is present in the river system in various stages of decomposition ranging from relatively fresh algal and other aquatic plant material, leaf and branch material from the surrounding forest, and degraded brown-colored organic “fluff”.

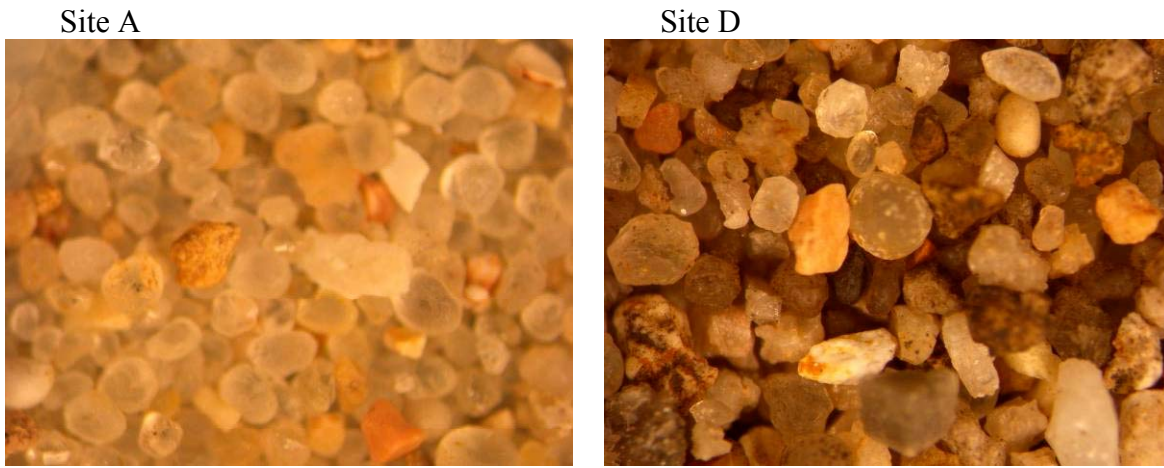
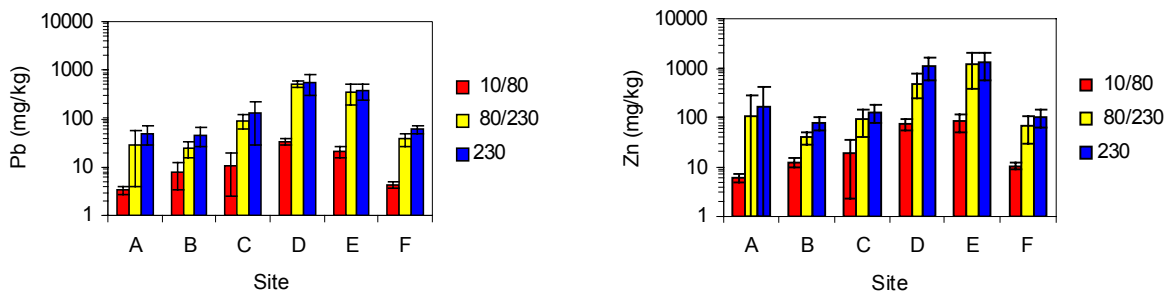


Figure 3. Optical microscopy images of panned concentrated sediments from the West Fork of the Black River, Sites A and D. Sediments from Site D are visibly noted to have more Mn and Fe oxyhydroxides coatings. Scanning Electron Microscopy – Energy Dispersive Spectroscopy analyses for the Mn and Fe oxyhydroxide particles (not shown) also indicate a higher contaminant metal content. The base of each photo is approximately 7.5 mm in length.

West Fork Sediments – Chemistry

Sediment samples were collected on the West Fork of the Black River from our six primary (Sites A through E) and eighteen auxiliary site locations between 2002 and 2005. Metal concentrations were typically greatest in the two smaller mesh size sediment fractions (80- to +230 and -230 mesh; Figure 4). The coarse fraction, however, dominates in volume, always being >50%, and usually >90% of the weight fraction of the sediments.



a. b.
 Figure 4. Lead and zinc concentrations in three size fractions of sediment. Samples from Sites A through F (10/80 represents sediments which passed through the #10 mesh and were retained in the #80 mesh (coarse to fine sand), 80/230 passed through the #80 mesh and were retained in the #230 mesh (fine to very fine sand), and 230 passed through the #230 mesh (silt and clay sized). Error bars represent one standard deviation from the average values shown.

Lead concentrations in the -230 mesh sediment fraction ranged from 2.4 to 960 $\mu\text{g/g}$ while Zn ranged from 4.3 to 2489 $\mu\text{g/g}$ at our six primary sites. Metal values for Pb and Zn increase between our regional background metal value (Sites X and W) and control Site A. Since Site A does not receive any surface drainage from the mines, this increase must result from an alternative processes. The highest Pb and Zn concentrations in the West Fork system were seen at Sites D and E, which are the two sites located directly downstream from the input point for the West Fork Mine effluent water. Zinc tended to be more enriched at the more distal Site E, while Pb was highest in the more proximal Site D. Concentrations of Co, Ni, and As also display large concentration increases at both of these locations, while Cu and Ba increases are noted, but are more subdued.

Three additional auxiliary sites were located between Site E and F, while an additional 11 auxiliary sites were located downstream of Site F (Figure 1). These additional sites allow us to characterize metal transport processes between our primary Sites A through E and Clearwater Lake. Most metal concentrations in the sediments decrease downstream away from Site D with concentrations returning to near Site A levels by the time sediments reach Site F (Figure 5). Concentrations still, however, remain above the regional background concentrations of Sites X and W. Nickel concentrations approach the regional background levels by the Fishtrap Hollow Site, while Zn and Pb remain slightly above regional background levels all the way to Clearwater Lake. Concentrations of Pb, Zn, and Cu increase slightly downstream of the confluence with the Center Fork of the Black River. The additional metals are likely derived from two mines that drain into the Center Fork. Nickel, Zn, Co and Cu, Fe, and Mn also show moderate increases further down river at the Warner Bay location. There are no known mines that occur within the Black River drainage basin in this region.

Manganese concentrations increase downstream from the point at which the river system passes the West Fork mine effluent. Iron concentrations also increase, but only at a fraction of the rate observed for Mn. The result is a notable increase in the Mn/Fe ratio in the sediment, especially in the smaller two sediment size fractions (Figure 6). This change can be correlated to the darkening in color of the sediments (Figure 3). An examination of the SEM-EDS spectra from the sedimentary particles from Sites D and E indicates that Pb, Cu, Co, Ni, and Zn are often associated with Mn and Fe-rich precipitate material. The solid Mn- and Fe-phase(s) are thus acting as a precipitation sink for metals released with the tailings pile waters. Other possible sinks for contaminant metals in sediment are represented by clay minerals and organic particles. Clays were not detected during XRD analyses of the -230 mesh sediment fraction (silt and clay sized) despite using a gravity flotation technique designed specifically concentrate clay-sized particles for analysis. Total Organic Carbon (TOC) determinations were made on a limited number of West Fork sediment samples from Sites A and D. Both sites display a progressive increase in TOC contents with decreasing sediment size. TOC concentrations in the -10/+80 mesh sediment fraction were 0.03 and 0.04 wt% for Sites A and D, respectively, whereas the corresponding -230 mesh fraction values were 3 and 4 wt%, respectively. Samples of degraded organic “fluff” were also collected at Sites A and E by siphoning off the low density river bottom sediment in slack-water areas using a plastic “turkey baster”. Enrichment ratios for metals in the organic fluff (concentration at Site E/ concentration at Site A) were highest for Pb, Ni, Zn and Mn (7.0, 6.2, 5.9, and 4.1 respectively). However, the metal contents in the organic fluff are less than those of the bulk -230 mesh fraction sediments indicating that the organic particles are not the only metal adsorbent, nor are they the dominant metal adsorbent in the sediment system.

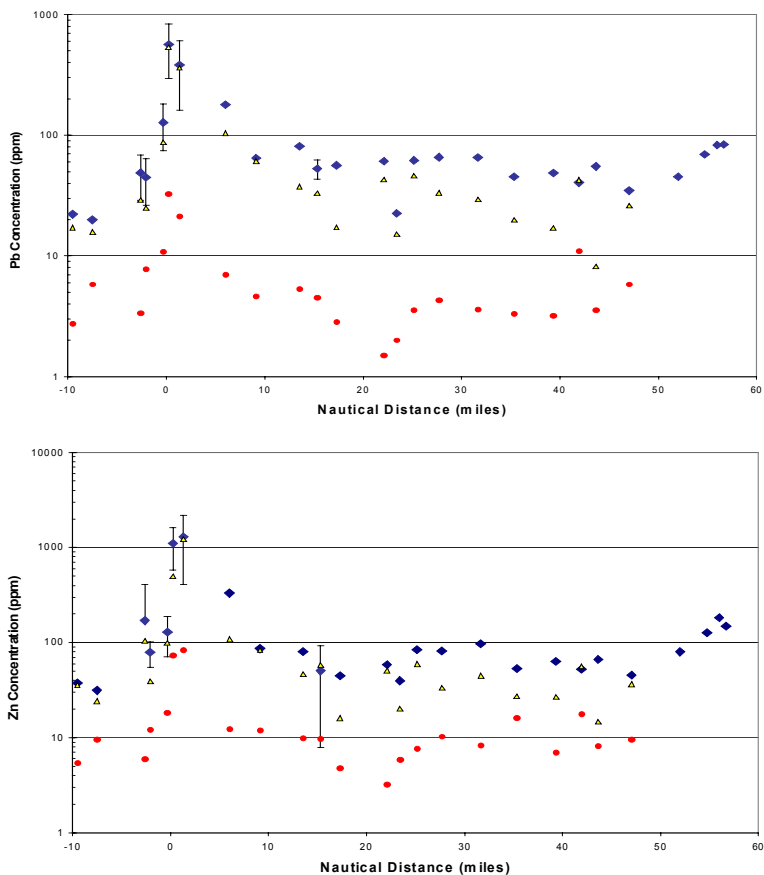
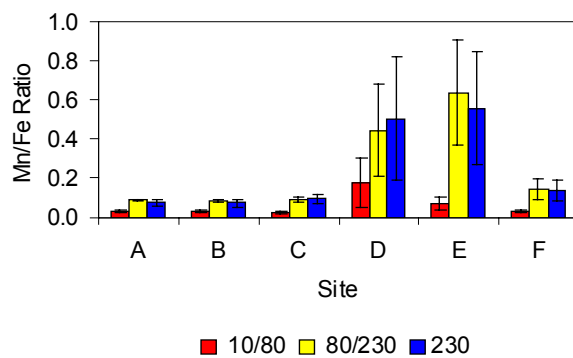


Figure 5. Lead and zinc concentrations in West Fork sediments as a function of downstream transport distance. The zero mile location represents the West Fork Tailings effluent point. One standard deviation bars are shown for Sites A through F. The blue diamond symbols are the -230 mesh size fraction, yellow triangles the -80/+230 mesh size fraction, and red circles the -10/+80 mesh size fraction. The four blue diamonds to the far right are the Clearwater Lake sediments.



a.

Figure 6. Average Mn/Fe ratios in three size fractions of West Fork sediment (error bars represent one standard deviation).

West Fork Water Column - Chemistry

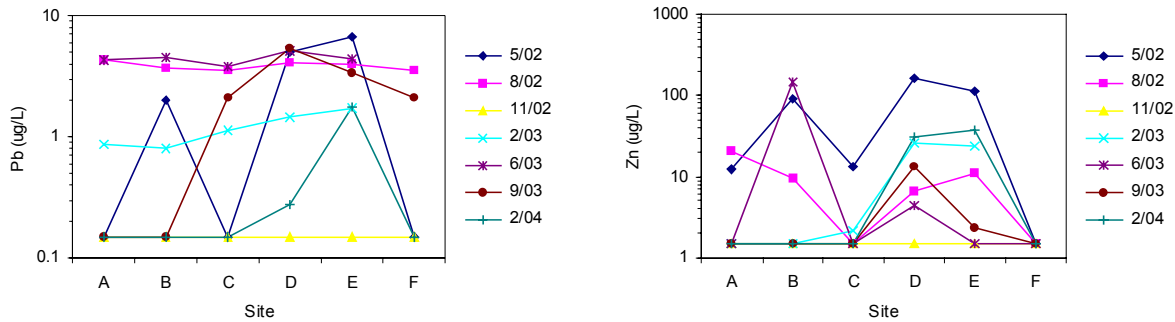
Six of the ten water column sampling trips on the West Fork were conducted when the river was exhibiting low-flow water conditions. The remaining sampling trips coincided with a high-flow period following a winter rain (2/03), a rising flow during a summer rain (6/03), a moderate flow period (5/02), and a gravel removal operation that occurred during low flow conditions (8/02). Flow rates were presented in Table 2 were calculated using on-line flow data recorded at the Lesterville and Annapolis USGS gauging stations (located downstream from our sampling sites), and then comparing the relative watershed sizes for these two stations against the size of the watershed encompassing our sampling sites.

West Fork river water pH varied from 7.6 to 8.2, while Eh values ranged from -4 to -75 mV for all sampling periods. Alkalinity values ranged from 100-186, and Ca-hardness from 61-105, and total hardness (Ca+Mg) from 109-229 mg/L. The Ca and total hardness values increased as the river waters received effluent water from the mine tailings and then decreased with increasing distance away from the mines. The mine effluent water at the point where it discharges into the West Fork has an alkalinity value of 155, Ca-hardness of 145, and total hardness of 291 mg/L.

The abundance of suspended sediment material in the water column is relatively limited as indicated by the low turbidity values associated with the West Fork waters. Turbidity values measured during low flow sampling events ranged from 0.2 to 2.1 nephelometric turbidity units (ntu). These values increased during high flow, peaking during storm flow at 17.7 ntu. Total suspended solid (TSS) values for non-flood events, ranged from 0.096 to 2.22 mg/L while total dissolved solid (TDS) values fell between 166 to 185 mg/L. Values for DOC (<0.45 μm filtered) were measured during the 2/04 sampling trip with values ranging from 4.15 to 5.02 mg/L.

All of the unfiltered water samples collected during normal flow periods had Pb concentrations that ranged from <0.15 to 6.7 $\mu\text{g/L}$ while Zn concentrations were between <0.15 and 163 $\mu\text{g/L}$ (all sampling periods except 8/02 and 6/03). For the proximal locations on the West Fork, Pb concentrations were lowest at Sites A, C, and F, all three of which are also located either upstream or far downstream from known mining operations. Lead concentrations increased at Site B, which receives effluent from the Brushy Creek Mine *via* Bills Creek; and at Sites D and E, which are located directly downstream from the West Fork Mine. Lead distributions in the water column appear to be dominated by particulate material > 0.45 μm in size. Zinc concentrations roughly parallel those of Pb with the highest concentrations occurring at Sites D and E.

Lead concentrations were elevated at control Site A during the high flow period in 2/03 (Figure 7). By contrast, Pb concentrations at Site D, directly downstream from the input point for West Fork effluent did not deviate with the river flow, but rather similar Pb values were obtained irregardless of flow rate. Zinc contents exhibited a closer correlation to flow, with concentrations increasing during low to moderate flow events, but decreasing during a period of high flow (2/03). The increased concentrations are believed to result from the suspension of Zn-bearing particulate matter, while the latter decrease may result from dilution effects associated with meteoric water input.



a. b.
 Figure 7. Metal concentrations in unfiltered water samples from the West Fork of the Black River; a) Pb concentrations, b) Zn concentrations.

Our sampling on 6/03 was conducted during a period of summer rain and corresponding increase in river flow. Three sets of samples were taken from Sites C and D throughout the day and night capturing a normal flow, two inch rise, and peak flow after a 2.75 inch total rise. Contaminant metal concentrations in the water column notably increased during flood event. Our maximum Pb concentration of 65.5 $\mu\text{g/L}$ was collected during the rapid rise period. This was the highest Pb concentration detected during all sampling events on the West Fork. The corresponding concentrations in the 5.0, 0.45, and 0.02 μm filtered fractions for this sample were 36.8, 30.4, and 4.7 $\mu\text{g/L}$, respectively. This distribution suggests that the particulate distribution of Pb is a bimodal during flooding, with a significant contribution of Pb occurring in two particle size ranges; 0.02 to 0.45 μm (39% of total) and $>5.0 \mu\text{m}$ (44% of total). Concentrations of both Pb and Zn decreased later in the day when we collected our third set of samples.

Our 8/02 sampling trip unintentionally coincided with a period of low water bridge construction and gravel removal upstream from the sampling reach. This disturbance event allowed us to examine potential river bed scouring effects associated with flooding, but without the dilution effect associated with increased meteoric water runoff. Figure 8 shows Pb and Zn concentrations throughout the sampling reach during the 8/02 construction period versus the 9/03 sampling when a similar river flow rate was in effect (47 and 52 cfs, respectively). High Pb concentrations were detected at control Site A following the disturbance. These levels remained elevated throughout the entire sampling reach (Sites A through F) masking any contribution from the mine tailings effluent. A large proportion of the Pb was contained in the $<0.02 \mu\text{m}$ fraction as opposed to distributions during normal flow events when the $>5.0 \mu\text{m}$ fraction was dominant. Zinc concentrations also increased at Site A as a result of the gravel operation, but notably decreased by Site C, and then increased again downstream of the effluent input at Site D. The differences between Pb and Zn behavior suggest that the transport of these two metals is influenced by sedimentary particles with contrasting densities.

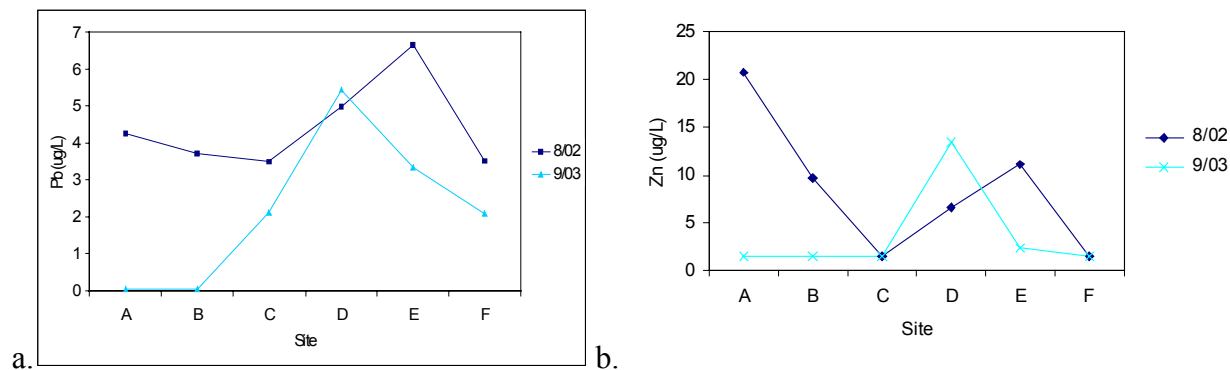


Figure 8. Lead and zinc concentrations in unfiltered water during the 8/02 period of bridge construction and gravel removal upstream of the sampling reach. Shown in relation to a period of similar flow conditions at 9/03.

Most of the Mn and Fe in the water column samples is present in a dissolved or fine-grained colloidal state. Samples taken from Site D on 9/03 had Mn concentrations of 129, 127, 124, and 119 $\mu\text{g/L}$ and Fe concentrations of 628, 616, 550 and 556 $\mu\text{g/L}$ in the unfiltered, 5.0, 0.45, and 0.02 μm filtered fractions, respectively. Samples for all sites showed a similar size distribution for Mn and Fe, irregardless of the concentration or river flow rate. Dissolved Organic Carbon (DOC; $<0.45 \mu\text{m}$ filtered sample) samples were collected during our sampling trips in February 2004 and June-July 2005. The DOC levels ranged varied 3.89 to 5.95 mg/L. There was no apparent dependence of the DOC values with respect to seasonal variation or distance from the mine water effluent input sites.

West Fork Batch Metal Adsorption Test

The potential effect of Mn, Fe, and organic phases on metal contaminant mobility was addressed experimentally in set of pilot-scale batch adsorption tests where unfiltered mine effluent water was added to vessels containing either West Fork organic particles from the Site X regional background location, hematite, hausmannite, or a control vessel without any solid phases. Metal distributions for the hematite and hausmannite tests did not differ from the control test and will not be further discussed. The 0.45 μm filtered sample aliquots collected from the control test during the first hour of testing contained Mn at a concentration of approximately 95 $\mu\text{m/L}$ (Figure 9a). These values began to fall after approximately two hours and dramatically decreased after eight hours of testing until they reached a level of about 3 $\mu\text{m/L}$ after 48 hours. By contrast, Fe remained at a relatively constant level of 750 - 900 $\mu\text{m/L}$ throughout the same interval. Concentrations of Pb and Co closely follow the changes observed with Mn (Figure 9b), suggesting these metals are being coprecipitated with Mn oxyhydroxide phases. Nickel and Zn contents also decreased, but only after 48 hours of testing, and these changes were not as dramatic as those involving Mn, Pb, and Co.

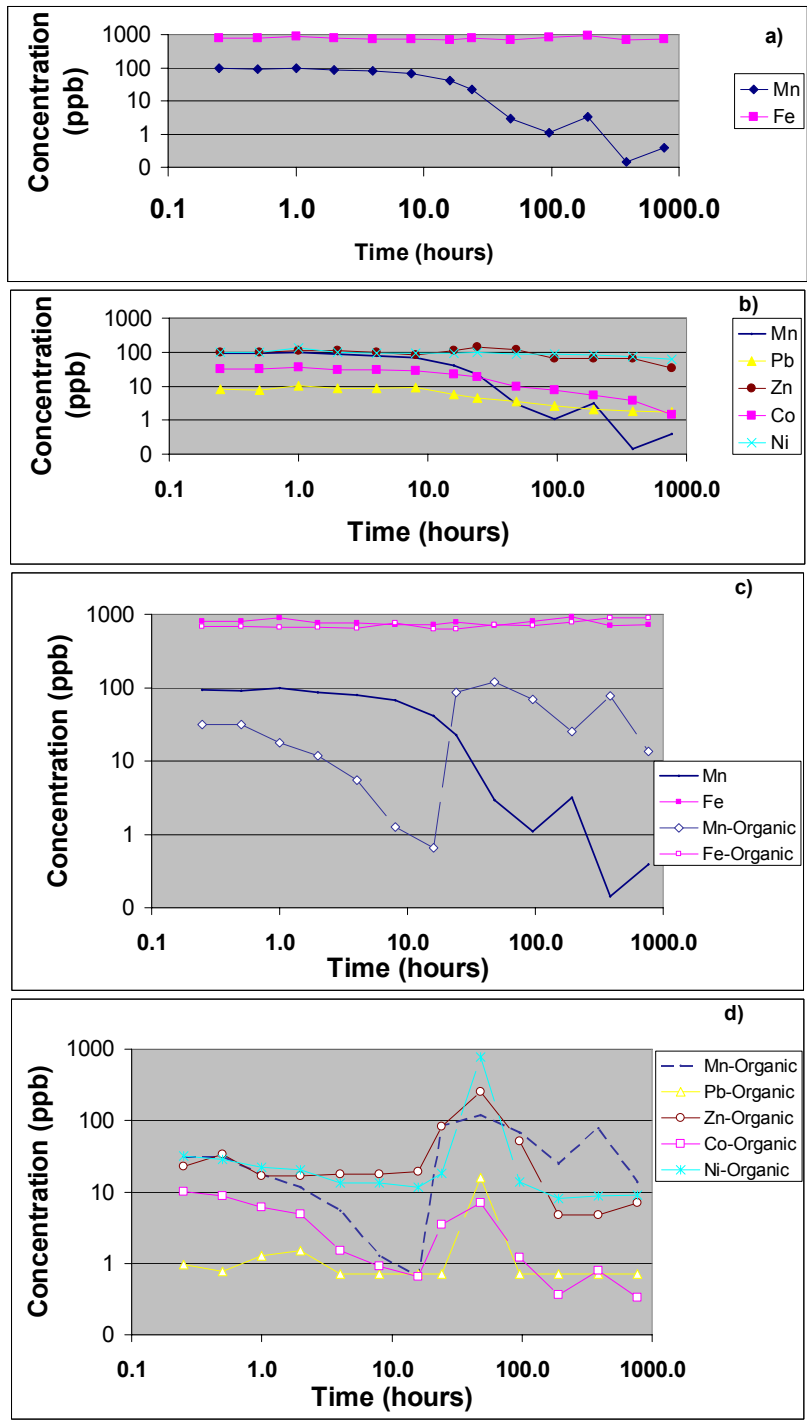


Figure 9. Time correlated metal distribution plots from batch adsorption tests using West Fork mine tailings effluent water. a) control test showing relationship between relatively static Fe and decreasing Mn concentrations, b) control test showing relationship between contaminant metals Pb, Zn, Co, and Pb versus Mn, c) variations between Fe and Mn distributions for tests with organic particulate material versus control test, d) organic particulate test showing relationship between contaminant metals Pb, Zn, Co, and Pb versus Mn.

Manganese concentrations initially decreased at a more rapid rate in the test containing organic particles (Figure 9c), but then reversed, showing an increase from between 16 to 48 hours. The Mn concentrations declined thereafter except for a temporary reversal at 348 hours. Iron concentrations were relatively static level over the entire testing period as they were in the control test. Contaminant metal concentration trends all evolved in parallel manner with Mn, with the concentrations of Pb, Zn, Ni, and Co all being relatively low in the initial stages, but then increasing again after 16 hours (Figures 9b and d). Nickel and Zn contents eventually exceeded the levels present in the starting test solution, with excess metals being derived from dissolution of colloidal particles that were present in the tailings water that was used to initiate the experiments. Lead distributions differed from the other metals with concentrations that were initially much lower than those in the control test (Figures. 9b and d). The pH and Eh values for the starting effluent water (leachant solution) were 8.33 and -54 mV. Final leachate values, after all aliquots had been removed, were pH = 8.07 and Eh = -81.7 for the control test, and pH = 7.33 and Eh = -36.9 for the sample with organic particles added.

Clearwater Lake Sediment Core Studies

There are no mines occurring in the Web Creek drainage basin, thus the sediment core from this branch offers a good baseline for evaluating regional background metal levels. Relatively little change is noted in the metal distributions in the vertical profile of this core with Pb remaining at a relatively constant 25 $\mu\text{g/g}$ and Zn at constant 55 $\mu\text{g/g}$. The Logan Creek branch receives drainage from Sweetwater Mine that is located at the southern extremity of the New Lead Belt district (Figure 1). Lead levels in Logan Branch sediments increase from 15 to 45 $\mu\text{g/g}$ from the base to the top of the core, while Zn contents similarly increased from 30 to 70 $\mu\text{g/g}$. The metal contents at the base of this core were the lowest observed in the Clearwater Lake Basin.

Three cores were collected in the Black River branch. The Upper Black core was collected furthest north and closest to the mouth of the Black River (Figure 1). This core displays a relatively small Pb concentration increase from 35 to 45 $\mu\text{g/g}$ and Zn increase from 75 to 80 $\mu\text{g/g}$ from bottom to top. The Middle Black core displayed a Pb increase from 50 to 70 and a Zn increase from 100 to 130 $\mu\text{g/g}$. The core furthest south in the Black River branch (near the boat marina) displayed a Pb increase from 35 to 90 $\mu\text{g/g}$ and Zn increase from 90 to 150 $\mu\text{g/g}$. Metal concentrations in these three cores thus display concentration increases from: 1) the bottom to the top of the cores, and 2) from sites closest to the mouth of the Black River to the sites furthest away. None of these three cores display a Cs-137 emission profile peak that correlates with peak atmospheric fallout in 1964, thus all three core segments likely accumulated after active mining was already underway in the New Lead Belt. None of these three cores penetrated the entire lake sedimentary sequence.

Our last core was taken closest to the Clearwater Dam Site. This core displayed the largest relative metal increase and the highest overall Pb content in the Clearwater Lake system. Lead and Zn concentrations at the base were 35 and 90 $\mu\text{g/g}$, respectively. These concentrations increased upwards to where Pb levels reached 90 and Zn levels reached 150 $\mu\text{g/g}$ at the top. The base of this core also contained tree roots fragments in a soil matrix, thus it appears to have penetrated the entire sediment profile of the Lake down to the 1948 soil surface.

Lead isotope concentrations were also determined for sediments in the Upper Black and Clearwater Dam Site cores and compared to published lead isotopic ratios for ore minerals in the New Lead Belt, mineralized Bonnetterre dolomite, unmineralized Bonnetterre dolomite, and

leaded gasoline used in Missouri prior to its EPA mandated phase out (Goldhaber et al., 1995). The Bonneterre Formation is the dominant host rock for the Pb-Zn ores of the New Lead Belt. The resulting $^{207}\text{Pb}/^{204}\text{Pb}$ versus $^{206}\text{Pb}/^{204}\text{Pb}$ isotopic determinations for the lake sediments fall along a well-defined mixing line located between unmineralized Bonneterre dolomite and ore minerals from the New Lead Belt (Figure 10). The isotopic character of the sediments progressively moves away from the Bonneterre end member and nearer to the New Lead Belt ore mineral source as we move from the bottom to the top of the cores (Figure 10b). The Pb isotopic patterns do not show any suggestion of being derived from Missouri leaded gasoline (Figure 10a).

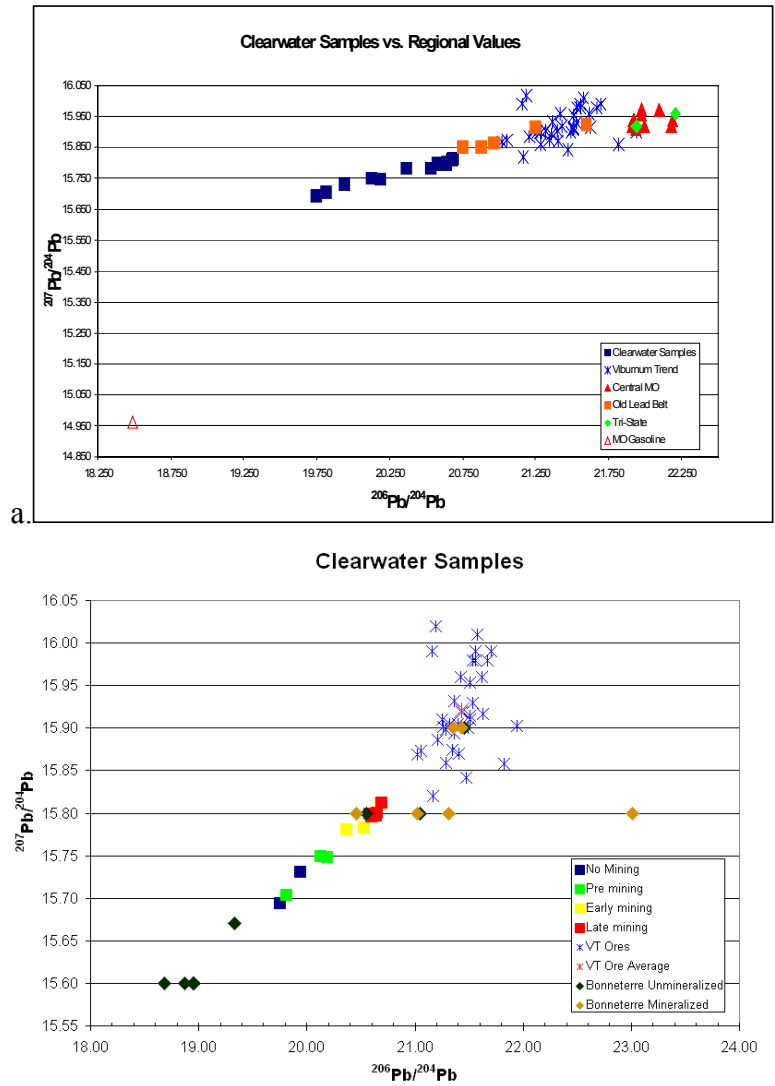


Figure 10. Lead isotopic trends in Clearwater Lake sediments and associated potential source materials (source data from Goldhaber et al., 1995). A) comparison of isotopic ratios from Clearwater sediments with Missouri leaded gasoline and lead ores from four regional mining districts, b) comparison of Clearwater sediments taken at various stratigraphic intervals (no mining, pre mining, early mining, late mining) with isotopic ratios from Viburnum Trend (New Lead Belt) ores and unmineralized carbonate rocks of the Bonneterre Formation.

Sequentially Extracted Metals

The sequential extraction procedure (Tessier et al., 1979) was used to determine the solid phase location of five separate fractions of contaminant metals including: 1) exchangeable, 2) carbonate, 3) Fe-Mn oxide (oxyhydroxide), 4) organic, and 5) residual. Spike recoveries for Pb, Zn, Cd, Ni, Co, Ba, Fe, and Mn ranged from 93 to 109%, while Cu recoveries were 77 to 110% for matrix (sample) and reagent spikes, respectively. Arsenic recoveries were only 24 to 27%, most likely due to the loss of volatiles containing As during digestion.

For the Black River system, the -230 mesh size Site A sediments upstream of the tailings water entry points contained most of its metal inventory in the residual and oxyhydroxide fractions. Significant amounts of lead were also contained in the organic and carbonate (~10% each), Cd in the exchangeable and carbonate, Cu in the organic, and Ba in the carbonate fractions. Changes in metal distributions were noted for the -230 mesh sediments below the tailings water entry point (Site D) where overall contaminant metal contents increased and the percentage of contaminant metals increased in the carbonate fraction for Pb, Zn, Cd, Cu, and Ni; oxyhydroxide fraction for Pb, Zn, Cu, Ni, Co, Fe, and Mn; exchangeable fraction for Cd; and organic fraction for Zn and Cd. The largest increases are typically associated with the oxyhydroxide fraction. A significant fraction of the Cu, Ba, and Fe were associated with the residual (silicate) fraction both above and below the tailings water entry points. Correlation coefficients (r) and their levels of significance (at $\alpha=0.05$) were determined for all sequential fractions, sum of fractions, and total metals (with no digestion) using Statistica® (Statsoft). The correlation analyses showed that all sequential extraction fractions (and totals) for Pb correlated well with the carbonate, Fe/Mn oxyhydroxide, and residual (silicate and/or sulfide) fractions. In contrast, only the residual Mn was found to correlate well with Pb. Zinc displayed a strong correlation with the Fe carbonate fraction, while both Zn and Pb showed the strongest correlations with the Fe/Mn oxyhydroxide and residual fractions. Sequential extraction tests on Big River sediments displayed similar contaminant metal distributions as those of Site D on the West Fork. There were notable increases in the percentages of Pb, Cd, Cu, Ni, Co, Fe, and Mn associated with the oxyhydroxide fraction, Cu with the organic fraction, and Zn with the residual fraction, between the Route 67 and Washington Park sites.

Hydrologic Characterization of the West Fork of the Black River

The mean size of field-measured gravels on the bed surface is 5.5". The calculated flow rate required to break a non-cohesive armored layer of this nature is 350 cfs. Our sieve analysis (ASTM D1140-54) of the representative bed channel material passing through the sieves at Site B yielded the following: Sieve Size = 2", 100.0, 1", 85.9%, 3/4" 76.6%, 1/2" 57.3%, 3/8" 45.5%, 1/4" 25.9%, #4, 22.2%, #20 3.5%, #40 1.6%, #50 0.6%, #100 0.1%, #200 0.0%, and Pan, 0.0%.

Big River and Associated Tributary Sediments – Chemistry

Only a single suite of sediment samples have been collected and analyzed from the six primary Big River sites. Concentrations of Fe and Mn are highest in sediments closest to the tailings piles, with Fe being present at levels that are approximately 10-fold higher than Mn. This trend is similar to what was observed in the West Fork sediments. Manganese concentrations ranged from 0.20 to 0.38% at sites near the tailings piles to 0.11 to 0.23 at sites furthest from the piles. Iron concentrations similarly ranged from 2.05 to 2.93% at proximal to

1.17 to 2.07% at more distal locations. Contaminant metals correlate well with Fe and Mn, especially at the more distal locations. Lead concentrations ranged up to 2800 and 24,800 $\mu\text{g/g}$ for the Big River channel and associated tributary streams draining tailings piles, respectively. Corresponding maximum Zn values were 1600 $\mu\text{g/g}$ and 26,400 $\mu\text{g/g}$. Remaining maximum values for the other metals (main Big River channel only) are Cd, 24.5; Cu, 73; Ni, 30; Co, 32; Ba, 670; As, 11; and Ag, 2.2 $\mu\text{g/g}$.

Big River and Associated Tributary Sediments – Mineralogy

X-ray diffraction analysis of the various sieve-sized sediment fractions from the tributary creeks which drain from the tailings piles into the Big River indicate that the sediments are dominated by dolomite ($(\text{CaMg})(\text{CO}_3)_2$) from the tailings piles, while sediments from the Big River channel are dominated by quartz. Most of the quartz is likely derived as a chemically resistant weathering residue from the surrounding soils.

Panned sediment concentrates of heavy minerals were collected from our eight primary sampling sites and 20 auxiliary sites located at $\frac{1}{2}$ nautical mile increments starting at the southeastern edge of the Desloge Tailings Pile. These sediments provide a record of the ability of the sulfide minerals to survive transport and corrosion processes, and the fate of the associated contaminant metals. Galena (PbS) was the most common sulfide mineral found, with particles recovered from sediments close to the Desloge pile still displaying their characteristic cubic morphology without significant rounding of corners and edges (Figure 11). Rounded and pitted sphalerite grains (ZnS ; Figures 11a and b) were only rarely encountered, even though sphalerite is the second most abundant ore mineral present in the Old Lead Belt ores. Pyrite (FeS_2) was also found, but only in sediments proximal to the tailings piles. These grains also displayed irregular pitted surfaces that suggest they have undergone significant chemical weathering (Figure 11e). At a transport distance of $2\frac{1}{2}$ miles, galena particles display minor rounding of corners and well-developed dissolution pits. Sphalerite is also found at this distance, but pyrite is not. All galena and sphalerite grains collected at distances of 4.0 to 7.4 miles from the Desloge Pile are highly rounded, indicating extensive mechanical abrasion during transport (Figure 12). Galena grains also display various surface alteration features such as an S, Fe, and Si enriched surface coatings (Figures 12b and c) and precipitation of cerussite (PbCO_3) crystals in dissolution pits. Sulfide particles were not detected at the St. Francois Park Site, located 12.5 miles downstream from the Desloge Tailings Pile, or any sites further downstream. At these more distal locations, contaminant metals in the sediments are found in Fe-, Mn-, and Si-rich particles. Fe- and Mn-oxyhydroxide particles at the St. Francois State Park Site contained Pb, Zn, and Cu, with up to 7.4 wt% Pb (Figure 13b). Sedimentary particles from the Highway Y Site (60 miles from the Desloge Pile) contained more Si and Al, but lesser Pb, Fe, and Mn than the St. Francois Park sample.

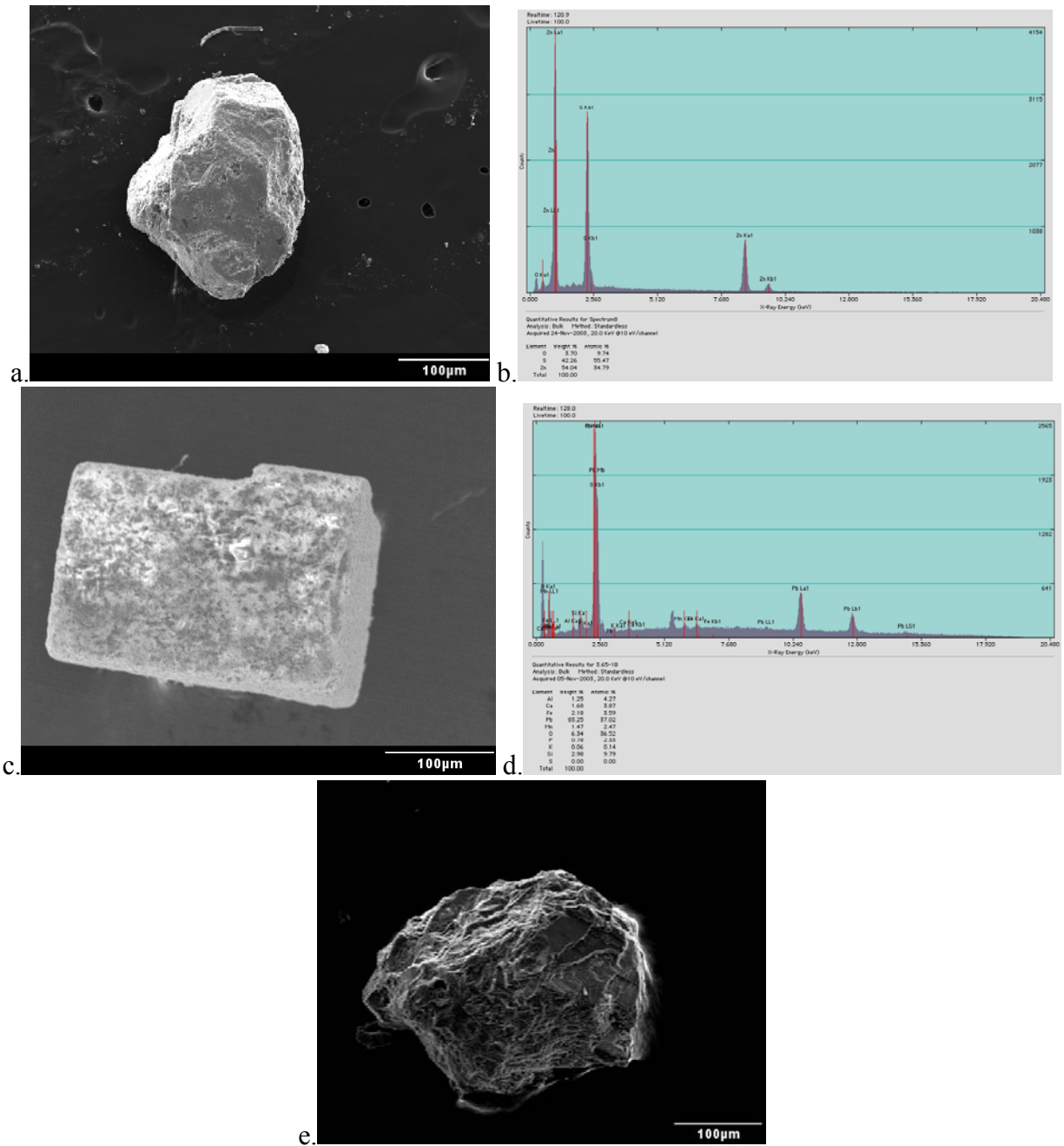


Figure 11. Sulfide grains recovered from Big River site ½ mile downstream of Desloge Tailings pile. All particles display minimal physical abrasion and are minimally rounded. a) lightly corroded sphaerite grain (ZnS), b) SEM/EDS compositional spectra from sphaerite grain in Figure 11a, c) cubic grain of galena (PbS) displaying development of fine grained alteration phases on surface, d) SEM/EDS compositional spectra from galena grain in Fig. 11c showing presence of Pb, S, and minor Si, Al, Ca, Mn, P, and Fe, e) moderately corroded pyrite grain (FeS₂).

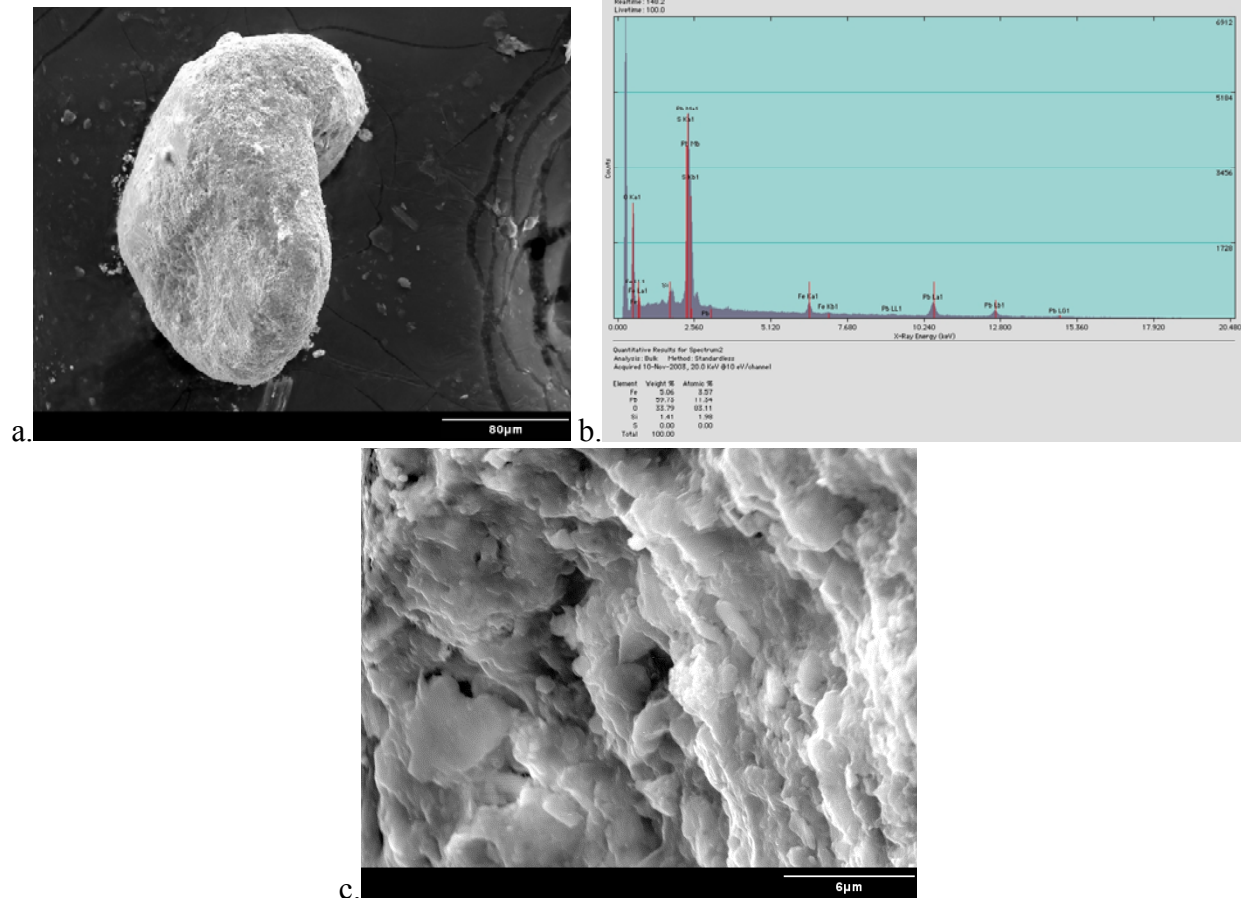


Figure 12. Altered galena (PbS) Particle from 4.0 miles downstream of Desloge Tailings pile. a) highly rounded morphology indicating abrasion during transport, b) SEM/EDS spectra displaying Pb- and S-rich composition with lesser Fe and Si, c) High magnification image of altered particle surface.

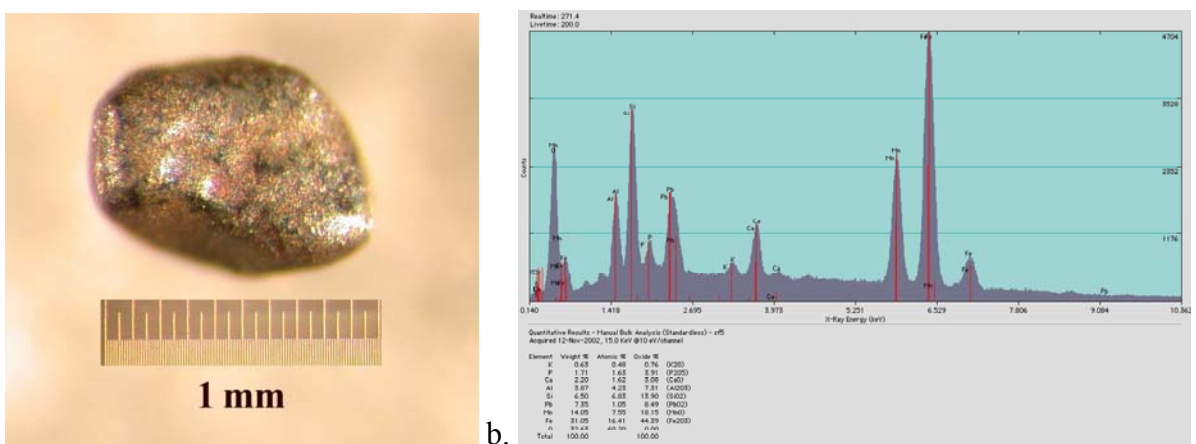


Figure 13. Sedimentary particle from the St. Francois State Park sampling site located 12.5 miles downstream from the Desloge tailings pile. a) optical image of rounded sediment particle displaying dark and mottled color with metallic reflective surface, b) EDS spectra for sediment particle displaying Fe-, Mn-, and Si-rich composition with lesser Al, Ca, Pb, and P.

Big River Tailings Pile Water - Chemistry

Waters emanating from the Elvins Pile (River Mines) tailings waters are enriched in Ca, Mg, sulfate, and bicarbonate. The waters are also mildly alkaline with a pH ranging from 7.6 - 8.0. The pH values tend to increase with time and distance as the waters migrate away from the tailings piles. Corresponding Eh values remain at a relatively constant -37 mV. Alkalinity values ranged from 96-149, Ca hardness from 354 to 755, and total hardness values from 620 to >4000 mg/L. In addition to Ca and Mg, dissolved contaminant metals (e.g., Zn) are likely contributing to the high hardness values. Two turbidity measurements were made on the Elvins pile waters. A value of 1.4 ntu was obtained during a non-rain sampling event, while turbidity increased up to 14 ntu following a period of heavy rainfall. Corresponding TSS values increased from 14.63 to 35.11 mg/L for the non-rainfall and rainfall events, while TDS values decrease from 1174 to 710 mg/L for the same samples. Values for DOC (<0.45 μm filtered) were below detection while total carbon (TC) concentrations were at 31.0 mg/L.

In the Old Lead Belt area, many of the metals are being released from the tailings piles in a soluble or colloidal form. Zinc contents are highest in tributary streams near the Elvins tailings pile (ranging up to 20,825 ppb) with up to 87% of the Zn passing through a 0.45 μm filter. The maximum Pb concentrations obtained from the Elvins waters was 623 ppb, with 23% of this Pb passing through 0.45 μm filter. The remaining maximum metal (and As) concentrations and percent passing through a 0.45 μm filter from the tributary creeks are as follows: Ba-63 ppb-100%; Cd-53 ppb-83%; Cu-26 ppb-45%; Ni-711 ppb-99%; Co-853ppb-98%; As-13 ppb-100%; Ag-0.53 ppb-<10%. Concentration trends for the metals present largely in a soluble form (e.g., Zn, Ni, and Co) were lowered following the heavy rains. By contrast, metals exhibit higher particulate fractions (e.g., Pb and Cu) display increased concentrations following rain events.

Big River Water - Chemistry

The pH values from the main channel of the Big River (Rt. 67, St. Francois, Washington Park, Highway Y, Byrnsville, and Irondale Sites) varied from 7.1 - 8.3, while Eh values ranged from -24 to -61 mV. Alkalinity ranged from 46-223, Ca hardness from 44-170, and total hardness from 71-340 mg/L. Flood water events are usually associated with the highest Eh, and lowest pH, alkalinity and hardness measurements. The highest Ca- and total hardness values occurred in portions of the river system located directly downstream and in closest proximity to the tailings piles.

Turbidity values measured during low water flow periods ranged from 1.4 to 18 ntu. These values increased dramatically during flooding, with a peak value of just over 300 ntu being determined from a sample collected during the January 2005 storm event. TSS values for a non-flood event ranged from 1.72 to 11.58 mg/L while the maximum flood values (1/05) ranged from 154 to 403 mg/L. TDS values for the non-flood event ranged between 264 to 374 mg/L, while flood values ranged from 91 to 167 mg/L. TSS, TDS, and the ntu turbidity values generally increased downstream in the Big River during both non-flood and flood events.

Metal concentrations in the Big River channel were generally lower than those of the tributary streams. During the moderate flood of March 2002, Zn concentrations increased to values that were between 144 and 227 $\mu\text{g/L}$, although concentrations were diminished downstream. Unfiltered concentrations for Zn during the January 2005 flood ranged from between 62 to 197 $\mu\text{g/L}$. These values were lower than those of the March 2002 flood. The location for the peak metal concentration also progressively moved downstream during flooding.

The highest Zn concentrations collected during the first sampling round in the 2005 flood (during rising water conditions) occurred at the Washington Park Site where 195 µg/L was detected. Later that night, as the flood waters were cresting, the peak concentration moved further downstream to the Highway Y Site where 197 µg/L was detected. Two days later, after flood crest had occurred, the Zn concentrations had evened out to approximately 120 µg/L at the Washington Park, Highway Y, and Byrnsville Sites.

Lead concentrations in unfiltered waters ranged between 16 to 82 µg/L during low water events, with concentrations increasing to between 197 and 286 µg/L during the March 2002 flood and between 26 and 560 µg/L during the January 2005 flood. In contrast to the diminishing Zn values, Pb levels continuously increased with distance downstream during flooding. At the Route 67 Site, Pb values peaked early during the 2005 flood at approximately 170 µg/L. As the flood waters subsided, the Pb values here were reduced to 26 µg/L. The position of the peak Pb concentration progressively moved down river during the course of the flood event. During our first sampling in the morning of January 5th, our peak Pb concentration was determined at Washington Park, where 560 µg/L was detected. That same night, the concentration at Washington Park fell to 265 µg/L as the peak concentration occurred downstream at the Highway Y Site where 529 µg/L Pb was detected. During the third sampling on January 7th, the highest concentration of Pb occurred at the Byrnsville Site where a concentration of 316 µg/L was detected. During this latter sampling, the corresponding Pb concentrations at Washington Park and Highway Y had fallen to 260 and 176 µg/L, respectively.

Determinations for TC and DOC (<0.45 µm filtered) from the January 2005 flood event indicate that DOC concentrations increased during the course of active flood rise, and then decreased on the tail end of the event as the flood crest had passed. The TC concentrations correspondingly continuously decreased over the entire course of the flood event. Determinations for IC did not display any consistent trends from site-to-site during the flooding.

Dissolution Processes Occurring in Tailings Piles

Metal release to fluvial systems from the tailings piles occurs in a complex and dynamic fashion. Tailings waters emanating from the base of the Elvins (River Mines) Tailings Pile contain high contaminant metal loadings (e.g., up to 20,825 ppb Zn) with the majority of this load passing through 0.02 and 0.45 µm filters. These filtered solutions may thus contain colloidal particles as well as ions that are truly dissolved in solution. Nearly the entire inventory of As and Ba is being transported in this soluble fraction while Ni and Co follow close behind at 99 and 98%, respectively. Zinc and Cd are released with an average of 87 and 83% occurring in the <0.45 µm filtered fraction, while Cu and Pb had the lowest proportion of soluble material with only 45% of the Cu and 25% of the Pb fraction passed through a 0.45 µm filter.

The relative order of the aqueous phase complex stability (as determined by % of total metal content passing through the 0.45 mm filter) from the Elvins Pile tailings water is:

$$\text{As} > \text{Ba} > \text{Ni} > \text{Co} > \text{Zn} > \text{Cd} > \text{Cu} > \text{Pb} \quad (1)$$

This sequence corresponds precisely with the relative order of for metal ion adsorption to hydrous oxide phases as determined by Dzombak and Morel (1990). However, in the Dzombak and Morel sorption series, the majority of the metals were adsorbed onto the hydrous oxide phases, while in the Elvins waters the majority of the metals were still present in a soluble form. The concentration of many metals in the Elvins waters also exceeds the established

solubility limit for metals with respect to various metal carbonate and sulfate phases. For example, the calculated equilibrium concentration for Zn in the presence of smithsonite (ZnCO_3) based off a $K_{sp} = 10^{-10}$ (Faure, 1998) would be 654 $\mu\text{g/L}$, much lower than the 10,116 to 18,248 $\mu\text{g/L}$ of Zn measured in <0.45 μm filtered waters the Elvins waters from our six sampling trips. Similarly, a solubility limit for Pb based upon the presence of cerussite (PbCO_3 ; $K_{sp} = 10^{-13.1}$) would be 58 $\mu\text{g/L}$, while our six filtered water samples ranged from 64 to 144 $\mu\text{g/L}$. Similar calculations for Cu, Cd, and Co would indicate a supersaturated state for the metals with relative to their respective carbonate phases. The solutions are clearly out of equilibrium with respect to the metal carbonate phases, an observation further substantiated by our inability to obtain stable conductivity readings from these waters while in the field. White crusty carbonate grains have also been observed to precipitate on the rocks adjacent to the tailings pile streams, and the precipitation of a Zn-Mg-carbonate phase has been induced by evaporating Elvins sample waters on a glass slide in the laboratory. High metal concentrations appear to be produced as oxygenated meteoric water comes in contact with tailings pile sulfide grains such as pyrite within the tailings piles. The water is acidified through the well-established oxidative-dissolution mechanism for sulfides and the formation of sulfuric acid, however, the acidified water is quickly neutralized through reactions with surrounding carbonate tailings sands (principally dolomite). High concentrations of SO_4^{2-} provide supporting evidence for the oxidative-dissolution process, while high Ca and Mg contents reflect the neutralization process that counters the acid formation.

Water seeping from the base of the Elvins pile is supersaturated with respect to many of the contaminant metals. These concentrations may be lowered when secondary minerals (e.g., carbonate and oxide phases) precipitate. A slight rise in pH is noted as the effluent water migrates away from the tailings pile and this rise is presumed to result from the loss of carbon dioxide to the atmosphere. The pH increase will induce the precipitation of additional carbonate minerals.

Concentration trends for the metals in the tailings water effluent that are dominantly in a soluble form (e.g., Zn, Ni, and Co) were lowered following the heavy rains of 3/02 and 1/05, while metals typically released as particles (e.g., Pb and Cu), display concentration increases. While localized variations in precipitation and a lag-time before a hydrologic flux is transmitted through a tailings pile may play a yet undetermined role in these patterns it does appear that the more soluble metal concentrations in tailings waters are being diluted by the rain water influx, while metals that are transported dominantly as particulates are increasing due to the flushing and dislodging of precipitated phases from the tailings piles grains.

Metal Concentration Changes with Transport Distance

The relatively minor increase in metal concentrations between our regional background (Sites X and W) and control (Site A) locations indicates that metal contents may be increased in the river systems *without* directly receiving effluent runoff from the mine tailings piles. Elevated levels of trace metals have been noted in water and sediment samples from non-mining influenced areas in other ore districts (Runnells et al., 1997). We have considered five potential contributing sources to the higher metal concentrations at Site A: 1) naturally elevated background metal concentrations resulting from geologic emplacement of ore metals by hydrothermal solutions, 2) subterranean transport of contaminated tailings or mine waters in a karsted terrain (caves) to an entry point that affects Site A, but not X and W, 3) wind blown dusts from tailings piles that influence the more proximal Site A sediments, 4) wind blown

smelter effluent from Pb-Zn smelter sites, and 5) other anthropogenic automotive exhaust. The potential for fugitive smelter dusts and automotive exhaust affecting the sediment compositions appear to be rather remote as both sources are relatively distant to the sediments and each would appear to have affected both Sites A and X sediments to a similar degree. Elevated natural background metal values and wind-blown tailings pile dusts appear to be the most likely sources for metal enrichment at Site A, while we do not have any basis on which to evaluate the possible migration of mine contaminated waters through a karsted geologic terrain.

Metal concentrations for the -230 mesh size sediments at Site D were ten-fold or higher for Pb, Ni, and Co; between five- and ten-fold for Zn, Cd, and Mn; and approximately four-fold higher for As relative to Site A (see Fig. 4 for Pb and Zn variability). Copper, Ba, Fe, Cr, Mo, Ca, and Mg display increases that were less than two-fold. The relatively large increase in contaminant metals at Site D provides a quantitative assessment of the impact of mining on the West Fork and the importance of mine effluent water in influencing the sediment metal loads. We normally expect samples with lower metal concentrations to also display the highest overall relative standard deviation values since the effect of analytical error is usually increased as analytical detection limits are approached. In the West Fork sediments we see the opposite trend. When comparing our six primary Sites, we find that Sites D and E display both highest metal concentrations and the highest relative standard deviation values for Pb, Co, Mn and As. Furthermore, Site E (but not D) also displays large relative standard deviations for Ni and Cd. Clearly the increase in contaminant metal concentrations at Sites D and E are accompanied by an increase in metal heterogeneity as well. Such a trend would logically reflect a disproportionate distribution of metals to a relatively limited quantity of sedimentary particles.

Concentration values for most metals return to Site A baseline levels by the time sediments reach Site F (Figure 5). Thus, the influence of the tailings waters on metal contaminant levels is only notable for a distance of approximately 15 nautical miles in the river sediments. At distances further than 15 miles the metal contents have decrease to levels that are difficult to distinguish from the Site A, however, these levels are still above the regional background values defined by Sites X and W sediments. Local exceptions to this trend are noted downstream of the confluence point between the West and Center Forks where metal concentrations again increase. Since the Center Fork receives drainage from two additional mine tailings piles in the New Lead Belt, it is likely that these mines are the source for the additional metals. Copper and Zn also show anomalously high concentrations further downstream at the Warner Bay collection location.

The Clearwater Lake impoundment acts as a receiving basin for all sediments being transported in the Black River and Logan Creek systems (Krizanich and Wronkiewicz, 2005). The concentration of contaminant metals in the top several inches of the Clearwater Lake core sediment are similar to those found in the -230 mesh sized fraction of sediments collected from the southern segments of the Black River system (Figure 5). Three additional sediment cores, the Lower Black River arm, the Marina, and the Dam Site occur successively further south and down current from the Upper Black River core location. Lead and Zn concentrations in these three cores progressively increase from north to south. This increase likely reflects a gravitational settling and segregation of particulate material across the lake where relatively larger silt-sized particles with lower metal concentrations preferentially settle out of the water column closest to the Upper Black River arm location. The finer grained and higher metal content fraction is transported further down current and deposited closer in proximity to the Marina and Clearwater Dam Sites. Additive contributions of other potential source(s) of

contamination, for example metals derived from recreational boating activities associated with the nearby Clearwater Lake Marina, cannot be ruled out as metal sources.

The cores collected in the Black River branch do not appear to represent a complete sedimentary section of the lake as our Cs-137 profile from the Upper Black River arm core displays a continuous decrease from the bottom to the top. The core collected from the Clearwater Dam Site does bottom out into pre-impoundment soils and the core displays a well defined rise and fall in Cs-137 values. The Dam Site core thus appears to have captured a metal emission profile that overlaps the onset of mining activities in the New Lead Belt. Metal concentrations in this core display a well-defined doubling in metal concentrations with a marked increase 1/2-way through the core profile. Lead isotope distributions in this core displays lead isotopic features that can be used to constrain the timing, source, and apportioned contributions of Pb to the sediments (Krizanich and Wronkiewicz, 2005; Figure 10). Isotopic patterns clearly fall along a mixing line between end member source contributions from New Lead Belt ore minerals and unmineralized Bonnetterre carbonate rocks. The contribution from the former increases upsection in the cores. Leaded gasoline has a distinctly different isotopic composition and does not appear to be making any significant contributing to the Pb patterns in Clearwater Lake sediments. The increasing contributions from a New Lead Belt source indicates that the rate of Pb exhumation has increased in the basin since the Clearwater Dam was constructed in 1948 and that this increase coincides with the initiation with mining activities in the basin in 1965. The increase probably has resulted from the emplacement of mine waste materials in tailings piles and the release of metals from the piles as they weather over time. Additional Pb may also be derived from soils naturally enriched in metals, with accelerated erosion of these soils possibly being due to construction activities associated with human development of the region. Lead may also be derived from smelter effluent as this source of Pb would have the same isotopic composition as the lead ores derived from the mines. Our current set of data does not completely discriminate between the various delivery mechanisms of Pb to the Clearwater Lake Basin.

Particulate Control on Contaminant Metal Transport

The transport of contaminant metals in water proximal to tailings piles is dominated by soluble aqueous phase complexes as previously noted. Since metal concentrations in these systems are supersaturated, their respective carbonate and sulfate metal bearing phases should precipitate by exothermic processes. As the contaminated waters and sediments migrate away from the tailings piles, they will be mixed with waters and sediments from regional drainage systems that have lower metal levels. Aqueous metal concentrations may be further reduced by this mixing to concentration levels below the previously established carbonate and sulfate phase saturation limits. This will result in the dissolution of previously formed metal bearing phases and the transfer of the contaminant metals as ions adsorbed onto various oxyhydroxide and organic particles with high K_d values. The overall effect of the near field to far field transfer is a partitioning of metals from the aqueous fraction, to mineral phases containing the metal contaminants as a major component, and finally to phases containing the contaminant metals as a trace component.

Particulate Organics

Particulate organic material in the West Fork sediments is present in various types of material and stages of decomposition. Most degraded organic material occurs as a brown-

colored organic “fluff” that settles from the water column and onto the sediment bed in areas where the flow of water is diminished. The abundance of finer grained organic colloids in the water column is probably limited as indicated by the low turbidity and TSS values associated with the West Fork waters. Previous investigators found that organic particulates were evenly distributed between different sized sediment fractions, and since contaminant metals seemed to display the same distribution patterns, they could be occurring as metal-organic complexes (Bolter et al., 1977). By contrast, Schmitt and Finger (1982) determined that only about 20 percent of the Pb and a minimal amount of Zn were associated with the organic fraction of sediments from the Black River.

Only a weak correlation was noted between TOC and contaminant metals contents (Figure 14). We also collected organic fluff material from the sediment bed at Sites A and D from the West Fork in order to further evaluate the role of organic particulates in transporting contaminant metals. These two sites represent samples located upstream and downstream, respectively, of mine effluent input points. Enrichment ratios for metals in the organic fluff (concentration at Site D/Site A) were highest for Pb, Ni, Zn and Mn (7.0, 6.2, 5.9, and 4.1 respectively), indicating that the organics are acting as adsorbents for metals. The corresponding enrichment ratio for contaminant metals in the -230 mesh Site D/Site A bulk sediment, however, exceeds the ratios observed for the organic fluff. For example, the -230 mesh sediment enrichment ratios at Site D/Site A for Pb, Ni, Zn and Mn were 7.8, 13.1, 7.6, and 8.5, respectively. If the metal transport was being dominated by organics, then the organic fraction should show the highest enrichment ratios. They generally do not. Only two elements show greater enrichment ratios in the organics relative to the bulk sediment; these being Cu (2.0 vs. 0.92) and Ag (1.6 vs. 0.5). Other metal adsorbents thus must be providing a greater contribution to the overall sediment metal inventory than the organic fluff.

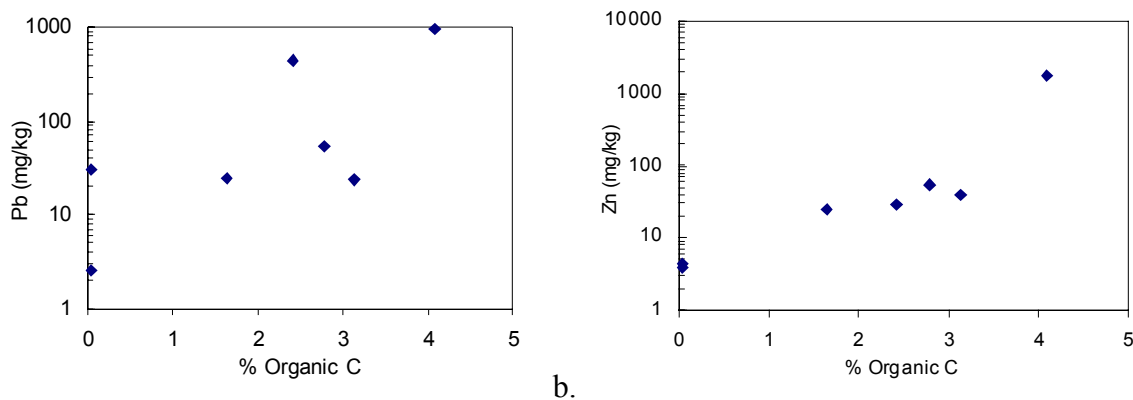


Figure 14. Correlation of lead and zinc with percent organic carbon in sediments from the West Fork; a) correlation between Pb and percent organic carbon, $n = 7$, $r^2 = 0.6640$, $p = 0.119$, b) correlation between Zn and percent organic carbon, $n = 7$, $r^2 = 0.6125$, $p = 0.144$.

Results from our sequentially extracted metal tests agree with the comparative metal distribution patterns observed in the bulk -230 mesh sediment and the organic fluff fractions. The concentration of most metals are dominated by the oxyhydroxide and/or residual fractions at points upstream of the mine tailings water input point on the West Fork. The only elements showing any notable variability are Cu with a 23% association with organics; Pb with a 11%

organic association; Cd, Ba, and Mn with a 19-32% association with carbonates; and Cd with a 11% exchangeable component. Downstream of the tailings input points there is a significant enrichment of metals in the oxyhydroxide and carbonate fractions for many metals, while the organic fraction displays minor percentage increases in contained Zn and Cd. Overall metal distribution patterns are in agreement with the trends reported by Schmitt and Finger (1982), while they conflict with the findings of Bolter (1977).

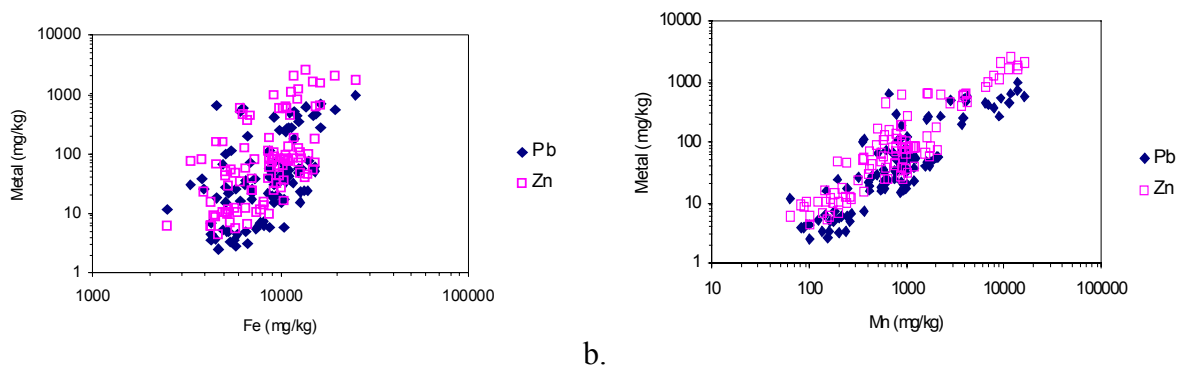
Dissolved Organic Carbon (<0.45 μm filtered; DOC) determinations from the January 2005 Big River flood event revealed an increase in DOC values increased during flood rise, then a decrease as flood waters were receding. The increase during flood rise probably reflects flushing of organic material into the river from the surrounding forest soils. The subsequent decrease in TOC values is attributed to a shifting of flood water contributions from deeply circulating groundwater on the tail end of the flood event. Total carbon concentrations also decreased over the entire course of the flood event, reflecting dilution of the river waters by the recent meteoric water input. Arsenic displayed only a weak association to TOC with a correlation coefficient value of 0.47. All remaining contaminant metals displayed even weaker correlations to DOC.

Clays

Both the exchangeable interlayer and relatively inert octahedral sites in the clay minerals represent a possible sink for contaminant metals in sediments. Clays were not detected during XRD analyses of the -230 mesh sediment fraction from either the West Fork or Big River systems, despite attempts to concentrate them for analysis. The XRD identification technique is relatively insensitive to detecting small quantities of minerals (<5%), however, thus the failure to detect clay mineral peaks by XRD analysis suggests that the clay mineral content in the sediments was probably minor rather than being truly being absent. Maximum Al concentrations in the -230 mesh Big River and West Fork sediments were 1.06 and 1.37 wt. %, respectively. These Al concentrations would correlate to a 5-7% weight fraction of clay minerals, assuming that the clays were either kaolinite or illite and assuming the entire inventory of Al in the sediments was incorporated into clays. Al correlations with most contaminant metals in the sediments were generally poor at locations close to the Elvins tailings pile (Table 3), but improved notably in far field areas of the Big River. Cadmium displayed the highest percentage association with the exchangeable fraction in the sequential extraction tests, suggesting that a significant proportion of the Cd may be associated with the clay minerals.

Mn and Fe oxyhydroxide

West Fork sediments were notably darker in color as they pass input points for mine effluent water (Figure 3). Increasing manganese concentrations can be correlated with this change (Figures 7 and 8), while SEM and sequentially extracted metal fraction analysis indicates that contaminant metals are being incorporated in the Mn- and Fe-oxyhydroxide fractions. Correlation coefficients are high for both Pb-Mn ($r^2 = 0.830$) and Zn-Mn ($r^2 = 0.943$) and moderate for the Pb-Fe ($r^2 = 0.513$) and Zn-Fe ($r^2 = 0.557$) pairings in bed load sediments of the West Fork (Figure 15). Similar associations have been noted in other contaminated water systems (O'Reilly, 2002).



a. b.

Figure 15. Elemental correlations for sediments from the West Fork – Black River. a) Iron correlations with Pb and Zn, calculated r^2 values are Pb-Fe 0.513, Zn-Fe 0.557, b) Manganese correlations with Pb and Zn, calculated r^2 values are Pb-Mn 0.830, Zn-Mn 0.943. All correlation coefficient calculations were determined to be significant ($p < 0.001$).

In order to more fully assess the near field transport behavior of metals, we ran a series of batch adsorption tests where mine effluent water was allowed to equilibrate with and without the presence of organic particles. Results from these tests show that many of the contaminant metals in a $< 0.45 \mu\text{m}$ filtered solution were closely coupled to Mn. As the Mn concentrations fell, the concentration of Pb, Co, Ni and Zn also fell in unison (Figures 9a and b). Iron did not display the same control on contaminant metals, with the difference believed to be related to Eh-pH changes affecting the mine effluent waters. Since the effluent waters were in a state of disequilibrium with their surroundings as they were emitted from the tailings piles, their pH and Eh values should both rise as CO_2 is lost and O_2 is absorbed into solution. The measured pH and Eh values of the tailings water was 8.33 and -54 mV, respectively. These values would plot on a standard pH-Eh plot at a position above the $\text{Fe}^{2+} - \text{Fe}(\text{OH})_3$ but below the $\text{Mn}^{2+} - \text{MnO}_2$ equilibrium lines. Any increase in Eh and/or pH values would thus not alter the oxidation state of Fe (and hence its solubility), but Mn concentrations may be lowered if they evolve from a 2+ to a 4+ valence state and precipitate from solution as solid Mn-oxyhydroxide particles.

Manganese concentrations initially decreased at a more rapid rate when particulate organic material was added to the batch reaction vessels (relative to the blank tests; Figure 9c). After 16 hours the trend was reversed, as Mn concentrations began to increase. They eventually reached a concentration that was higher than the original starting test solution. Colloidal particles present in the tailings water leachant were likely being dissolved and represent the source of the excess Mn. The increase was transient however, peaking after 48 hours, and then declining again except for a temporary reversal with the 348 hour sample. The initial decrease in Mn concentration during the first 16 hours is believed to result from the oxidation and conversion of Mn^{2+} into Mn^{4+} ions. The increase in Mn between 16 and 48 hours likely resulted from the reduction of the Eh and/or pH values in response to the presence of the organics, and the associated dissolution of solid Mn oxyhydroxide phases. The pH variability between the control test and the test with organics was 8.1 versus 7.3, while the corresponding Eh change was -82 mV for the control test and -37 mV for the test with the organics. It thus appears that the increasing acidity was responsible for the increasing solubility of Mn between 16 and 48 hours. The decreasing Mn concentrations observed after 48 hours may result from adsorption of Mn^{2+} ions onto the organic particles or the re-oxidation of manganese to Mn^{4+} as a result of the

interaction of the test solution with the progressive growth in the air-filled head space in the test vessels as solution aliquots were removed.

Concentrations of the various contaminant metals evolved in parallel manner to the Mn trends throughout both the control and organic batch adsorption tests. Lead, Zn, Ni, and Co were all relatively low in the initial stages of tests when organic particles were present (Figures 9b and d), but increased as the Mn particles were dissolving from between 16 and 48 hours. The Ni and Zn concentrations exceeded levels in the starting solution with the source being dissolving Mn-colloids captured during the start of the tests. Lead displays a strong affinity for adsorption on the organics relative to other metals (Figures 9b and d). Lead concentrations also did not increase after 16 hours like the other metals, but rather the increase was delayed until the 24 hour test. The Pb increase, and that of the other contaminant metals was only temporary, with concentrations decreasing again by the time the 96 hour samples were collected.

Metals being adsorbed onto river particulate material may become fractionated from each other as a function of transport distance if the metals display different solubility limits or if adsorbing phases have a significant density contrast. In the Big River, Zn contents tend to be diminished with increasing transport distance downstream, while Pb levels displayed the opposite trend, often increasing with downstream transport. This was true for both normal flow and flood conditions. A similar pattern was also noted following the disturbance event in the West Fork (Figure 8). The differences between the transport behavior of Pb and Zn, suggest that the former has a greater affinity to be adsorbed onto low density solids (e.g., clays and organics), while the latter may be more closely associated with a higher density phase(s) and thus may be more rapidly removed from the water column by particle adsorption and settling processes.

Correlation coefficients have been calculated for the remaining contaminant metals with respect their potential transport hosts containing Fe, Mn, or Al in the Big River System (Table 3). For the Elvins tributary system, correlation coefficients were weak for most metals. Lead displays the strongest correlation with Mn; Cu with Al; and Zn, Cd, Ni, and Co with Fe. Most correlation coefficient values increase from the near-field to far-field settings in the Big River system. Lead, Zn, Ni, and Co display the highest correlation coefficients while Cd, Cu, and Ba show weaker correlations with Mn, Fe, and Al. Neither the Mn, Fe, nor Al phases appear to display any distinctly superior ability to correlate to the contaminant metals relative to one another. Correlation coefficient data displayed an important change, however, when the January 2005 flood waters were evaluated. During this event, the strongest correlations were observed between Fe and the contaminant metals, with Al being intermediate, and Mn correlations being lowest. The high correlations noted for Fe during flood stage on the Big River contrast with the high correlations noted for Mn for the proximal sites of the West Fork. Scouring of buried sediment with higher Fe-contaminant metal associations is believed to be responsible for this change. The different associations between surficial and buried sediments are hypothesized to result from redox variations and their potential effect on the stability of Mn- *versus* Fe-oxyhydroxide phases.

Table 3. Correlation Coefficients for Metals and Organics in Big River Water Column

Element Pair	Tributary Sites			Big River					Combined Sites Big River
	Elvins Pile	Eaton Creek	Flat River	Highway 67	Saint Francois	Wash. Park	Highway Y	Byrnsville	January 2005 Flood
Fe-Mn	0.54	0.63	0.96	0.68	0.64	0.96	0.99	0.98	0.61
Fe-Al	0.19	-0.02	0.90	0.98	0.99	0.99	1.00	1.00	0.99
Mn-Al	0.70	-0.39	0.91	0.92	0.93	0.94	0.98	0.97	0.55
Fe-Pb	0.51	0.30	0.93	0.96	0.99	0.94	0.98	0.99	0.91
Fe-Zn	0.69	0.67	0.09	0.45	0.66	0.96	0.97	0.79	0.80
Fe-Cd	0.64	0.69	0.25	0.55	0.44	0.71	0.60	0.25	0.68
Fe-Cu	0.04	0.54	0.75	0.68	0.59	0.15	0.98	0.66	0.85
Fe-Ni	0.79	0.73	0.04	0.17	0.55	0.88	0.84	0.88	0.94
Fe-Co	0.65	0.74	0.13	0.92	0.94	0.88	0.99	0.97	0.97
Fe-Ba	0.36	0.22	0.37	0.53	0.34	0.67	0.71	0.16	0.77
Fe-As	-0.38	0.08	0.44	0.53	0.57	0.58	0.80	0.73	0.77
Mn-Pb	0.89	-0.16	0.96	0.67	0.77	0.96	0.98	0.93	0.61
Mn-Zn	0.48	0.91	0.09	0.29	0.56	0.94	0.96	0.80	0.66
Mn-Cd	0.44	0.84	0.15	0.34	0.30	0.75	0.85	0.57	0.64
Mn-Cu	0.66	0.52	0.80	0.46	0.33	0.15	0.97	0.65	0.53
Mn-Ni	0.34	0.84	-0.01	0.09	0.28	0.83	0.85	0.86	0.56
Mn-Co	0.30	0.98	0.12	0.64	0.63	0.87	0.99	0.99	0.65
Mn-Ba	0.13	0.14	0.33	0.25	0.13	0.70	0.74	0.26	0.39
Mn-As	-0.02	-0.30	0.46	0.46	0.51	0.50	0.77	0.73	0.54
Al-Pb	0.71	0.84	0.89	0.95	0.97	0.93	0.97	0.89	0.86
Al-Zn	0.19	-0.38	-0.24	0.30	0.61	0.95	0.96	0.77	0.75
Al-Cd	0.08	-0.30	-0.22	0.39	0.25	0.65	0.81	0.43	0.60
Al-Cu	0.92	0.39	0.80	0.74	0.57	0.11	0.97	0.63	0.80
Al-Ni	-0.25	-0.43	-0.34	0.05	0.50	0.86	0.82	0.89	0.92
Al-Co	-0.04	-0.41	-0.20	0.86	0.91	0.84	0.98	0.96	0.93
Al-Ba	0.31	-0.53	0.02	0.44	0.20	0.61	0.71	0.09	0.74
Al-As	0.03	0.77	0.60	0.57	0.58	0.59	0.80	0.70	0.75
Fe-DOC									-0.37
Mn-DOC									-0.68
Al-DOC									-0.29
DOC-Pb									-0.50
DOC-Zn									-0.56
DOC-Cd									-0.58
DOC-Cu									0.09
DOC-Ni									-0.24
DOC-Co									-0.62
DOC-Ba									0.06
DOC-As									0.47

A comparison of the overall batch adsorption, sequential extraction, and analysis of river sediment material reveals a transient nature for the transport of metal contaminants in the West Fork and Big River systems. Initial release of Pb, Zn, and other metals within the tailings piles occurs as dissolved ions in an acidified aqueous solution. Neutralization of acidic waters occurs quickly within the tailings piles through reactions with the dolomite host rock, resulting in metal precipitation. Continued chemical changes occur as the tailings effluent waters lose dissolved CO₂ or incorporate O₂ from the atmosphere. Contaminant metals may be incorporated into newly formed Mn-oxyhydroxide or carbonate phases. As the mine effluent water and sediments move into the main river channels they will undergo further chemical changes associated with metal dilution processes. Previously formed solid phases may dissolve under the influence of either lower concentration river water or lower Eh-pH pore waters in contact with buried river sediments. Metals may thus be re-released back into solution and then adsorbed onto new phases. Organic particles and Fe-oxyhydroxides are more abundant in the river system and thus may play an increasingly more important role in the adsorption process.

Sulfides

Panned sediment concentrates of heavy minerals were collected from both the West Fork and Big Rivers in order to assess the mineral composition, sulfide phase survivability, and locations for metal adsorption in these river systems. Metal sulfide grains were not recovered in sediments of the West Fork. Direct transfer of sulfide particles into the West Fork by erosion processes thus does not appear to be taking place to any notable degree. The presence of sulfide minerals in the Big River sediments is one of the major differences noted in sediments from rivers draining the New and Old Lead Belts. The Desloge Tailings Pile on the Big River was the site of a catastrophic overflow of a retaining dam wall in 1977, when 450,000 ft³ of tailings piles were released directly into the Big River. In addition to this event, continuous erosion of tailings pile material by headwater seep and wind erosion has been observed from several tailings piles in the district. Sulfide minerals have been identified as part of the bed load sediment at sites downstream from mine tailings on the Big River and are believed to be largely responsible for the higher metal contents of these sediments. Galena and sphalerite have been found at distances of up to eight nautical miles from the tailings piles, defining the region of influence these phases may directly affect the distribution patterns of metals. Although the concentration of total sulfide particles decreases with transport distance, galena appears to become relatively more predominant, indicating that it has the highest survivability rate of all sulfides present. Pyrite is restricted to locations only a short distance from the tailings piles indicating that it is least resistance to weathering effects. The rapid attrition rate of pyrite reflects a higher chemical dissolution rate, as its relatively high mineral hardness value (H=6) should make it resistant to physical abrasion effects during transport. High galena/sphalerite ratios in the sediments and high dissolved Zn concentrations in the fluids emanating from the Elvins tailings pile also indicate that sphalerite dissolution is also occurring faster than galena.

Flood Effects on Contaminant Metal Transport

Water turbidity and TSS values increase dramatically during flooding in both the West Fork and Big Rivers. Metal bearing particles can easily be suspended in the water column during flooding and contribute to the overall metal transport process. For the West Fork system, Pb concentrations at control Site A were elevated during periods of high water flow to a point where they were high enough to mask any metal input from the West Fork Mine tailings water

(Figure 7). One sample collected during a period of flood rise had an unfiltered Pb concentration of 65.5 µg/L. This was the highest Pb concentration detected on the West Fork. Corresponding concentrations in the 5.0, 0.45, and 0.02 µm filtered fractions from this same sample were 36.8, 30.4, and 4.7 µg/L, respectively. Concentrations of Zn at Sites A and D increased during low and moderate flow events, but then decreased again during a period of high flow (2/03). The lowering concentration of Zn during the high flow period likely resulted from dilution by meteoric water input.

Our sampling during the West Fork disturbance event resulted in the collection of suspended sediments which normally would have only been moved into the water column by scouring events associated with a high flood stage condition. This river bed disturbance thus allowed us to examine potential effects associated with a flooding, but without the dilution effects related to increased meteoric water input into the river system. High Pb concentrations were detected at the control Site A during the disturbance, and these Pb levels remained elevated throughout the sampling reach of Sites A through F (Figure 8). The elevated Pb contents were also high enough to mask the contribution from the mine effluent waters at Sites D and E. Zinc concentrations were also elevated at control Site A following the disturbance event, but quickly dropped off by the time they reached Site C. Zinc contents increased again below the mining effluent input at Site D due to the contribution of the tailings water. The differences between Pb and Zn behavior suggest that at least a portion of the Pb transport is more closely associated with low-density organic or clay particles that easily remain suspended in the water column. Alternatively, Zn transport is controlled by particles that more rapidly settle from the water column.

The Big River was sampled once during a moderate (March 2002) and major flood event (January 2005). The latter flood stage sampling included repeat collections at some sites for three different over a three day period. The proportion of suspended particulate material and associated metal loads increased dramatically during flooding. The maximum total metal concentration (in µg/L) from the Big River channel unfiltered water samples and percent metal associated with greater than 0.45 µm particles collected during the March 2002 flood were: Pb-286-98%; Zn-227-92%; Cd-4.05-90%; Cu-17.7-85%; Ni-11.4-85%; Co-11.0-94%; Ba-317-67%; Fe-6152-92%; Mn-892-97%; and Al-6227-87%. Both the bulk metal concentrations and the proportion metals contained in sedimentary particles were even higher during the January 2005 flood where the distribution pattern for metals was Pb-560-99.4%; Zn-197-95%; Cd-2.81-84%; Cu-16.5-87%; Ni-10.7-82%; Co-6.46-98%; Ba-747-77%; Fe-8268-99.2%; Mn-520-99.7%; Al-10,797-99.8%. Such a trend is consistent with the erosion of contaminant metal laden river bed (or soil) material in the river and turbulent suspension of these particles. Dissolved Organic Carbon determinations from this latter event initially rose and then fell in unison with the flood waters. The contaminant metals displayed only weak correlations to the DOC contents (Table 3). Barium and Cd contents increased only slightly during flooding, yet the particulate fraction displayed a disproportionately large increase relative to the total metal variation. Overall Ni concentrations even decreased during flooding, and still the proportion of Ni contained on >0.45 µm particles increased. The trend for these latter three metals suggests that they may be scavenged by sedimentary particles that are suspended into the water column during flooding.

Conclusions

- High metal concentrations occur in tailings effluent waters, with many metals being supersaturated with respect to their respective carbonate mineral phases at the near-neutral pH values of the water. Acidic waters must be generated within the tailings piles as this is the only satisfactory explanation for the origin of the high metal contents. Acid neutralization occurs by reaction with dolomite in the tailings piles.
- Contaminant metals in tailings pile waters are transported in both soluble and colloidal forms. Metals are transferred from the former to the latter with increasing transport distance and time.
- Both Fe and Mn occur naturally in discrete oxyhydroxide particles and coatings. Mn/Fe ratios increase in the sediments as they pass the mine tailings piles. In the West Fork system, Pb and Zn display the strongest affinity for Mn-oxyhydroxide phases close to the tailings piles. An affinity for Fe-oxyhydroxides is also evident.
- Mn, Fe, and Al all display high correlations with contaminant metals in more distal locations. The correlation with Fe is enhanced when flood waters were evaluated from the Big River.
- Transfer of metal contaminants occurs between the soluble load and particulate host phases as the metal-bearing waters move between the tailings piles, tailings outflow streams, and the main river channels. Changes in water chemistry (CO₂ loss, O₂ absorption, pH, Eh) and flooding affect these changes.
- Most contaminant metals display only weak correlations with DOC when bulk sediment or water column samples are analyzed. Lead appears to be more easily suspended in the water column and remains in the water column for longer transport distances than Zn. A higher portion of Pb is associating with low-density particulate organics. By contrast, Zn displays a stronger association with Mn and Fe, and settles out from the water column more quickly than Pb.
- Sulfide minerals containing Pb, Zn, and Fe and other metals have been recovered from the bed load sediment material in the Big River at sites up to eight nautical miles from the tailings piles. Resistance to combined mechanical and chemical changes for the three most common sulfide phases occur in the order: galena>sphalerite>pyrite. The survivability of these phases influences metal transport properties. Sulfides were not found in sediments from the West Fork.
- Lower metal concentrations are also associated with the New Lead Belt (West Fork – Black River) drainage systems relative to the Old Lead Belt (Big River). The difference reflects the improved metallurgical processing and environmental practices employed in the New Lead Belt.
- Increases in Pb and Zn concentrations in sediments of Clearwater Lake suggest a doubling of the metal flux following the initiation of mining activities in the New Lead Belt. Lead isotopic analyses indicate that the excess lead is derived from ore minerals (galena). The delivery mechanism for these metals is not as clear. They may be derived from Pb in tailings pile effluent water, wind blown tailings particles, dusts from lead-zinc smelters, or enhanced erosion of a Pb-enriched soil residuum from the New Lead Belt vicinity.

Literature Cited

- ASARCO Inc. (1996) West Fork Fact Sheet. <http://www.asarco.com/factsheets/westfork.html>
Assessed 3/23/04.
- Bolter, E., Gale, N.L., Hemphill, D.D., Jennett, C.J., Koirtyohann, S.R., Pierce, J.O., Lowsley, I.H. Jr., Tranter, W.H., and Wixon, B.G. (1977) The Missouri Lead Study—An Interdisciplinary Investigation of Environmental Pollution by Lead and Other Heavy Metals from Industrial Development in the New Lead Belt of Southeastern MO—Final Report to the National Science Foundation Research Applied to National Needs, User Agencies and Industries for the Period 5/72 to 5/77.
- Dzomback, D.A., and Morel, F.M.M., (1990) Surface Complexation Modeling. Wiley, NY.
- Faure, G., (1998) Principals and Applications of Geochemistry. 2nd Edition. Prentice Hall, NJ.
- Goldhaber, M.B., Church, S.E., Doe, B.R., Aleinikoff, J.N., Brannon, J.C., Podosek, F.A., Mosier, E.L., Taylor, C.D., and Gent, C.A. (1995) Lead and Sulfur Isotope Investigation of Paleozoic Sedimentary Rocks from the Southern Midcontinent of the United States; Implications for Paleohydrology and Ore Genesis of the Southeast Missouri Lead Belts. *Economic Geology*, v. 90:1875-1910.
- Krizanich, G.W., and Wronkiewicz, D.J. (2005) Trace Element and Isotopic Trends in Sediment Cores from Clearwater Lake, Southeast Missouri, *Geol. Soc. Amer. 2005 Annual Fall Meeting*, abstract, Salt Lake, UT.
- O'Reilly, S.E. (2002) Lead Sorption Efficiencies of Natural and Synthetic Mn and Fe-oxides. Doctoral Dissertation. Virginia Polytechnic Institute and State University.
- Petersen, J.C., Adamski, J.C., Davis, J.V., Femmer, S.R., Freiwald, D.A., and Joseph, R.L. (1998) Water Quality in the Ozark Plateaus, Arkansas, Kansas, Missouri, and Oklahoma, 1992-95. U.S. Geological Survey Circular 1158 <http://water.usgs.gov/pubs/circ1158>. Accessed 3/02/04.
- Runnells, D.D., Dupon, D.P., Jones, R.L., and Cline, D.J. (1997) Determination of Natural Background Concentrations in Water at Mining, Milling, and Smelting Sites. *Proceedings of the Fourth International Conference on Tailings and Mine Waste '97*, Fort Collins, CO, USA, A.A. Balkema, Rotterdam.
- Schmitt, C. J., and Finger, S. E. (1982) The Dynamics of Metals from Past and Present Mining Activities in the Big and Black River Watersheds, Southeastern Missouri, U.S. Fish and Wildlife Service Final Report for the U.S. Army Corps of Engineers. Columbia National Fisheries Research Laboratory, Columbia, MO.
- Smith, B.J., and Schumacher, J.G. (1991) Hydrochemical and Sediment Data for the Old Lead Belt, Southeastern Missouri: 1988-89, U.S. Geological Survey Open-File Report 91-211.
- Warner, B., and Rickmar, M. (1970) St. Joe Headframe. The History of St. Joe Lead Company; St. Joe Minerals Corporation, Bonne Terre, MO; Special Edition, Fall 1970. http://www.rootsweb.com/~mostfran/mine_history/stjoe_history.htm Accessed 4/9/04.
- Wharton, H.M., Larsen, K.G., Sweeny, P.H., Harrison, E., Bradly, M., Davis, J.H., Rogers, R.K., Brown, W.J., Paarlberg, N.L., Evans, L.L., Mouat, M.M., and Clendenin, C.W. Jr. (1975) Missouri Geological Survey and Water Resources Report of Investigation #58, Guidebook to the Geology and Ore Deposits of Selected Mines in the Viburnum Trend, Missouri. Missouri Department of Natural Resources.

A Test of the Biotic Ligand Model: Fish Exposed to Time-varying Concentrations of Copper and Zinc

Joseph S. Meyer
Department of Zoology and Physiology
University of Wyoming
Laramie, WY 82071-3166

Annual Report prepared for:
Center for the Study of the Bioavailability of Metals in the Environment

Introduction

The biotic ligand model (BLM) of the acute toxicity of metals to aquatic organisms provides a useful tool for regulating aqueous discharges of metals (Di Toro et al. 2001, Paquin et al. 2002). Although the BLM is based on data from toxicity tests conducted under constant-exposure conditions (Santore et al. 2001), concentrations of metals and routine water quality parameters often vary temporally in the real-world (e.g., Nimick et al. 2003, Morris et al. 2005). Therefore, to more realistically mimic real-world situations, time-variable exposures might have to be incorporated into a unit world model and/or into site-specific analyses of metals.

In concept, the BLM is designed to account for variations in concentrations of total metal and free metal ions by accounting for variations in the amount of metal accumulated at the biotic ligand of an organism over time (Di Toro et al. 2001, Paquin et al. 2002). However, appropriate experiments are needed to test this concept. Therefore, a major objective of this research project was to conduct acute toxicity tests with fathead minnow (FHM -- *Pimephales promelas*) larvae exposed to Cu or Zn in time-variable water quality and then compare those results to predictions using a model of time-variable toxicity (e.g., Meyer et al. 1995) modified to incorporate the BLM-predicted amount of Cu or Zn accumulated on the FHM biotic ligand. We chose Cu and Zn as model divalent cationic metals because considerable background information is available about those two metals, and their physiological modes of toxicity to fish differ. Copper disrupts Na homeostasis, whereas Zn disrupts Ca homeostasis (Paquin et al. 2002).

Before we could use a model of toxicity for time-variable water quality conditions, we needed reliable Cu and Zn BLMs for FHM. Although a reliable Cu BLM has been available for several years (Santore et al. 2001) and is being incorporated into an upcoming revision of the U.S. Environmental Protection Agency's water quality criteria for Cu (USEPA 2003), only a preliminary Zn BLM (Santore et al. 2002) was available when the current research project was initiated. That preliminary Zn BLM had been parameterized for FHM solely using information published until 2000, and the available studies did not include tests of the protective effects of specific major cations (Ca^{2+} , Mg^{2+} , Na^{+} and K^{+}) and dissolved organic matter (DOM) against Zn toxicity to FHM. We performed toxicity tests with preliminary funding and with Year 1 funding for this project to help refine the parameterization of the Zn BLM. Those results are reported in the Year 1 progress report for this research project (Meyer et al. 2004) and in Bringolf et al. (2006).

In this report, we present results of acute toxicity tests in which we exposed larval FHM to constant or time-varying (i.e., pulsed) concentrations of Cu at various combinations of pH, water hardness and DOM concentration. We used the continuous-exposure data in constant water-quality conditions to calibrate the Cu BLM for our fish and to parameterize a one-compartment uptake-depuration (OCUD) model for predicting the toxicity of Cu during the time-variable exposures. We hypothesized that only an OCUD model linked to the BLM-calculated concentration of Cu bound to the FHM biotic ligand (as opposed to using a dissolved species of Cu) could accurately predict the acute toxicity of Cu to FHM in time-variable exposures under a variety of water quality conditions. To test that hypothesis, we compared the Cu LA50s (median lethal accumulations) predicted by our OCUD model to the observed Cu LA50s in the continuous- and pulsed-exposure tests. Because of funding limitations, we did not have enough resources to conduct similar toxicity tests and develop a linked BLM-OCUD model for Zn.

Methods

Toxicity Tests

To calibrate the BLM to our fish (i.e., to be able to calculate the concentration of Cu bound to the FHM biotic ligand at exposure times ranging from 1 to 96 h), we conducted a series of 96-h continuous-exposure, static-renewal toxicity tests in which we exposed FHM larvae to Cu at pH 6, 7 or 8 and at a water hardness of 0.5 (pH 7 only) or 2.0 mEq/L (pH 6, 7 and 8) with no dissolved organic matter (DOM) added. Additionally, we conducted a continuous-exposure toxicity test at pH 7 and 2.0 mEq/L hardness in the presence of DOM isolated from the Suwannee River, Georgia, USA (at 20 mg DOC/L). Then to test the predictions of the OCUD model that we fitted to the continuous-exposure data (see Models section below), we conducted a series of 72-h pulse-exposure toxicity tests in which we exposed larval FHM to Cu in the presence or absence of Suwannee River DOM at the same combinations of pH and water hardness as we used in the continuous-exposure tests. We conducted 72-h exposures instead of 96-h exposures for the pulse-exposure tests to conserve staff time and costs, because preliminary trials indicated that pulse Cu LC50s usually approach an asymptote at exposure times ≥ 72 h. The dates and exposure conditions of all continuous- and pulse-exposure toxicity tests included in this report are listed in Table 1.

Table 1. Dates and exposure conditions of continuous- and pulse-exposure toxicity tests conducted with fathead minnow (*Pimephales promelas*) larvae exposed to Cu

Start date	Nominal pH	Nominal hardness (mEq/L)	Nominal DOC (mg/L)	Duration (h)	Type of exposure	Daily time exposed to Cu (h)	Daily time in clean water (h)	Exposure times at which LC50s could be calculated (h)
7/26/04	7	25	0	96	Continuous	24	0	1,2,4,8,24,48,72,96
8/2/04	7	25	0	72	Pulse	2	22	24,48,72
8/2/04	7	25	0	72	Pulse	8	16	24,48,72
8/9/04	7	100	0	96	Continuous	24	0	1,2,4,8,24,48,72,96
4/19/05	7	100	0	72	Continuous	24	0	24,48,72
4/26/05	7	100	0	72	Pulse	8	16	24,48,72
4/26/05	7	100	0	72	Pulse	2	22	24,48,72
5/10/05	7	100	0	72	Pulse	8	16	24,48,72
5/10/05	7	100	20	72	Pulse	8	16	24,48,72
5/17/05	7	100	0	72	Pulse	2	22	24,48,72
5/17/05	7	100	20	72	Pulse	2	22	24,48,72
5/25/05	7	100	0	72	Continuous	24	0	24,48,72
5/25/05	7	100	20	72	Continuous	24	0	24,48,72
10/24/05	7	100	0	72	Continuous	24	0	24,48,72
11/9/05	8	100	0	96	Continuous	24	0	8,24,48,72,96
11/22/05	7	100	0	96	Continuous	24	0	1,2,4,8,24,48,72,96
11/29/05	6	100	0	96	Continuous	24	0	2,4,8,48,72,96
1/4/06	6	100	0	96	Continuous	24	0	2,4,8,24,48,72,96
1/24/06	6	100	0	72	Pulse	2	22	24,48,72
1/25/06	6	100	20	72	Pulse	2	22	24,48,72
1/18/06	6	100	0	72	Pulse	8	16	24,48,72
1/18/06	6	100	20	72	Pulse	8	16	24,48,72

In the pulse-exposure tests, we exposed the fish to either (1) Cu for 2 h followed by “recovery” in uncontaminated dilution water for the remaining 22 h of each 24-h pulse-and-recovery cycle (i.e., a 2-h pulse of Cu) or (2) Cu for 8 h followed by “recovery” in uncontaminated dilution water for the remaining 16 h of each 24-h pulse-and-recovery cycle

(i.e., an 8-h pulse of Cu). We performed all continuous-exposure toxicity tests according to standard procedures (ASTM 1993, USEPA 2002), with transfer of the fish into renewal water every 24 h. We followed the same standard procedures for the pulse-exposure tests, except on each day in the pulse-exposure tests we transferred the FHM from Cu-contaminated water to uncontaminated dilution water at the end of the pulse-exposure period (either 2 or 8 h) and from uncontaminated dilution water back into Cu-contaminated water at the beginning of the next day. This manual transfer from Cu-contaminated water to uncontaminated water (and vice versa) produced square-wave pulse exposures (*sensu* Wang and Hanson 1985, Meyer et al. 1995).

The dilution water in all toxicity tests was a mixture of well water and reverse-osmosis(RO)-treated/deionized water at 0.5 or 2.0 mEq/L hardness, with the following nominal water quality before pH adjustment: 25°C, pH 7.0, alkalinity of 0.1 mEq/L, and dissolved organic carbon (DOC) concentration of ≤ 0.5 mg/L. The Suwannee River DOM was isolated in June 1999 using a commercial RO unit (RealSoft, Norcross, Georgia, USA) with pre-treatment of the river water through a column containing H⁺-saturated cation-exchange resin. We filtered the refrigerated DOM stock solution through a 0.4- μ m polycarbonate membrane (Millipore) before using the DOM in toxicity tests.

For all of the tests, we used ≤ 24 -h-old FHM larvae produced by stock populations of adult FHM maintained at the University of Wyoming. Different stock populations of FHM were used during the three testing periods (July-August 2004, April-May 2005, and October 2005 - January 2006). Each FHM brood stock was reared in well water (pH 8, alkalinity and hardness of 4 mEq/L, and DOC concentration of ≤ 0.5 mg/L), but each batch of FHM eggs was hatched in the dilution water in which they were tested. To avoid complications associated with the sorption of metals onto food, we did not feed the larvae.

Physical and Chemical Analyses

Extensive water quality analyses, including temperature (by hand-held thermometer), pH (by meter), dissolved oxygen (by meter), alkalinity (by titration), major inorganic anions (by ion chromatography), major inorganic cations (by flame atomic absorption spectrophotometry), DOC concentration (by combustion; 0.45- μ m filtered), and dissolved (0.45- μ m filtered) and total Cu (by graphite furnace or flame atomic absorption spectrophotometry, depending on the concentration range used in each toxicity test), were conducted on all exposure waters in each test using standard methods (USEPA 1979, APHA et al. 1995). These analytical techniques are described in more detail in the UW QAPP for this research project.

For analyses of Cu, the major inorganic cations and anions, and DOC, we performed QA/QC analyses that included sample duplicates and spikes, initial and continuing verification standards, initial and continuing calibration blanks, and external QC samples. We reanalyzed all samples in any analytical run in which we did not obtain acceptable QA/QC results according to USEPA (1994) guidelines. The instrument detection limit for Cu was ~ 0.01 μ M.

Models

Biotic ligand model

We used Version 2.1.1 of the BLM (dated 3/26/04; available at <http://www.hydroqual.com/blm>) in speciation mode to calculate (1) the concentrations of the various species of dissolved Cu at the LC50 in each exposure water, and (2) the corresponding concentration of Cu bound to the biotic ligand of FHM (i.e., the $\Sigma\text{Cu-BL} = \text{Cu-BL} + \text{CuOH-BL}$, which equals the LA50 at the 50%-mortality exposure conditions). For each test, we entered

measured water chemistry values into the BLM. We did not run the BLM in toxicity mode to predict LC50s and LA50s because the 96-h Cu LC50s and LA50s in our continuous-exposure tests differed from the corresponding BLM-predicted Cu LC50s and LA50s (see Results and Discussion section), indicating that our FHM larvae were less sensitive than the default parameterization of the FHM Cu BLM predicted.

To modify the BLM to produce ln(LA50) vs. ln(time) curves that fit the OCUD model (i.e., an increasingly steeper negative slope as exposure time decreases; see next section), we altered the default log K values for Cu-BL, CuOH-BL, Ca-BL, Na-BL, and/or H-BL binding in the BLM file titled “Cu_Fathead_Minnow_04-03-26.DAT”.

One-Compartment Uptake-Depuration Models

Mancini (1983) proposed the following OCUD model (as modified by Meyer et al. 1995) for the acute toxicity of chemicals to aquatic organisms, based on the assumption that 50% mortality occurs when the chemical accumulates to a specified concentration in the internal compartment at which the toxic action occurs:

$$\frac{dC_{\text{soa}}}{dt} = k_u \cdot C_w^y - k_{\text{dep}} \cdot C_{\text{soa}} \quad (1)$$

where C_w = concentration of chemical in the exposure water (M), C_{soa} = concentration of chemical at the site of action (moles of chemical/g tissue), k_u = uptake rate constant (L/(g tissue·h)), k_{dep} = depuration rate constant (/h), t = exposure time (h), and y = a unitless fitting term. The LC50 at any exposure time is predicted to be (modified from Meyer et al. 1995):

$$\text{LC50} = \left[\frac{k_{\text{dep}}}{\frac{k_u}{C_{L,50}} \cdot (1 - e^{-k_{\text{dep}} \cdot t})} \right]^{1/y} \quad (2)$$

where $C_{L,50}$ = concentration of chemical at the site of action that causes 50% mortality (moles of chemical/g tissue). Unlike concentration×time toxicity models that do not consider depuration of a chemical (e.g., the dashed line in Fig. 1), an OCUD model (e.g., the solid curve in Fig. 1) predicts that initially the LC50 decreases rapidly as exposure time is increased (like a concentration×time model) but eventually a steady-state LC50 (the incipient lethal level -- C_{ILL}) is approached at long exposure times. That C_{ILL} equals $[k_{\text{dep}}/(k_u/C_{L,50})]^{1/y}$ (Meyer et al. 1995).

Although the OCUD model originally was developed for aqueous concentrations of chemicals, our objective was to test whether the BLM-predicted accumulations of Cu at the site of toxic action fit the OCUD model (i.e., whether they have the same type of shape as shown in Figure 1). In that case, the units for k_u are “/h” instead of “L/(g tissue·h)”.

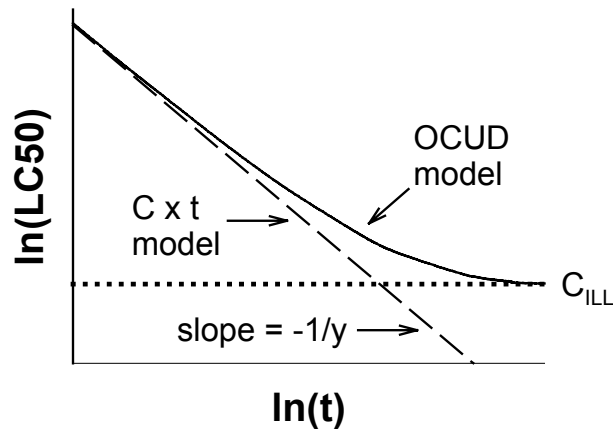


Figure 1. Comparison of one-compartment uptake-depuration (OCUD; Eqn. 2) and concentration×time ($C \times t$) models.

Although the OCUD model originally was developed for aqueous concentrations of If the OCUD model fits the continuous-exposure data, the following equation predicts the LC50 (or LA50) for square-wave pulse exposures (modified from Meyer et al. 1995):

$$LC50_{\text{pulse}} = \left[\frac{k_{\text{dep}} \cdot \left(1 - e^{-k_{\text{dep}} \cdot t_{\text{total}}}\right)}{\frac{k_u}{C_{L,50}} \cdot \left(1 - e^{-k_{\text{dep}} \cdot t_{\text{pulse}}}\right) \cdot \left(1 - e^{-N \cdot k_{\text{dep}} \cdot t_{\text{total}}}\right)} \right]^{1/y} \quad (3)$$

where N = number of pulse-and-recovery cycles (e.g., number of days in this study), t_{pulse} = duration of pulse exposure during one pulse-and-recovery cycle (e.g., 2 or 8 h in this study), t_{total} = duration of a pulse-and-recovery cycle (e.g., 24 h in this study), and $t_{\text{total}} - t_{\text{pulse}}$ = amount of time spent in uncontaminated water during one pulse-and-recovery cycle (e.g., 22 or 16 h in this study). Figure 2 in Meyer et al. (1995) graphically defines these pulse-exposure time periods.

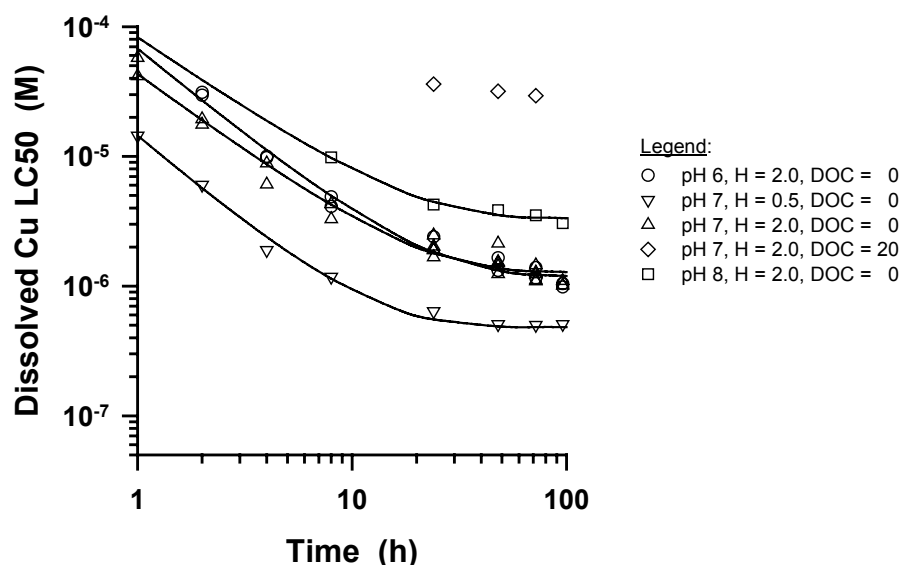


Figure 2. Fit of a one-compartment uptake-depuration model (OCUD model, Eqn. 2) to dissolved Cu LC50s for fathead minnow larvae in 96-h continuous-exposure tests conducted from July 2004 through January 2006. Nominal exposure conditions were: 25°C; either pH 6, 7 or 8 (with corresponding alkalinities of 0.02, 0.1 and 0.5 mEq/L); hardness (H) of 0.5 or 2.0 mEq/L; and dissolved organic carbon (DOC) concentration of 0 or 20 mg/L. The constants for the four OCUD curves are listed in Table 2. No LC50s were calculated for exposure times <8 h at pH 8 because some of the Cu precipitated in the high-concentration exposure waters. The LC50s at pH 7, H = 2.0 and DOC = 20 were not included in the regression for the combination of pH 7 and H = 2.0.

Table 2. Nonlinear-regression coefficients for a one-compartment uptake-depuration model (Eqn. 2) fitted to LC50s or LA50s in continuous-exposure toxicity tests conducted with fathead minnow (*Pimephales promelas*) larvae exposed to Cu^a

Form of Cu and endpoint ^a	Exposure conditions ^b	$k_u/C_{L,50}$	k_{dep} (/h)	y
Dissolved Cu LC50	pH 6, H = 2.0 mEq/L, DOC = 0 mg/L	1,095 L/(mol Cu·h)	0.05455	0.7261
	pH 7, H = 0.5 mEq/L, DOC = 0 mg/L	2,315 L/(mol Cu·h)	0.01004	0.6907
	pH 7, H = 2.0 mEq/L, DOC = 0 mg/L	3,355 L/(mol Cu·h)	0.05938	0.8106
	pH 8, H = 2.0 mEq/L, DOC = 0 mg/L	3,874 L/(mol Cu·h)	0.06186	0.8757
Σ Cu-BL LA50 ^c	All continuous-exposure tests ^d	0.02067 g tissue/(mol Cu·h)	0.02911	0.9805

^aLC50 = median lethal concentration, LA50 = medial lethal accumulation.

^bH = water hardness, DOC = dissolved organic carbon.

^cLA50 for the sum of Cu and CuOH bound to the FHM biotic ligand (BL). These regression coefficients only apply to Σ Cu-BL LA50s calculated with $\log K_{Cu-BL} = 7.4$, $\log K_{CuOH-BL} = -1.3$, $\log K_{Ca-BL} = 5.6$, $\log K_{H-BL} = 8.9$, and $\log K_{Na-BL} = 3.0$.

^dIncluding pH 7 test with 2.0 mEq/L water hardness and 20 mg DOC/L

Statistical Analyses

We calculated LC50s (median lethal concentrations) for the Cu toxicity tests using the maximum likelihood logit procedure or the trimmed Spearman-Kärber procedure (only when

partial mortality occurred in only one concentration or when the logit procedure did not converge) in TOXCALC Version 5.0 (Ives 1996). For pulse-exposure tests, the $LA50_{\text{pulse}}$ values were based on the Cu concentrations during the 2-h or 8-h pulse-exposure period (i.e., the LC50s were not based on average Cu concentrations time-weighted over the entire 24-h pulse-and-recovery cycle). To estimate $k_u/C_{L,50}$, k_{dep} and y , we fitted Equation 2 to LC50 or LA50 data from continuous-exposure toxicity tests using nonlinear regression in Version 10 of SPSS for Windows (SPSS Inc., Chicago, Illinois, USA). Because k_u and $C_{L,50}$ appear only in the term $k_u/C_{L,50}$ in Equation in 2, separate k_u and $C_{L,50}$ values cannot be estimated by this method..

Results and Discussion

Fitting the OCU D Model to the Continuous-Exposure LC50 Data

In 96-h continuous-exposure toxicity tests, LC50s for dissolved Cu (Figure 2) and Cu^{2+} (Figure 3) at each combination of pH, hardness and DOC concentration fit Equation 2 well. However, the observed 96-h LC50s and the corresponding LA50s were $2\times$ to $4\times$ higher than the corresponding 96-h LC50s and LAC50s calculated by the Cu BLM with its default parameterization for FHM. Therefore, we used the Cu BLM in speciation mode to calculate Cu^{2+} and $\text{Cu}^{2+} + \text{CuOH}^+$ LC50s and $\Sigma\text{Cu-BL}$ LA50s for our FHM, using the water chemistry and dissolved Cu concentrations at 50% mortality in our toxicity tests (see Methods section).

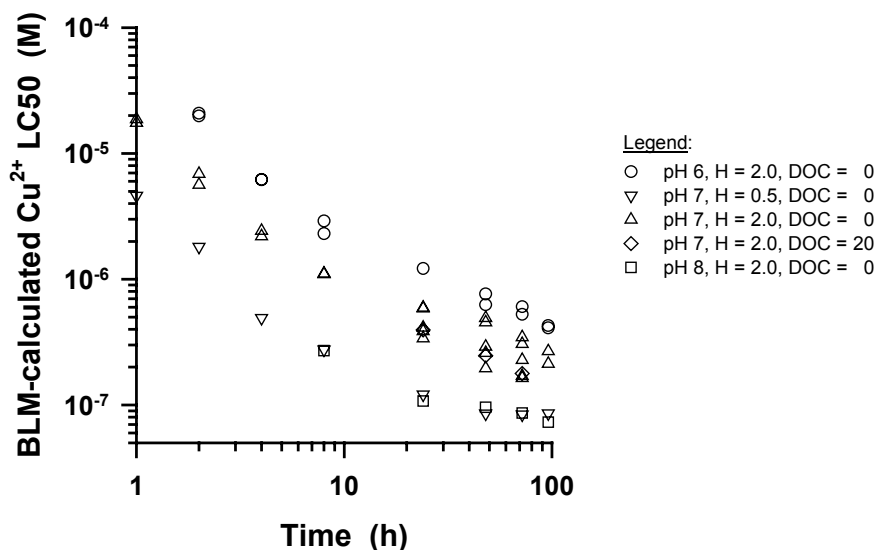


Figure 3. BLM-calculated Cu^{2+} LC50s for fathead minnow larvae in 96-h continuous-exposure tests conducted from July 2004 through January 2006 (same tests as plotted in Figure 2). Nominal exposure conditions are listed in the caption for Figure 2. No LC50s were calculated for exposure times <8 h at pH 8 because some of the Cu precipitated in the high-concentration exposure waters.

As expected, the locations of the curves for each combination of pH, water hardness and DOC concentration differed because neither dissolved Cu concentration nor Cu^{2+} concentration alone is a good predictor of the acute toxicity of Cu to aquatic organisms when water hardness or pH is varied (Meyer et al. 1999, Santore et al. 2001, Meyer et al. 2002). Therefore, one would

need to know the equation for each separate combination of pH and water hardness of interest to accurately predict (1) continuous-exposure LC50s at untested exposure times, and/or (2) pulse-exposure LC50s across a wide range of combinations of pH and water hardness.

Reassuringly, all the dissolved Cu LC50s at pH 7, 2.0 mEq/L hardness and 0 mg DOC/L and at the same exposure times were similar (Figure 2), suggesting similar sensitivity of the three separate FHM brood populations during this study. In contrast, the dissolved Cu LC50s at pH 7, 0.5 mEq/L hardness and 0 mg DOC/L were 2× to 5× lower than the corresponding LC50s at 2.0 mEq/L hardness (Figure 2) because of the protective effect of water hardness on Cu toxicity (Meyer et al. 1999, Santore et al. 2001, Meyer et al. 2002); and the dissolved Cu LC50s at pH 7, 2.0 mEq/L hardness and 20 mg DOC/L were 20× to 30× greater than the corresponding LC50s at 0 mg DOC/L (Figure 2) because of the protective effect of DOM on Cu toxicity (Santore et al. 2001). Moreover, the dissolved Cu LC50s at pH 8, 2.0 mEq/L hardness and 0 mg DOC/L were ~3× greater than the corresponding dissolved Cu LC50s at pH 7 (Figure 2) because of the protective effect of alkaline pH on Cu toxicity (Santore et al. 2001, Meyer et al. 2002). In agreement with BLM predictions, the dissolved Cu LC50s at pH 6, 2.0 mEq/L hardness and 0 mg DOC/L did not differ considerably from the dissolved Cu LC50s at pH 7, 2.0 mEq/L hardness and 0 mg DOC/L.

The OCUD curves we fitted to the four sets of dissolved Cu LC50 data in Figure 2 were approximately parallel, suggesting that the dissolved Cu LC50s in the different data sets differed by approximately constant factors. However, the OCUD curve for the pH 8, 2.0 mEq/L hardness and 0 mg DOC/L data (the squares in Figure 2) deviated slightly from being parallel with the other curves at exposure times <8 h because that portion of the OCUD curve was extrapolated from the data for 8- to 96-h exposures (i.e., reliable LC50s could not be determined for 1-h, 2-h and 4-h exposures because some of the Cu precipitated from the high Cu concentrations that were selected to bracket the 1-h, 2-h and 4-h LC50s in that toxicity test).

As expected, basing the LC50s on Cu^{2+} concentration instead of dissolved Cu concentration brought the data for pH 7, 2.0 mEq/L hardness and 20 mg DOC/L very close to the corresponding data for pH 7, 2.0 mEq/L hardness and 0 mg DOC/L (i.e., the diamonds are nestled among the upward-pointing triangles in Figure 3) because pH and water hardness were constant in those toxicity tests. However, this moved all the Cu^{2+} LC50s determined at pH 7, 2.0 mEq/L hardness and 0 mg DOC/L in 2005 away from the corresponding Cu^{2+} LC50s determined at pH 7, 2.0 mEq/L hardness and 0 mg DOC/L in 2004 because the background DOC concentrations in the dilution water differed enough between those two years (0.2-0.3 mg DOC/L in 2004, and ~0.5 mg DOC/L in 2005) to cause a moderately large difference in the calculated amounts of Cu-DOM complexation (and thus, a moderately large difference in calculated Cu^{2+} concentrations) at 50% mortality. Moreover, the Cu^{2+} LC50s determined at pH 8, 2.0 mEq/L hardness and 0 mg DOC/L nestled with the Cu^{2+} LC50s determined at pH 7, 0.5 mEq/L hardness and 0 mg DOC/L, which were 2× to 5× lower than the Cu^{2+} LC50s determined at pH 7, 2.0 mEq/L hardness and 0 mg DOC/L. Finally, the Cu^{2+} LC50s determined at pH 6, 2.0 mEq/L hardness and 0 mg DOC/L remained considerably higher than the Cu^{2+} LC50s determined at pH 7, 2.0 mEq/L hardness and 0 mg DOC/L.

When the sum of BLM-calculated Cu^{2+} and CuOH^+ concentrations at 50% mortality were used as predictors of toxicity, the relative positions of the data sets under the different combinations of pH, water hardness and DOC concentration remained approximately the same as for the Cu^{2+} LC50s. The only major difference was that the $\text{Cu}^{2+} + \text{CuOH}^+$ LC50s determined at pH 8, 2.0 mEq/L hardness and 0 mg DOC/L moved considerably closer to the $\text{Cu}^{2+} + \text{CuOH}^+$

LC50s determined at pH 7, 2.0 mEq/L hardness and 0 or 20 mg DOC/L, and those $\text{Cu}^{2+} + \text{CuOH}^+$ LC50s determined at pH 7, 2.0 mEq/L hardness and 0 or 20 mg DOC/L moved slightly closer to the $\text{Cu}^{2+} + \text{CuOH}^+$ LC50s determined at pH 6, 2.0 mEq/L hardness and 0 mg DOC/L (results not shown). However, the $\text{Cu}^{2+} + \text{CuOH}^+$ LC50s determined at pH 7, 0.5 mEq/L hardness and 0 mg DOC/L remained considerably lower than the $\text{Cu}^{2+} + \text{CuOH}^+$ LC50s determined at pH 7, 2.0 mEq/L hardness and 0 mg DOC/L.

Fitting the OCUD Model to the Continuous-Exposure LA50 Data

Because a separate curve is needed to fit the OCUD model to dissolved Cu LC50s, Cu^{2+} LC50s, or $\text{Cu}^{2+} + \text{CuOH}^+$ LC50s at each water hardness (thus requiring an almost infinite number of curves for the almost infinite number of possible combinations of water hardness and other water quality parameters in laboratory toxicity tests and in real-world surface waters), a predictor of Cu toxicity that is independent of water quality is needed to simplify this otherwise difficult-to-manage task. Based on the demonstrated ability of a single BLM-calculated concentration of Cu bound to the FHM biotic ligand to predict Cu toxicity across a wide range of water quality conditions at a specified exposure time (Santore et al. 2001), we hypothesized that the BLM-calculated concentration of Cu bound to the FHM biotic ligand might also accurately predict toxicity when Cu concentrations and/or water quality are time-variable.

Using the default parameterization of the FHM Cu BLM, the calculated $\Sigma\text{Cu-BL}$ LA50s (i.e., $\text{Cu-BL} + \text{CuOH-BL}$ at 50% mortality) for all the continuous-exposure toxicity tests were much closer together (Figure 4) than were the LC50s based on dissolved Cu (Fig. 2) or Cu^{2+} (Fig. 3). However, closer inspection of the $\Sigma\text{Cu-BL}$ LA50s (Figure 5) shows that they did not fit the OCUD model illustrated in Figure 1 because the plot of $\ln(\text{LA50})$ vs. $\ln(t)$ had a decreasing slope that approached a horizontal asymptote as exposure time decreased, which is opposite of the trend for a generalized OCUD model (e.g., Figure 4). The plot of $\ln(\text{LA50})$ vs. $\ln(t)$ approached a horizontal asymptote as exposure time decreased because the BLM-calculated binding of Cu and CuOH with the biotic ligand approached saturation (e.g., >90% of the binding sites were occupied by Cu at exposure times ≤ 2 h) when the default parameterization of the FHM Cu BLM was used to calculate the LA50s. One way to circumvent this undesirable feature would be to alter one or more of the cation-BL binding constants (i.e., $K_{\text{Cu-BL}}$, $K_{\text{CuOH-BL}}$, $K_{\text{H-BL}}$, $K_{\text{Ca-BL}}$ and $K_{\text{Na-BL}}$) in the Cu BLM, thus decreasing the percentage saturation of the biotic ligand with Cu.

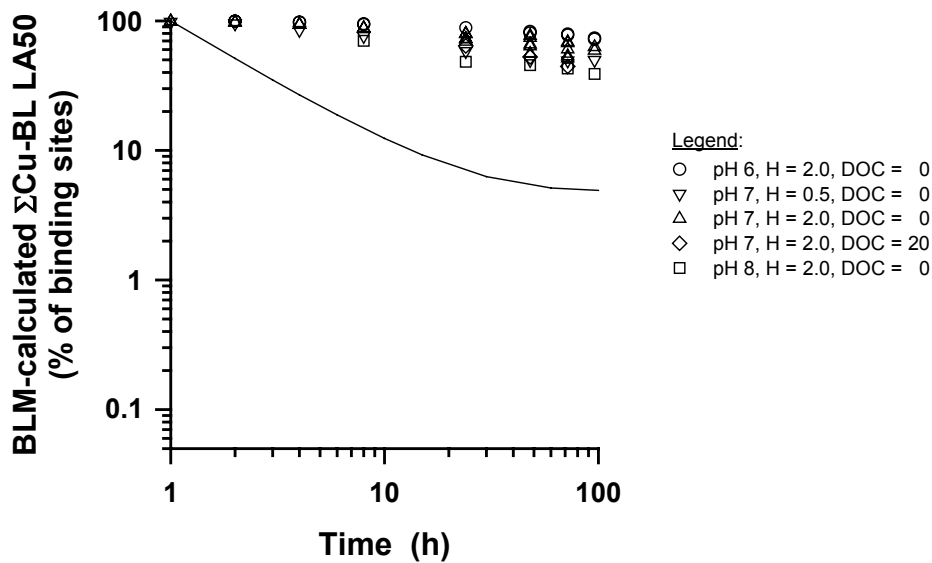


Figure 4. Σ Cu-BL LA50s for fathead minnow larvae in 96-h continuous-exposure Cu toxicity tests (same tests as plotted in Figures 2 and 3), calculated using the default parameterization of FHM Cu BLM Version 2.1.1. Nominal exposure conditions are listed in the caption for Figure 2. The solid curve is a generalized one-compartment uptake-depuration model (not fitted to the data).

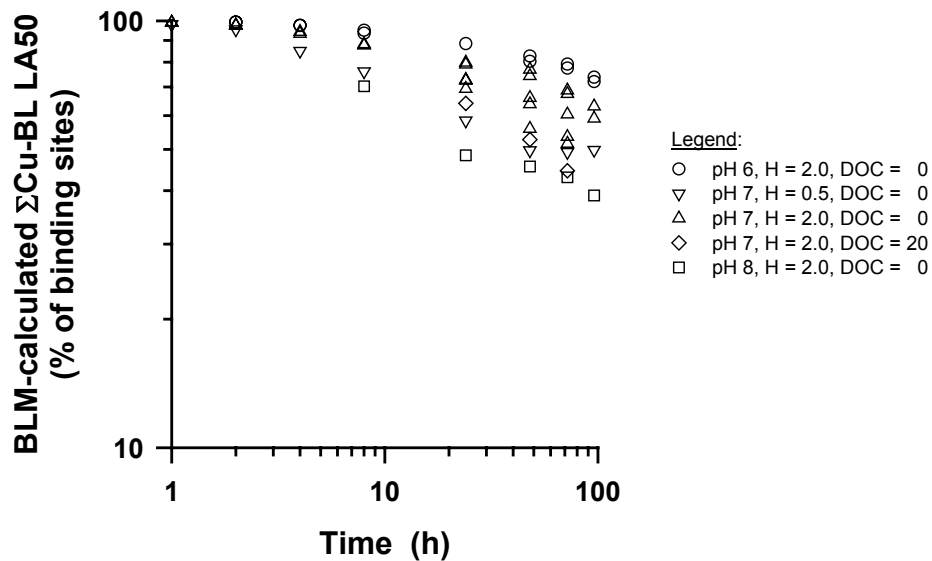


Figure 5. Σ Cu-BL LA50s for fathead minnow larvae in 96-h continuous-exposure Cu toxicity tests (same tests as plotted in Fig. 4 but at higher resolution), calculated using the default parameterization of FHM Cu BLM Version 2.1.1. Nominal exposure conditions are listed in the caption for Figure 2.

Our first attempt to decrease the percentage of BL binding sites occupied by Cu was to decrease all five cation-BL binding constants in the BLM proportionally. For example, when we

decreased all BL binding constants by 2 log units (i.e., by 100×), the plot of $\ln(\text{LC50})$ vs. $\ln(t)$ fit the OCUD model in Equation 2 (e.g., compare Figure 6 with Figure 1). However, with this new parameterization of the BLM, the LA50s at 0.5 and 2.0 mEq/L hardness were approximately as far apart as the corresponding Cu^{2+} LC50s (compare the upward- and downward-pointing triangles in Figure 6 with those in Figure 3), producing an ad hoc solution that is incompatible with the underlying concept of the BLM that the LA50 is independent of water quality at a specified exposure time. This occurred because decreasing the binding of all the cations (H^+ , Na^+ , Ca^{2+} , Cu^{2+} , and CuOH^+) to the biotic ligand effectively eliminated competition among the cations for binding at the BL sites, leaving no mechanism in the model for water hardness (represented by Ca^{2+} in the BLM) to decrease Cu binding to the biotic ligand.

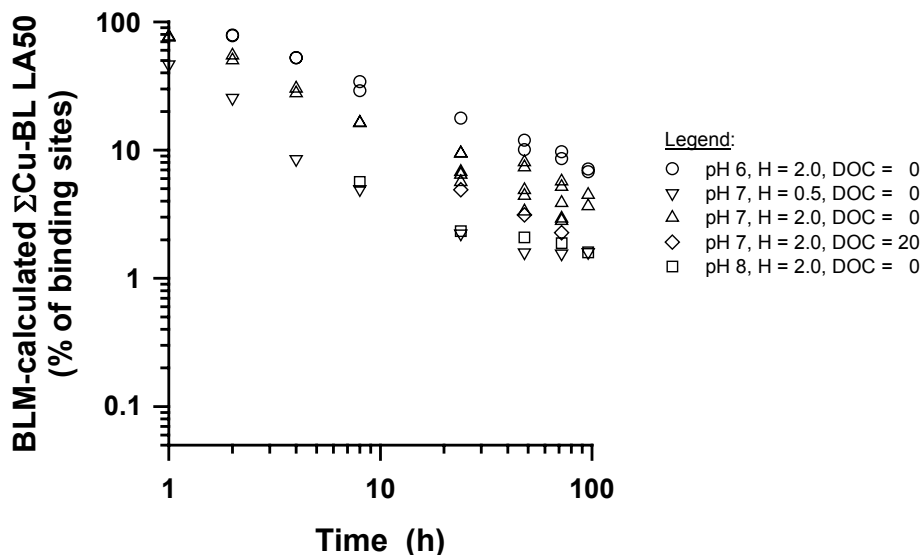


Figure 6. $\Sigma\text{Cu-BL}$ LA50s for fathead minnow larvae in 96-h continuous-exposure Cu toxicity tests, calculated using values for $K_{\text{Cu-BL}}$, $K_{\text{CuOH-BL}}$, $K_{\text{H-BL}}$, $K_{\text{Ca-BL}}$ and $K_{\text{Na-BL}}$ that were 2 log units lower than in the default parameterization of FHM Cu BLM Version 2.1.1. Nominal exposure conditions are listed in the caption for Figure 2.

Next we decreased only the Cu-BL and CuOH-BL binding constants in the BLM by 1 to 3 log units but left all three other cation-BL binding constants at the default BLM values; however, that did not bring the two sets of $\Sigma\text{Cu-BL}$ LA50s together, either (results not shown). Finally, we increased only the Ca-BL and H-BL binding constants by various amounts and left the other three cation-BL binding constants at the default BLM values. With the binding constants listed in Table 3, the $\Sigma\text{Cu-BL}$ LA50s for all the continuous-exposure tests came together, and the variation in $\Sigma\text{Cu-BL}$ LA50s was minimized (Figures 7 and 8).

Table 3. Comparison of the default cation-BL binding constants in FHM Cu BLM Version 2.1.1 and the modified set of binding constants used to obtain the best fit of a one-compartment uptake-depuration (OCUD) model to the BLM-predicted $\Sigma\text{Cu-BL}$ LA50s shown in Figure 7.^a

Cation-BL complex ^a	log K of default binding constant in BLM	log K of best-fit binding constant in this study
Ca-BL	3.6	5.6
Cu-BL	7.4	7.4
CuOH-BL	-1.3	-1.3
H-BL	5.4	8.9
Na-BL ^b	3.0	3.0

^a BL = biotic ligand.

^b $K_{\text{Na-BL}}$ was not modified when fitting the OCUD model to the $\Sigma\text{Cu-BL}$ LA50s because Na concentration was not varied in the toxicity tests used to generate the $\Sigma\text{Cu-BL}$ LA50s.

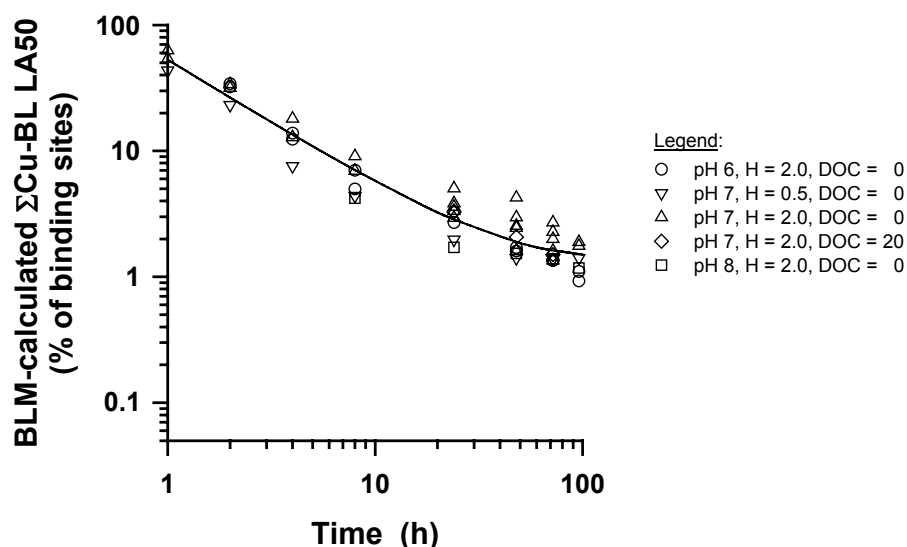


Figure 7. $\Sigma\text{Cu-BL}$ LA50s for fathead minnow larvae in 96-h continuous-exposure Cu toxicity tests, calculated using values for $K_{\text{Ca-BL}}$ and $K_{\text{H-BL}}$ that were, respectively, 2 and 3.5 log units greater than in the default parameterization of FHM Cu BLM Version 2.1.1. Nominal exposure conditions are listed in the caption for Figure 2. The cation-BL binding constants are listed in Table 3, and the nonlinear-regression constants for the fit to a one-compartment uptake-depuration model (the curve) are listed in Table 2.

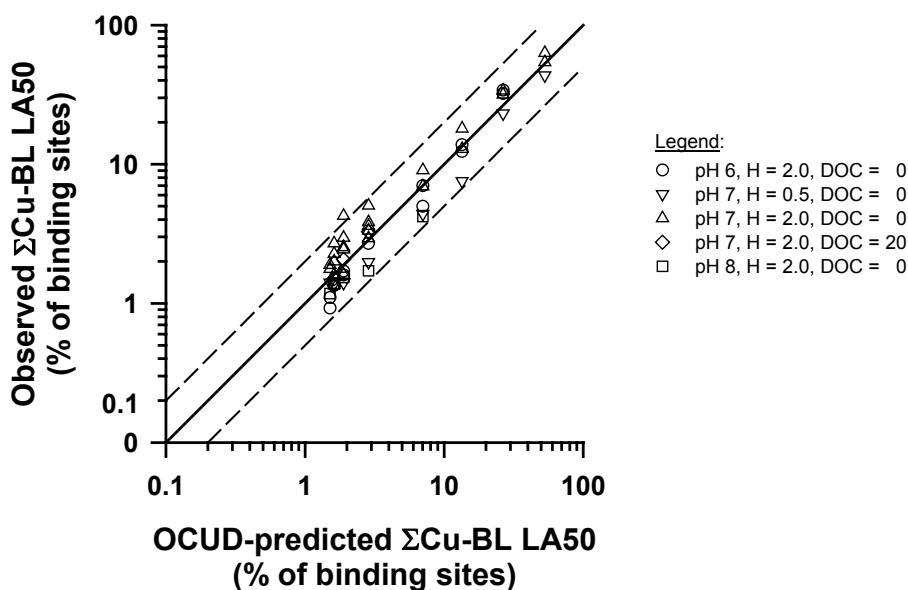


Figure 8. Comparison of observed continuous-exposure $\Sigma\text{Cu-BL LA50s}$ and the corresponding $\Sigma\text{Cu-BL LA50s}$ predicted by the one-compartment uptake-depuration model fitted to the observed continuous-exposure $\Sigma\text{Cu-BL LA50s}$ in Figure 7. The solid diagonal line is the 1:1 line of perfect agreement; the two dashed diagonal lines bracket the range of observed:predicted ratios of 0.5 to 2.0.

The good fit of the OCUD model using the modified set of BLM binding constants is shown in Figures 7 and 8, and the coefficients for the nonlinear-regression fit of the OCUD model to the $\Sigma\text{Cu-BL LA50s}$ are listed in Table 2. The maximum range of observed $\Sigma\text{Cu-BL LA50s}$ at a given exposure time was only 3-fold (at 48 h; Figure 7), and only one continuous-exposure $\Sigma\text{Cu-BL LA50}$ fell outside the $0.5\times$ to $2\times$ range of agreement between observed and OCUD-predicted $\Sigma\text{Cu-BL LA50s}$ (i.e., outside the region bounded by the dashed diagonal lines in Fig. 8). Therefore, increasing the default $K_{\text{Ca-BL}}$ in the BLM by 2 log units and the default $K_{\text{H-BL}}$ in the BLM by 3.5 units provides an acceptable solution that simultaneously is consistent with the generalized form of an OCUD model and fits the continuous-exposure toxicity data well.

The important components of this re-parameterization of the cation-BL binding constants in the BLM were that (1) $\log K_{\text{Ca-BL}}$ was ≥ 2 units greater than the default value of 3.6, and (2) $\log K_{\text{H-BL}}$ was increased by 1.5 units more than $\log K_{\text{Ca-BL}}$ was increased. These conditions reflect the need to have Ca^{2+} and H^+ increase their competition with Cu^{2+} and CuOH^+ for binding to the biotic ligand on FHM, and the need to have H^+ increase its binding strength relative to that of Ca^{2+} . Otherwise, the OCUD model would not be satisfied while simultaneously collapsing the $\Sigma\text{Cu-BL LA50s}$ into a narrow range of values at each exposure time. Additionally, the need to increase $\log K_{\text{H-BL}}$ more than $\log K_{\text{Ca-BL}}$ explains why decreasing only $K_{\text{Cu-BL}}$ and $K_{\text{CuOH-BL}}$ did not provide a satisfactory solution.

The good fit of the data to the $\ln(\text{LA50})$ vs. $\ln(t)$ curve in Figure 7 indicates that it is possible to have a linked BLM-OCUD model in which simultaneously (1) only one $\Sigma\text{Cu-BL LA50}$ is calculated for FHM larvae across a range of water quality conditions at a specified exposure time, and (2) the $\ln(\text{LA50})$ vs. $\ln(t)$ curve is consistent with the traditional OCUD model. However, achieving both criteria requires that the Ca-BL and H-BL binding constants in

FHM Cu BLM Version 2.1.1 must be increased considerably and, as a consequence, the BLM-calculated 96-h Σ Cu-BL LA50 (and by extension, the Σ Cu-BL LA50 at all other exposure times) decreases considerably. To cover an even a wider range of water quality conditions (e.g., different Na^+ concentrations), $K_{\text{Na-BL}}$ might also have to be increased.

Observed versus Predicted Pulse-Exposure LA50

We used Equation 3 and the OCUD parameters determined in the previous section (i.e., the Σ Cu-BL LA50 coefficients listed in Table 2) to predict Σ Cu-BL LA50s for all the 72-h pulse-exposure tests conducted during this study (see Table 1). Then we compared the predicted pulse Σ Cu-BL LA50s to the corresponding observed pulse Σ Cu-BL LA50s. Because of the wide range of dissolved Cu, Cu^{2+} , and $\text{Cu}^{2+} + \text{CuOH}^+$ LC50s in the continuous-exposure tests at various combinations of pH, water hardness and DOC concentration, we could not generate a single set of OCUD parameters that would reliably predict continuous-exposure LC50s across a wide range of water quality conditions. Therefore, we did not attempt to use the OCUD model to predict 2-h and 8-h LC50s for dissolved Cu, Cu^{2+} , or $\text{Cu}^{2+} + \text{CuOH}^+$ in the pulse-exposure tests.

In most cases, the predicted pulse Σ Cu-BL LA50s agreed relatively well with the corresponding observed pulse Σ Cu-BL LA50s, when the LA50s were calculated for the end of each 24-h pulse-and-recovery cycle (i.e., most of the predicted pulse Σ Cu-BL LA50s were within $0.5\times$ to $2\times$ of the corresponding observed pulse Σ Cu-BL LA50s; Figure 9). Therefore, using one composite OCUD equation and the modified cation-BL binding constants in the FHM Cu BLM, the acute toxicity of Cu during time-variable exposures can be predicted relatively accurately across a moderately wide range of pH (6-8), water hardness (0.5-2.0 mEq/L) and DOC concentrations (0-20 mg/L).

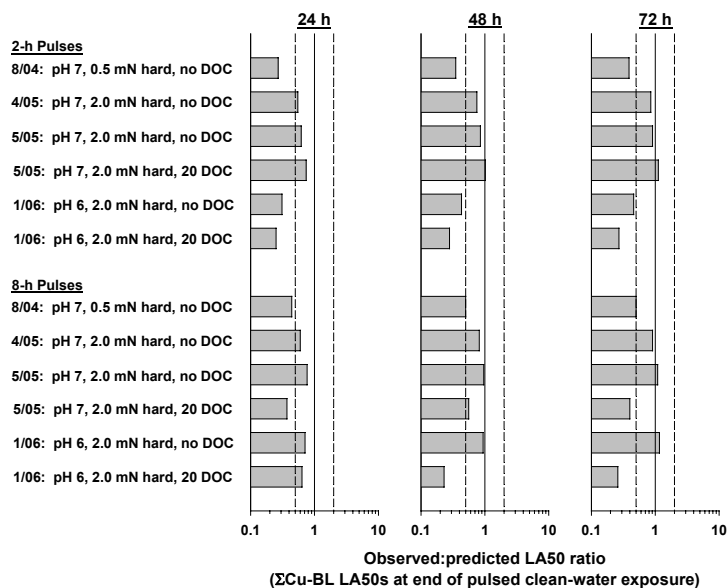


Figure 9. Ratios of observed pulse-exposure Σ Cu-BL LA50 to the corresponding pulse-exposure Σ Cu-BL LA50 predicted by Equation 3, using a one-compartment uptake-depuration model fitted to the observed continuous-exposure Σ Cu-BL LA50s in Figure 7. All the observed and predicted LA50s were calculated for the end of the clean-water exposure period of each 24-h pulse-and-recovery cycle (i.e., at 24, 48 and 72 h of each pulse-exposure test).

On closer inspection of Figure 9, though, almost every predicted pulse Σ Cu-BL LA50 was greater than the corresponding observed pulse Σ Cu-BL LA50 (i.e., the observed: predicted LA50 ratio almost always was <1), suggesting that the OCUD model tended to slightly under-predict the acute toxicity of Cu pulses to FHM larvae. This under-prediction of the pulse toxicity of Cu occurred because some of the fish killed by the pulse Cu exposures died while they were in uncontaminated water during the recovery period of each pulse-and-recovery cycle, especially after the first 2-h or 8-h Cu pulse (Table 4). Therefore, for example, the continuous-exposure 2-h LA50 predicted by the OCUD model using the regression coefficients listed in Table 2 can not accurately predict the 24-h Σ Cu-BL LA50 when the fish are exposed to a 2-h pulse of Cu but some fish to die during the subsequent 22-h recovery period in uncontaminated water.

Table 4. Qualitative scoring of the amount of fathead minnows that died during the recovery phases (i.e., during the 22 or 16 h that the fish were in uncontaminated water) in 2-h or 8-h Cu pulse-exposure toxicity tests

Test type and start date ^b	Exposure conditions	Relative number of deaths during the recovery period ^a		
		First (2-24 h or 8-24 h) recovery period	Second (26-48 h or 32-48 h) recovery period	Third (50-72 h or 56-72 h) recovery period
<u>2-h pulses</u>				
4/05	pH 7, H = 2.0 mEq/L, DOC = 0 mg/L	***	*	*
5/05	pH 7, H = 2.0 mEq/L, DOC = 0 mg/L	***	*	*
5/05	pH 7, H = 2.0 mEq/L, DOC = 20 mg/L	***	*	*
1/06	pH 6, H = 2.0 mEq/L, DOC = 0 mg/L	***	*	*
1/06	pH 6, H = 2.0 mEq/L, DOC = 20 mg/L	**	*	*
<u>8-h pulses</u>				
4/05	pH 7, H = 2.0 mEq/L, DOC = 0 mg/L	**	*	*
5/05	pH 7, H = 2.0 mEq/L, DOC = 0 mg/L	**	*	*
5/05	pH 7, H = 2.0 mEq/L, DOC = 20 mg/L	***	*	*
1/06	pH 6, H = 2.0 mEq/L, DOC = 0 mg/L	**	*	*
1/06	pH 6, H = 2.0 mEq/L, DOC = 20 mg/L	**	*	*

^a*** = large number of deaths, ** = intermediate number of deaths, * = small number of deaths.

^bDeaths during the uncontaminated-water recovery periods were not recorded in the 2-h pulse and 8-h pulse tests conducted in August 2004.

To test that explanation for the apparently biased underestimates of pulse-exposure Cu toxicity, we recalculated the Σ Cu-BL LA50s with the toxicity data at the end of each Cu-exposure period (i.e., at 2, 26, and 50 h in the 2-h Cu-pulse/22-h recovery tests, or at 8, 32 and 56 h in the 8-h Cu-pulse/16-h recovery tests). As expected, this increased most of the observed:predicted LA50 ratios, placing all of the 2-h or 8-h LA50 ratios, all but two of the 26-h or 32-h LA50 ratios, and all but three of the 50-h or 56-h LA50 ratios within an acceptable range of 0.5 to 2.0 (Figure 10). Interestingly, three of the four tests with 20 mg DOC/L produced the most biased underestimates of Cu-pulse toxicity.

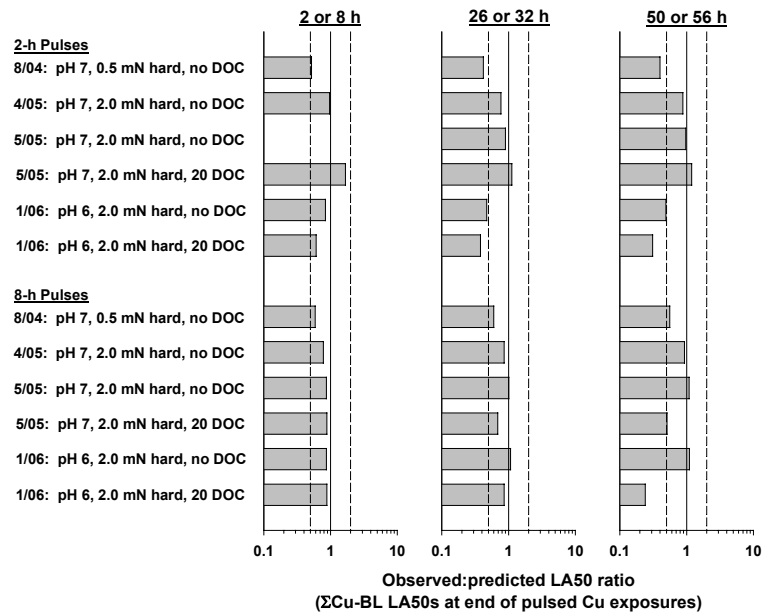


Figure 10. Ratios of observed pulse-exposure Σ Cu-BL LA50 to the corresponding pulse-exposure Σ Cu-BL LA50 predicted by Equation 3, using a one-compartment uptake-depuration model fitted to the observed continuous-exposure Σ Cu-BL LA50s in Figure 7. These are the same toxicity tests as in Figure 9; however, all the observed and predicted LA50s were calculated for the end of the Cu-exposure period of each pulse-and-recovery cycle (i.e., at 2, 26 and 50 h of each 2-h pulse test, or at 8, 32 and 56 h of each 8-h pulse test), instead of at the end of each pulse-and-recovery cycle.

The OCUD model is best at predicting pulse-exposure LA50s at the end of the first Cu-exposure period because the model does not have to account for delayed deaths that will occur during subsequent recovery periods in uncontaminated water. However, predictions of pulse-exposure LA50s at the end of the second and third Cu pulses (and at the end of each pulse-and-recovery cycle) become less reliable because of the delayed mortalities not accounted for in continuous-exposure 2-h or 8-h LA50s. This is inevitable for toxicants like Cu that cause delayed deaths, because a key assumption of the OCUD model used here is that an organism dies as soon the concentration at the site of action equals the median lethal accumulation (the $C_{L,50}$).

Framework for Using the Linked BLM-OCUD Model for Predicting Acute Toxicity of Copper

The results presented in the previous section demonstrate that a single linked BLM-OCUD model can be used to relatively reliably predict across a range of water quality conditions (1) the continuous-exposure LC50s for FHM exposed to Cu at non-standard exposure times (i.e., at other than 96 h), and (2) pulse-exposure LC50s for FHM exposed to Cu. This universal applicability of a single BLM-OCUD equation circumvents the need to know a separate OCUD equation for each of a potentially infinite number of combinations of water quality conditions, a situation that is encountered when concentrations of dissolved Cu, Cu^{2+} or $\text{Cu}^{2+} + \text{CuOH}^+$ are used instead of Σ Cu-BL as the predictor of toxicity.

Predicting continuous-exposure LC50s for dissolved Cu at exposure times other than 96 h is relatively easy. Simply use Equation 2 and the OCUD regression coefficients for Σ Cu-BL in

Table 2 to predict the Σ Cu-BL LA50 at the specified exposure time. Then use FHM Cu BLM Version 2.1.1 (but with $\log K_{Ca-BL} = 5.6$ and $\log K_{H-BL} = 8.9$ in file titled “Cu_Fathead_Minnow_04-03-26.DAT”, instead of using the default values for those two binding constants) to iteratively calculate the dissolved Cu concentration that produces the same Σ Cu-BL LA50 that you calculated in the previous step. That dissolved Cu concentration is the predicted continuous-exposure Cu LC50.

Predicting square-wave pulse-exposure LC50s for dissolved Cu at exposure times other than 96 h is just as easy as predicting continuous-exposure LC50s for dissolved Cu. Simply use Equation 3 and the OCUD regression coefficients for Σ Cu-BL in Table 2 to predict the pulse Σ Cu-BL LA50 at the specified exposure time. Then use FHM Cu BLM Version 2.1.1 (but with $\log K_{Ca-BL} = 5.6$ and $\log K_{H-BL} = 8.9$ in file titled “Cu_Fathead_Minnow_04-03-26.DAT”, instead of using the default values for those binding constants) to iteratively calculate the dissolved Cu concentration that produces the same pulse Σ Cu-BL LA50 that you calculated in the previous step. That dissolved Cu concentration is the predicted pulse-exposure Cu LC50.

Predicting pulse-exposure LC50s for dissolved Cu in time-variable exposures that do not produce square-wave pulses is more complicated than explained in the previous paragraph because Equation 3 (which is specific for square-wave pulses) must be modified for the pulsing pattern of interest. Wang and Hanson (1985) discussed the general approach for deriving appropriate substitute equations and even derived the equations for some specific pulsing patterns like triangle pulses. However, after an appropriate substitute for Equation 3 is derived, use the same steps as described for square-wave pulses in the previous paragraph to calculate the pulse-exposure LC50 for dissolved Cu.

Conclusions

One global OCUD equation linked to a re-parameterized FHM Cu BLM can be used to predict the acute toxicity of continuous and pulse exposures of Cu to FHM larvae relatively accurately across the range of combinations of pH, water hardness and DOC concentration tested in this study. However, the default parameterization of FHM Cu BLM Version 2.1.1 predicts Σ Cu-BL LA50s that do not fit the generalized form of an OCUD model and thus cannot be used to accurately predict pulse-exposure LC50s of dissolved Cu. Although the re-parameterized Ca-BL and H-BL binding constants selected in this study might be improved by fitting the OCUD model to a larger set of continuous-exposure Cu toxicity data generated across an even wider range of water quality conditions and with a variety of types of DOM, more pressing research needs should be addressed in the near term. First, linked BLM-OCUD models should be developed for FHM exposed other cationic metals (e.g., Ag, Cd, Ni, Pb, Tl, Zn) and for other regulatorily important aquatic organisms exposed to all cationic metals of concern, so at least first-approximation pulse-exposure LC50s can be calculated for a wide range of cationic metals of general concern. Second, the apparently biased underestimates of pulse Cu toxicity that our linked BLM-OCUD model produced should be addressed by modifying the OCUD model framework to account for delayed mortality. The phenomenon of delayed mortality is often overlooked or not even recognized because it can be relatively unimportant at the end of standard continuous-exposure toxicity tests (e.g., 48 h for invertebrates and 96 h for fish). However, delayed mortality can be substantial at shorter exposure times (Zhao and Newman 2004, Kolts et al. 2006, Zhao and Newman 2004, and this study) and has important implications for predicting pulse-exposure toxicity of Cu (and perhaps other metals) to aquatic organisms. A generalized

unit world model for metals and site-specific analyses of metal toxicity could be improved by increasing the accuracy of the linked BLM-OCUD models for a variety of metals.

Acknowledgements

Jeffrey Morris and Connie Boese (University of Wyoming) conducted the time-varying toxicity tests and performed the chemical analyses. Dr. Herbert Allen (University of Delaware) supplied the Suwannee River DOM. Dr. Peter Campbell (Université du Québec) provided helpful advice about the design of the pulse-exposure toxicity tests.

Literature Cited

- APHA, AWWA, and WEF (American Public Health Association, American Water Works Association, and Water Environment Foundation). (1995) *Standard Methods for the Examination of Water and Wastewater. 19th Edition*. American Public Health Association, Washington, District of Columbia, USA.
- ASTM (American Society for Testing and Materials). (1993) *ASTM Standards on Aquatic Toxicology and Hazard Evaluation*. American Society for Testing and Materials, Philadelphia, Pennsylvania, USA.
- Di Toro, D.M., Allen, H.E., Bergman, H.L., Meyer, J.S., Paquin, P.R., and Santore, R.C. (2001) Biotic Ligand Model of the Acute Toxicity of Metals. 1. Technical Basis. *Environ. Toxicol. Chem.* 20:2383-2396.
- Kolts, J.M., Boese, C.J., and Meyer, J.S. (2006) Acute Toxicity of Copper and Silver to *Ceriodaphnia dubia* in the Presence of Food. *Environ. Toxicol. Chem.* (in press).
- Ives, M.A. (1996) TOXCALC 5.0. Tidepool Scientific Software, McKinleyville, California, USA.
- Mancini, J.L. (1983) A Method for Calculating Effects, on Aquatic Organisms, of Time-Varying Concentrations. *Water Res.* 10:1355-1362.
- Meyer, J.S., Bringolf, R.B., and Morris, B.A. (2004) A Test of the Biotic Ligand Model: Fish Exposed to Time-Variable Concentrations of Copper And Zinc -- Progress report for Year 1 of a three-year project. University of Wyoming, Laramie, Wyoming, USA. pp.8.
- Meyer, J.S., Boese, C.J., and Collyard, S.A. (2002) Whole-Body Accumulation of Copper Predicts Acute Toxicity to an Aquatic Oligochaete (*Lumbriculus variegatus*) as pH and Calcium are Varied. *Comp. Biochem. Physiol. Part C Toxicol. Pharm* 133:99-109.
- Meyer, J.S., Gulley, D.D., Goodrich, M.S., Szmania, D.C., and Brooks, A.S. (1995) Modeling Toxicity Due to Intermittent Exposure of Rainbow Trout and Common Shiners to Monochloramine. *Environ. Toxicol. Chem.* 14:165-175.
- Meyer, J.S., Santore, R.C., Bobbitt, J.P., DeBrey, L.D., Boese, C.J., Paquin, P.R., Allen, H.E., Bergman, H.L., and Di Toro, D.M. (1999) Binding of Nickel and Copper to Fish Gills Predicts Toxicity When Water Hardness Varies, but Free-ion Activity Does Not. *Environ. Sci. Technol.* 33:913-916.
- Morris, J.M., Farag, A.M., Nimick, D.M., and Meyer, J.S. (2005) Does Biofilm Contribute to Diel Cycling of Zn in High Ore Creek, Montana? *Biogeochemistry* 76:233-259.

- Nimick D.A., Gammons, C.H., Cleasby, T.E., Madison, J.P., Skaar, D., and Brick, C.M. (2003) Diel Cycles in Dissolved Metal Concentrations in Streams -- Occurrence and Possible Causes. *Water Resources Research* 39: citation no. 1247, doi:10.1029/WR001571.
- Paquin, P.R., Gorsuch, J.W., Apte, S., Batley, G.E., Bowles, K.C., Campbell, P.G.C., Delos, C.G., Di Toro, D.M., Dwyer, R.L., Galvez, F., Gensemer, R.W., Goss, G.G., Hogstrand, C., Janssen, C.R., McGeer, J.C., Naddy, R.B., Playle, R.C., Santore, R.C., Schneider, U., Stubblefield, W.A., Wood, C.M., and Wu, K.B. (2002) The Biotic Ligand Model: A Historical Overview. *Comp. Biochem. Physiol. Part C Toxicol. Pharm.* 133:3-35
- Santore, R.C., Di Toro, D.M., Paquin, P.R., Allen, H.E., and Meyer, J.S. (2001) Biotic Ligand Model of the Acute Toxicity of Metals. 2. Application to Acute Copper Toxicity in Freshwater Fish and *Daphnia*. *Environ. Toxicol. Chem.* 20:2397-2402.
- Santore, R.C., Mathew, R., Paquin, P.R., and Di Toro, D.M. (2002) Application of the Biotic Ligand Model to Predicting Zinc Toxicity to Rainbow Trout, Fathead Minnow, and *Daphnia magna*. *Comp. Biochem. Physiol. Part C Toxicol. Pharm.* 133:271-285.
- USEPA (U.S. Environmental Protection Agency). (1979) Methods for Chemical Analysis of Water and Wastes. EPA 600/4-79-020. U.S. Environmental Protection Agency, Environmental Monitoring and Support Laboratory, Cincinnati, Ohio, USA.
- USEPA (U.S. Environmental Protection Agency). (1994) USEPA Contract Laboratory Program National Functional Guidelines for Inorganic Data Review. EPA 540/R-94/013. Office of Emergency and Remedial Response, U.S. Environmental Protection Agency, Washington, District of Columbia, USA.
- USEPA (U.S. Environmental Protection Agency). (2002) Methods for Measuring the Acute Toxicity of Effluents and Receiving Waters to Freshwater and Marine Organisms, Fifth Edition. EPA-821-R-02-012. U.S. Environmental Protection Agency, Washington, District of Columbia, USA.
- USEPA (U.S. Environmental Protection Agency). (2003) Draft Update of Ambient Water Quality Criteria for Copper. EPA 822-R-023-026. U.S. Environmental Protection Agency, Office of Water, Washington, District of Columbia, USA.
- Wang, M.P., and Hanson, S.A. (1985) The acute toxicity of chlorine on freshwater organisms: Time-concentration relationships of constant and intermittent exposures. pp. 213-232 in: R.C. Bahner and D.J. Hansen (eds.). *Aquatic Toxicology and Hazard Assessment: Eighth Symposium*. STP 891. American Society for Testing and Materials, Philadelphia, Pennsylvania, USA.
- Zhao, Y., and Newman, M.C. (2004) Shortcomings of the laboratory-derived median lethal concentration for predicting mortality in field populations: Exposure duration and latent mortality. *Environ. Toxicol. Chem.* 23:2147-2153.

APPENDIX II

Publications

Ecotoxicology of Mining-Related Metal Oxides in a High Gradient Mountain Stream

James Ranville
Department of Chemistry and Geochemistry
Colorado School of Mines
Golden, CO 80401

Philippe Ross
Department of Environmental Science and Engineering
Colorado School of Mines
Golden, CO 80401

and

Barbara Butler
Department of Environmental Science and Engineering
Colorado School of Mines
Golden, CO 80401

Publications

Presentations:

- Ranville, J.F., 2005. Simple Methods for Mine Waste Evaluations and Bioaccessibility Assessments. US EPA Abandoned Mine Lands Workshop Series. Acid Mine Water: Treatment Technologies Workshop. May 10-12, 2005, Denver, CO.
- Butler, B.A., Ranville, J.F., and Ross, P.E. Comparing equilibrium and transport modeling predictions to observed particulate metal transport in a mining-impacted stream (North Fork Clear Creek, CO). 26th Annual North American Conference of the Society of Environmental Toxicology & Chemistry, Baltimore, MD, November 13-17, 2005.
- Butler, B.A., Ranville, J.F., and Ross, P.E. Comparison between observed and model predicted particulate metal transport in a mining-impacted stream (North Fork Clear Creek, Colorado). 22nd Annual Meeting of the American Society of Mining and Reclamation, Breckenridge, CO, June 18-23, 2005.
- Butler, B.A. and Ranville, J.F. Assessing dissolved and particulate metals (Cu, Fe, Mn, & Zn) in North Fork Clear Creek, Colorado. Invited speaker at the monthly meeting of the Upper Clear Creek Watershed Association, Idaho Springs, CO, April 14, 2005.
- Butler, B.A., Ranville, J.F., and Ross, P.E. Seasonal trends in metal transport in an acid-mine drainage (AMD) impacted stream: North Fork Clear Creek (NFCC), Colorado: 2005. 15th Annual Colorado School of Mines Research Fair, Golden, CO, April 6, 2005.
- Butler, B.A., Ranville, J.F., and Ross, P.E. Seasonal trends in metal transport in North Fork Clear Creek, Colorado: A mining-impacted stream. 18th Annual Meeting of the Rocky Mountain Regional Chapter of the Society of Environmental Toxicology & Chemistry, Leadville, CO, April 1, 2005.
- Butler, B.A., Ranville, J.F., and Ross, P.E. Comparison of methods to determine suspended sediment associated metals in a mining-impacted stream. 4th World Congress Meeting of the Society of Environmental Toxicology & Chemistry, Portland, OR, November 14-18, 2004.
- Harvey, B.A.B., Ranville, J.F., and Ross, P.E. Seasonal trends in metal transport in a mining-impacted stream: North Fork Clear Creek, Colorado. Annual Meeting of the Geologic Society of America, Denver, CO, November 7-10, 2004.
- Harvey, B.B., Ranville, J.F., and Ross, P.E. Comparison of methods to determine suspended sediment associated metals. 17th Annual Meeting of the Rocky Mountain Regional Chapter of the Society of Environmental Toxicology & Chemistry, Laramie, WY, April 2, 2004.
- Harvey, B.B., Ranville, J.F., and Ross, P.E. Seasonal changes in the characteristics of suspended sediment metal transport in a mining-impacted stream. Joint Conference of the 9th Billings Land Reclamation Symposium and the 20th Annual Meeting of the American Society of Mining and Reclamation, Billings, MT, June 1-7, 2003.
- Butler, B.A. and Ranville, J.F. Sediment and metal transport in a high-gradient stream receiving acid-mine drainage. Invited speaker at the monthly meeting of the Upper Clear Creek Watershed Association, Idaho Springs, CO, February 13, 2002.

Posters

- Ranville, J.F., B.A. Butler, P. Ross. 2005. Application of the biotic ligand model to identify water quality parameters influencing aquatic metal toxicity in Clear Creek, Colorado. 18th

Annual Meeting of the Rocky Mountain Regional Chapter of the Society of Environmental Toxicology & Chemistry, Leadville, CO, April 1, 2005.

Blumenstein, E. P., Ranville, J.F., Choate, L.M., Ross P.E., 2005. Assessing the Validity of Enzyme Bioassays for Rapid Screening for Metals Contamination in Mining Influenced Water. Poster presented at the 18th Annual Meeting of the Rocky Mountain Regional Chapter of the Society of Environmental Toxicology & Chemistry, Leadville, CO, April 1, 2005.

Butler, B.A., Ranville, J.F., and Ross, P.E. Behavior of metals in North Fork Clear Creek, Colorado. Invited presentation at the Clear Creek Watershed Forum 2005: Creating a Sustainable Future, Co-sponsored by the Clear Creek Watershed Foundation and the Upper Clear Creek Watershed Association, Empire, CO, September 27, 2005

Harvey, B.B., Ranville, J.F., Ross, P.E., Pearson, J., Walksi, K., and Clements, W. Transport and metal chemistry of sediments in a high-gradient mountain stream impacted by mining. 16th Annual Meeting of the Rocky Mountain Regional Chapter of the Society of Environmental Toxicology & Chemistry, Denver, CO, April 16, 2003. *Best student poster presentation award.*

Harvey, B.B., Ranville, J.F., Ross, P.E., Pearson, J., Walski, K., and Clements, W. Transport and metal chemistry of sediments in a high-gradient mountain stream impacted by mining. 23rd Annual North American Conference of the Society of Environmental Toxicology & Chemistry, Salt Lake City, UT, November 10-14, 2002.

Harvey, B.B., Ranville, J.F., and Ross, P.E. Transport and metal chemistry of sediments in a high-gradient mountain stream impacted by mining. Annual Meeting of the Geologic Society of America, Denver, CO, October 27-30, 2002.

Peer-Reviewed Papers

Gillis P.L., Chow-Fraser P., Ranville J.F., Ross P.E., Wood C.M. 2005. Daphnia need to be gut-cleared too: the effect of exposure to and ingestion of metal-contaminated sediment on the gut-clearance patterns of *D. magna*. *Aquatic Toxicology*, 71 (2) 143-154.

Gillis P.L., Wood, C.M., Ranville J.F., Chow-Fraser P. 2006. Bioavailability of sediment-associated copper and zinc to *Daphnia Magna*. *Aquatic Toxicology*, 72 (5) 402-411.

Kangas, K., Ayers, J., Ranville, J. F., and Ross, P.E. 2005. The toxicity of binary metal mixtures to *ceriodaphnia dubia* in mining-influenced waters . *in* Proceedings of the 2005 National Meeting of the American Society of Mining and Reclamation, Breckenridge, Colorado, June 19-23, 2005. ASMR, Lexington, KY.

Butler, B.A., Ranville, J.F., and Ross, P.E. **2005**. Comparison between observed and model predicted particulate metal transport in a mining-impacted stream (North Fork Clear Creek, Colorado). Proceedings of the 2005 National Meeting of the American Society of Mining and Reclamation, 3134 Montavesta Rd., Lexington, KY 40502.

Harvey, B.B., Ranville, J.F., and Ross, P.E. **2003**. Seasonal changes in the characteristics of suspended sediment metal transport in a mining-impacted stream. Proceedings for the Joint Conference of the 9th Billings Land Reclamation Symposium and the 20th Annual Meeting of the American Society of Mining and Reclamation, 3134 Montavesta Rd., Lexington, KY 40502.

Butler, B.A., Ranville, J.F., and Ross, P.E. **In Review**. Direct versus indirect determination of suspended sediment associated metals in mining-influenced waters. (Submitted to Applied Geochemistry)

Butler, B.A., Ranville, J.F., and Ross, P.E. **In Prep**. Seasonal trends in metal distribution between sediment and water in the water column of a mining-impacted stream.

Butler, B.A., Ranville, J.F., and Ross, P.E. **In Prep**. Spatial trends in the fate and transport of metals downstream from mining sources.

Butler, B.A., Ranville, J.F., and Ross, P.E. **In Prep**. Sorption studies of copper and zinc onto field derived solids: HFO, HMO, and suspended sediments.

Published Abstracts

Ranville, J. F., Wildeman, T.R., Choate, L.M., Smith K.S. 2005. Integrating bioaccessibility approaches into metal contaminated waters. International Chemical Congress of Pacific Basin Societies. Honolulu, Hawaii, USA, December 15-20, 2005.

Gillis, P, Chow-Fraser, P, Ranville, J, Wood, C . 2005. Are ingested sediments a significant source of bioavailable Cu to *Daphnia magna*?. Abstracts from the 26th Annual North American Conference of the Society of Environmental Toxicology & Chemistry, Pensacola, FL.

Butler, B.A, Ranville, J.F., and Ross, P.E. **2005**. Comparing equilibrium and transport modeling predictions to observed particulate metal transport in a mining-impacted stream (North Fork Clear Creek, CO). Abstracts from the 26th Annual North American Conference of the Society of Environmental Toxicology & Chemistry, Pensacola, FL, p. 16.

Butler, B.A, Ranville, J.F., and Ross, P.E. **2004**. Comparison of methods to determine suspended sediment associated metals in a mining-impacted stream. Abstracts from the 4th World Congress and 25th Annual North American Conference of the Society of Environmental Toxicology & Chemistry, Pensacola, FL, p. 38.

Harvey, B.A.B., Ranville, J.F., and Ross, P.E. **2004**. Seasonal trends in metal transport in a mining-impacted stream: North Fork Clear Creek, Colorado. GSA Abstracts with Programs, Volume 36, No. 5. Published by the Geological Society of America, Boulder, CO, p29.

Harvey, B.B., Ranville, J.F., Ross, P.E., Pearson, J., Walski, K., and Clements, W. **2002**. Transport and metal chemistry of sediments in a high-gradient mountain stream impacted by mining. Abstracts from the 23rd Annual Meeting of the Society of Environmental Toxicology & Chemistry, Pensacola, FL, p. 219.

Harvey, B.B., Ranville, J.F., Ross, P.E., Pearson, J., Walski, K., and Clements, W. **2002**. Transport and metal chemistry of sediments in a high-gradient mountain stream impacted by mining. GSA Abstracts with Programs, Volume 34, No. 6. Published by the Geological Society of America, Boulder, CO.

Modeling Cu and Zn Desorption Kinetics from Soil Particles

Herbert E. Allen and Zhenqing Shi
Department of Civil and Environmental Engineering
University of Delaware
Newark, DE 19716

Publications

Papers

Zhenqing Shi, Dominic M. Di Toro, Herbert E. Allen and Alexander A. Ponizovsky. Modeling kinetics of Cu and Zn release from soils. *Environmental Science and Technology*. 2005, 39, 4562-4568.

Herbert E. Allen, Zhenqing Shi, Sagar Thakali, Alexander A. Ponizovsky, David Metzler and Dominic M. Di Toro. Partitioning of metal between soil and soil solution: a key process controlling the risk of metals to soil organisms. *Proceedings of the Copper 2003 - Cobre 2003 International Conference*. November 30 - December 3, 2003. Santiago, Chile. G.E. Lagos, A.E.M. Warner and M. Sanchez (eds.). Canadian Institute of Mining, Metallurgy and Petroleum. Volume II. pp. 567-580 (2003).

Zhenqing Shi, Dominic M. Di Toro, Alexander A. Ponizovsky and Herbert E. Allen. Modeling effects of pH and dissolved organic matter on kinetics of Cu and Zn desorption from soils. The 228th ACS National Meeting, Philadelphia, PA. August 22-26, 2004, CD-ROM.

Manuscripts in Preparation

Zhenqing Shi, Dominic M. Di Toro, and Herbert E. Allen. A WHAM based kinetics model for Zn adsorption and desorption on soils.

Zhenqing Shi, Herbert E. Allen, Dominic M. Di Toro, Suen-Zone Lee, and Steve Lofts. Predicting cadmium adsorption on soil.

Presentations

Zhenqing Shi, Dominic M. Di Toro, Alexander A. Ponizovsky and Herbert E. Allen. Modeling effects of pH and dissolved organic matter on kinetics of Cu and Zn desorption from soils. The 228th ACS National Meeting, Philadelphia, PA. August 22-26, 2004.

Quantitative Structure Activity Relationships for Toxicity and Fate Parameters of Metals and Metal Compounds

Dominic M. Di Toro
Department of Civil and Environmental Engineering
University of Delaware
Newark, DE 19716

and
Richard Carbonaro
Department of Environmental Engineering
Manhattan College
Riverdale, NY 10471

Publications

Presentations

Carbonaro, R.F., Di Toro, D.M. "Estimation of formation constants of metal complexes: Monodentate binding to oxygen and nitrogen donor atoms." American Chemical Society, San Francisco, CA September 10-14, 2006.

Carbonaro, R.F., Di Toro, D.M. "Investigation of metal-ligand interactions of model ligands for modeling metal-organic carbon binding." Society of Toxicology and Environmental Chemistry, 26th Annual Meeting in North America, Baltimore MD, November 13-17, 2005.

Books

Paquin, P. R., K. Farley, R. C. Santore, C. D. Kavvas, K. G. Mooney, R. P. Winfield, K. B. Wu, and D. M. Di Toro, eds. (2003). *Metals in Aquatic Systems: A Review of Exposure, Bioaccumulation, and Toxicity Models*, SETAC Press, Pensacola, FL.

Reiley, M. C., W. A. Stubblefield, W. J. Adams, D. M. Di Toro, P. V. Hodson, R. J. Erickson, and E. J. Keating Jr., eds. (2003). *Reevaluation of the State of the Science for Water Quality Criteria Development*, SETAC Press, Pensacola, FL.

Di Toro, D. M., Berry, W. J., Burgess, R. M., Mount, D., R., O'Connor, T. P., & Swartz, R. C. (2004). Predictive ability of sediment quality guidelines derived using equilibrium partitioning. In R. J. Wenning, G. E. Batley, C. E. Ingersoll, & D. W. Moore (Eds.), Use of sediment quality guidelines and related tools for the assessment of contaminated sediments. Society of Environmental Toxicology and Chemistry. Pensacola, FL:

Papers

Allen, H.E., Z. Shi, S. Thakali, A.A. Ponizovsky, D.M. Metzler, and D.M. Di Toro (2003). Partitioning of metal between soil and soil solution: a key process controlling the risk of metals to soil organisms. *Proceedings of the Copper 2003 - Cobalt 2003 International Conference*. Santiago, Chile, Canadian Institute of Mining, Metallurgy and Petroleum.

Di Toro, D. M., McGrath, J. M., Hansen, D. J., Berry, W. J., Paquin, P. R., Mathew, R., Wu, K. B., & Santore, R. C. (2005). Predicting Sediment Metal Toxicity Using a Sediment Biotic Ligand Model: Methodology and Initial Application. *Environ. Toxicol. Chem.*, 24(10), 2410-2427.

Carbonaro, R., Mahony, J., Walter, A., Halper, E., & Di Toro, D. (2005). Experimental and Modeling Investigation of Metal Release from Metal-Spiked Sediments. *Environ. Toxicol. Chem.*, 24(12), 3007-3019.

Shi, Z., Di Toro, D. M., Allen, H. E., & Ponizovsky, A. A. (2005). Modeling Kinetics of Cu and Zn Release from Soils. *Environ. Sci. Technol.*, 39(12), 4562-4568.

Miller, B. E., Rader, K. J., & Farley, K. J. (2006). Tableau Input Coupled Kinetic Equilibrium Transport (TICKET) Model. Submitted, Environmental Sci Tech.

Developing a Unit World Model for Metals in Aquatic Environments

Dominic M. Di Toro
Department of Civil and Environmental Engineering
University of Delaware
Newark, DE 19716

George W. Luther III
College of Marine and Earth Studies
University of Delaware
Lewes, DE 19958

and
Kevin J. Farley
Department of Environmental Engineering
Manhattan College
Riverdale, NY 10471

Publications

Presentations

- “Bioavailability of Metals and Organics in the Water Column and Sediment”, Ecotoxicology: A Hudson River Case Study, Department of Environmental Medicine, New York University, October 9, 2003
- Hudson-Delaware Chapter of SETAC Fall Workshop, Environmental Ecological Modeling and its Relationship to Criteria Development “Overview of Environmental Ecological Modeling and its Relationship to Criteria Development”, September 26, 2003
- Metal Unit World Workshop, Center for the Study of Metals in the Environment, University of Delaware, Newark, Delaware, February 3–5, 2003
- Hazard Identification Approach for Metals and Metal Substances, A SETAC-Sponsored Workshop, SETAC Technical Workshop on Hazard Identification for Metals, “Assessing Persistence”, May 3–8, 2003
- 48th Institute in Water Pollution Control, Manhattan College, Bronx NY, “Sediment Quality Criteria for Toxic Organic Contaminants and Metals”, June 9–13, 2003
- Frontiers in Assessment Methods for the Environment (FAME), NSF Sponsored Workshop, University of Minnesota, “High Resolution Large Scale Hydrodynamic/Chemical/Biological/Water Quality Models: The State of the Art in Practice”, August 10–13, 2003
- EPA Stakeholders Meeting, Papers Addressing Scientific Issues in the Risk Assessment on Metals, “Exposure Assessment: The Unit World Approach”, Washington DC, October 29, 2003
- Water Environment Research Foundation Multi-Metal Meeting, “A (Very) Short History of the *BLM*”, Miami, FL, October 22–24, 2003
- Farley, K.J., Rader, K.J., Costanzo, R., Nemesh, J., Hellweger, F., and DiToro, D.M. “Development of a Unit World Model for Metals in Aquatic Environments,” Platform Presentation, SETAC 24th Annual Meeting, Austin TX, November 9-13, 2003.
- SETAC Annual Meeting, Austin, TX, Short Course: Characterization and Remediation of Contaminated Sediments “Introduction and Overview”, “EqP Sediment Quality Guidelines Criteria”, November 9, 2003
- R. Mathew, R. C. Santore, P. R. Paquin, K. J. Heim, D. P. Galya, and D. M. DiToro, “Site-Specific Water Quality Criteria for Copper-Validation and Application of the BLM”, SETAC Annual Meeting, Austin, TX, November 12, 2003.
- P. R. Paquin, D. Damiani, K. J. Farley, R. Mathew, R. C. Santore, D. M. DiToro, “Metals Bioaccumulation and Effects: Consideration of Intracellular Speciation”, SETAC Annual Meeting, Austin, TX, November 12, 2003.
- Understanding Bioavailability and Mechanisms of Toxicity: Impacting Risk Assessment and Criteria Development, Invited Keynote Address, Workshop: Internal Exposure- Linking Bioavailability to Effects, International Conference Center Stefano Franscini, Monte Vérita, Ascona, Switzerland, August 22 - 27, 2004
- Farley, K.J. “Unit World Model,” Invited Presentation, Minerals and Metals Technical Working Group (MMTWG), Aberdeen UK, September 1-2, 2004

Farley, K.J., Costanzo, R., Carbonaro, R.F., and Di Toro, D.M. "Development of a "Unit World" Model for Metals in Aquatic Environments," Platform Presentation, Fourth SETAC World Congress and 25th Annual Meeting, Portland OR, November 14-18, 2004.

Toxicology, Chemistry and Theory: The Past and the Future, Invited Kenote Address - Perspectives Session, SETAC 2004, November 17, 2004

Predicting Sediment Metal Toxicity Using a Sediment Biotic Ligand Model, Platform Presentation, SETAC 2004

Modern Water and Sediment Quality Criteria for Toxic Metals: The Biotic Ligand Model and its Applications, Department of Environmental Medicine, New York University School of Medicine and Nelson Institute of Environmental Medicine, January 14, 2005

Point-Counterpoint: The scientific reliability of the Acid Volatile Sulfide/Simultaneously Extracted Metal (AVS/SEM) to assess metals bioavailability and sediment toxicity, Sediment Management Work Group, University of Maryland University Conference Center, Adelphi, Maryland, April 11, 2005

Farley, K.J., Carbonaro, R.F., and Di Toro, D.M. "Development of a "Unit World" (Model) Simulation for Metals in Aquatic Environments," Invited Presentation, Metal Environmental Risk Assessment Guidance Document (MERAG) Science Consolidation Workshop, London UK, May 10-11, 2005.

Development of Water and Sediment Quality Criteria, Manhattan College Summer Institute 50th Anniversary Symposium, Manhattan College, June 17, 2005

Modern Water Quality and Sediment Criteria: Toxicological and Chemical Interactions, Simon W. Freese Environmental Engineering Award and Lecture, Watershed Management Conference, Williamsburg VA, July 19, 2005

Bioavailability of Metals and Organics in the Water Column and Sediment Ecotoxicology: A Hudson River Case Study, Department of Environmental Medicine, New York University, October 6, 2005

Modern Water and Sediment Quality Criteria: Toxicological and Chemical Interactions, Superfund Basic Research Program, National Institute of Environmental Health Science Bioavailability Workshop, Newark NJ, November 9-10, 2005

Farley, K.J., Carbonaro, R.F., and Di Toro, D.M. "Evaluation of Critical Metal Loads Using the "Unit World" Model for Lakes," Platform Presentation, SETAC 26th Annual Meeting, Baltimore, MD November 13-17, 2005.

Papers

J. J. Tsang, T. F. Rozan, H. Hsu-Kim, K. M. Mullaugh and G. W. Luther, III. Pseudopolarographic determination of Cd²⁺ complexation in freshwater. *Environmental Science Technology*, in press. DOI: 10.1021/es0525509

J. J. Tsang, C. Kraiya, Shufen Ma and George W. Luther, III. Pseudopolarographic determination of zinc speciation in estuarine and fresh waters in the mid-Atlantic region. *Environmental Toxicology and Chemistry*, submitted.

A third one is being written on:

The preparation of trace metal clean NaCl and NaNO₃ for ionic strength adjustment in laboratory experiments.

Evaluation of Automobile sources for Metals in Urban Areas

Akash Sondhi, Paul T. Imhoff, Herbert E. Allen and Steven, K. Dentel
Department of Civil and Environmental Engineering
University of Delaware
Newark, DE 19716

Publications

Sondhi, A., P.T. Imhoff, H.E. Allen, and S.K. Dentel (2004) Dissolution of Metals from Brake Pad Wear Debris Under Conditions Simulating Leaching in Urban Areas, Society of Environmental Toxicology and Chemistry (SETAC)-25th National Meeting, Portland, OR.

Sondhi, A., P.T. Imhoff, H.E. Allen, and S.K. Dentel (2004) Evaluation of Metal Emissions from Brake Pad Wear Debris in Urban Runoff, American Chemical Society (ACS)-National Meeting. Philadelphia, PA.

Papers (to be submitted)

A comparison of the physico-chemical properties of brake pad wear debris generated under different laboratory conditions and collected in the environment

Dissolution of Copper from brake pad wear debris for four automobile types under urban environment conditions.

The Impact of Surface Precipitation on Sequestrian and Bioavailability of Metals in Soils

Donald L. Sparks and Edward Peltier
Department of Plant and Soil Sciences
University of Delaware
Newark, DE 19716

and
Danial van der Lelie
Biology Department
Brookhaven National Laboratory
Upton, NY 11973

Publications

Presentations

- Peltier, E.F., Allada, R. A., Navrotsky, A. and Sparks, D. L. Formation and Stability of Nickel Soil Precipitates. 228th ACS National Meeting, Philadelphia, PA August 22-26.
- Sparks, D.L., 2004. Multi-scale assessment of ion sorption kinetics at the mineral/water interface. 228th ACS National Meeting, Philadelphia, PA August 22-26.
- Sparks, D.L. 2004. Shedding light on metal speciation at mineral surfaces: The role of synchrotron-based spectroscopic techniques. 228th ACS National Meeting, Philadelphia, PA. August 22-26.
- Peltier, E. McNear Jr., D. H., and Sparks, D. L. "Formation and Stability of Mixed Metal Hydroxide Phases in Contaminated Soils" 20th Annual International Conference on Soils, Sediments and Water, Amherst MA, October 18-21, 2004.
- Peltier, E. and Sparks, D. L. "Predicting Nickel Precipitate Formation in Contaminated Soils" Soil Science Society of America National Meeting, Seattle, WA, October 31-November 4, 2004.
- Sparks, D.L. 2005. Kinetics of Chemical Reactions in Environmental Systems: Research Needs and Challenges. Keynote Talk. NSLS Users' Meeting, In-situ Analyses in Environmental Systems, Brookhaven National Laboratory, Upton, NY, May 23-25.
- Sparks, D.L. 2005. The Role of XAFS in Advancing the Frontiers of Molecular Environmental Science. Keynote Talk. 4th Summer School on Condensed Matters Research, Zuoz, Switzerland, August 14-21.
- Sparks, D.L. 2005. Advances in Elucidating Biogeochemical Processes in Soils: It's About Scale and Interfaces. Keynote Talk. 7th International Symposium on Geochemistry of the Earth's Surface (GES-7), Aix-en-Provence, August 23-27.
- Sparks, D.L. 2005. Grand Challenges and Opportunities in the Environmental Sciences: The Importance of Basic Research and Technology. 2005 Sterling B. Hendricks Memorial Lecture, American Chemical Society Meeting, Washington, DC, August 31.
- Sparks, D.L. 2005. Frontiers in Contaminant Speciation and Reactivity in Terrestrial Environments: The Role of Synchrotron Radiation. Plenary Talk. Japanese Society of Soil Science and Plant Nutrition Meeting, Matsue, Japan, September 6-8.
- Sparks, D.L. 2005. Frontiers in Soil Science: Technology and the Information Age. Plenary Talk. Frontiers of Soil Science- Messages from Soil Scientists in Asia, Japan Council of Science, Tokyo, Japan, September 12.
- Peltier, E. and Sparks, D. L. "Identifying Nickel Precipitates in Contaminated Soils" Synchrotron Environmental Science III, Brookhaven, NY (September 18-20, 2005)
- Sparks, D.L. 2005. Future Directions in Basic Soil Science Research: Opportunities and Challenges. Plenary Talk. International Symposium 2005, Application of Emerging Soil Science Research and its Role in the Conservation of Agricultural Ecosystems. Seoul, Korea, September 28-29.
- Peltier, E. and Sparks, D. L. "Formation and Stability of Ni Surface Precipitates in Delaware Soils" National Science Foundation Sponsored Workshop Frontiers in Exploration of the Critical Zone, Newark, DE (October 24-26, 2005)

Peltier, E. and Sparks, D. L. "The Influence of Surface Precipitation on Nickel Solubility, Bioavailability, and Fate in Contaminated Soils" 18th World Congress of Soil Science, Philadelphia, PA (July 9-16, 2006)

Published Articles

Peltier, E., Allada, R. K., Navrotsky, A. and Sparks, D. L. (2006) "Nickel Solubility and Precipitation in Soils: A Thermodynamic Study" *Clays and Clay Minerals* **54**:153-164.

Peltier E. and Sparks, D. L. "Kinetics of Nickel Surface Precipitate Formation in Soils" in preparation

Peltier E., van der Lelie, D. and Sparks, D. L. "Stability and Bioavailability of Ni LDH Soil Precipitates" in preparation

Transport Processes of Mining Related Metals in the Black River of Missouri's New Lead Belt

David J. Wronkiewicz
Department of Geology and Geophysics
University of Missouri - Rolla
Rolla, MO 65409
and

Craig D. Adams and Cesar Mendosa
Department of Environmental Engineering
University of Missouri - Rolla
Rolla, MO 65409

Publications

- Faeth, A.M., Wronkiewicz, D.J., Adams, C.D., Mendoza, C., McBurnett, J.D., Wolf, S.F., Krizanich, G.W., Lead and Zinc Transport Processes in the Black River of Missouri's New Lead Belt, Environmental Science and Technology (in prep).
- Krizanich, G.W. and Wronkiewicz, D.J., Trace element and isotopic trends in sediment cores from Clearwater Lake, southeast Missouri, Geol. Soc. Amer. 2005 annual fall meeting, abstract, Salt Lake, UT.
- Faeth, A.M., Lead and Zinc Transport in the West Fork Black River of Missouri's New Lead Belt, University of Missouri – Rolla MS Thesis, student graduated August 2004.
- Krizanich, G.W. and Wronkiewicz, D.J., Trace element trends in sediment cores from Clearwater Lake, southeast Missouri, Geol. Soc. Amer. 2004 annual fall meeting, abstract, Denver, CO, v.. 36, No. 5, p. 288.
- Faeth, A.M., Wronkiewicz, D.J., Adams, C.D., Mendoza, C., McBurnett, J.D., Wolf, S.F., Krizanich, G.W., Struttman, S.R., and Hemmann, R., “Heavy Metal Transport Processes in the Black River of Missouri's New Lead Belt”, Geol. Soc. Amer. 2004 Sectional Meeting abstract, St. Louis, MO (2004).
- McBurnett, J. D., Wronkiewicz, D., and Faeth, A.M., “Energy Dispersive Spectroscopy of Big River Sediments”, Geol. Soc. Amer. 2004 Sectional Meeting abstract, St. Louis, MO (2004).
- Faeth, A.M., Wronkiewicz, D.J., Adams, C.D., Mendoza, C., McBurnett, J.D., Wolf, S.F., Krizanich, “Processes Affecting Metal Transport in the Black River of Missouri's New Lead Belt”, Missouri Groundwater Conference 2004 annual meeting, abstract, Columbia, MO (2004).
- Hemmann, Robert J. and David J. Wronkiewicz, “Alteration Phase Development During the Oxidative Weathering of Remnant Sulfide Ores”, MO Acad. Sci. 2004 annual meeting, abstract, Kansas City, MO (2004).
- Wronkiewicz, D. J., Mendoza, C., Adams, C. Fate and Transport of Metal Contaminants in the Big and Black River Systems of Missouri. Missouri Water News. 2003, 10, No. 1.
- Wronkiewicz, D.J., McBurnett, J.D., Faeth, A.M., Wolf, S.F., Mendoza, C., Krizanich, G.W., Struttman, S.R., Hemmann, R., and Adams, C.D., “Lead and Zinc Migration in the Big River System, Southeastern Missouri”, Soc. Environ. Toxicology and Chem. 2003 annual meeting, abstract, Austin, TX, p. 81 (2003).
- Faeth, A.M., Wronkiewicz, D.J., Adams, C.D., Mendoza, C., McBurnett, J.D., Wolf, S.F., Krizanich, G.W., and Struttman, S.R., “Metal Speciation and Transport in the Black River of Missouri's New Lead Belt”, Soc. Environ. Toxicology and Chem. 2003 annual meeting, abstract, Austin, TX, p. 316 (2003).
- McBurnett, J.D. and Wronkiewicz, D.J., “Geochemical Impact of Lead Mining Waste Water on Strother Creek”, MO Acad. Sci. 2003 annual meeting, abstract, Warrensburg, MO (2003).
- Wronkiewicz, D.J., Crenshaw, T.L., Davidson, D.A., Faeth, A.M., Goss, A.K., Knobbe, S.J., Krizanich, G.W., McBurnett, J.D., McNeil, A.G., Stanke, B.D., and Struttman, S.R., “Controls on Heavy Metal Contaminant Migration in the Big River Watershed, Southeastern Missouri”, Inter. Conf. Basement Tectonics, 2002 annual meeting, extended abstract, Rolla, MO, p. 50-51 (2002).

Wronkiewicz, D.J., Faeth, A.M., Krizanich, G.W., and Struttman, S.R., "Fate and transport of heavy metal contaminants in the Big River, Old Lead Belt, Southeastern Missouri", Geol. Soc. Amer. 2002 annual fall meeting, abstract, Denver, CO, p. 214 (2002).

A Test of the Biotic Ligand Model: Fish Exposed to Time-varying Concentrations of Copper and Zinc

Joseph S. Meyer
Department of Zoology and Physiology
University of Wyoming
Laramie, WY 82071-3166

Publications

Journal articles containing acknowledgement of funding from CSME that either were published or have been accepted for publication in scientific journals:

Clearwater, S.J., A.M. Farag and J.S. Meyer. 2002. Bioavailability and toxicity of dietborne copper and zinc to fish. *Comparative Biochemistry and Physiology Part C* 132:269-313.

Morris, J.M., A.M. Farag, D.M. Nimick and J.S. Meyer. 2005. Does biofilm contribute to diel cycling of Zn in High Ore Creek, Montana? *Biogeochemistry* 76:233-259.

Brooks, M.L., C.J. Boese and J.S. Meyer. 2006. Complexation and time-dependent accumulation of copper by larval fathead minnows (*Pimephales promelas*): Implications for modeling toxicity. *Aquatic Toxicology* 78:42-49.

Meyer, J.S., M.J. Suedkamp, A.M. Farag and J.M. Morris. 2006. Leachability of protein and metals incorporated into aquatic invertebrates: Are species and metals-exposure history important? *Archives of Environmental Contamination and Toxicology* 50:79-87.

Morris, J.M. and J.S. Meyer. 2006. Extracellular and intracellular uptake of Zn in a photosynthetic biofilm matrix. *Bulletin of Environmental Contamination and Toxicology* 77:30-35.

Bringolf, R.B., B.A. Morris, C.J. Boese, R.C. Santore, H.E. Allen and J.S. Meyer. 200_. Influence of dissolved organic matter on acute toxicity of zinc to larval fathead minnows (*Pimephales promelas*). *Archives of Environmental Contamination and Toxicology*: in press.

Kolts, J.M., C.J. Boese and J.S. Meyer. 200_. Acute toxicity of copper and silver to *Ceriodaphnia dubia* in the presence of food. *Environmental Toxicology and Chemistry*: in press.

Morris, J.M., A.M. Farag, D.A. Nimick and J.S. Meyer. 200_. Light-mediated Zn uptake in photosynthetic biofilm. *Hydrobiologia*: in press.

Morris, J.M. and J.S. Meyer. 200_. Photosynthetically mediated Zn removal from the water column in High Ore Creek, Montana. *Water, Air, and Soil Pollution*: in press.

Books published:

Meyer, J.S., W.J. Adams, K.V. Brix, S.N. Luoma, D.R. Mount, W.A. Stubblefield and C.M. Wood (eds.). 2005. *Toxicity of Dietborne Metals to Aquatic Organisms*. SETAC Press, Pensacola, Florida, USA. 303 pp.

Book chapters published:

Benson, W.H., H.E. Allen, J.P. Connolly, C.G. Delos, L.W. Hall, Jr., S.N. Luoma, D. Maschwitz, J.S. Meyer, J.W. Nichols and W.A. Stubblefield. 2003. Exposure analysis. p. 15-51 in: M.C. Reiley, W.A. Stubblefield, W.J. Adams, D.M. Di Toro, P.V. Hodson, R.J. Erickson and F.J. Keating, Jr. (eds.). *Reevaluation of the State of the Science for Water-quality Criteria Development*. SETAC Press, Pensacola, Florida, USA.

Campbell, P.G.C., S.J. Clearwater, P.B. Brown, N.S. Fisher, C. Hogstrand, G.R. Lopez, L.M. Mayer and J.S. Meyer. 2005. Digestive physiology, chemistry, and nutrition. p. 13-57 in: J.S. Meyer, W.J. Adams, K.V. Brix, S.N. Luoma, D.R. Mount, W.A. Stubblefield and C.M. Wood (eds.), *Toxicity of Dietborne Metals to Aquatic Organisms*, SETAC Press, Pensacola, Florida, USA.

Meyer, J.S., W.J. Adams, K.V. Brix, S.N. Luoma, D.R. Mount, W.A. Stubblefield and C.M. Wood. 2005. Workshop summary and conclusions. p. 191-201 in: J.S. Meyer, W.J. Adams, K.V. Brix, S.N. Luoma, D.R. Mount, W.A. Stubblefield and C.M. Wood (eds.), *Toxicity of Dietborne Metals to Aquatic Organisms*, SETAC Press, Pensacola, Florida, USA.

Manuscripts containing acknowledgement of funding from CSME that are in review for publication in scientific journals:

Brooks, M.L. and J.S. Meyer. 200_. Toxicity of copper to larval *Pimephales promelas* in the presence of photodegraded natural dissolved organic matter. Submitted to *Canadian Journal of Fisheries and Aquatic Sciences*.

Kolts, J.M., M.L. Brooks, B.D. Cantrell, C.J. Boese, R.A. Bell and J.S. Meyer. Dissolved fraction of standard laboratory cladoceran food alters acute toxicity of waterborne silver to *Ceriodaphnia dubia*. Submitted to *Environmental Science and Technology*.

Morris, J.M. and J.S. Meyer. Extracellular and intracellular uptake of Zn in a photosynthetic biofilm matrix. Submitted to *Bulletin of Environmental Contamination and Toxicology*.

Manuscripts containing acknowledgement of funding from CSME that are in preparation for submission to scientific journals:

Brooks, M.L., J.S. Meyer and D.M. McKnight. Changes in copper complexation during photolysis of wetland and riverine dissolved organic matter. (to be submitted to *Photobiology*).

Clearwater, S.J., A.M. Farag and J.S. Meyer. Bioavailability and toxicity of dietborne silver, aluminum, cadmium and lead to fish. (to be submitted to *Comparative Biochemistry and Physiology Part C Toxicology and Pharmacology*).

Kolts, J.M., C.J. Boese and J.S. Meyer. Toxicity of dietborne copper and silver to *Ceriodaphnia dubia*. (to be submitted to *Aquatic Toxicology*).

Morris, B.A., R.B. Bringolf, C.J. Boese, R.C. Santore and J.S. Meyer. Influence of pH, calcium, magnesium, sodium and potassium on zinc toxicity to larval fathead minnows (*Pimephales promelas*). (to be submitted to *Archives of Environmental Toxicology and Chemistry*).

Morris, J.M., D.A. Nimick, A.M. Farag and J.S. Meyer. Vertical profiles of pH and Zn²⁺ concentration in biofilm explain possible mechanism(s) of diel Zn cycling in mining-impacted streams. (to be submitted to *Limnology and Oceanography*).

Morris, J.M., D.A. Nimick, A.M. Farag and J.S. Meyer. A conceptual model of how photosynthetic biofilm controls diel Zn cycling in mining-impacted streams. (to be submitted to *Biogeochemistry*).

Presentations at scientific meetings:

Lovvorn, M.B. and J.S. Meyer. 2001. Photochemically altered dissolved organic matter from natural waters: implications for copper-organic binding and toxicity. Presented at the Fourteenth Annual Meeting of the Rocky Mountain Chapter of the Society of Environmental Toxicology and Chemistry. Denver, CO. 6 April.

Lovvorn, M.B. and J.S. Meyer. 2001. Sunlight effects on natural waters: humic substances, copper complexation, and toxicity. Presented at the Twenty-second Annual Meeting of the Society of Environmental Toxicology and Chemistry. Baltimore, MD. 11-15 November.

- Moffett, J.W. and J.S. Meyer. 2001. Application of the biotic ligand model to the marine environment: opportunities and challenges. Presented at the Twenty-second Annual Meeting of the Society of Environmental Toxicology and Chemistry. Baltimore, MD. 11-15 November.
- Morris, J.M., S.A. Collyard and J.S. Meyer. 2001. Does exposure to copper alter nutritional content of *Hyalella azteca*? Presented at the Twenty-second Annual Meeting of the Society of Environmental Toxicology and Chemistry. Baltimore, MD. 11-15 November.
- Lovvorn, M.B. and J.S. Meyer. 2002. Sunlight effects on natural waters: humic substances, copper complexation, and toxicity. Presented at the Fifteenth Annual Meeting of the Rocky Mountain Chapter of the Society of Environmental Toxicology and Chemistry. Fort Collins, CO. 19 April.
- Lovvorn, M.B. and J.S. Meyer. 2002. Photoreactivity and copper complexation by wetland versus riverine DOM. Presented at the Twenty-third Annual Meeting of the Society of Environmental Toxicology and Chemistry. Salt Lake City, UT. 16-20 November.
- Meyer, J.S., W.J. Adams, K.V. Brix, S.N. Luoma, D.R. Mount, W.A. Stubblefield, and C.M. Wood. 2002. Toxicity of dietborne metals to aquatic biota: emerging science and regulatory implications. Presented at the Twenty-third Annual Meeting of the Society of Environmental Toxicology and Chemistry. Salt Lake City, UT. 16-20 November.
- Morris, J.M., A.M. Farag, D.A. Nimick and J.S. Meyer. 2002. Biofilm and the diel cycling of aqueous metals in mountain streams. Presented at the Fifteenth Annual Meeting of the Rocky Mountain Chapter of the Society of Environmental Toxicology and Chemistry. Fort Collins, CO. 19 April.
- Morris, J.M., A.M. Farag, D.A. Nimick and J.S. Meyer. 2002. Biofilm and the diel cycling of aqueous metals in mountain streams. Presented at the Twenty-third Annual Meeting of the Society of Environmental Toxicology and Chemistry. Salt Lake City, UT. 16-20 November.
- Wu, K.B., V. Navab, R. Mathew, R.C. Santore, P.R. Paquin, J.S. Meyer, K.V. Brix and D.M. Di Toro. 2002. An application of the biotic ligand model (BLM) framework to nickel. Presented at the Twenty-third Annual Meeting of the Society of Environmental Toxicology and Chemistry. Salt Lake City, UT. 16-20 November.
- Bringolf, R.B., B.A. Morris, S.A. Collyard, C.J. Boese, R.C. Santore, H.E. Allen and J.S. Meyer. 2003. Effects of pH and dissolved organic matter on acute toxicity of zinc to larval fathead minnows. Presented at the Twenty-fourth Annual Meeting of the Society of Environmental Toxicology and Chemistry. Austin, TX. 9-13 November.
- Kolts, J.M., C.J. Boese and J.S. Meyer. 2003. Toxicity of dietborne and waterborne copper and silver to *Ceriodaphnia dubia*. Presented at the Twenty-fourth Annual Meeting of the Society of Environmental Toxicology and Chemistry. Austin, TX. 9-13 November.
- Morris, B.A., R.B. Bringolf, C.J. Boese and J.S. Meyer. 2003. Protective effects of inorganic salts against zinc toxicity to larval fathead minnows. Presented at the Twenty-fourth Annual Meeting of the Society of Environmental Toxicology and Chemistry. Austin, TX. 9-13 November.
- Morris, J.M., B. Mueller, A.M. Farag and J.S. Meyer. 2003. Profiling photosynthetic biofilm using miniaturized ion-selective electrodes. Presented at the Sixteenth Annual Meeting of

the Rocky Mountain Chapter of the Society of Environmental Toxicology and Chemistry. Denver, CO. 16 April.

- Morris, J.M., D.A. Nimick, A.M. Farag and J.S. Meyer. 2003. Biotic influences on diel cycling of Zn in High Ore Creek, Montana. Presented at the Twenty-fourth Annual Meeting of the Society of Environmental Toxicology and Chemistry. Austin, TX. 9-13 November.
- Kolts, J.M., B.L. Denier, C.J. Boese, R.A. Bell and J.S. Meyer. 2004. Acute toxicity of waterborne silver to *Ceriodaphnia dubia* in the presence of dissolved organic matter. Presented at the Twenty-fifth Annual Meeting (Fourth World Congress) of the Society of Environmental Toxicology and Chemistry. Portland, OR. 14-18 November.
- Morris, B.A., R.B. Bringolf, C.J. Boese and J.S. Meyer. 2004. Protective effects of inorganic salts against zinc toxicity to larval fathead minnows. Presented at the Seventeenth Annual Meeting of the Rocky Mountain Chapter of the Society of Environmental Toxicology and Chemistry, Laramie, Wyoming. 1-2 April.
- Morris, J.M., B. Morris, A.M. Farag and J.S. Meyer. 2004. Photosynthetically mediated Zn uptake in biofilm in High Ore Creek, Montana. Presented at the Seventeenth Annual Meeting of the Rocky Mountain Chapter of the Society of Environmental Toxicology and Chemistry, Laramie, Wyoming. 1-2 April.
- Morris, J.M., B. Morris, A.M. Farag, D.A. Nimick and J.S. Meyer. 2004. Photosynthetically mediated Zn uptake in biofilm in High Ore Creek, Montana. Presented at the Twenty-fifth Annual Meeting (Fourth World Congress) of the Society of Environmental Toxicology and Chemistry. Portland, OR. 14-18 November.
- Schmidt, T.S., J.S. Meyer and W.H. Clements. 2004. Field test of the biotic ligand model in Colorado Rocky Mountain streams. Presented at the Twenty-fifth Annual Meeting (Fourth World Congress) of the Society of Environmental Toxicology and Chemistry. Portland, OR. 14-18 November.
- Morris, J.M., A. Farag and J.S. Meyer. 2005. pH and Zn profiles in photosynthetic biofilm using ion-selective electrodes: An explanation for diel metal cycling? Presented at the Twenty-sixth Annual Meeting of the Society of Environmental Toxicology and Chemistry. Baltimore, MD. 13-17 November.
- Meyer, J.S., C.J. Boese and J.M. Morris. 2006. Adapting the biotic ligand model to predict toxicity of time-variable Cu exposures to fathead minnows. To be presented at the Twenty-seventh Annual Meeting of the Society of Environmental Toxicology and Chemistry. Montreal, Québec, Canada. 5-9 November.

APPENDIX III

Students Supported

Ecotoxicology of Mining-Related Metal Oxides in a High Gradient Mountain Stream

Colorado School of Mines
Department of Chemistry and Geochemistry
Department of Environmental Science and Engineering

Students Fully Supported

Dr. Barbara Ann Butler, PhD thesis May 2005 - Title: Assessing the Fate and Transport of Metals in a High Gradient Acid Mine Drainage Impacted Mountain Stream, North Fork, Clear Creek, Colorado

Students Partially Supported

Kathryn Kangas, MS thesis December 2005 - Title: The Toxicity of Binary Metal Mixtures to *Ceriodaphnia dubia*

Eric Blumenstein, MS thesis May 2006 – Title: Evaluating Aquatic Bioassays for Copper and Zinc Toxicity In Mining Influenced Waters

Marti Adams, MS thesis May 2006 - Title: Applicability of the Biotic Ligand Model for Mining Influenced Waters and Influence of Variations in Natural Organic Matter Characteristics on Copper Toxicity to *Ceriodaphnia dubia*

Modeling Cu and Zn Desorption Kinetics from Soil Particles

Department of Civil and Environmental Engineering
University of Delaware

Students Supported

Zhenqing Shi, Ph.D. thesis February 2006- Title: Kinetics of Trace Metals Sorption on and Desorption from Soils: Developing Predictive Models

Sagar Thakali, Ph.D. thesis May 2006 – Title: Terrestrial Biotic Ligand Model (tBLM) for Copper, and Nickel Toxicities to Plants, Invertebrates, and Microbes in Soils

Amanda Ackerman, Undergraduate Student

Quantitative Structure Activity Relationships for Toxicity and Fate Parameters of Metals and Metal Compounds

Department of Civil and Environmental Engineering
University of Delaware

Department of Environmental Engineering
Manhattan College

Students Supported
Undine Kipka, Graduate Student
Yasemin Atalay Graduate Student

Developing a Unit World Model for Metals in Aquatic Environments

Department of Civil and Environmental Engineering
University of Delaware

Department of Environmental Engineering
Manhattan College

Students Supported
Robert Costanzo, a graduate student (ME 2004)
Jason Ragona, M.S.
Feryal Guler, M.S. thesis May 2005 – Title: Modeling Metal Sorption to Algae Using

WHAM

Kevin Rader, Ph.D candidate
Kathy Phillips, Ph.D. candidate

Postdoctoral Students Partially Supported
Charoenkwan Kraiya
Jeffrey J. Tsang

Evaluation of Automobile sources for Metals in Urban Areas

Department of Civil and Environmental Engineering
University of Delaware

Students Supported

Akash Sondhi (Degree - Ph.D., expected graduation – Winter-2007)

Amanda Lucas (Degree – B.S. Env. Engg., 2009)

Francis Bonkowski (Degree – B.S. Env. Engg., 2008)

Jessica Kessler (Degree – B.S. Env. Engg., 2008)

The Impact of Surface Precipitation on Sequestrian and Bioavailability of Metals in Soils

University of Delaware
Department of Plant and Soil Sciences

Brookhaven National Laboratory
Biology Department

Students Supported

A number of studies have appeared in the literature on the formation of metal (e.g., Co, Ni, and Zn) hydroxide precipitates on mineral and mineral-coated surfaces. These phases occur at surface loadings often below monolayer coverage and at pHs.

Transport Processes of Mining Related Metals in the Black River of Missouri's New Lead Belt

University of Missouri – Rolla
Department of Geology and Geophysics
Department of Environmental Engineering

Student Supported

Gary W. Krizanich, Ph.D. candidate, Geological Sciences and Engineering, is Gary W. Krizanich, Ph.D. candidate, Geological Sciences and Engineering, is continuing with his research activities on the Clearwater Lake Sediments. This project is supported by the U.S. Geological Survey and the Geological Sciences and Engineering Department.

Anne M. Faeth, MS graduate, Department of Environmental Engineering / Geological Sciences and Engineering, graduated in May 2005. Her research focus and thesis related to the studies of the West Fork sediments and waters.

Joshua D. McBurnett, MS candidate, Department of Geological Sciences and Engineering, Big River sediment study. Student withdrew from graduate program without completing his degree requirements.

H. Carrie Bender, MS candidate, Department of Geological Sciences and Engineering, began her graduate studies in January 2006 with the intention of investigating metal transport in the Big River System.

Justin Davis, MS candidate, Department of Geological Sciences and Engineering, began his graduate studies in January, 2006 with the intention of investigating mineral alteration patterns in tailings piles.

Robert Hemmann, BS graduate, undergraduate research study investigating relative corrosion rates of sulfide minerals, Department of Geological Sciences and Engineering, graduated in December 2004.

Graeme Stroker, BS graduate, undergraduate research study investigating microbial influence on sulfide corrosion in tailings pile waters, Department of Geological Sciences and Engineering, is expected to graduate in December 2005.

Russell Pate, BS graduate, undergraduate work-study student, Department of Geological Sciences and Engineering, is expected to graduate in December 2005.

T. Crenshaw, D. Davison, A. Faeth, M. Goss, S. Knobbe, G. Krizanich, J. McBurnett, A. McNiel, B. Stanke and S. Struttman, undergraduate participants in GEOL 372 class, applied geochemistry in investigation into “Composition and Size Distribution of Contaminants Associated with Mined Wastes in the Big and Flat Rivers of Southern Missouri” (2002).

A Test of the Biotic Ligand Model: Fish Exposed to Time-varying Concentrations of Copper and Zinc

University of Wyoming
Department of Zoology and Physiology

Students Supported

Jeffrey M. Morris, Ph.D. thesis December 2005 - Title: Mechanisms and Effects of Light-Mediated Zinc Uptake by Photosynthetic Biofilm: Implications for Diel Metal Cycling in Mining-Impacted Streams

Brady A. Morris, M.S. (anticipated December 2006). Thesis title: Toxicity of Sodium Bicarbonate to Fathead Minnows in Water Mimicking the Tongue River in Montana